RADIAL: a Fortran subroutine package for the solution of the radial Schrödinger and Dirac wave equations

Francesc Salvat and José M. Fernández-Varea

Facultat de Física (FQA and ICC). Universitat de Barcelona.
Diagonal 645, E-08028 Barcelona, Catalonia

Abstract

The Fortran subroutine package RADIAL for the numerical solution of the Schrödinger and Dirac wave equations of electrons in central potentials $V(r)$ is described. The considered potentials are such that the function $\mathcal{V}(r) \equiv rV(r)$ is finite for all r and tends to constant values for $r \to 0$ and $r \to \infty$. This includes finite-range potentials as well as combinations of Coulomb and finite-range potentials. The function $\mathcal{V}(r)$ used in the numerical calculation is the natural cubic spline that interpolates a table of values provided by the user. The radial wave equations are solved by using piecewise exact power series expansions of the radial functions, which are summed up to the prescribed accuracy so that truncation errors can be completely avoided. The RADIAL subroutines compute radial wave functions, eigenvalues for bound states and phase shifts for free states. Specific subroutines are also provided for computing the radial functions and phase shifts for free states of complex optical potentials having an absorptive imaginary part of finite range. The present report contains a detailed study of Coulomb wave functions (*i.e.*, solutions of the radial wave equations for pure Coulomb potentials), which are used to normalise the radial functions of free states and to verify the accuracy of the numerical integration algorithm. Practical applications of the RADIAL subroutines are presented: the self-consistent solution of the Dirac–Hartee–Fock–Slater equations for neutral atoms and positive ions, and the calculation of cross sections for elastic scattering of electrons and positrons by atoms and of nucleons by nuclei.

Keywords: Schrödinger equation. Dirac equation. Central potentials. Bound states, eigenvalues. Free states, phase shifts. Coulomb functions. Bessel functions. Dirac–Hartree–Fock–Slater self-consistent equations for atoms. Scattering of electrons and positrons by atoms. Scattering of nucleons by nuclei.

Date: 22 January, 2019

Contents

1 Introduction

The calculation of central-potential radial wave functions is a basic tool in atomic and nuclear physics. In spite of its practical importance, computer programs, capable of solving the radial wave equations for an arbitrary potential $V(r)$ given in numerical form, are not generally available. In this report we describe an algorithm, and a Fortran subroutine package called RADIAL, for the numerical solution of the radial Schrödinger and Dirac equations for a wide class of central potentials. The potentials considered are such that the function $\mathcal{V}(r) \equiv rV(r)$ is finite for all r and reaches constant values when $r \to 0$ and $r \to \infty$. This includes finite-range potentials, Coulomb potentials, and any combination of both (the so-called *modified Coulomb potentials*).

The present report is intended to serve as a manual of the subroutine package. For the sake of completeness, we offer a detailed description of the solution algorithm, including the complete collection of formulas and numerical recipes implemented in the programs. In particular, we present a detailed study of Coulomb and Bessel functions, which are used to normalise the radial functions of free states. This information may be helpful to correct possible bugs in the computer code, which do have a tendency to come into action when programs leave the author's hand.

The numerical procedure adopted to solve the radial differential equations was proposed by Salvat and Mayol (1991), and is based on a similar method employed by Bühring (1965). The function $\mathcal{V}(r)$ used in the calculations is the natural cubic spline (see Appendix A) that interpolates the values of a table provided by the user. Interpolation errors introduced by the spline approximation can be made as small as required by simply specifying the values of the potential function on a sufficiently dense grid of radii. The responsibility for ensuring that the effect of these interpolation errors on the calculation results is negligible rests with the user. In this respect, it may be helpful to plot the input potential table together with the spline interpolation and check that the spline does not wiggle between the input data points. The radial wave equations for the cubic-spline potential are solved by using the *exact* power-series expansions of the radial functions, which are summed up to a prescribed accuracy. This procedure allows a complete control of truncation errors. The calculation results are thus only affected by unavoidable round-off errors. In practice, the algorithm permits different levels of accuracy; the price to be paid for a more accurate result is merely a longer calculation time. With double-precision arithmetic, results accurate to up to 13 or 14 decimal figures can be obtained.

The Fortran subroutine package RADIAL described here has been tailored to be as easy to use as possible. Although it is largely based on the RADWEQ package of Salvat and Mayol (1991), it is considerably more versatile and general. A first version of RADIAL was written by Salvat, Fernández-Varea, and Williamson, and published in *Computer Physics Communications* in 1995. Since then the subroutines have been em-

ployed by a number of research groups in calculations of atomic collisions, photoabsorption, bremsstrahlung emission, nuclear β decay, etc. We have used RADIAL intensively, mostly in calculations of elastic and inelastic collisions of electrons and positrons with atoms and ions (Salvat, 2003; Salvat *et al.*, 2005; Segui *et al.*, 2002, 2003; Bote and Salvat, 2008) and of the atomic photoeffect (Sabbatucci and Salvat, 2016). We have introduced various refinements to improve the accuracy and robustness of the subroutines, and to ease their use. The most significant improvement affected the normalisation of bound states, which now is performed to the same accuracy as the integration of the differential equations. The source files of RADIAL have been rewritten and new auxiliary subroutines have been included. In the current version of the subroutines and documentation, Dirac wave functions conform to the phase convention of Rose (1961), which is more commonly used than the alternative convention adopted by Salvat *et al.* (1995). Finally, the calculation of free-state radial functions and phase shifts has been extended to the case of complex optical potentials that occur in studies of atomic and nuclear collisions.

The present report is organised as follows. In Section 2 we briefly review basic aspects of the solutions of the Schrödinger and Dirac wave equations for central potentials, and we describe normalisation conventions for bound and free states. Section 3 is devoted to the study of the radial wave functions of a particle in a Coulomb potential, the so-called Coulomb functions. In the limit of null potential strength, the Coulomb functions reduce to spherical Bessel functions. Analytical expressions for the Coulomb functions are derived, and robust algorithms for computing these functions are described. In Section 4 we present the power-series method for solving the radial Schrödinger and Dirac equations. Sections 5 and 6 deal with the practical calculation of radial functions of bound and free states, respectively; we also give basic formulas for calculations with distorted plane waves. General asymptotic expansions of the radial functions for large radii, where the potential is purely Coulombian, are presented in Section 7. The structure and operation of the RADIAL library are detailed in Section 8. Section 9 describes the generic main programs `demorad`, `zdemorad`, and `numpoten`, which calculate radial functions of electrons in modified Coulomb potentials. Sections 10 to 12 present examples of practical applications: the self-consistent solution of the Dirac–Hartree–Fock–Slater equations for neutral atoms and positive ions; the calculation of differential cross sections for scattering of electrons and positrons in the electrostatic field of neutral atoms by means of the Schrödinger and Dirac partial-wave expansion methods; and the calculation of elastic collisions of nucleons with nuclei by the partial-wave expansion method with a global optical-model potential. The Appendices contain information on numerical methods (cubic spline interpolation and evaluation of continued fractions), and an analysis of the nodes of radial wave functions.

2 Radial wave equations

For the sake of concreteness, we will assume that the particles described by the Schrödinger and Dirac equations are electrons (mass $\mathrm{m_e}$, charge $-e$) or positrons (mass $\mathrm{m_e}$, charge $+e$). In Sections 2 and 3, which deal with general theoretical considerations, formulas

are written in the Gaussian-cgs system of units, with all fundamental constants indicated explicitly. In the description of the numerical solution algorithms, and in the computer programs, it is expedient to use Hartree atomic units. In these units, the reduced Planck constant $\hbar$, the elementary charge e (*i.e.*, the absolute value of the electron charge), and the mass $\mathrm{m_e}$ of the electron are taken as unity, with no dimensions. The atomic unit of length is the Bohr radius

$$a_0 \equiv \frac{\hbar^2}{\mathrm{m_e} e^2} = 0.529\,177\,211 \text{ Å}, \tag{2.1}$$

and the unit of energy is the Hartree energy,

$$E_\mathrm{h} \equiv \frac{\mathrm{m_e} e^4}{\hbar^2} = 27.211\,386 \text{ eV}. \tag{2.2}$$

In atomic units, the speed of light in vacuum is $c = c\hbar/e^2 = \alpha^{-1} = 137.035\,999$, *i.e.*, the inverse of the fine-structure constant α. The numerical values of fundamental physical constants adopted in the programs were taken from Mohr *et al.* (2016).

The theory and the computer code are valid also for particles other than electrons and positrons; we only need to replace $\mathrm{m_e}$ by the mass M of the particle. The corresponding "generalised" system of atomic units is then defined by setting $M = e = \hbar = 1$. That is, the generalised atomic units of length and energy are $a_M = (\mathrm{m_e}/M)a_0$ and $E_M = (M/\mathrm{m_e})E_\mathrm{h}$, respectively. Notice that the potential function $\mathcal{V} = rV(r)$ has dimensions of length×energy and, hence, its numerical value is independent of the mass M of the particle.

2.1 Schrödinger equation

In non-relativistic quantum mechanics, the stationary states of an electron (or positron) in a central potential $V(r)$ are described by the time-independent Schrödinger equation

$$\mathcal{H}_\mathrm{S}\,\psi(\mathbf{r}) = E\,\psi(\mathbf{r}) \tag{2.3}$$

with the Hamiltonian

$$\mathcal{H}_\mathrm{S} = -\frac{\hbar^2}{2\mathrm{m_e}}\,\nabla^2 + V(r) = -\frac{\hbar^2}{2\mathrm{m_e}}\left(\frac{1}{r}\,\frac{\partial^2}{\partial\, r^2} r - \frac{1}{r^2} L^2\right) + V(r). \tag{2.4}$$

Since the orbital angular momentum operator[1] (in units of $\hbar$) $\mathbf{L} = (1/\hbar)\mathbf{r}\times\mathbf{p}$ commutes with $\mathcal{H}_\mathrm{S}$, we can construct simultaneous eigenfunctions of $\mathcal{H}_\mathrm{S}$, L^2 and L_z. These solutions of the Schrödinger equation are known as *central-field orbitals* or *spherical waves*; they are of the form (Schiff, 1968; Merzbacher, 1970)

$$\psi_{E\ell m}(\mathbf{r}) = \frac{1}{r}\,P_{E\ell}(r)\,Y_{\ell m}(\hat{\mathbf{r}}), \tag{2.5}$$

[1] In the coordinate representation, the linear momentum operator takes the form $\mathbf{p} = -\mathrm{i}\hbar\nabla$.

where the spherical harmonics $Y_{\ell m}(\hat{\mathbf{r}})$ are eigenfunctions of L^2 and L_z [with eigenvalues $\ell(\ell+1)$ and m, respectively] and the reduced radial function $P_{E\ell}(r)$ satisfies the radial Schrödinger equation

$$-\frac{\hbar^2}{2\mathrm{m_e}}\frac{\mathrm{d}^2 P_{E\ell}}{\mathrm{d}r^2}+\left[\frac{\hbar^2}{2\mathrm{m_e}}\frac{\ell(\ell+1)}{r^2}+V(r)\right]P_{E\ell}=E\,P_{E\ell}\,. \tag{2.6}$$

Since $rV(r)$ is finite everywhere, we can require that the wave function $\psi(\mathbf{r})$ also be finite in all space. This implies that the radial function $P_{E\ell}(r)$ behaves as $r^{\ell+1}$ near the origin (see Subsection 4.1). The allowed values of the orbital angular momentum quantum number ℓ are the non-negative integers and, for each ℓ, the magnetic quantum number m may have one of the $2\ell+1$ values $-\ell, -\ell+1, \ldots, \ell$.

When $V(r)$ takes negative values in a certain region, bound states may exist, where the particle is constrained to move within a limited volume, for a discrete set of negative eigenvalues. Discrete energy levels can be identified by the angular momentum quantum number ℓ and the principal quantum number n. Alternatively, instead of n, the radial quantum number, $n_\mathrm{r} \equiv n-(\ell+1)$, can be used to label the negative energy levels. The radial quantum number has a more direct geometrical significance: it gives the number of nodes of the radial function, *i.e.*, the zeros of $P_{n\ell}(r)$ other than those at $r=0$ and $r=\infty$. If bound states with a given principal quantum number n exist, ℓ may take any value from 0 to $n-1$ and, therefore, the possible values of n_r are 0, 1, ..., $n-1$.

As Eq. (2.6) does not depend on the magnetic quantum number m, each energy level $E_{n\ell}$ is at least $2\ell+1$ times degenerate (the energy levels of a pure Coulomb potential are also degenerate with respect to ℓ). For bound states ($E<0$) the radial function is normalised by requiring that

$$\int \psi^*_{n\ell m}(\mathbf{r})\,\psi_{n\ell m}(\mathbf{r})\,\mathrm{d}\mathbf{r}=\int_0^\infty P^2_{n\ell}(r)\,\mathrm{d}r=1. \tag{2.7}$$

For free states ($E>0$, continuum spectrum), the wave function will be normalised to the asymptotic form

$$P_{E\ell}(r)\underset{r\to\infty}{\sim}\sin\left(kr-\ell\frac{\pi}{2}-\eta\ln(2kr)+d_\ell\right), \tag{2.8}$$

where

$$k\equiv\frac{p}{\hbar}=\sqrt{2\mathrm{m_e}E}/\hbar \tag{2.9}$$

is the particle wave number, η is a constant [$=0$ for finite-range potentials, see Eq. (3.5)] and d_ℓ is the phase shift. The set of spherical waves (bound and free) constitutes a complete orthogonal basis of the complex vector space of particle states.

2.2 Dirac equation

Stationary states of a relativistic electron (and of other elementary particles with spin 1/2) in the potential $V(r)$ are described by the Dirac equation (Rose, 1961; Sakurai, 1967)

$$\mathcal{H}_\mathrm{D}\,\psi(\mathbf{r})=W\,\psi(\mathbf{r}) \tag{2.10}$$

with the Hamiltonian

$$\mathcal{H}_{\rm D} = -{\rm i}\, c\hbar\, \widetilde{\boldsymbol{\alpha}} \cdot \nabla + \widetilde{\beta}\, {\rm m_e} c^2 + V(r), \tag{2.11}$$

where $\widetilde{\boldsymbol{\alpha}} = (\alpha_1, \alpha_2, \alpha_3)$ and $\widetilde{\beta}$ are 4×4 matrices. In the spinor representation

$$\widetilde{\boldsymbol{\alpha}} = \begin{pmatrix} 0 & \boldsymbol{\sigma} \\ \boldsymbol{\sigma} & 0 \end{pmatrix}, \qquad \widetilde{\beta} = \begin{pmatrix} {\rm I}_2 & 0 \\ 0 & -{\rm I}_2 \end{pmatrix}. \tag{2.12}$$

Here, $\boldsymbol{\sigma} = (\sigma_1, \sigma_2, \sigma_3)$ stands for the familiar set of Pauli spin matrices

$$\sigma_1 = \begin{pmatrix} 0 & 1 \\ 1 & 0 \end{pmatrix}, \quad \sigma_2 = \begin{pmatrix} 0 & -{\rm i} \\ {\rm i} & 0 \end{pmatrix}, \quad \sigma_3 = \begin{pmatrix} 1 & 0 \\ 0 & -1 \end{pmatrix}, \tag{2.13}$$

and ${\rm I}_2$ is the 2×2 unit matrix. In this representation, $\psi(\mathbf{r})$ is a four-component function. The eigenvalue W in Eq. (2.10) is the total energy of the electron, inclusive of the rest energy ${\rm m_e} c^2$.

The Dirac spin operator is given by (Rose, 1961; Sakurai, 1967)

$$\boldsymbol{\Sigma} = \frac{1}{2} \begin{pmatrix} \boldsymbol{\sigma} & 0 \\ 0 & \boldsymbol{\sigma} \end{pmatrix} = \begin{pmatrix} \mathbf{S}_{\rm P} & 0 \\ 0 & \mathbf{S}_{\rm P} \end{pmatrix}, \tag{2.14}$$

where $\mathbf{S}_{\rm P} = \frac{1}{2}\boldsymbol{\sigma}$ is Pauli's non-relativistic spin operator. Note that all angular momenta are expressed in units of $\hbar$. The total angular momentum operator, $\mathbf{J} \equiv \mathbf{L} + \boldsymbol{\Sigma}$, commutes with the Dirac Hamiltonian. It is convenient to introduce the operator

$$\mathcal{K} \equiv -\widetilde{\beta}\,(2\boldsymbol{\Sigma} \cdot \mathbf{L} + 1) = \begin{pmatrix} -\left(J^2 - L^2 + \frac{1}{4}\right) {\rm I}_2 & 0 \\ 0 & \left(J^2 - L^2 + \frac{1}{4}\right) {\rm I}_2 \end{pmatrix}, \tag{2.15}$$

which commutes with $\mathcal{H}_{\rm D}$, J^2 and J_z. Therefore, we can construct simultaneous eigenfunctions of $\mathcal{H}_{\rm D}$, J^2, J_z and $\mathcal{K}$, with eigenvalues W, $j(j+1)$, m and κ, respectively. These solutions of the Dirac equation are the *spherical waves* or *central-field orbitals*[2]

$$\psi_{W\kappa m}(\mathbf{r}) = \frac{1}{r} \begin{pmatrix} P_{W\kappa}(r)\, \Omega_{\kappa,m}(\hat{\mathbf{r}}) \\ {\rm i} Q_{W\kappa}(r)\, \Omega_{-\kappa,m}(\hat{\mathbf{r}}) \end{pmatrix}, \tag{2.16}$$

where $P(r)$ and $Q(r)$ are the upper- and lower-component radial functions and the spherical spinors

$$\Omega_{\kappa m}(\hat{\mathbf{r}}) \equiv \Omega^{\ell}_{jm}(\hat{\mathbf{r}}) = \sum_{\mu=\pm 1/2} \langle \ell, 1/2, m-\mu, \mu | j, m \rangle\, Y_{\ell,m-\mu}(\hat{\mathbf{r}})\, \chi_\mu \tag{2.17}$$

are simultaneous eigenfunctions of the operators L^2, $S^2_{\rm P}$, $J^2_{\rm P}$ and $J_{{\rm P}z}$ (where $\mathbf{J}_{\rm P} = \mathbf{L} + \mathbf{S}_{\rm P}$ is the non-relativistic total angular momentum) with eigenvalues $\ell(\ell+1)$, $3/4$, $j(j+1)$

[2]The Dirac wave function (2.16) conforms to the habitual phase convention (Rose, 1961); in the alternative phase convention (used in Salvat *et al.*, 1995) the radial function $Q(r)$ has the opposite sign.

and m, respectively. The quantities $\langle \ell, 1/2, m-\mu, \mu | j, m\rangle$ are Clebsch–Gordan coefficients, and the spinors χ_μ are eigenstates of $S_{\rm P}^2$ and $S_{{\rm P}z}$ with eigenvalues $3/4$ and $\mu = \pm 1/2$,

$$\chi_{+1/2} = \begin{pmatrix} 1 \\ 0 \end{pmatrix} \qquad \text{and} \qquad \chi_{-1/2} = \begin{pmatrix} 0 \\ 1 \end{pmatrix}. \tag{2.18}$$

The quantum number κ is conventionally used as short-hand notation for j and ℓ. The values of κ, j and ℓ are related by[3]

$$\kappa = (\ell - j)\,(2j+1) = -(j+\tfrac{1}{2})\,\sigma \tag{2.19a}$$

where $\sigma \equiv -\text{sign}(\kappa) = -\kappa/|\kappa|$. That is

$$\kappa = \begin{cases} -(j+\frac{1}{2}) & \text{if } \; j = \ell + \frac{1}{2}\,, \\ \quad j+\frac{1}{2} & \text{if } \; j = \ell - \frac{1}{2}\,, \end{cases} \qquad \text{or} \qquad \kappa = \begin{cases} -\ell - 1 & \text{if } \; j = \ell + \frac{1}{2}\,, \\ \ell & \text{if } \; j = \ell - \frac{1}{2}\,, \end{cases} \tag{2.19b}$$

and

$$j = |\kappa| - \tfrac{1}{2} = \ell + \tfrac{1}{2}\,\sigma\,, \tag{2.19c}$$

$$\ell = |\kappa| - \tfrac{1}{2}(1+\sigma) = j - \tfrac{1}{2}\,\sigma = \begin{cases} |\kappa| - 1 & \text{if } \; \kappa < 0, \\ |\kappa| & \text{if } \; \kappa > 0\,, \end{cases} \tag{2.19d}$$

Notice that

$$\kappa(\kappa+1) = \ell(\ell+1) \tag{2.19e}$$

An alternative convention is used in x-ray physics, where the angular momentum quantum numbers are specified by a single numerical label, i, defined by

$$i \equiv 2|\kappa| - \tfrac{1}{2}\,(1+\sigma) = \begin{cases} 2|\kappa| - 1 & \text{if } \; \kappa < 0, \\ 2|\kappa| & \text{if } \; \kappa > 0\,, \end{cases} \tag{2.19f}$$

which takes positive integer values. The inverse relation is

$$\kappa = \tfrac{1}{2}\,[i - (2i+1)\,\text{mod}(i,2)] = \begin{cases} \frac{1}{2}\,i & \text{if } i \text{ is even}, \\ -\frac{1}{2}(i+1) & \text{if } i \text{ is odd}. \end{cases} \tag{2.19g}$$

Table 1 shows the correspondence between these alternative representations of angular momentum quantum numbers.

[3] Considering the relations (2.19c) and (2.19d), and the analytical expressions of the Clebsch–Gordan coefficients (see, *e.g.*, Edmonds, 1960), the spherical spinors can be written in the compact form

$$\Omega^{\ell}_{\ell\pm1/2,m}(\hat{\mathbf{r}}) = \frac{1}{\sqrt{2\ell+1}} \begin{pmatrix} \pm\sqrt{\ell \pm m + \frac{1}{2}}\; Y_{\ell,m-1/2}(\hat{\mathbf{r}}) \\ \sqrt{\ell \mp m + \frac{1}{2}}\; Y_{\ell,m+1/2}(\hat{\mathbf{r}}) \end{pmatrix}.$$

Table 1: Correspondence between various conventions to designate angular momentum eigenstates; $(\ell,\, j)$, κ, spectroscopic notation (s.n.), and x-ray notation.

ℓ	0	1	1	2	2	3	3	4	4	5
j	$\frac{1}{2}$	$\frac{1}{2}$	$\frac{3}{2}$	$\frac{3}{2}$	$\frac{5}{2}$	$\frac{5}{2}$	$\frac{7}{2}$	$\frac{7}{2}$	$\frac{9}{2}$	$\frac{9}{2}$
κ	-1	$+1$	-2	$+2$	-3	$+3$	-4	$+4$	-5	$+5$
s.n.	$s_{1/2}$	$p_{1/2}$	$p_{3/2}$	$d_{3/2}$	$d_{5/2}$	$f_{5/2}$	$f_{7/2}$	$g_{7/2}$	$g_{9/2}$	$h_{9/2}$
	s	$\bar{p}$	p	$\bar{d}$	d	$\bar{f}$	f	$\bar{g}$	g	$\bar{h}$
x ray, i	1	2	3	4	5	6	7	8	9	10

It should be noted that the relativistic wave function (2.16) is not an eigenfunction of L^2; the index ℓ used in the spectroscopic notation is the eigenvalue of the upper-component spinor and serves to indicate the parity of $\psi_{W\kappa m}(\mathbf{r})$. The radial functions $P_{W\kappa}(r)$ and $Q_{W\kappa}(r)$ satisfy the coupled equations (Rose, 1961)

$$\begin{aligned}\frac{\mathrm{d}P_{W\kappa}}{\mathrm{d}r} &= -\frac{\kappa}{r}\,P_{W\kappa} + \frac{W + \mathrm{m_e}c^2 - V}{c\hbar}\,Q_{W\kappa},\\ \frac{\mathrm{d}Q_{W\kappa}}{\mathrm{d}r} &= \frac{-W + \mathrm{m_e}c^2 + V}{c\hbar}\,P_{W\kappa} + \frac{\kappa}{r}\,Q_{W\kappa},\end{aligned} \tag{2.20}$$

which will be referred to as the radial Dirac equations.

A peculiarity of relativistic wave equations is that they have positive and negative energy eigenvalues, which correspond to particle and antiparticle states, respectively. Thus, the Dirac equation for free particles (*i.e.*, with $V \equiv 0$) has eigenstates with energies $W \geq \mathrm{m_e}c^2$ and $W \leq -\mathrm{m_e}c^2$. Wave functions with positive energies $W = E + \mathrm{m_e}c^2$ represent states of ordinary electrons (negatrons) with kinetic energy E. According to Dirac's hole theory (see, *e.g.*, Sakurai, 1967), states with negative energies $W \leq -\mathrm{m_e}c^2$ are unobservable and filled with electrons (Dirac sea); radiative transitions of electrons in positive-energy states to these negative-energy states are forbidden by the Pauli exclusion principle. However, an electron in a state of negative energy $W = -E - \mathrm{m_e}c^2$ can be excited to positive-energy states (*e.g.*, by absorption of a high-energy photon) leaving a hole in the Dirac sea. This hole is observable as a particle of mass $\mathrm{m_e}$, charge $+e$, and energy $-W = E + \mathrm{m_e}c^2$; this particle is the positron.

In the case of a central potential $V(r)$, the radial functions of orbitals with "positive" energies $W = E + \mathrm{m_e}c^2$ are given by the radial equations (2.20). It is convenient to express these equations in terms of the reduced eigenvalue $E \equiv W - \mathrm{m_e}c^2$ $(W > 0)$

$$\begin{aligned}\frac{\mathrm{d}P_{E\kappa}}{\mathrm{d}r} &= -\frac{\kappa}{r}\,P_{E\kappa} + \frac{E + 2\mathrm{m_e}c^2 - V}{c\hbar}\,Q_{E\kappa},\\ \frac{\mathrm{d}Q_{E\kappa}}{\mathrm{d}r} &= \frac{-E + V}{c\hbar}\,P_{E\kappa} + \frac{\kappa}{r}\,Q_{E\kappa},\end{aligned} \tag{2.21}$$

where $P_{E\kappa} = P_{W\kappa}$ and $Q_{E\kappa} = Q_{W\kappa}$. In the non-relativistic limit $(c \to \infty)$, the reduced eigenvalues E tend to the eigenvalues of the radial Schrödinger equation (2.6)

(see below). As in the non-relativistic theory, when $V(r)$ takes negative values in a certain region, bound states may exist for a discrete set of negative reduced eigenvalues ($E < 0$). Note that, for attractive potentials that are strong enough, we may have bound states of ordinary electrons with $E < -\mathrm{m_e}c^2$ and $W = E + \mathrm{m_e}c^2 < 0$, that is, deeply bound "positive" levels may have negative total energies[4].

Let us now consider states with "negative" total energy, $W = -E - \mathrm{m_e}c^2$, of a central potential $V(r)$. Their radial functions can be calculated by solving the same radial Dirac equations (2.21) as for "positive"-energy states, but for the potential $-V(r)$. This is readily seen by introducing the quantities

$$\overline{W} \equiv -W = E + \mathrm{m_e}c^2, \qquad \bar{\kappa} \equiv -\kappa, \qquad \begin{aligned} \overline{P}_{W\bar{\kappa}} &\equiv Q_{W\kappa}, \\ \overline{Q}_{W\bar{\kappa}} &\equiv P_{W\kappa}, \end{aligned} \tag{2.22}$$

and expressing the radial Dirac equations (2.20) as

$$\begin{aligned} \frac{\mathrm{d}\overline{Q}_{W\bar{\kappa}}}{\mathrm{d}r} &= +\frac{\bar{\kappa}}{r}\,\overline{Q}_{W\bar{\kappa}} + \frac{-\overline{W} + \mathrm{m_e}c^2 - V}{c\hbar}\,\overline{Q}_{W\bar{\kappa}}, \\ \frac{\mathrm{d}\overline{P}_{W\bar{\kappa}}}{\mathrm{d}r} &= \frac{\overline{W} + \mathrm{m_e}c^2 + V}{c\hbar}\,\overline{Q}_{W\bar{\kappa}} - \frac{\bar{\kappa}}{r}\,\overline{P}_{W\bar{\kappa}}. \end{aligned}$$

Indeed, these equations differ from Eqs. (2.20) only in the sign of the potential. Hence, the "negative"-energy orbitals (with $W = -E - \mathrm{m_e}c^2$) are of the form

$$\psi_{W\kappa m}(\mathbf{r}) = \frac{1}{r}\begin{pmatrix} \overline{Q}_{E\bar{\kappa}}(r)\,\Omega_{\kappa,m}(\hat{\mathbf{r}}) \\ \mathrm{i}\overline{P}_{E\bar{\kappa}}(r)\,\Omega_{-\kappa,m}(\hat{\mathbf{r}}) \end{pmatrix}, \tag{2.23}$$

where the radial functions $\overline{P}_{E\bar{\kappa}}(r)$ and $\overline{Q}_{E\bar{\kappa}}(r)$ satisfy the radial equations [cf. Eqs. (2.21)]

$$\begin{aligned} \frac{\mathrm{d}\overline{P}_{E\bar{\kappa}}}{\mathrm{d}r} &= -\frac{\bar{\kappa}}{r}\,\overline{P}_{E\bar{\kappa}} + \frac{E + 2\mathrm{m_e}c^2 + V}{c\hbar}\,\overline{Q}_{E\bar{\kappa}}\,, \\ \frac{\mathrm{d}\overline{Q}_{E\bar{\kappa}}}{\mathrm{d}r} &= \frac{-E - V}{c\hbar}\,\overline{Q}_{E\bar{\kappa}} + \frac{\bar{\kappa}}{r}\,\overline{Q}_{E\bar{\kappa}}\,. \end{aligned} \tag{2.24}$$

The wave function (2.23) represents the "negative"-energy state that, when emptied, is observable as a positron with reduced energy E, angular momentum $j = |\kappa| - 1/2$ and magnetic quantum number $-m$. Bound "negative"-energy states may exist whenever the potential $-V(r)$ is negative in a sufficiently wide region; for these states the reduced eigenvalue E is negative.

In the following, we will limit ourselves to consider "positive"-energy states of an ordinary electron in a central potential $V(r)$, with total energy $W = E + \mathrm{m_e}c^2$. "Negative"-energy states, when needed, will be obtained as "positive"-energy solutions of the radial Dirac equations for the potential $-V(r)$.

[4]The feature that characterizes the "positive"-energy states is the following. Consider the family of potentials $aV(r)$, where a is a positive constant. The states of a particle in these potentials vary continuously with a, and reduce to the states of a free particle when $a \to 0$. The "positive"-energy states of the potential $V(r)$ ($a = 1$) are those which, in the limit $a \to 0$ become positive-energy states. Similar considerations apply to "negative"-energy states.

Discrete (bound) energy levels ($E < 0$), when they exist, are identified by the quantum number κ and either the principal quantum number n or the radial quantum number n_r. As in the non-relativistic theory, $n_\mathrm{r} = n - (\ell + 1)$ gives the number of nodes of $P(r)$. Notice that, for a given n, ℓ can take the values 0, 1, ..., $n - 1$; the possible values of κ are $-n$, ..., -1, 1, ..., $n - 1$. Each bound level is, at least, $2j + 1$ times degenerate (the eigenstates of a pure Coulomb potential with the same ℓ and $j = \ell \pm 1/2$ have the same energy). Adequate normalisation for bound states is

$$\int \psi^\dagger_{n\kappa m}(\mathbf{r})\, \psi_{n\kappa m}(\mathbf{r})\, \mathrm{d}\mathbf{r} = \int_0^\infty \left[P^2_{n\kappa}(r) + Q^2_{n\kappa}(r)\right] \mathrm{d}r = 1. \tag{2.25}$$

Dirac free states ($E > 0$) will be normalised in such a way that the radial function $P(r)$ asymptotically oscillates with unit amplitude [cf. Eq. (2.8)],

$$P_{E\kappa}(r) \underset{r\to\infty}{\sim} \sin\left(kr - \ell\frac{\pi}{2} - \eta \ln(2kr) + d_\kappa\right), \tag{2.26}$$

where

$$k \equiv \frac{p}{\hbar} = \frac{\sqrt{E(E + 2\mathrm{m_e}c^2)}}{c\hbar} \tag{2.27}$$

is the relativistic wave number, η is a constant [=0 for finite-range potentials, see Eq. (3.107)] and d_κ is the phase shift. The set of spherical waves (with positive *and* negative energies) constitute a complete orthogonal basis of the vector space of states of an electron.

It is worth noting that in the limit $E - V \ll 2\mathrm{m_e}c^2$, the radial Eqs. (2.21) for "positive"-energy states reduce to

$$Q = \frac{c\hbar}{2\mathrm{m_e}c^2}\left(\frac{\kappa}{r}P + \frac{\mathrm{d}P}{\mathrm{d}r}\right) \tag{2.28}$$

and

$$\frac{\mathrm{d}^2P}{\mathrm{d}r^2} = \left[\frac{\kappa(\kappa+1)}{r^2} - \frac{2\mathrm{m_e}}{\hbar^2}(E - V)\right] P. \tag{2.29}$$

Equation (2.28) shows that the lower ("small") component $Q(r)$ vanishes in the non-relativistic limit ($c \to \infty$). Using the fact that $\kappa(\kappa + 1) = \ell(\ell + 1)$, Eq. (2.29) is seen to coincide with the radial Schrödinger equation (2.6), and therefore, in the non-relativistic limit the upper ("large") component $P(r)$ reduces to the Schrödinger radial function. The non-relativistic limit of the radial equations (2.24) for "negative"-energy states is given by Eqs. (2.28) and (2.29) with the potential $-V(r)$ and with $\bar\kappa$ replacing κ. Because $\bar\kappa(\bar\kappa + 1) = \ell(\ell + 1)$, in the limit $c \to \infty$ the lower (large) component $\overline{P}(r)$ tends to the Schrödinger radial function for the potential $-V(r)$ and the upper-component $\overline{Q}(r)$ vanishes.

2.3 Schrödinger–Pauli equation

The non-relativistic limit ($E \ll \mathrm{m_e}c^2$) of the Dirac equation for positive-energy states is the Schrödinger–Pauli wave equation (see, *e.g.*, Bethe and Salpeter, 1957),

$$\mathcal{H}_\mathrm{SP}\, \psi(\mathbf{r}) = E\, \psi(\mathbf{r}) \tag{2.30}$$

with the Hamiltonian

$$\mathcal{H}_{\rm SP} = \left[-\frac{\hbar^2}{2{\rm m}_{\rm e}} \nabla^2 + V(r) \right] I_2, \tag{2.31}$$

which was introduced by Pauli to describe the interaction of the electron spin with magnetic fields. The wave function $\psi(\mathbf{r})$ is a spinor, which corresponds to the non-relativistic limit of the upper spinor of the Dirac wave function.

Since the Hamiltonian (2.31) is independent of the spin, its eigenvalues are the same as those of the Schrödinger Hamiltonian (2.4). In atomic physics, the equation may be complemented by adding to the Hamiltonian (2.31) the spin-orbit potential,

$$V_{\rm so}(r) = \frac{\hbar^2}{2{\rm m}_{\rm e}^2 c^2} \frac{1}{r} \frac{{\rm d}V}{{\rm d}r} \mathbf{L}\cdot\mathbf{S}_{\rm P}, \tag{2.32}$$

which represents the interaction of the spin with the magnetic field that is observed in the electron's reference frame. The potential (2.32) is obtained as part of the fine-structure Hamiltonian, the non-relativistic limit to order $E/({\rm m}_{\rm e}c^2)$ of the Dirac Hamiltonian for positive-energy states (see, *e.g.*, Bransden and Joachain, 1983, Appendix 7). Wave equations with spin-dependent potentials proportional to $\mathbf{L}\cdot\mathbf{S}_{\rm P}$ are also found in nuclear physics (Hodgson, 1971).

The space of one-electron states admits a basis of central-field orbitals of the type[5]

$$\psi_{E\kappa m}(\mathbf{r}) = \frac{1}{r} P_{E\kappa}(r)\, \Omega_{\kappa m}(\hat{\mathbf{r}}), \tag{2.33}$$

that are simultaneous eigenfunctions of the mutually commuting operators $\mathcal{H}_{\rm SP}$, L^2, $S_{\rm P}^2$, J^2, and J_z, with corresponding eigenvalues E, $\ell(\ell+1)$, $3/4$, $j(j+1)$, and m. The reduced radial functions $P_{E\kappa}(r)$ satisfy the radial Schrödinger equation (2.6). When the Hamiltonian includes a spin-orbit term, the radial equation takes the form

$$-\frac{\hbar^2}{2{\rm m}_{\rm e}} \frac{{\rm d}^2 P_{E\kappa}}{{\rm d}r^2} + \left[\frac{\hbar^2}{2{\rm m}_{\rm e}} \frac{\ell(\ell+1)}{r^2} + V_\kappa(r) \right] P_{E\kappa} = E P_{E\kappa}\,, \tag{2.34}$$

with a potential

$$V_\kappa(r) = V(r) + \frac{\hbar^2}{2{\rm m}_{\rm e}^2 c^2} \frac{1}{r} \frac{{\rm d}V}{{\rm d}r} \frac{1}{2} \left[j(j+1) - \ell(\ell+1) - \frac{3}{4} \right] \tag{2.35}$$

that depends on the quantum number κ or, equivalently, on ℓ and j. Notice that the power-series method implemented in the RADIAL subroutines (see Section 4) can be used to solve the radial equation (2.34) only when the function $r\,V_\kappa(r)$ is finite at $r = 0$. This requirement is met by the electrostatic plus spin-orbit interaction of an electron with a finite nucleus (represented, *e.g.*, as a uniformly charged sphere), but not by the spin-orbit interaction of an electron moving in the field of a point nucleus.

[5] Alternatively, for central potentials $V(r)$, we could consider orbitals of the type (uncoupled representation)

$$\psi_{E\ell m\mu} = \frac{1}{r} P_{E\ell}(r)\, Y_{\ell m}(\hat{\mathbf{r}})\, \chi_\mu.$$

However, these orbitals are not eigenfunctions of Hamiltonians with spin-orbit terms.

Discrete (bound) energy levels are identified by the quantum number κ and either the principal quantum number n or the radial quantum number $n_{\rm r}$; each bound level is $2j+1$ times degenerate. Bound states are normalised to unity

$$\int \psi^{\dagger}_{n\kappa m}(\mathbf{r})\,\psi_{n\kappa m}(\mathbf{r})\,\mathrm{d}\mathbf{r} = \int_0^{\infty} P^2_{n\kappa}(r)\,\mathrm{d}r = 1. \tag{2.36}$$

and the normalisation of free states ($E > 0$) is such that

$$P_{E\kappa}(r) \underset{r\to\infty}{\sim} \sin\left(kr - \ell\frac{\pi}{2} - \eta\ln(2kr) + d_{E\kappa}\right), \tag{2.37}$$

where k is the wave number, $k = (2\mathrm{m_e}E)^{1/2}/\hbar$, and η is a constant.

2.4 Normalisation of free-state radial wave functions

As free-state wave functions are not square integrable, they cannot be assigned a finite norm. Instead it is natural to require that their scalar product be proportional to a delta function. In certain applications, it is convenient to use Dirac free-state wave functions normalised on the energy scale, *i.e.*,

$$\int_0^{\infty} [P_{E\kappa}(r)P_{E'\kappa}(r) + Q_{E\kappa}(r)Q_{E'\kappa}(r)]\,\mathrm{d}r = \delta(E-E'). \tag{2.38}$$

For Schrödinger free states, the energy normalisation condition reads

$$\int_0^{\infty} P_{E\ell}(r)P_{E'\ell}(r)\,\mathrm{d}r = \delta(E-E'), \tag{2.39}$$

which can be considered as the non-relativistic limit ($c\to\infty$) of Eq. (2.38). Radial functions normalised on the energy scale have the asymptotic form [cf. Eqs. (2.8) and (2.26)]

$$P_{E\kappa}(r) \underset{r\to\infty}{\sim} A_E\,\sin\left(k_E r - \ell\frac{\pi}{2} - \eta_E\ln(2k_E r) + d_E\right), \tag{2.40}$$

where A_E, η_E and d_E are constants and k_E is the wave number given by Eqs. (2.9) or (2.27). The asymptotic behaviour of the lower-component Dirac function is determined by the first of Eqs. (2.21). Neglecting terms of order $(1/r)$, we get

$$Q_{E\kappa}(r) \underset{r\to\infty}{\sim} A_E\sqrt{\frac{E}{E+2\mathrm{m_e}c^2}}\cos\left(k_E r - \ell\frac{\pi}{2} - \eta_E\ln(2k_E r) + d_E\right). \tag{2.41}$$

To determine the normalisation constant A_E, we consider the radial Eqs. (2.21)

$$P'_{E\kappa} + \frac{\kappa}{r}\,P_{E\kappa} = \frac{E-V+2\mathrm{m_e}c^2}{c\hbar}\,Q_{E\kappa}, \tag{2.42}$$

$$Q'_{E\kappa} - \frac{\kappa}{r}\,Q_{E\kappa} = -\frac{E-V}{c\hbar}\,P_{E\kappa}, \tag{2.43}$$

where the primes denote differentiation with respect to r. Multiplying Eqs. (2.42) and (2.43) from the left by $Q_{E'\kappa}$ and $P_{E'\kappa}$, respectively,

$$\begin{aligned} Q_{E'\kappa}P'_{E\kappa} + \frac{\kappa}{r}\,Q_{E'\kappa}P_{E\kappa} &= \frac{E-V+2\mathrm{m_e}c^2}{c\hbar}\,Q_{E'\kappa}Q_{E\kappa}, \\ P_{E'\kappa}Q'_{E\kappa} - \frac{\kappa}{r}\,P_{E'\kappa}Q_{E\kappa} &= -\,\frac{E-V}{c\hbar}\,P_{E'\kappa}P_{E\kappa}, \end{aligned}$$

and subtracting from each of these two equations the analogous ones obtained by interchanging E and E' everywhere, we get

$$\begin{aligned} Q_{E'\kappa}P'_{E\kappa} - Q_{E\kappa}P'_{E'\kappa} + \frac{\kappa}{r}\,(Q_{E'\kappa}P_{E\kappa} - Q_{E\kappa}P_{E'\kappa}) &= \frac{E-E'}{c\hbar}\,Q_{E'\kappa}Q_{E\kappa}, \\ P_{E'\kappa}Q'_{E\kappa} - P_{E\kappa}Q'_{E'\kappa} - \frac{\kappa}{r}\,(P_{E'\kappa}Q_{E\kappa} - P_{E\kappa}Q_{E'\kappa}) &= \frac{E'-E}{c\hbar}\,P_{E'\kappa}P_{E\kappa}. \end{aligned}$$

Subtracting the second from the first of these equations we have

$$P_{E\kappa}P_{E'\kappa} + Q_{E\kappa}Q_{E'\kappa} = \frac{c\hbar}{E-E'}\,\frac{\mathrm{d}}{\mathrm{d}r}\left(Q_{E\kappa}P_{E'\kappa} - P_{E\kappa}Q_{E'\kappa}\right).$$

Then, for any value of R,

$$\int_0^R (P_{E\kappa}\,P_{E'\kappa} + Q_{E\kappa}\,Q_{E'\kappa})\,\mathrm{d}r = \frac{c\hbar}{E-E'}\left[Q_{E\kappa}(R)\,P_{E'\kappa}(R) - P_{E\kappa}(R)\,Q_{E'\kappa}(R)\right] \quad (2.44)$$

since $P_{E\kappa}(0) = Q_{E\kappa}(0) = 0$. Notice that Eq. (2.44) applies to free *and* bound states. When $R \to \infty$, it shows that a bound state is orthogonal to all states with different energies.

In practical calculations with free states ($E, E' > 0$), the limit $R \to \infty$ of the integral (2.44) takes the form of a distribution, and it occurs only as a factor in the integrand of integrals over the energy E. For free states and large enough R-values, the main contribution to the integral (2.44) comes from large radial distances, where the asymptotic forms (2.40) and (2.41) are valid. Introducing these expressions into Eq. (2.44) we obtain

$$\begin{aligned} &\int_0^R (P_{E\kappa}P_{E'\kappa} + Q_{E\kappa}Q_{E'\kappa})\,\mathrm{d}r = \\ &= \frac{c\hbar}{E-E'}\,A_E A_{E'}\left\{\sqrt{\frac{E}{E+2\mathrm{m_e}c^2}}\cos\phi_E\sin\phi_{E'} - \sin\phi_E\sqrt{\frac{E'}{E'+2\mathrm{m_e}c^2}}\cos\phi_{E'}\right\} \\ &= \frac{c\hbar}{E-E'}\,A_E A_{E'}\left\{\sqrt{\frac{E}{E+2\mathrm{m_e}c^2}}\sin\Big[\,(k_E-k_{E'})\,R\Big] + X_{E,E'}(R)\right\}, \end{aligned} \quad (2.45)$$

where

$$\phi_E \equiv k_E R - \ell\frac{\pi}{2} - \eta_E\ln(2k_E R) + d_E \quad (2.46)$$

is the argument of the trigonometric functions in expressions (2.40) and (2.41). The quantity

$$X_{E,E'}(R) \equiv \sqrt{\frac{E}{E+2\mathrm{m_e}c^2}}\left(\cos\phi_E\,\sin\phi_{E'} - \sin\Big[\,(k_E-k_{E'})\,R\Big]\right) - \sqrt{\frac{E'}{E'+2\mathrm{m_e}c^2}}\,\sin\phi_E\,\cos\phi_{E'} \tag{2.47}$$

is seen to vanish when $E = E'$. If $E \neq E'$, $X_{E,E'}(R)$ oscillates infinitely rapidly as $R \to \infty$ and contributes nothing to integrals over E. Hence

$$\begin{aligned}
&\int_0^\infty (P_{E\kappa}P_{E'\kappa} + Q_{E\kappa}Q_{E'\kappa})\,\mathrm{d}r = \\
&= A_E A_{E'}\,c\hbar\sqrt{\frac{E}{E+2\mathrm{m_e}c^2}}\,\frac{k_E-k_{E'}}{E-E'}\,\lim_{R\to\infty}\left\{\frac{1}{k_E-k_{E'}}\sin\Big[\,(k_E-k_{E'})\,R\Big]\right\} \\
&= A_E A_{E'}\,\frac{E}{k_E}\,\frac{k_E-k_{E'}}{E-E'}\,\pi\,\delta(k_E-k_{E'}) = A_E A_{E'}\,\frac{E}{k_E}\,\pi\,\frac{k_{E'}-k_E}{E'-E}\,\frac{\mathrm{d}E}{\mathrm{d}k_E}\,\delta(E-E') \\
&= A_E^2\,\frac{\pi E}{k_E}\,\delta(E-E').
\end{aligned} \tag{2.48}$$

Comparing this result with Eq. (2.38), we see that

$$A_E = \sqrt{\frac{k_E}{\pi E}} \qquad \text{(Dirac)}. \tag{2.49}$$

Therefore, the radial function $P_{E\kappa}(r)$ of Dirac free states normalised on the energy scale oscillates asymptotically with amplitude A_E. The normalising factor for Schrödinger waves can be obtained as the non-relativistic limit of expression (2.49),

$$A_E = \sqrt{\frac{k_E}{\pi E}} = \sqrt{\frac{2\mathrm{m_e}}{\hbar^2}\,\frac{1}{\pi k_E}} \qquad \text{(Schrödinger)}. \tag{2.50}$$

The subroutine package RADIAL gives free-state radial functions normalised to unit amplitude and, therefore, they must be multiplied by the constant factor A_E to get wave functions normalised on the energy scale.

Another normalisation for free states, frequently used in scattering theory, is the so-called "wave-number" normalisation,

$$\int_0^\infty [P_{E\kappa}(r)P_{E'\kappa}(r) + Q_{E\kappa}(r)Q_{E'\kappa}(r)]\,\mathrm{d}r = \delta(k_E-k_{E'}). \tag{2.51}$$

From the relation

$$\delta(E-E') = \frac{\mathrm{d}k_E}{\mathrm{d}E}\,\delta(k_E-k_{E'})$$

it follows that the wave-number normalisation constant is

$$A_E^{(\mathrm{wn})} = A_E\sqrt{\frac{\mathrm{d}E}{\mathrm{d}k_E}} = \sqrt{\frac{E+2\mathrm{m_e}c^2}{\pi\,(E+\mathrm{m_e}c^2)}} \qquad \text{(Dirac)}, \tag{2.52}$$

where use has been made of Eq. (2.27). In the non-relativistic limit, we obtain the well-known result

$$A_E^{(\mathrm{wn})} = \sqrt{\frac{2}{\pi}} \qquad \text{(Schrödinger)}. \tag{2.53}$$

3 Coulomb functions

Let us consider the motion of an electron or positron (charge $Z_1 e$, with $Z_1 = -1$ or $Z_1 = +1$, respectively) in the Coulomb field produced by a point charge $Z_2 e$ fixed at the origin of coordinates. The interaction potential energy is

$$V(r) = \frac{Z_\infty e^2}{r}. \tag{3.1a}$$

where $Z_\infty = Z_1 Z_2$. The solutions of the radial Schrödinger and Dirac wave equations for this potential are known as *Coulomb functions* and they can be expressed in closed analytical form in terms of Whittaker's functions. Solutions for attractive Coulomb potentials, with $Z_\infty < 0$, describe, *e.g.*, the motion of an electron in the presence of a (point) nucleus with charge number $Z_2 = -Z_\infty$. In this case, negative-energy Coulomb functions represent bound states of the hydrogen atom ($Z_2 = 1$) and hydrogenic ions ($Z_2 > 1$). Repulsive potentials, with $Z_\infty > 0$, describe, *e.g.*, the scattering of positrons by point nuclei. Positive-energy Coulomb functions are important in scattering theory. In particular, they are useful to determine the phase shifts and the normalisation of free states of particles in modified Coulomb potentials (see Section 6). The Coulomb tail of a modified Coulomb potential has the form (3.1a) with

$$Z_\infty = e^{-2} \lim_{r\to\infty} rV(r) = e^{-2} \lim_{r\to\infty} \mathcal{V}(r), \tag{3.1b}$$

and beyond the onset r_c of the Coulomb tail the radial wave functions are linear combinations of the regular and irregular Coulomb functions. In the present Section we derive analytical expressions for the Coulomb functions and we present efficient numerical algorithms to compute them.

3.1 Schrödinger–Coulomb functions

The radial Schrödinger equation for an electron or positron in the Coulomb potential (3.1) reads

$$-\frac{\hbar}{2\mathrm{m_e}} \frac{\mathrm{d}^2}{\mathrm{d}r^2} P(r) + \left[\frac{\hbar^2}{2\mathrm{m_e}} \frac{\ell(\ell+1)}{r^2} + \frac{Z_\infty e^2}{r} \right] P(r) = E\, P(r). \tag{3.2}$$

It can be recast in a dimensionless form by introducing the independent variable $x = kr$ with

$$k = \sqrt{\frac{2\mathrm{m_e}}{\hbar^2} E}. \tag{3.3}$$

We have

$$\left(\frac{\mathrm{d}^2}{\mathrm{d}x^2} + 1 - \frac{2\eta}{x} - \frac{\ell(\ell+1)}{x^2}\right) U_\ell(\eta, x) = 0, \tag{3.4}$$

where the dimensionless quantity

$$\eta \equiv \frac{Z_\infty e^2\, k}{2E} \tag{3.5}$$

is the *Sommerfeld parameter*. For free states ($E > 0$), k is the wave number and

$$\eta = \frac{Z_\infty e^2\, \mathrm{m_e}}{\hbar^2 k} = \frac{Z_\infty e^2}{\hbar v}, \tag{3.6}$$

where $v = \hbar k/\mathrm{m_e}$ is the velocity of the electron. For bound states ($E < 0$), k and η are purely imaginary numbers.

Alternatively, we can introduce the variable $z = -2\mathrm{i}x = -2\mathrm{i}kr$, and reduce the wave equation to Whittaker's standard form of the confluent hypergeometric equation (Erdélyi, 1953),

$$\frac{\mathrm{d}^2 P(z)}{\mathrm{d}z^2} + \left[-\frac{1}{4} - \frac{\mathrm{i}\eta}{z} + \frac{\frac{1}{4} - (\ell + \frac{1}{2})^2}{z^2}\right] P(z) = 0. \tag{3.7}$$

3.1.1 Confluent hypergeometric and Whittaker functions

The solutions of the Whittaker equation

$$\frac{\mathrm{d}^2 f}{\mathrm{d}z^2} + \left[-\frac{1}{4} + \frac{\chi}{z} + \frac{1/4 - \mu^2}{z^2}\right] f = 0 \tag{3.8}$$

are conveniently expressed in terms of the Kummer function (Abramowitz and Stegun, 1974; Olver *et al.*, 2010),

$$\begin{aligned} {}_1F_1(a;b;z) \;&=\; 1 + \frac{a}{b}\,z + \frac{a(a+1)}{b(b+1)}\,\frac{z^2}{2!} + \frac{a(a+1)(a+2)}{b(b+1)(b+2)}\,\frac{z^3}{3!} + \ldots \\ &= \sum_{n=0}^{\infty} \frac{(a)_n}{(b)_n}\,\frac{z^n}{n!}. \end{aligned} \tag{3.9}$$

The quantities $(a)_n$ are known as Pochhammer symbols,

$$(a)_0 = 1, \quad (a)_n = a(a+1)\ldots(a+n-1) = \Gamma(a+n)/\Gamma(a), \tag{3.10}$$

where $\Gamma(a)$ is Euler's complex gamma function (see, *e.g.*, Abramowitz and Stegun, 1974). The last expression for $(a)_n$ follows from the property $\Gamma(1+a) = a\Gamma(a)$. For large $|z|$, with a and b fixed, the Kummer function admits the following asymptotic expansion (Erdélyi, 1953),

$$\begin{aligned} {}_1F_1(a;b;z) \;=\; &\frac{\Gamma(b)}{\Gamma(b-a)} \left(\frac{\exp(\mathrm{i}\pi\epsilon)}{z}\right)^a \left[\sum_{n=0}^{R-1} \frac{(a)_n\,(1+a-b)_n}{n!\,(-z)^n} + O(|z|^{-R})\right] \\ &+ \frac{\Gamma(b)}{\Gamma(a)}\,\exp(z)\,z^{a-b} \left[\sum_{n=0}^{S-1} \frac{(b-a)_n\,(1-a)_n}{n!\,z^n} + O(|z|^{-S})\right], \end{aligned} \tag{3.11}$$

where $\epsilon = +1$ if $\mathrm{Im}(z) > 0$ and $\epsilon = -1$ if $\mathrm{Im}(z) < 0$.

The Whittaker equation (3.8) has an irregular singularity at $x = 0$ and a regular singularity at ∞ (see Olver *et al.*, 2010). The solution regular at the origin is

$$\mathcal{M}_{\chi,\mu}(z) = z^{\mu+1/2}\,\mathrm{e}^{-z/2}\,{}_1F_1(\tfrac{1}{2}+\mu-\chi;1+2\mu;z), \tag{3.12}$$

and a solution regular at ∞ is

$$\mathcal{W}_{\chi,\mu}(z) = \frac{\Gamma(-2\mu)}{\Gamma(\frac{1}{2}-\mu-\chi)}\,\mathcal{M}_{\chi,\mu}(z) + \frac{\Gamma(2\mu)}{\Gamma(\frac{1}{2}+\mu-\chi)}\,\mathcal{M}_{\chi,-\mu}(z)\,. \tag{3.13}$$

The Wronskian of these solutions is

$$W\{\mathcal{W}_{\chi,\mu}(z),\mathcal{M}_{\chi,\mu}(z)\} \equiv \mathcal{W}_{\chi,\mu}(z)\,\mathcal{M}'_{\chi,\mu}(z) - \mathcal{W}'_{\chi,\mu}(z)\,\mathcal{M}_{\chi,\mu}(z) = \frac{\Gamma(1+2\mu)}{\Gamma(\frac{1}{2}+\mu-\chi)}\,. \tag{3.14}$$

The Whittaker functions, Eqs. (3.12) and (3.13), admit the following asymptotic expansions for large z,

$$\begin{aligned}
\mathcal{M}_{\chi,\mu}(z) \;=\; & (-1)^{1/2+\mu-\chi}\,z^{\chi}\,\mathrm{e}^{-z/2}\frac{\Gamma(1+2\mu)}{\Gamma(\frac{1}{2}+\mu+\chi)} \\
& \times\left[\sum_{n=0}^{R-1}\frac{(\frac{1}{2}+\mu-\chi)_n\,(\frac{1}{2}-\mu-\chi)_n}{n!\,(-z)^n} + O(|z|^{-R})\right] \\
+\; & z^{-\chi}\,\mathrm{e}^{z/2}\,\frac{\Gamma(1+2\mu)}{\Gamma(\frac{1}{2}+\mu-\chi)} \\
& \times\left[\sum_{n=0}^{S-1}\frac{(\frac{1}{2}+\mu+\chi)_n\,(\frac{1}{2}-\mu+\chi))_n}{n!\,z^n} + O(|z|^{-S})\right]
\end{aligned} \tag{3.15}$$

and

$$\mathcal{W}_{\chi,\mu}(z) \;=\; z^{\chi}\,\mathrm{e}^{-z/2}\left[\sum_{n=0}^{R-1}\frac{(\frac{1}{2}+\mu-\chi)_n\,(\frac{1}{2}-\mu-\chi)_n}{n!\,(-z)^n} + O(|z|^{-R})\right]. \tag{3.16}$$

3.1.2 Coulomb functions of free states

Let us now consider the solutions of the radial equation (3.4) for free states ($E > 0$, $x = kr$),

$$\left[\frac{\mathrm{d}^2}{\mathrm{d}x^2} + 1 - \frac{2\eta}{x} - \frac{\lambda(\lambda+1)}{x^2}\right] U_\lambda(\eta,x) = 0. \tag{3.17}$$

In the non-relativistic Schrödinger theory, the orbital angular momentum quantum number ℓ takes only non-negative integer values. For the sake of generality, however, here we assume that λ can take arbitrary real values larger than -1. In Section 3.2.1, we will see that the radial functions for free states of a relativistic (Dirac) electron in a

Coulomb potential can be expressed in terms of the functions $U_\lambda(\eta, x)$ with non-integer values of the parameter λ.

The regular solution of Eq. (3.17) is defined by

$$\begin{aligned} F_\lambda(\eta, x) &= C_\lambda(\eta) \left(\frac{\mathrm{i}}{2}\right)^{\lambda+1} \mathcal{M}_{-\mathrm{i}\eta,\lambda+1/2}(-2\mathrm{i}x) \\ &= C_\lambda(\eta)\, x^{\lambda+1}\, \exp(\mathrm{i}x)\, {}_1F_1(\lambda+1+\mathrm{i}\eta; 2\lambda+2; -2\mathrm{i}x)\,, \end{aligned} \tag{3.18}$$

where the constant $C_\lambda(\eta)$ fixes the normalisation of the state. The asymptotic behaviour of this function at large x is given by Eq. (3.15). Using the property $\Gamma(a^*) = [\Gamma(a)]^*$, we have

$$\begin{aligned} F_\lambda(\eta, x) &\underset{x\to\infty}{\sim} C_\lambda(\eta)\, \frac{\mathrm{i}}{2} \left[\left(\frac{\mathrm{i}}{2}\right)^{\lambda} (-2\mathrm{i}x)^{\mathrm{i}\eta}\, \mathrm{e}^{-\mathrm{i}x} \frac{\Gamma(2\lambda+2)}{\Gamma(\lambda+1+\mathrm{i}\eta)} - \text{c.c.} \right] \\ &= C_\lambda(\eta)\, \frac{\exp(\eta\pi/2)\Gamma(2\lambda+2)}{2^\lambda |\Gamma(\lambda+1+\mathrm{i}\eta)|}\, \frac{\mathrm{i}}{2} \left\{ \exp\left[\mathrm{i}\frac{\pi}{2}\lambda + \mathrm{i}\eta \ln(2x) - \mathrm{i}x - \mathrm{i}\,\mathrm{arg}\Gamma(\lambda+1+\mathrm{i}\eta) \right] - \text{c.c.} \right\}, \end{aligned}$$

where the notation "c.c." denotes the complex conjugate of the quantity that precedes it. The normalisation defined by Eq. (2.8) is obtained by setting

$$C_\lambda(\eta) = 2^\lambda\, \exp(-\eta\pi/2)\, \frac{|\Gamma(\lambda+1+\mathrm{i}\eta)|}{\Gamma(2\lambda+2)}\,. \tag{3.19}$$

Thus, at large r the regular radial function oscillates with unit amplitude,

$$F_\lambda(\eta, x) \underset{x\to\infty}{\sim} \sin\left[x - \lambda\frac{\pi}{2} - \eta\ln(2x) + \Delta_\lambda \right], \tag{3.20}$$

where

$$\Delta_\lambda = \arg\Gamma\left(\lambda+1+\mathrm{i}\eta\right) \tag{3.21}$$

is the *Coulomb phase shift*. Notice that

$$\Delta_{\lambda+1} = \Delta_\lambda + \arctan(\eta/\lambda). \tag{3.22}$$

Examples of the functions $F_\lambda(\eta, x)$ are displayed in Fig. 1. Note that, for small values of x,

$$F_\lambda(\eta, x) \underset{x\to 0}{\sim} C_\lambda(\eta)\, x^{\lambda+1}. \tag{3.23}$$

For reasons that will become evident below, it is convenient to consider a second solution of Eq. (3.17), $G_\lambda(\eta, x)$, with the asymptotic behaviour

$$G_\lambda(\eta, x) \underset{x\to\infty}{\sim} \cos\left[x - \lambda\frac{\pi}{2} - \eta\ln(2x) + \Delta_\lambda \right]. \tag{3.24}$$

This solution is irregular at $x = 0$. This can be easily seen by noting that the Wronskian $W\{G_\lambda, F_\lambda\} \equiv G_\lambda F'_\lambda - G'_\lambda F_\lambda$ is independent of x [because F_λ and G_λ are solutions of the

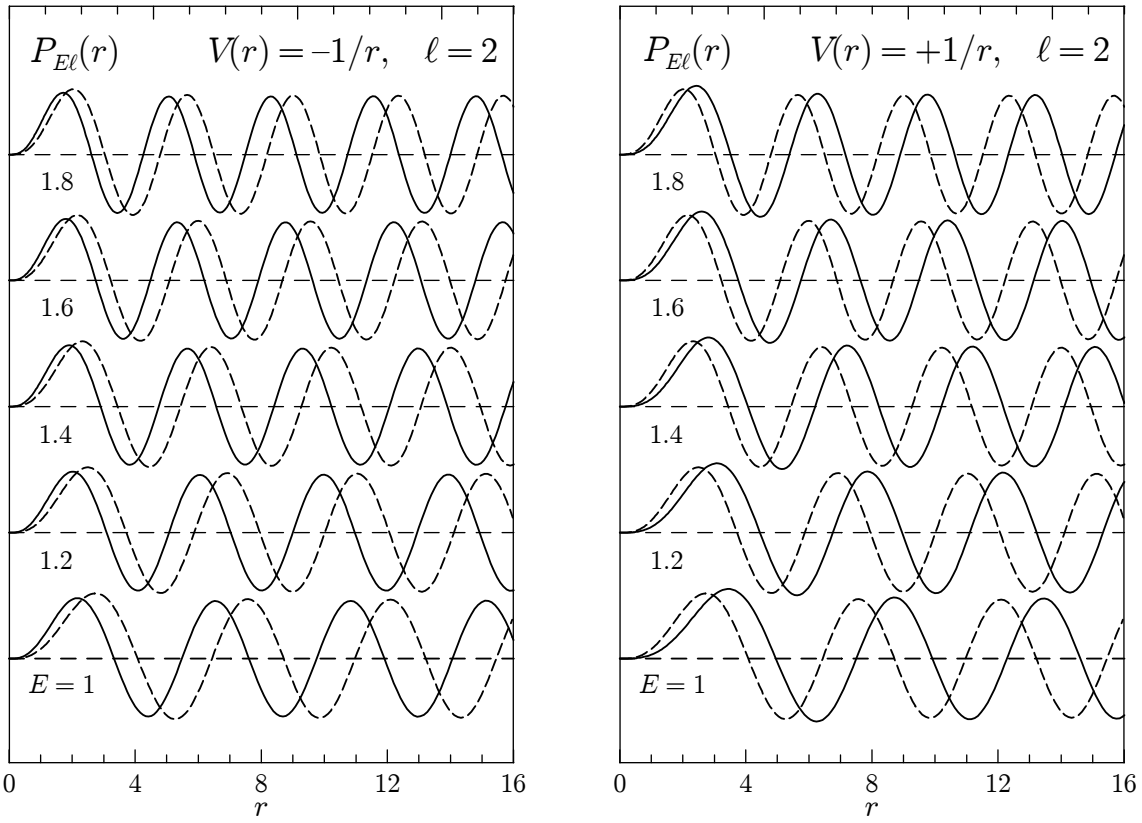

Figure 1: Regular Schrödinger–Coulomb functions $P_{E\ell}(r) = F_\ell(\eta, x)$ of free states of energy E and orbital angular momentum $\ell = 2$ for Coulomb potentials with $Z_\infty = \pm 1$. The dashed curves represent radial functions for the null potential, $P_{E\ell}(r) = kr\, j_\ell(kr)$. All states are normalised in the form (3.20) and are plotted with the same scale. All quantities in atomic units.

differential equation (3.17)]. Moreover, in the asymptotic region $W\{G_\lambda, F_\lambda\} = 1$ and, therefore,

$$W\{G_\lambda, F_\lambda\} = G_\lambda F'_\lambda - G'_\lambda F_\lambda = 1 \qquad \forall x. \tag{3.25}$$

Let us assume that for $x \ll 1$

$$G_\lambda(\eta, x) \underset{x\to 0}{\sim} A x^b.$$

Then,

$$W\{G_\lambda, F_\lambda\} \underset{x\to 0}{\sim} A(\lambda + 1 - b) C_\lambda(\eta)\, x^{\lambda+b} = 1,$$

and it follows that $b = -\lambda$ and $A = 1/[(2\lambda + 1)C_\lambda(\eta)]$. That is,

$$G_\lambda(\eta, x) \underset{x\to 0}{\sim} x^{-\lambda}/[(2\lambda + 1)C_\lambda(\eta)], \tag{3.26}$$

which shows that, for $\lambda > 0$, $G_\lambda(\eta, x)$ is irregular at $x = 0$, q.e.d.

A more compact definition of the functions $F_\lambda(\eta, x)$ and $G_\lambda(\eta, x)$ is provided by the following equality (see, *e.g.*, Olver *et al.*, 2010),

$$G_\lambda(\eta, x) + \mathrm{i}F_\lambda(\eta, x) = (-\mathrm{i})^\lambda \exp\left[\eta\,\frac{\pi}{2} + \mathrm{i}\,\mathrm{arg}\Gamma(\lambda + 1 + \mathrm{i}\eta)\right] \mathcal{W}_{-\mathrm{i}\eta,\lambda+1/2}(-2\mathrm{i}x)\,, \quad (3.27)$$

where $\mathcal{W}_{-\mathrm{i}\eta,\lambda+1/2}(-2\mathrm{i}x)$ is the Whittaker function (3.13). To verify that this equality does define the two Coulomb functions, we observe that the function on the right-hand side is a solution of the Whittaker equation (3.7). Moreover, from the asymptotic expansion (3.16), we have

$$G_\lambda(\eta, x) + \mathrm{i}F_\lambda(\eta, x) \;=\; \exp(\mathrm{i}\theta_\lambda)\left[\sum_{n=0}^{R-1} \frac{(\lambda + 1 + \mathrm{i}\eta)_n\,(-\lambda + \mathrm{i}\eta)_n}{n!\,(2\mathrm{i}x)^n} + O(|2x|^{-R})\right]\,, \quad (3.28)$$

with

$$\theta_\lambda \equiv x - \lambda\frac{\pi}{2} - \eta\ln(2x) + \Delta_\lambda. \quad (3.29)$$

Hence, the real and imaginary parts of expression (3.27) have the asymptotic forms (3.24) and (3.20), respectively. We thus conclude that the identity (3.27) is consistent with our previous definitions of the regular and irregular Coulomb functions.

From the differential equation (3.17), it is seen that the Coulomb functions F_λ and G_λ have a classical turning point (*i.e.*, an inflexion point – see Appendix C) at

$$x_{\mathrm{TP}}[\lambda] = \eta + \sqrt{\eta^2 + \lambda(\lambda + 1)}. \quad (3.30)$$

For $x < x_{\mathrm{TP}}[\lambda]$, F_λ and G_λ are positive; F_λ increases monotonously and G_λ decreases monotonously with increasing x. For $x > x_{\mathrm{TP}}[\lambda]$, F_λ and G_λ have an oscillatory behaviour.

The series (3.28) provides a simple method for computing the Coulomb functions. However, this series is convergent only in the asymptotic sense, *i.e.*, for relatively large values of x ($x > x_{\mathrm{TP}}[\lambda]$), and the summation must be terminated just after adding the term with the smallest absolute magnitude (which normally gives a good estimate of the absolute error of the result).

3.1.3 Steed's continued fraction method

Although the Coulomb functions are expressed in terms of confluent hypergeometric functions, the strict summation of the hypergeometric series is of little help for the numerical evaluation of the Coulomb functions, except for x values in limited intervals (see, *e.g.*, Bardin *et al.*, 1972). A variety of procedures to compute Schrödinger–Coulomb functions can be found, *e.g.*, in the papers of Fröberg (1955) and Bardin *et al.* (1972). An exhaustive list of references on this topic is given by Barnett *et al.* (1981). The calculation algorithm adopted here is the continued-fraction method due to Steed (Barnett *et al.*, 1974), which is generally applicable for $x > x_{\mathrm{TP}}[\lambda]$. For sufficiently large values of x, however, we use the asymptotic expansion (3.28), which is more effective. In the

following, we quote the properties of positive-energy Coulomb functions required for the derivation of Steed's algorithm.

The Coulomb functions for successive λ-values are linked by recurrence relations (see, *e.g.*, Fröberg, 1955). The downward recursion, for decreasing orders, is

$$R_\lambda\, U_{\lambda-1} = S_\lambda\, U_\lambda + U'_\lambda, \tag{3.31a}$$

$$U'_{\lambda-1} = S_\lambda\, U_{\lambda-1} - R_\lambda\, U_\lambda, \tag{3.31b}$$

and the upward recursion is

$$R_{\lambda+1}\, U_{\lambda+1} = S_{\lambda+1}\, U_\lambda - U'_\lambda, \tag{3.32a}$$

$$U'_{\lambda+1} = R_{\lambda+1}\, U_\lambda - S_{\lambda+1}\, U_{\lambda+1}. \tag{3.32b}$$

Here again U_λ stands for either F_λ or G_λ, and the primes denote differentiation with respect to x. The coefficients for $\lambda \neq 0$ are

$$R_\lambda = \frac{1}{\lambda}\sqrt{\lambda^2+\eta^2}, \qquad S_\lambda = \frac{\lambda}{x} + \frac{\eta}{\lambda}. \tag{3.33}$$

Combining the relations (3.32a) and (3.32b) we obtain

$$U_{\lambda+1} = \frac{S_{\lambda+1}+S_\lambda}{R_{\lambda+1}}\, U_\lambda - \frac{R_\lambda}{R_{\lambda+1}}\, U_{\lambda-1}. \tag{3.34}$$

The relation

$$W_\lambda \equiv F_\lambda\, G_{\lambda+1} - F_{\lambda+1}\, G_\lambda = 1/R_{\lambda+1} \tag{3.35}$$

follows from Eq. (3.25) by eliminating the derivatives with the aid of Eq. (3.32a).

Recursion relations are said to be stable when the quantities obtained from them do not decrease monotonously. Otherwise, there is a gradual loss of accuracy, due to the finite number of digits in the floating point representation, which may eventually invalidate the results. For $x < x_{\rm TP}[\lambda]$, F_λ decreases and G_λ increases for decreasing λ. Thus, the downward recursion for F_λ and the upward recursion for G_λ are stable. For $x > x_{\rm TP}[\lambda]$ the functions are always of the order of unity and, hence, both recursions are stable.

Steed's method for the evaluation of Coulomb functions (Barnett *et al.*, 1974) is based on the fact that, for $x \geq x_{\rm TP}[\lambda]$, the quantities

$$f_\lambda \equiv \frac{F'_\lambda}{F_\lambda} \qquad \text{and} \qquad p_\lambda + \mathrm{i}q_\lambda \equiv \frac{G'_\lambda + \mathrm{i}F'_\lambda}{G_\lambda + \mathrm{i}F_\lambda} \tag{3.36}$$

can be expressed as rapidly converging continued fractions. We evaluate these continued fractions by using the modified Wallis' algorithm described in Appendix B. Equations (3.36) can then be solved for F'_λ, G_λ and G'_λ in terms of F_λ,

$$F'_\lambda = f_\lambda F_\lambda, \qquad G_\lambda = \frac{f_\lambda - p_\lambda}{q_\lambda}\, F_\lambda, \qquad G'_\lambda = \frac{p_\lambda\,(f_\lambda - p_\lambda) - q_\lambda^2}{q_\lambda}\, F_\lambda. \tag{3.37}$$

The absolute value of F_λ, *i.e.*, the scaling factor in expressions (3.37), is determined from the Wronskian (3.25),

$$F_\lambda = \pm \left(\frac{q_\lambda}{(f_\lambda - p_\lambda)^2 + q_\lambda^2} \right)^{1/2}, \tag{3.38}$$

and, finally, its sign is obtained during the evaluation of f_λ (see below). Notice that

$$q_\lambda = \frac{1}{F_\lambda^2 + G_\lambda^2}. \tag{3.39}$$

• **Continued fraction for f_λ**

Consider the sequences (n = 0,1,2, ...)

$$\begin{aligned} A_n &\equiv c_{11}\, F_{n+\lambda+1} + c_{12}\, G_{n+\lambda+1}, \\ B_n &\equiv c_{21}\, F_{n+\lambda+1} + c_{22}\, G_{n+\lambda+1}, \end{aligned} \tag{3.40}$$

where c_{ij} are four constants. According to Eq. (3.34), A_n and B_n satisfy the recurrence relations

$$\begin{aligned} A_n &= A_{n-1}\, b_n + A_{n-2}\, a_n, \\ B_n &= B_{n-1}\, b_n + B_{n-2}\, a_n, \end{aligned} \tag{3.41}$$

with

$$a_n = -\frac{R_{n+\lambda}}{R_{n+\lambda+1}} = -\sqrt{\frac{(n+\lambda)^2+\eta^2}{(n+\lambda+1)^2+\eta^2}}\, \frac{n+\lambda+1}{n+\lambda} \tag{3.42a}$$

and

$$b_n = \frac{S_{n+\lambda+1} + S_{n+\lambda}}{R_{n+\lambda+1}} = \frac{2(n+\lambda)+1}{\sqrt{(n+\lambda+1)^2+\eta^2}} \left(\frac{n+\lambda+1}{x} + \frac{\eta}{n+\lambda} \right). \tag{3.42b}$$

The constants c_{ij} are fixed so that

$$\begin{aligned} A_{-1} &= c_{11}\, F_\lambda + c_{12}\, G_\lambda = 1, \qquad A_0 = c_{11}\, F_{\lambda+1} + c_{12}\, G_{\lambda+1} = b_0, \\ B_{-1} &= c_{21}\, F_\lambda + c_{22}\, G_\lambda = 0, \qquad B_0 = c_{21}\, F_{\lambda+1} + c_{22}\, G_{\lambda+1} = 1. \end{aligned} \tag{3.43}$$

Using the properties (3.25) and (3.35) of the Coulomb functions, we obtain

$$\begin{aligned} c_{11} &= (G_{\lambda+1} - b_0\, G_\lambda)\, R_{\lambda+1}, & c_{12} &= (b_0\, F_\lambda - F_{\lambda+1})\, R_{\lambda+1}, \\ c_{21} &= -G_\lambda\, R_{\lambda+1}, & c_{22} &= F_\lambda\, R_{\lambda+1}. \end{aligned} \tag{3.44}$$

From Eqs. (3.41) and (3.43), and making use of the results given in Appendix B [Eqs. (B.4) to (B.6)], it is clear that

$$\lim_{n\to\infty} \frac{A_n}{B_n} = b_0 + \frac{a_1}{b_1+}\, \frac{a_2}{b_2+}\, \frac{a_3}{b_3+\cdots}.$$

On the other hand, since $F_{n+\lambda+1} \to 0$ and $G_{n+\lambda+1} \to \infty$ as $n \to \infty$, from Eq. (3.40) it follows that

$$\lim_{n\to\infty} \frac{A_n}{B_n} = \frac{c_{12}}{c_{22}} = b_0 - \frac{F_{\lambda+1}}{F_\lambda}. \tag{3.45}$$

Therefore,

$$\frac{F_{\lambda+1}}{F_\lambda} = -\frac{a_1}{b_1+}\,\frac{a_2}{b_2+}\,\frac{a_3}{b_3+\cdots}. \tag{3.46}$$

With the help of Eq. (3.32a), we eliminate $F_{\lambda+1}$ to obtain the following continued fraction for f_λ

$$f_\lambda = \frac{F'_\lambda}{F_\lambda} = S_{\lambda+1} + R_{\lambda+1}\frac{a_1}{b_1+}\,\frac{a_2}{b_2+}\,\frac{a_3}{b_3+\cdots}. \tag{3.47}$$

The final step is to recast this continued fraction in a form that is more convenient for numerical evaluation. By means of the equivalence transformation (see Appendix B)

$$c_n = x(n+\lambda)(n+\lambda+1)R_{n+\lambda+1} = x(n+\lambda)\sqrt{(n+\lambda+1)^2+\eta^2},$$

we obtain the transformed continued fraction

$$f_\lambda = S_{\lambda+1} + \frac{H_1}{K_1+}\,\frac{H_2}{K_2+}\,\frac{H_3}{K_3+\cdots} \tag{3.48}$$

with

$$\begin{aligned} H_1 &= c_1 R_{\lambda+1} a_1 = -\,\frac{\lambda+2}{\lambda+1}\left[(\lambda+1)^2+\eta^2\right] x, \\ H_n &= c_{n-1}c_n a_n = -\left[(n+\lambda)^2-1\right]\left[(n+\lambda)^2+\eta^2\right] x^2, \qquad (n>1) \\ K_n &= c_n b_n = \left[2(n+\lambda)+1\right]\left[(n+\lambda)(n+\lambda+1)+\eta x\right]. \end{aligned} \tag{3.49}$$

The sign of F_λ, see Eq. (3.38), is obtained during the calculation of f_λ using the following trick. We observe that as $n \to \infty$ the value of B_n, Eq. (3.40), tends to $c_{22}\, G_{n+\lambda+1} = F_\lambda\, R_{\lambda+1}\, G_{n+\lambda+1}$ and $G_{n+\lambda+1} \to +\infty$. Therefore, the sign of F_λ is the sign of the n-th denominator B_n when the continued fraction has converged.

• **Continued fraction for $p_\lambda + \mathrm{i}q_\lambda$**

A continued fraction for $p_\lambda + \mathrm{i}q_\lambda$ is obtained by considering the asymptotic form given by Eq. (3.28), which suggests the replacement

$$G_\lambda + \mathrm{i}F_\lambda = \exp(\mathrm{i}\theta_\lambda)\, y_\lambda(\eta, x) \tag{3.50}$$

with θ_λ given by Eq. (3.29). The function $y_\lambda(\eta, x)$ then satisfies the differential equation

$$\left(\frac{\mathrm{d}^2}{\mathrm{d}x^2} + 2\mathrm{i}(1-\eta/x)\,\frac{\mathrm{d}}{\mathrm{d}x} + (\mathrm{i}\eta-\lambda)(\mathrm{i}\eta+\lambda+1)\frac{1}{x^2}\right) y_\lambda(\eta, x) = 0. \tag{3.51}$$

Introducing the variable $z \equiv (2\mathrm{i}x)^{-1}$, this equation transforms into the hypergeometric equation

$$\left(z^2\,\frac{\mathrm{d}^2}{\mathrm{d}z^2} + [z(a+b+1)-1]\,\frac{\mathrm{d}}{\mathrm{d}z} + ab\right) y_\lambda(\eta, z) = 0 \tag{3.52}$$

with $a = \mathrm{i}\eta - \lambda$ and $b = \mathrm{i}\eta + \lambda + 1$. The solution with the required asymptotic behaviour, $\lim_{x\to\infty} y_\lambda(\eta, x) = 1$, is the generalised hypergeometric function

$$\begin{aligned} {}_2F_0\,(a, b; z) &\equiv 1 + \frac{a\,b}{1!}\,z + \frac{a(a+1)\,b(b+1)}{2!}\,z^2 + \dots \\ &= \sum_{n=0}^{\infty} \frac{(a)_n\,(b)_n}{n!}\,z^n\,. \end{aligned} \tag{3.53}$$

That is,

$$y_\lambda(\eta, x) = {}_2F_0\left(\mathrm{i}\eta - \lambda, \mathrm{i}\eta + \lambda + 1; (2\mathrm{i}x)^{-1}\right)\,. \tag{3.54}$$

From the differentiation property

$${}_2F_0'(a, b; z) \equiv \frac{\mathrm{d}\ {}_2F_0}{\mathrm{d}z} = ab\ {}_2F_0(a+1, b+1; z), \tag{3.55}$$

we find

$$p_\lambda + \mathrm{i}q_\lambda \equiv \frac{G_\lambda' + \mathrm{i}F_\lambda'}{G_\lambda + \mathrm{i}F_\lambda} = \mathrm{i}\left(1 - \frac{\eta}{x}\right) + \mathrm{i}\,\frac{ab}{2x^2}\,\frac{{}_2F_0(a+1, b+1; z)}{{}_2F_0(a, b; z)}. \tag{3.56}$$

Also, using (3.55) in Eq. (3.52), dividing by ${}_2F_0'$ and rearranging we obtain

$$\frac{{}_2F_0(a, b; z)}{{}_2F_0(a+1, b+1; z)} = 1 - z(a+b+1) - z^2(a+1)(b+1)\,\frac{{}_2F_0(a+2, b+2; z)}{{}_2F_0(a+1, b+1; z)}.$$

Taking the reciprocal of this equation,

$$\frac{{}_2F_0(a+1, b+1; z)}{{}_2F_0(a, b; z)} = \frac{1}{1 - z(a+b+1) - z^2(a+1)(b+1)\,\dfrac{{}_2F_0(a+2, b+2; z)}{{}_2F_0(a+1, b+1; z)}},$$

and applying it repeatedly gives the continued fraction

$$\frac{{}_2F_0(a+1, b+1; z)}{{}_2F_0(a, b; z)} = \frac{1}{1 - z(a+b+1) -}\ \frac{z^2(a+1)(b+1)}{1 - z(a+b+3) -}\ \frac{z^2(a+2)(b+2)}{1 - z(a+b+5) - \cdots}.$$

Replacing the constants a and b, introducing $z = (2\mathrm{i}x)^{-1}$ and making an equivalence transformation with $c_n = 2x$ we get

$$\frac{{}_2F_0(a+1, b+1; z)}{{}_2F_0(a, b; z)} = \frac{2x}{2(x - \eta + \mathrm{i}) +}\ \frac{(\mathrm{i}\eta - \lambda + 1)(\mathrm{i}\eta + \lambda + 2)}{2(x - \eta + 2\mathrm{i}) +}\ \frac{(\mathrm{i}\eta - \lambda + 2)(\mathrm{i}\eta + \lambda + 3)}{2(x - \eta + 3\mathrm{i}) + \cdots}$$

Finally, from Eq. (3.56), we have

$$p_\lambda + \mathrm{i}q_\lambda = \frac{\mathrm{i}}{x}\left(K_0 + \frac{H_1}{K_1 +}\ \frac{H_2}{K_2 +}\ \frac{H_3}{K_3 + \cdots}\right), \tag{3.57}$$

with

$$\begin{aligned} K_0 &= x - \eta, \\ K_n &= 2(x - \eta + \mathrm{i}n), \qquad (n \geq 1) \\ H_n &= (\mathrm{i}\eta - \lambda - 1 + n)(\mathrm{i}\eta + \lambda + n). \end{aligned} \tag{3.58}$$

The Fortran subroutine FCOUL calculates Coulomb functions and their derivatives for real η, real $\lambda > -1$ and real $x > 0$. It combines Steed's method with the asymptotic expansion (3.53) using double-precision arithmetic. If $x > x_{\rm TP}[\lambda]$, the asymptotic expansion is tentatively evaluated, and the relative error of the result is estimated from the magnitude of the term with the smallest absolute value. If this error is less than 10^{-15}, the Coulomb functions and their derivatives are delivered. Otherwise, Steed's algorithm is applied, using a maximum of 1000 iterations to evaluate the continued fractions. When these have converged, or when the 1000 iterations have been completed, the relative error of the resulting function values is determined from the differences between the last calculated convergents of the continued fractions. Among the results obtained with the two methods, the subroutine selects the ones with the lesser relative uncertainty. For $x > x_{\rm TP}[\lambda]$, the delivered values are usually accurate to 13 or 14 decimal figures.

For $x < x_{\rm TP}[\lambda]$, only Steed's method is applicable. In this case the accuracy of the algorithm worsens with decreasing x, due to the fact that G_λ and G'_λ increase without limit, while F_λ goes to zero. Thus, when x decreases, the ratio $|q_\lambda/p_\lambda|$ increases rapidly and, as a consequence, there is a gradual loss of significance. This difficulty is partially avoided by means of the following trick (Barnett *et al.*, 1981). For $x < x_{\rm TP}[\lambda]$, the continued fraction for f_λ, Eq. (3.48), is evaluated first and the downward recursions for F and F' [Eqs. (3.31)] are applied to obtain the value of $f_{\rm L}$ for an index L which is less than 1 or such that x is larger than $x_{\rm TP}[{\rm L}]$, the turning point for the angular momentum L. The continued fraction for $p_{\rm L} + {\rm i}q_{\rm L}$ is then evaluated and the functions $G_{\rm L}$ and $G'_{\rm L}$ obtained from Eqs. (3.37). The upward recursions for G and G' [Eqs. (3.32)] are used to obtain G_λ and G'_λ. Finally, the Wronskian, Eq. (3.25), together with the previously computed value of f_λ, determine F_λ and F'_λ. In this way, Coulomb functions can be calculated for all x larger than a value $x_{\rm crit}$ of the order of the turning point $x_{\rm TP}[0]$ for $\lambda = 0$. When $x \ll x_{\rm TP}[\lambda]$, the irregular functions may take exceedingly large values; to prevent computer overflows, the calculation is discontinued and an error code is returned to the main program when $G_\lambda(\eta, x)$ is larger than $\sim 10^{30}$. For x-values less than $x_{\rm crit}$ or such that $G_\lambda(\eta, x) > 10^{30}$, regular Coulomb functions may be obtained either by summing the hypergeometric series [see Eqs. (3.9) and (3.18)] or by numerical integration of their differential equation (3.17) (*e.g.*, by using the subroutine SCH included in the RADIAL package).

3.1.4 Bessel functions

The Bessel functions of the first kind, $J_\nu(x)$, and of the second kind, $Y_\nu(x)$, are the solutions of the differential equation (see, *e.g.*, Abramowitz and Stegun, 1974)

$$\frac{{\rm d}^2\,\omega_\nu(x)}{{\rm d}x^2} + \frac{1}{x}\,\frac{{\rm d}\,\omega_\nu(x)}{{\rm d}x} + \left(1 - \frac{\nu^2}{x^2}\right)\omega_\nu(x) = 0, \tag{3.59}$$

with the asymptotic behaviour

$$J_\nu(x) \underset{x\to\infty}{\sim} \sqrt{\frac{2}{\pi x}}\,\sin\left(x - \nu\frac{\pi}{2} + \frac{\pi}{4}\right) \tag{3.60a}$$

and

$$Y_\nu(x) \underset{x\to\infty}{\sim} -\sqrt{\frac{2}{\pi x}}\,\cos\left(x-\nu\frac{\pi}{2}+\frac{\pi}{4}\right). \tag{3.60b}$$

We remove the first derivative in Eq. (3.59) with the transformation

$$\omega_\nu(x) = x^{-1/2}\,\mathrm{w}_\nu(x), \tag{3.61}$$

which yields

$$\frac{\mathrm{d}^2\,\mathrm{w}_\nu(x)}{\mathrm{d}x^2}+\left(1-\frac{\nu^2-1/4}{x^2}\right)\mathrm{w}_\nu(x)=0. \tag{3.62}$$

This equation is of the form (3.17) with $\eta = 0$ and $\lambda = \nu - 1/2$ and, therefore, for $\nu > -1/2$,

$$J_\nu(x)=\sqrt{\frac{2}{\pi x}}\,F_{\nu-1/2}\,(0,x) \qquad \text{and} \qquad Y_\nu(x)=-\sqrt{\frac{2}{\pi x}}\,G_{\nu-1/2}\,(0,x). \tag{3.63}$$

Subroutine `FCOUL` can then be used to compute Bessel functions of orders $\nu > -1/2$, and their derivatives, for $x > 0$ to high accuracy. The idea of employing Steed's algorithm to calculate Bessel functions is due to Barnett *et al.* (1981).

The *spherical Bessel functions* (Abramowitz and Stegun, 1974) satisfy the differential equation

$$\frac{\mathrm{d}^2\,\omega_\nu(x)}{\mathrm{d}x^2}+\frac{2}{x}\,\frac{\mathrm{d}\,\omega_\nu(x)}{\mathrm{d}x}+\left(1-\frac{\nu(\nu+1)}{x^2}\right)\omega_\nu(x)=0, \tag{3.64}$$

Particular solutions are the spherical Bessel functions of the first kind

$$j_\nu(x)\equiv\sqrt{\frac{\pi}{2x}}\,J_{\nu+1/2}\,(x)=\frac{1}{x}\,F_\nu\,(0,x), \tag{3.65a}$$

the spherical Bessel functions of the second kind

$$n_\nu(x)\equiv\sqrt{\frac{\pi}{2x}}\,Y_{\nu+1/2}\,(x)=-\frac{1}{x}\,G_\nu\,(0,x)\,, \tag{3.65b}$$

and the spherical Bessel functions of the third kind

$$h^{(1)}_\nu(x)=j_\nu(x)+\mathrm{i}n_\nu(x) \qquad \text{and} \qquad h^{(2)}_\nu(x)=j_\nu(x)-\mathrm{i}n_\nu(x). \tag{3.65c}$$

The functions $j_\nu(x)$, $n_\nu(x)$, and $h^{(i)}_\nu(x)$ are also known as spherical Bessel, Neumann, and Hankel functions, respectively. They have the following asymptotic behaviours:

$$j_\nu(x)\underset{x\to\infty}{\sim}\frac{1}{x}\,\sin\left(x-\nu\frac{\pi}{2}\right), \tag{3.66a}$$

$$n_\nu(x)\underset{x\to\infty}{\sim}-\frac{1}{x}\,\cos\left(x-\nu\frac{\pi}{2}\right), \tag{3.66b}$$

and

$$h^{(1)}_\nu(x)\underset{x\to\infty}{\sim}\frac{1}{x}\,\exp\left[\mathrm{i}\left(x-\nu\frac{\pi}{2}\right)\right], \tag{3.66c}$$

$$h_\nu^{(2)}(x) \underset{x\to\infty}{\sim} \frac{1}{x}\,\exp\left[-\mathrm{i}\left(x-\nu\frac{\pi}{2}\right)\right]. \tag{3.66d}$$

The spherical Bessel functions of non-negative integer orders ($\ell \geq 0$) are given by the following expressions

$$j_\ell(x) = (-x)^\ell \left(\frac{1}{x}\frac{\mathrm{d}}{\mathrm{d}x}\right)^\ell \frac{\sin x}{x}\,, \tag{3.67a}$$

$$n_\ell(x) = -(-x)^\ell \left(\frac{1}{x}\frac{\mathrm{d}}{\mathrm{d}x}\right)^\ell \frac{\cos x}{x}\,. \tag{3.67b}$$

Therefore, these functions can be expressed as sums of products of $\sin x$ and $\cos x$ by polynomials in x^{-1}. Those of orders $\ell = 0$ to 3 are

$$j_0(x) = \frac{1}{x}\,\sin x, \tag{3.68a}$$

$$j_1(x) = \frac{1}{x^2}\,\sin x - \frac{1}{x}\,\cos x, \tag{3.68b}$$

$$j_2(x) = \left(\frac{3}{x^3}-\frac{1}{x}\right)\sin x - \frac{3}{x^2}\,\cos x, \tag{3.68c}$$

$$j_3(x) = \left(\frac{15}{x^4}-\frac{6}{x^2}\right)\sin x - \left(\frac{15}{x^3}-\frac{1}{x}\right)\cos x, \tag{3.68d}$$

and

$$n_0(x) = -\frac{1}{x}\,\cos x, \tag{3.69a}$$

$$n_1(x) = -\frac{1}{x^2}\,\cos x - \frac{1}{x}\,\sin x, \tag{3.69b}$$

$$n_2(x) = \left(-\frac{3}{x^3}+\frac{1}{x}\right)\cos x - \frac{3}{x^2}\,\sin x\,, \tag{3.69c}$$

$$n_3(x) = \left(-\frac{15}{x^4}+\frac{6}{x^2}\right)\cos x - \left(\frac{15}{x^3}-\frac{1}{x}\right)\sin x\,. \tag{3.69d}$$

These functions are displayed in Fig. 2.

For small values of the argument, the spherical Bessel functions of non-negative integer order ($\ell = 0, 1, 2, \ldots$) can be calculated from the ascending series

$$j_\ell(x) = \frac{x^\ell}{1\cdot 3\cdot 5\cdots(2\ell+1)}\left(1-\frac{\frac{1}{2}x^2}{1!(2\ell+3)}+\frac{(\frac{1}{2}x^2)^2}{2!(2\ell+3)(2\ell+5)}-\ldots\right) \tag{3.70a}$$

and

$$n_\ell(x) = -\frac{1\cdot 3\cdot 5\cdots(2\ell+1)}{x^{\ell+1}}\left(1-\frac{\frac{1}{2}x^2}{1!(1-2\ell)}+\frac{(\frac{1}{2}x^2)^2}{2!(1-2\ell)(3-2\ell)}-\ldots\right). \tag{3.70b}$$

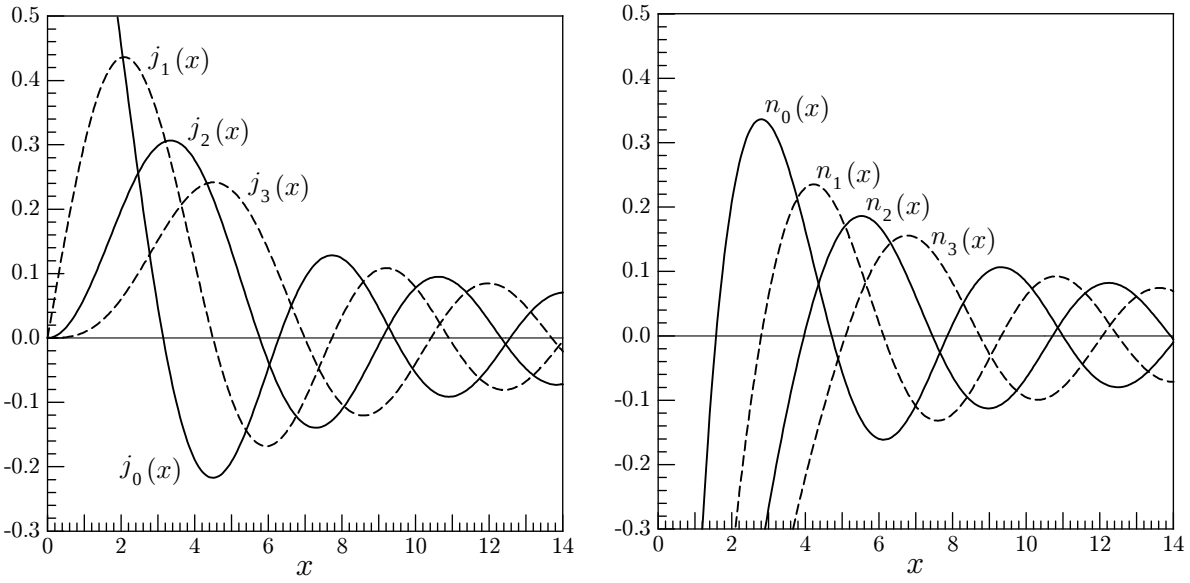

Figure 2: Spherical Bessel functions of orders $\ell = 0$ to 3.

The spherical Bessel and Neumann functions of integer order ($\ell = 0, \pm 1, \pm 2, \ldots$) are related by

$$n_\ell(x) = (-1)^{\ell+1}\, j_{-\ell-1}(x)\,, \tag{3.71}$$

and satisfy the following recurrence relations

$$f_{\ell-1}(x) + f_{\ell+1}(x) = (2\ell+1)x^{-1} f_\ell(x), \tag{3.72a}$$

$$\ell f_{\ell-1}(x) - (\ell+1) f_{\ell+1}(x) = (2\ell+1)\,\frac{\mathrm{d}}{\mathrm{d}x} f_\ell(x), \tag{3.72b}$$

$$\frac{\ell+1}{x} f_\ell(x) + \frac{\mathrm{d}}{\mathrm{d}x} f_\ell(x) = f_{\ell-1}(x), \tag{3.72c}$$

$$\frac{\ell}{x} f_\ell(x) - \frac{\mathrm{d}}{\mathrm{d}x} f_\ell(x) = f_{\ell+1}(x), \tag{3.72d}$$

where $f_\ell(x)$ stands for either $j_\ell(x)$, $n_\ell(x)$, or $h_\ell^{(i)}(x)$. These relations can be derived from the recurrence relations obeyed by the Coulomb functions.

Spherical Bessel functions of integer orders ($\ell \geq 0$) are used by RADIAL to normalise free states for finite-range potentials (see Section 6). Although these functions could be calculated by means of subroutine `FCOUL`, it is faster to generate them from the exact expressions of $j_0(x)$, $j_1(x)$ and $n_0(x)$, $n_1(x)$, Eqs. (3.68) and (3.69), using the recurrence relation (3.72a). Notice that the upward recursion for $j_\ell(x)$ and $x < \ell$ is unstable; in this case, Miller's downward recursion method (Abramowitz and Stegun, 1974) can be applied. This is the procedure adopted in function `SBESJN`, which delivers accurate values of spherical Bessel and Neumann functions of integer order for any $x > 0$[6].

[6]The function `BESFJN` in the previous versions of RADIAL contained a bug that caused an overflow when using Miller's method with the argument x equal to an integer multiple of π. The name of that

3.1.5 Coulomb functions of bound states

When $Z_\infty < 0$, the Coulomb potential (3.1) holds an infinite number of bound states with negative energy E. The radial functions of bound states have the same analytical form as the regular Coulomb functions, Eq. (3.18), but only those values of the energy which yield square-integrable wave functions are allowed. To deal only with real quantities, we write

$$k = \sqrt{\frac{2\mathrm{m_e}}{\hbar^2}\,E} = \mathrm{i}a \qquad \text{and} \qquad \eta = \frac{Z_\infty e^2\,k}{2E} = \mathrm{i}\overline{\eta}, \tag{3.73}$$

where

$$a = \sqrt{\frac{2\mathrm{m_e}}{\hbar^2}\,(-E)} \qquad \text{and} \qquad \overline{\eta} = Z\sqrt{\frac{1}{2(-E)}\,E_\mathrm{h}} \tag{3.74}$$

with

$$Z \equiv -Z_\infty. \tag{3.75}$$

The regular solution of the radial equation (3.2) is [see Eq. (3.18)]

$$\begin{aligned} P(r) &= N\,\mathcal{M}_{\overline{\eta},\ell+1/2}(2ar) \\ &= N\,(ar)^{\ell+1}\,\exp(-ar)\;{}_1F_1\left(\ell+1-\overline{\eta};2\ell+2;2ar\right), \end{aligned} \tag{3.76}$$

where N is a normalisation constant. In general, the Kummer function in this last expression diverges as $\exp(2ar)$ when r tends to ∞ [see Eq. (3.11)]. Since the radial functions of bound states are square integrable, the series (3.9) for the Kummer function must terminate after a finite number of terms. That is, the first argument of the ${}_1F_1$ function must be a negative integer or zero,

$$\ell + 1 - \overline{\eta} = -n_\mathrm{r}, \tag{3.77}$$

in which case the series (3.9) becomes a polynomial of degree n_r.

The condition (3.77) can also be obtained by noting that the radial functions of bound states are regular at $r = 0$ and at $r = \infty$, that is, they are represented simultaneously by the Whittaker functions $\mathcal{M}_{\overline{\eta},\ell+1/2}(2ar)$ and $\mathcal{W}_{\overline{\eta},\ell+1/2}(2ar)$, which differ at most by a multiplicative constant. Consequently, the Wronskian of these solutions vanishes and, from Eq. (3.13), we can write

$$W\{\mathcal{W}_{\overline{\eta},\ell+1/2}(z), \mathcal{M}_{\overline{\eta},\ell+1/2}(z)\} = \frac{\Gamma(2\ell+2)}{\Gamma(\ell+1-\overline{\eta})} = 0\,, \tag{3.78}$$

which implies that the argument of the gamma function in the denominator must be a negative integer or zero. The equality of the solutions regular at $r = 0$ and at $r = \infty$ for the bound levels of a Coulomb potential is overlooked in many quantum mechanics textbooks. Rose (1961) shows how this equality can be used to determine

function has been changed to `SBESJN` to avoid conflicting with the name of an internal function of the Fortran compiler of the GNU Compiler Collection (`https://gcc.gnu.org/`).

the normalisation constant of Coulomb bound states without having to evaluate the normalisation integral.

Hence, for bound states of a Coulomb field we have

$$\overline{\eta} = \ell + 1 + n_{\rm r} = n, \tag{3.79}$$

and the second equation in (3.74) determines the discrete energy levels,

$$E_n = -\frac{Z^2}{2n^2}\, E_{\rm h}, \tag{3.80}$$

where $E_{\rm h}$ is the Hartree energy, Eq. (2.2). Evidently, $n_{\rm r}$ is the radial quantum number and n is the principal quantum number which, by definition, may take the values $\ell+1$, $\ell+2$, ... The energy levels (3.80) do not depend on the quantum number ℓ, a peculiarity of the Coulomb potential. Hence, the degeneracy of the level E_n is

$$\sum_{\ell=0}^{n-1}(2\ell+1) = n + 2\sum_{\ell=0}^{n-1}\ell = n + n(n-1) = n^2. \tag{3.81}$$

The radial wave functions corresponding to the eigenvalues E_n are given by the expression (3.76) with

$$a = \sqrt{-\frac{2{\rm m_e}}{\hbar^2}\, E_{n\ell}} = \frac{Z}{n}\,\frac{1}{a_0}, \tag{3.82}$$

where a_0 is the Bohr radius, Eq. (2.1). That is,

$$\begin{aligned} P_{n\ell}(r) &= N_{n\ell}\, \mathcal{M}_{n,\ell+1/2}(2ar) \\ &= N_{n\ell}\, (2ar)^{\ell+1} \exp(-ar)\, {}_1F_1\left(\ell+1-n; 2\ell+2; 2ar\right). \end{aligned} \tag{3.83}$$

The constant $N_{n\ell}$ is determined by the normalisation condition (2.7). The calculation of the integral in (2.7) is facilitated by expressing the radial functions in terms of the associated Laguerre polynomials, and using the orthogonality properties of these polynomials.

• Associated Laguerre polynomials

The associated Laguerre polynomials are defined by[7]

$$L_n^q(x) = \frac{(q+n)!}{q!\, n!}\, {}_1F_1(-n; q+1; x), \tag{3.84}$$

or by means of their generating function

$$U_q(x,t) = \frac{1}{(1-t)^{q+1}}\, \exp\left(\frac{tx}{t-1}\right) = \sum_{n=0}^{\infty} L_n^q(x)\, t^n, \qquad (|t|<1). \tag{3.85}$$

[7]In the literature we find different families of Laguerre polynomials, with different values of the constant on the right-hand side of Eq. (3.84). The definition adopted here is the one given by Gradshteyn and Ryzhik (1980).

The index n is a non-negative integer and q can take any real non-negative value. Notice that, to simplify the formulas, we set $q! \equiv \Gamma(q+1)$. For the present purposes, the variable x is real and takes values in the interval $(0, \infty)$.

The integrals

$$I^{\tau}_{qn;q'n'} \equiv \int_0^{\infty} \mathrm{e}^{-x} x^{\tau} L^q_n(x) L^{q'}_{n'}(x)\, \mathrm{d}x \tag{3.86}$$

can be evaluated in a systematic manner by the following considerations. Because of the relation (3.85), we have

$$\int_0^{\infty} \mathrm{e}^{-x} x^{\tau} U_q(x,s) U_{q'}(x,t)\, \mathrm{d}x = \sum_{n=0}^{\infty}\sum_{n'=0}^{\infty} I^{\tau}_{qn;q'n'}\, s^n t^{n'}. \tag{3.87}$$

The integral on the left-hand side is

$$\begin{aligned}
&\int_0^{\infty} \mathrm{e}^{-x} x^{\tau} U_q(x,s) U_{q'}(x,t)\, \mathrm{d}x \\
&\quad = \frac{1}{(1-s)^{q+1}(1-t)^{q'+1}} \int_0^{\infty} \exp\left(-x + \frac{sx}{s-1} + \frac{tx}{t-1}\right) x^{\tau}\, \mathrm{d}x \\
&\quad = \frac{1}{(1-s)^{q+1}(1-t)^{q'+1}} \left(1 + \frac{s}{1-s} + \frac{t}{1-t}\right)^{-(\tau+1)} \tau! \\
&\quad = \frac{(1-s)^{\tau-q}\,(1-t)^{\tau-q'}}{(1-st)^{\tau+1}}\, \tau!,
\end{aligned} \tag{3.88}$$

where we have used the identity

$$\int_0^{\infty} x^a\, \mathrm{e}^{-bx}\, \mathrm{d}x = \frac{a!}{b^{a+1}}. \tag{3.89}$$

Now, the integrals $I^{\tau}_{qn;q'n'}$ can be obtained by expanding the expression (3.88) as a series in powers of s and t and comparing the coefficients with those on the right-hand side of the equality (3.87). Thus, for instance, to obtain the integral $I^{q}_{qn;qn'}$, we consider the function (3.88) with $\tau = q' = q$,

$$\frac{q!}{(1-st)^{q+1}} = q! \sum_{n=0}^{\infty} \frac{(q+n)!}{n!q!} (st)^n = \sum_{n=0}^{\infty} \frac{(q+n)!}{n!} (st)^n = \sum_{n=0}^{\infty}\sum_{n'=0}^{\infty} I^{q}_{qn,qn'}\, s^n t^{n'},$$

and conclude that

$$I^{q}_{qn;qn'} = \int_0^{\infty} \mathrm{e}^{-x} x^q L^q_n(x) L^q_{n'}(x)\, \mathrm{d}x = \frac{(q+n)!}{n!}\, \delta_{n,n'}. \tag{3.90}$$

That is, the Laguerre polynomials are orthogonal in the interval (0,∞). In a similar manner, we can obtain the following integrals,

$$I^{q+1}_{qn;qn} = \int_0^{\infty} \mathrm{e}^{-x} x^{q+1} L^q_n(x) L^q_n(x)\, \mathrm{d}x = (q+2n+1)\frac{(q+n)!}{n!} \tag{3.91}$$

and

$$I^{q+1}_{q-1,n;q+1,n-1} = \int_0^\infty \mathrm{e}^{-x} x^{q+1} L_n^{q-1}(x) L_{n-1}^{q+1}(x)\,\mathrm{d}x = -2\,\frac{(q+n)!}{(n-1)!}, \tag{3.92}$$

which are useful for normalising negative-energy Coulomb wave functions.

Introducing the Laguerre polynomials, Eq. (3.84), the radial functions (3.83) can be expressed as

$$P_{n\ell}(r) = N_{n\ell}\,\frac{(2\ell+1)!(n-\ell-1)!}{(n+\ell)!}\,(2ar)^{\ell+1}\exp(-ar)\,L^{2\ell+1}_{n-\ell-1}(2ar). \tag{3.93}$$

The normalisation integral (2.7) can now be evaluated by using Eq. (3.90), and the normalisation constant $N_{n\ell}$ can thus be determined analytically. The result is

$$N_{n\ell} = \frac{1}{n(2\ell+1)!}\left[\frac{(n+\ell)!}{(n-\ell-1)!}\,\frac{Z}{a_0}\right]^{1/2}. \tag{3.94}$$

The Coulomb wave functions of the bound states with the lowest energies are

$$P_{10}(r) = \left(\frac{Z}{a_0}\right)^{3/2} 2r\ \exp(-Zr/a_0), \tag{3.95a}$$

$$P_{20}(r) = \left(\frac{Z}{a_0}\right)^{3/2} \frac{1}{\sqrt{2}}\,r\left[1-\frac{1}{2}\left(\frac{Zr}{a_0}\right)\right]\exp(-Zr/2a_0), \tag{3.95b}$$

$$P_{21}(r) = \left(\frac{Z}{a_0}\right)^{3/2} \frac{1}{2\sqrt{6}}\,\frac{Zr^2}{a_0}\exp(-Zr/2a_0), \tag{3.95c}$$

$$P_{30}(r) = \left(\frac{Z}{a_0}\right)^{3/2} \frac{2}{3\sqrt{3}}\,r\left[1-\frac{2}{3}\left(\frac{Zr}{a_0}\right)+\frac{2}{27}\left(\frac{Zr}{a_0}\right)^2\right]\exp(-Zr/3a_0), \tag{3.95d}$$

$$P_{31}(r) = \left(\frac{Z}{a_0}\right)^{3/2} \frac{8}{27\sqrt{6}}\,\frac{Zr^2}{a_0}\left[1-\frac{1}{6}\left(\frac{Zr}{a_0}\right)\right]\exp(-Zr/3a_0), \tag{3.95e}$$

$$P_{32}(r) = \left(\frac{Z}{a_0}\right)^{3/2} \frac{4}{81\sqrt{30}}\,\frac{Z^2r^3}{a_0^2}\exp(-Zr/3a_0). \tag{3.95f}$$

Figure 3 displays the radial wave functions for the Coulomb potential with $Z = -1$, $V(r) = -e^2/r$. It is interesting to note that the radial functions $R_{n\ell}(r) = r^{-1}P_{n\ell}(r)$ scale with Z,

$$R^{(Z)}_{n\ell}(r) = Z^{3/2}\,R^{(Z=1)}_{n\ell}(Zr), \tag{3.96}$$

where $R^{(Z)}_{n\ell}(r)$ is the radial function corresponding to the indicated value of Z.

3.2 Dirac–Coulomb functions

Free-state ($E > 0$) solutions of Dirac's equation for the Coulomb potential (3.1) are usually obtained by directly solving the coupled pair of first order radial differential

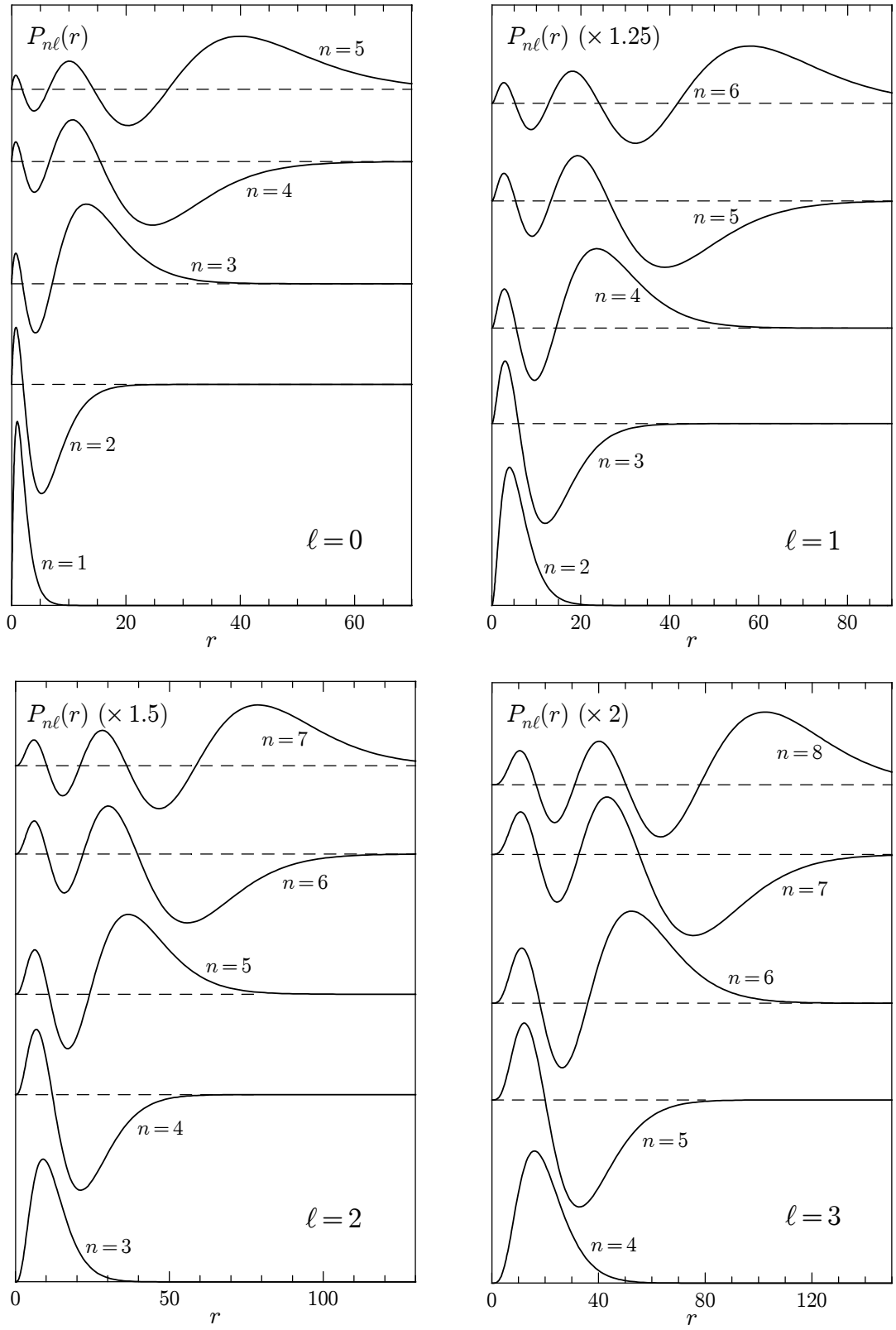

Figure 3: Schrödinger–Coulomb radial functions $P_{n\ell}(r)$ of the states with the indicated values of n and ℓ for $Z_\infty = -1$. The scale of the vertical axes is the same in all plots, but the functions have been multiplied by the indicated factors. All quantities are in atomic units.

equations (2.21),

$$\begin{aligned} \frac{\mathrm{d}\,u_\kappa^{(\mathrm{u})}}{\mathrm{d}r} &= -\frac{\kappa}{r}\,u_\kappa^{(\mathrm{u})} + \frac{W+\mathrm{m_e}c^2}{c\hbar}\,u_\kappa^{(\mathrm{l})} - \frac{\alpha Z_\infty}{r}\,u_\kappa^{(\mathrm{l})}, \\ \frac{\mathrm{d}\,u_\kappa^{(\mathrm{l})}}{\mathrm{d}r} &= -\frac{W-\mathrm{m_e}c^2}{c\hbar}\,u_\kappa^{(\mathrm{u})} + \frac{\alpha Z_\infty}{r}\,u_\kappa^{(\mathrm{u})} + \frac{\kappa}{r}\,u_\kappa^{(\mathrm{l})}, \end{aligned} \tag{3.97}$$

where $W \equiv E + \mathrm{m_e}c^2$ is the total energy, and $u_\kappa^{(\mathrm{u})}$ and $u_\kappa^{(\mathrm{l})}$ stand for the upper and lower spinor radial functions, respectively.

The solutions $u_\kappa^{(\mathrm{u})}$, $u_\kappa^{(\mathrm{l})}$ of Eqs. (3.97) can be expressed as linear combinations of two confluent hypergeometric functions with complex arguments (Rose, 1961; Greiner, 1990). However, to obtain the form that corresponds with the non-relativistic limit it is necessary to perform intricate manipulations using the properties of the confluent hypergeometric functions. Moreover, the numerical evaluation of the irregular Dirac–Coulomb functions is a difficult problem except for large radii, where the asymptotic expansions of the confluent hypergeometric functions converge to the desired accuracy.

In the present calculations, we use an alternative method that is free from these difficulties. The method is based on the, not widely known, fact that Eqs. (3.97) can be transformed to a pair of equations of the form (3.4) with non-integer λ's[8]. The transformation shows, in a natural way, that the regular and irregular solutions of the Dirac equation (3.97) are linear combinations of Schrödinger–Coulomb functions. Our transformation is similar to one described by Kolsrud (1966), who only considered the regular solutions. We have generalised the final steps of the derivation so as to also include the irregular solution. This transformation has been formulated in a different way by Auvil and Brown (1978), who applied it to bound states of the hydrogen atom.

3.2.1 Dirac–Coulomb functions of free states

Introducing the dimensionless variable $x = kr$, where k is the relativistic wave number [Eq. (2.27)]

$$k = \frac{\sqrt{W^2 - \mathrm{m_e}^2c^4}}{\hbar c}, \tag{3.98}$$

Eqs. (3.97) can be written in the following matrix form:

$$\begin{pmatrix} \dfrac{\mathrm{d}}{\mathrm{d}x} + \dfrac{\kappa}{x} & -\dfrac{W+\mathrm{m_e}c^2}{k\hbar c} + \dfrac{\alpha Z_\infty}{x} \\ \dfrac{W-\mathrm{m_e}c^2}{k\hbar c} - \dfrac{\alpha Z_\infty}{x} & \dfrac{\mathrm{d}}{\mathrm{d}x} - \dfrac{\kappa}{x} \end{pmatrix} u_\kappa(x) = 0, \qquad u_\kappa(x) \equiv \begin{pmatrix} u_\kappa^{(\mathrm{u})}(x) \\ u_\kappa^{(\mathrm{l})}(x) \end{pmatrix}, \tag{3.99}$$

or, in terms of the Pauli matrices (2.13),

$$\left[\frac{\mathrm{d}}{\mathrm{d}x} + \frac{1}{x}\left(\kappa\sigma_3 + \mathrm{i}\alpha Z_\infty\sigma_2\right) - \frac{\mathrm{i}}{k\hbar\,c}\left(W\sigma_2 - \mathrm{i}\mathrm{m_e}c^2\sigma_1\right)\right] u_\kappa(x) = 0. \tag{3.100}$$

[8] However, it is well known that the Klein–Gordon equation (also called the relativistic Schrödinger equation) for a Coulomb potential can be reduced to a form equivalent to Eq. (3.4) (see Schiff, 1968).

From the structure of this equation, it is natural to define the matrices

$$\Xi \equiv \frac{1}{k\hbar\, c}\left(W\sigma_2 - \mathrm{i}m_e c^2\sigma_1\right) = \frac{1}{k\hbar\, c}\begin{pmatrix} 0 & -\mathrm{i}\,(W+m_e c^2) \\ \mathrm{i}\,(W-m_e c^2) & 0 \end{pmatrix} \tag{3.101}$$

and

$$\Lambda \equiv \frac{1}{\lambda}\left(\kappa\sigma_3 + \mathrm{i}\alpha Z_\infty \sigma_2\right) = \frac{1}{\lambda}\begin{pmatrix} \kappa & \alpha Z_\infty \\ -\alpha Z_\infty & -\kappa \end{pmatrix} \tag{3.102}$$

with

$$\lambda \equiv \sqrt{\kappa^2 - (\alpha Z_\infty)^2}. \tag{3.103}$$

The global factors in these matrices are such that

$$\Xi^2 = \Lambda^2 = I_2 \qquad \text{and} \qquad \Lambda\,\Xi + \Xi\,\Lambda = \frac{2\mathrm{i}\,\alpha Z_\infty W}{\lambda\, k\hbar\, c}\, I_2. \tag{3.104}$$

Equation (3.100) can now be written in the more compact form

$$\frac{\mathrm{d}u_\kappa}{\mathrm{d}x} = \left(-\frac{\lambda}{x}\,\Lambda + \mathrm{i}\,\Xi\right) u_\kappa. \tag{3.105}$$

Following Kolsrud (1966), this equation is "squared" as

$$\frac{\mathrm{d}^2 u_\kappa}{\mathrm{d}x^2} = \frac{\lambda}{x^2}\,\Lambda\, u_\kappa + \left(-\frac{\lambda}{x}\,\Lambda + \mathrm{i}\,\Xi\right)^2 u_\kappa. \tag{3.106}$$

Using the properties (3.104) of the Ξ and Λ matrices, and introducing the *relativistic Sommerfeld parameter* [cf. Eq. (3.6)]

$$\eta = \frac{\alpha Z_\infty W}{k\hbar\, c} = \alpha Z_\infty \frac{c}{v} = \frac{Z_\infty e^2}{\hbar v} \tag{3.107}$$

we obtain

$$\left(\frac{\mathrm{d}^2}{\mathrm{d}x^2} + 1 - \frac{2\eta}{x} - \frac{\lambda(\lambda+\Lambda)}{x^2}\right) u_\kappa = 0, \tag{3.108}$$

which has a clear resemblance with the non-relativistic equation (3.17). An even closer similarity is obtained by introducing a linear transformation D that diagonalises Λ,

$$D\;\Lambda\; D^{-1} = \sigma_3. \tag{3.109}$$

The required transformation is

$$D = \Lambda + \sigma_3 = \frac{1}{\lambda}\begin{pmatrix} \kappa+\lambda & \alpha Z_\infty \\ -\alpha Z_\infty & -\kappa-\lambda \end{pmatrix}, \qquad D^{-1} = \frac{\lambda}{2(\kappa+\lambda)} D, \tag{3.110}$$

and the transformed second-order equation reads

$$\left(\frac{\mathrm{d}^2}{\mathrm{d}x^2} + 1 - \frac{2\eta}{x} - \frac{\lambda(\lambda+\sigma_3)}{x^2}\right) D u_\kappa = 0. \tag{3.111}$$

It then follows that

$$Du_\kappa = \begin{pmatrix} q_1\, U_\lambda(\eta, x) \\ q_2\, U_{\lambda-1}(\eta, x) \end{pmatrix}, \tag{3.112}$$

where the functions $U_\lambda(\eta, x)$ are solutions of the equation (3.17), *i.e.*, the usual Schrödinger–Coulomb functions, with the indicated parameters. This is the essential result obtained by Kolsrud (1966) and by Auvil and Brown (1978).

The ratio of the coefficients q_1 and q_2 is determined by transforming the first-order equation (3.105),

$$\left(\frac{\mathrm{d}}{\mathrm{d}x} + \frac{\lambda}{x}\,\sigma_3 - \mathrm{i}\, D\,\Xi\, D^{-1}\right) Du_\kappa = 0. \tag{3.113}$$

A simple calculation shows that

$$-\mathrm{i}\, D\,\Xi\, D^{-1} = \frac{1}{\lambda\, k\hbar\, c} \begin{pmatrix} \alpha Z_\infty\, W & \lambda\, \mathrm{m_e}c^2 + \kappa\, W \\ \lambda\, \mathrm{m_e}c^2 - \kappa\, W & -\alpha Z_\infty\, W \end{pmatrix},$$

and Eq. (3.113) takes the form

$$\begin{pmatrix} \dfrac{\mathrm{d}}{\mathrm{d}x} + \dfrac{\lambda}{x} + \dfrac{\eta}{\lambda} & \dfrac{1}{\lambda\, k\hbar\, c}\left(\lambda\, \mathrm{m_e}c^2 + \kappa\, W\right) \\ \dfrac{1}{\lambda\, k\hbar\, c}\left(\lambda\, \mathrm{m_e}c^2 - \kappa\, W\right) & \dfrac{\mathrm{d}}{\mathrm{d}x} - \dfrac{\lambda}{x} - \dfrac{\eta}{\lambda} \end{pmatrix} \begin{pmatrix} q_1\, U_\lambda(\eta, x) \\ q_2\, U_{\lambda-1}(\eta, x) \end{pmatrix} = 0. \tag{3.114}$$

Using the recurrence relations (3.31b) and (3.32a) of the Coulomb functions, we get the couple of linearly dependent equations

$$\begin{aligned} \sqrt{\lambda^2 + \eta^2}\; k\hbar\, c\; q_1 + \left(\lambda\, \mathrm{m_e}c^2 + \kappa\, W\right) q_2 \;&=\; 0, \\ \left(\lambda\, \mathrm{m_e}c^2 - \kappa\, W\right) q_1 - \sqrt{\lambda^2 + \eta^2}\; k\hbar\, c\; q_2 \;&=\; 0, \end{aligned} \tag{3.115}$$

which give

$$\frac{q_1}{q_2} = \frac{\sqrt{\lambda^2 + \eta^2}\; k\hbar\, c}{\lambda\, \mathrm{m_e}c^2 - \kappa\, W}. \tag{3.116}$$

We can thus write

$$\begin{pmatrix} u_\kappa^{(\mathrm{u})}(\eta, x) \\ u_\kappa^{(\mathrm{l})}(\eta, x) \end{pmatrix} = N D^{-1} \begin{pmatrix} \sqrt{\lambda^2 + \eta^2}\; k\hbar\, c\; U_\lambda(\eta, x) \\ \left(\lambda\, \mathrm{m_e}c^2 - \kappa\, W\right)\; U_{\lambda-1}(\eta, x) \end{pmatrix}, \tag{3.117}$$

where N is a normalisation constant. Hence, the Dirac–Coulomb radial functions can be expressed in the form

$$\begin{aligned} u_\kappa^{(\mathrm{u})}(\eta, x) &= N\left[(\kappa + \lambda)\sqrt{\lambda^2 + \eta^2}\; k\hbar\, c\; U_\lambda(\eta, x) + \alpha Z_\infty \left(\lambda\, \mathrm{m_e}c^2 - \kappa\, W\right)\; U_{\lambda-1}(\eta, x)\right], \\ u_\kappa^{(\mathrm{l})}(\eta, x) &= -N\left[\alpha Z_\infty \sqrt{\lambda^2 + \eta^2}\; k\hbar\, c\; U_\lambda(\eta, x) + (\kappa + \lambda)\left(\lambda\, \mathrm{m_e}c^2 - \kappa\, W\right)\; U_{\lambda-1}(\eta, x)\right]. \end{aligned} \tag{3.118}$$

Finally, the normalisation constant N is fixed by requiring that $u_\kappa^{(\mathrm{u})}(\eta, x)$ oscillates asymptotically with unit amplitude.

We recall that the form (3.118) applies to *both* the regular and irregular Dirac–Coulomb functions, which will be denoted as $f_\kappa^{(\mathrm{u,l})}(x)$ and $g_\kappa^{(\mathrm{u,l})}(x)$, respectively. Considering this, and the asymptotic behaviour of the Coulomb functions [Eqs. (3.20) and (3.24)], we have

$$g_\kappa^{(\mathrm{u})}(x) + \mathrm{i} f_\kappa^{(\mathrm{u})}(x) \sim N \Big[(\kappa+\lambda)\sqrt{\lambda^2+\eta^2}\; k\hbar\, c\; \exp(\mathrm{i}\Delta\theta) + \alpha Z_\infty \left(\lambda\, \mathrm{m_e}c^2 - \kappa\, W\right) \Big] \exp(\mathrm{i}\theta_{\lambda-1}).$$

From the definitions (3.21) and (3.29), using the properties of the Γ function, we find that the phase difference $\Delta\theta \equiv \theta_\lambda - \theta_{\lambda-1}$ is

$$\Delta\theta = -\frac{\pi}{2} + \arg\frac{\Gamma(\lambda+1+\mathrm{i}\eta)}{\Gamma(\lambda+\mathrm{i}\eta)} = -\frac{\pi}{2} + \arg(\lambda+\mathrm{i}\eta) \tag{3.119}$$

and

$$\exp(\mathrm{i}\Delta\theta) = \frac{\eta - \mathrm{i}\lambda}{\sqrt{\lambda^2+\eta^2}}. \tag{3.120}$$

Therefore,

$$\begin{aligned} g_\kappa^{(\mathrm{u})}(x) + \mathrm{i} f_\kappa^{(\mathrm{u})}(x) &\sim N \left[(\kappa+\lambda)\; k\hbar\, c\; (\eta - \mathrm{i}\,\lambda) + \alpha Z_\infty \left(\lambda\, \mathrm{m_e}c^2 - \kappa\, W\right) \right] \exp(\mathrm{i}\theta_{\lambda-1}) \\ &= N\lambda \left[\alpha Z_\infty \left(W + \mathrm{m_e}c^2\right) - \mathrm{i}\; (\kappa+\lambda)\; k\hbar\, c \right] \exp(\mathrm{i}\theta_{\lambda-1}). \end{aligned} \tag{3.121}$$

We obtain the desired asymptotic behaviour by setting

$$N = \pm\, \frac{1}{\lambda} \left[(\alpha Z_\infty)^2 \left(W + \mathrm{m_e}c^2\right)^2 + (\kappa+\lambda)^2 (k\hbar\, c)^2 \right]^{-1/2}, \tag{3.122}$$

so that

$$g_\kappa^{(\mathrm{u})}(x) + \mathrm{i} f_\kappa^{(\mathrm{u})}(x) \sim \pm \exp\left[\mathrm{i}\,(\nu + \theta_{\lambda-1})\right] \tag{3.123}$$

with

$$\nu = \arg\left[\alpha Z_\infty \left(W + \mathrm{m_e}c^2\right) - \mathrm{i}\; (\kappa+\lambda)\; k\hbar\, c \right]. \tag{3.124}$$

This completes the derivation of the normalised Dirac–Coulomb radial functions. The simplicity of this last step is in marked contrast with the elaborate manipulations needed to obtain the normalisation constant in the standard derivation (see, *e.g.*, Rose, 1961; Greiner, 1990).

As a matter of fact, there is a physically irrelevant sign ambiguity in expression (3.122). The "good" sign is obtained by requiring that, in the non-relativistic limit $c \to \infty$ ($E \ll \mathrm{m_e}c^2$, $\lambda \to |\kappa|$), the small radial functions $u_\kappa^{(\mathrm{l})}$ vanish and the large functions reduce to the non-relativistic Coulomb functions

$$f_\kappa^{(\mathrm{u})}(x) \xrightarrow{\text{n.r.}} F_\ell(\eta, x), \qquad g_\kappa^{(\mathrm{u})}(x) \xrightarrow{\text{n.r.}} G_\ell(\eta, x), \tag{3.125}$$

where ℓ stands for the orbital angular momentum quantum number ($\ell = \kappa$ if $\kappa > 0$ and $\ell = -\kappa - 1$ if $\kappa < 0$). This is accomplished by taking the minus sign in Eq. (3.122) when Z_∞ *and* κ are negative, and the plus sign otherwise. That is,

$$N = (1 - 2\mathcal{S}_{Z_\infty,\kappa})\,\frac{1}{\lambda}\,\left[(\alpha Z_\infty)^2\left(W + \mathrm{m_e}c^2\right)^2 + (\kappa+\lambda)^2(k\hbar\,c)^2\right]^{-1/2}, \tag{3.126}$$

where $\mathcal{S}_{Z_\infty,\kappa} = 1$ if $Z_\infty < 0$ and $\kappa < 0$, and $= 0$ otherwise.

Asymptotically, the upper-component radial functions behave as

$$f_\kappa^{(\mathrm{u})}(x) \sim \sin\,\phi_\kappa \qquad \text{and} \qquad g_\kappa^{(\mathrm{u})}(x) \sim \cos\,\phi_\kappa, \tag{3.127}$$

with

$$\phi_\kappa = \nu + \theta_{\lambda-1} - \mathcal{S}_{Z_\infty,\kappa}\,\pi.$$

We can write this last expression in the more conventional form

$$\phi_\kappa = x - \ell\frac{\pi}{2} - \eta\,\ln(2x) + \Delta_\kappa. \tag{3.128}$$

where we have introduced the Dirac–Coulomb phase shift defined as

$$\Delta_\kappa \equiv \nu - (\lambda - \ell - 1)\frac{\pi}{2} + \arg\Gamma(\lambda + \mathrm{i}\eta) - \mathcal{S}_{Z_\infty,\kappa}\,\pi. \tag{3.129}$$

With the adopted sign convention, Dirac–Coulomb phase shifts vanish in the zero potential limit. The asymptotic behaviour of the lower component functions is easily obtained by means of the first of the Dirac equations (3.97),

$$u_\kappa^{(\mathrm{l})} \sim \frac{\hbar k\,c}{W + \mathrm{m_e}c^2}\,\frac{\mathrm{d}u_\kappa^{(\mathrm{u})}(x)}{\mathrm{d}x} = \sqrt{\frac{W - \mathrm{m_e}c^2}{W + \mathrm{m_e}c^2}}\,\frac{\mathrm{d}u_\kappa^{(\mathrm{u})}(x)}{\mathrm{d}x}, \tag{3.130}$$

which gives

$$f_\kappa^{(\mathrm{l})}(x) \sim \sqrt{\frac{W - \mathrm{m_e}c^2}{W + \mathrm{m_e}c^2}}\,\cos\,\phi_\kappa \qquad \text{and} \qquad g_\kappa^{(\mathrm{l})}(x) \sim -\sqrt{\frac{W - \mathrm{m_e}c^2}{W + \mathrm{m_e}c^2}}\,\sin\,\phi_\kappa. \tag{3.131}$$

In the limit of zero potential strength ($Z_\infty \to 0, \lambda = |\kappa|$), we find

$$\begin{aligned} &u_\kappa^{(\mathrm{u})}(x) = U_\kappa(0,x), \qquad u_\kappa^{(\mathrm{l})}(x) = \sqrt{\frac{W - \mathrm{m_e}c^2}{W + \mathrm{m_e}c^2}}\,U_{\kappa-1}(0,x) \qquad \text{if } \kappa > 0, \\ &u_\kappa^{(\mathrm{u})}(x) = U_{-\kappa-1}(0,x), \quad u_\kappa^{(\mathrm{l})}(x) = -\sqrt{\frac{W - \mathrm{m_e}c^2}{W + \mathrm{m_e}c^2}}\,U_{-\kappa}(0,x) \quad \text{if } \kappa < 0. \end{aligned} \tag{3.132}$$

With the aid of the relations (3.65a) and (3.65b), we are lead to the familiar result that free particle Dirac radial functions are spherical Bessel functions (see, *e.g.*, Rose, 1961, p. 161).

The RADIAL package includes the subroutine `DCOULF`, which computes the free-state Dirac–Coulomb functions $f_\kappa^{(\mathrm{u,l})}(r)$ and $g_\kappa^{(\mathrm{u,l})}(r)$ by using the values of the Schrödinger–Coulomb functions delivered by subroutine `FCOUL`.

3.2.2 Dirac–Coulomb functions of bound states

Let us now consider the Dirac–Coulomb wave functions of bound states ($E < 0$, $W < \mathrm{m_e}c^2$) of an attractive Coulomb potential ($Z_\infty < 0$). As in the non-relativistic theory, the wave functions of bound states have the same analytical form as the regular free waves, but only those values of the energy which yield square-integrable wave functions are allowed. Denoting, as usually, the large and small radial wave functions by $P(r)$ and $Q(r)$, and using the expression (3.18) of the non-relativistic regular Coulomb functions, Eq. (3.117) implies that

$$\begin{pmatrix} P(r) \\ Q(r) \end{pmatrix} = N\, D^{-1} \begin{pmatrix} X \\ Y \end{pmatrix} \tag{3.133}$$

where N is a global normalisation constant, which includes common constant factors,

$$\begin{aligned} X &\equiv x^\lambda\, \exp(\mathrm{i}x)\, \sqrt{\lambda^2+\eta^2}\, c\hbar k\, x\; {}_1F_1(\lambda+1+\mathrm{i}\eta; 2\lambda+2; -2\mathrm{i}x), \\ Y &\equiv x^\lambda\, \exp(\mathrm{i}x)\, \left(\lambda \mathrm{m_e}c^2 - \kappa W\right) \frac{C_{\lambda-1}(\eta)}{C_\lambda(\eta)}\; {}_1F_1(\lambda+\mathrm{i}\eta; 2\lambda; -2\mathrm{i}x) \\ &= x^\lambda\, \exp(\mathrm{i}x)\, \left(\lambda \mathrm{m_e}c^2 - \kappa W\right) \frac{\lambda(2\lambda+1)}{\sqrt{\lambda^2+\eta^2}}\; {}_1F_1(\lambda+\mathrm{i}\eta; 2\lambda; -2\mathrm{i}x) \end{aligned} \tag{3.134}$$

and $x = kr$. To write the last expression for Y, we have used the relation [see Eq. (3.19)]

$$\frac{C_{\lambda-1}(\eta)}{C_\lambda(\eta)} = \frac{\lambda(2\lambda+1)}{|\lambda+\mathrm{i}\eta|} = \frac{\lambda(2\lambda+1)}{\sqrt{\lambda^2+\eta^2}}. \tag{3.135}$$

In order to deal only with real quantities, we set

$$k = \frac{\sqrt{W^2 - \mathrm{m_e}^2c^4}}{\hbar c} = \mathrm{i}a \qquad \text{and} \qquad \eta = \frac{Z_\infty e^2}{\hbar c}\,\frac{W}{c\hbar k} = \mathrm{i}\overline{\eta}, \tag{3.136}$$

with

$$a \equiv \frac{\sqrt{\mathrm{m_e}^2c^4 - W^2}}{\hbar c} \qquad \text{and} \qquad \overline{\eta} \equiv -\,\frac{\alpha Z_\infty\, W}{c\hbar a}\,. \tag{3.137}$$

Note that $\overline{\eta}$ is positive (otherwise, bound states would not exist). We can then write (apart from a common constant factor)

$$\begin{aligned} X &= (2ar)^\lambda\, \exp(-ar)\, \frac{\lambda^2-\overline{\eta}^2}{\lambda \mathrm{m_e}c^2 - \kappa W}\, c\hbar a\, 2ar\; {}_1F_1(\lambda+1-\overline{\eta}; 2\lambda+2; 2ar), \\ Y &= -(2ar)^\lambda\, \exp(-ar)\, 2\lambda(2\lambda+1)\; {}_1F_1(\lambda-\overline{\eta}; 2\lambda; 2ar). \end{aligned}$$

Noting that

$$\frac{\lambda^2-\overline{\eta}^2}{\lambda \mathrm{m_e}c^2 - \kappa W} = \frac{\lambda \mathrm{m_e}c^2 + \kappa W}{\mathrm{m_e}^2c^4 - W^2} = \frac{\lambda \mathrm{m_e}c^2 + \kappa W}{(c\hbar a)^2}, \tag{3.138}$$

we have

$$\begin{aligned} X &= (2ar)^\lambda\, \exp(-ar)\, \frac{\lambda \mathrm{m_e}c^2 + \kappa W}{c\hbar a}\, 2ar\; {}_1F_1(\lambda+1-\overline{\eta}; 2\lambda+2; 2ar), \\ Y &= -(2ar)^\lambda\, \exp(-ar)\, 2\lambda(2\lambda+1)\; {}_1F_1(\lambda-\overline{\eta}; 2\lambda; 2ar). \end{aligned} \tag{3.139}$$

Inserting these expressions in Eq. (3.133), and writing [see Eq. (3.110)]

$$D^{-1} \sim \begin{pmatrix} \kappa+\lambda & \alpha Z_\infty \\ -\alpha Z_\infty & -\kappa-\lambda \end{pmatrix},$$

we obtain the following expressions for the large and small radial functions,

$$\begin{aligned} P(r) = N\,(2ar)^\lambda \exp(-ar)\,\Big[&-\alpha Z_\infty\, 2\lambda(2\lambda+1)\;{}_1F_1(\lambda-\overline{\eta};2\lambda;2ar) \\ &+ (\kappa+\lambda)\,\frac{\lambda \mathrm{m_e}c^2+\kappa W}{c\hbar a}\,2ar\;{}_1F_1(\lambda+1-\overline{\eta};2\lambda+2;2ar)\Big], \\ Q(r) = N\,(2ar)^\lambda\,\exp(-ar)\,\Big[&(\kappa+\lambda)\,2\lambda(2\lambda+1)\;{}_1F_1(\lambda-\overline{\eta};2\lambda;2ar) \\ &- \alpha Z_\infty\,\frac{\lambda \mathrm{m_e}c^2+\kappa W}{c\hbar a}\,2ar\;{}_1F_1(\lambda+1-\overline{\eta};2\lambda+2;2ar)\Big]. \end{aligned} \tag{3.140}$$

The confluent hypergeometric functions ${}_1F_1$ diverge like $\exp(2ar)$ when r tends to infinity [see Eq. (3.11)]. Hence, to obtain a square-integrable wave function, the series (3.9) for ${}_1F_1(\lambda-\overline{\eta};2\lambda;2ar)$ must terminate after a finite number of terms. That is, $\lambda-\overline{\eta}$ must be a negative integer,

$$\lambda-\overline{\eta} = -n', \qquad n' = 0,1,2,\ldots \tag{3.141}$$

This condition determines the energy levels, which are given by

$$W = \mathrm{m_e}c^2\left(1+\frac{(\alpha Z_\infty)^2}{(n'+\lambda)^2}\right)^{-1/2}. \tag{3.142}$$

That is,

$$W_{n\kappa} = \mathrm{m_e}c^2\left(1+\frac{(\alpha Z_\infty)^2}{\left(n-|\kappa|+\sqrt{\kappa^2-(\alpha Z_\infty)^2}\right)^2}\right)^{-1/2}, \tag{3.143}$$

where we have introduced the principal quantum number

$$n \equiv |\kappa| + n' \tag{3.144}$$

and indicated that each individual level is identified by the values of the quantum numbers n and κ. Alternatively, instead of κ we can specify ℓ and j [see Eqs. (2.19) and Table 1].

Thus, when $n'>0$, the Kummer functions in Eqs. (3.140) reduce to Laguerre polynomials, Eq. (3.84), and the wave function is indeed square integrable. The case $n'=0$ ($|\kappa|=n$, $\lambda=\overline{\eta}$) requires special consideration, because the function ${}_1F_1(1;2\lambda+2;2ar)$ diverges when $r\to\infty$. If $n'=0$, κ can take the values $\pm n$, which correspond to

$$j = n-\tfrac{1}{2} \quad \text{and} \quad \ell = \begin{cases} n-1 & \text{if } \kappa=-n, \\ n & \text{if } \kappa=n. \end{cases}$$

Moreover,

$$W_{n,\kappa=\pm n} = \mathrm{m_e}c^2 \left(1 + \frac{(\alpha Z_\infty)^2}{\lambda^2}\right)^{-1/2} = \mathrm{m_e}c^2 \frac{\lambda}{|\kappa|}, \tag{3.145}$$

so that

$$\lambda \mathrm{m_e}c^2 + \kappa W_{n,\kappa=\pm n} = \lambda \mathrm{m_e}c^2 \left(1 + \frac{\kappa}{|\kappa|}\right). \tag{3.146}$$

To get a square-integrable wave function, the last quantity must vanish to remove the second terms in expressions (3.140). This implies that states with $\kappa = n$ (*i.e.*, with $\ell = n$) do not exist. Consequently, a bound level $W_{n\kappa}$ exists only if $n > \ell$; this condition holds also in the non-relativistic theory. Summarizing, for a given value of κ, bound energy levels $W_{n\kappa}$ exist for all $n \geq |\kappa|$, except when κ is positive, in which case the level with $n = \kappa$ does not occur. Conversely, for a given value of n, we have bound levels $W_{n\kappa}$ with κ from $-n$ to $n-1$. Note that the energies $W_{n\kappa}$ are independent of the sign of κ, that is, levels with the same principal quantum number and opposite values of κ (*i.e.*, with the same j and with $\ell = j \pm 1/2$) are degenerate.

It is convenient to introduce the quantity

$$\tau \equiv \frac{-\alpha Z_\infty}{\lambda + n'}, \tag{3.147}$$

and write[9]

$$a = \frac{\mathrm{m_e}c}{\hbar}\sqrt{\frac{\tau^2}{1+\tau^2}}, \qquad \frac{W_{n\kappa}}{c\hbar a} = \frac{1}{\tau} \qquad \text{and} \qquad \frac{\mathrm{m_e}c^2}{c\hbar a} = \frac{\sqrt{1+\tau^2}}{\tau}. \tag{3.148}$$

Thus, the radial functions (3.140) take the form

$$P_{n\kappa}(r) = N_{n\kappa}\,(2ar)^\lambda\,\exp(-ar)\left[-\alpha Z_\infty\, 2\lambda(2\lambda+1)\;{}_1F_1(-n';2\lambda;2ar)\right.$$
$$\left. + (\kappa+\lambda)\,\frac{\kappa+\lambda\sqrt{1+\tau^2}}{\tau}\,2ar\;{}_1F_1(-n'+1;2\lambda+2;2ar)\right], \tag{3.149a}$$

$$Q_{n\kappa}(r) = N_{n\kappa}\,(2ar)^\lambda\,\exp(-ar)\left[(\kappa+\lambda)\,2\lambda(2\lambda+1)\;{}_1F_1(-n';2\lambda;2ar)\right.$$
$$\left. - \alpha Z_\infty\,\frac{\kappa+\lambda\sqrt{1+\tau^2}}{\tau}\,2ar\;{}_1F_1(-n'+1;2\lambda+2;2ar)\right]. \tag{3.149b}$$

To determine the normalisation constant, $N_{n\kappa}$, we replace the Kummer functions by the corresponding Laguerre polynomials [see Eq. (3.84)],

$${}_1F_1(-n';2\lambda;y) = \frac{(2\lambda-1)!\,n'!}{(2\lambda-1+n')!}\,L_{n'}^{2\lambda-1}(y),$$

[9] $\hbar/(\mathrm{m_e}c) = \alpha a_0 = 3.861\,593 \times 10^{-11}$ cm is the reduced Compton wavelength (Mohr *et al.*, 2016).

we set $y = 2ar$ and write

$$P_{n\kappa}(r) = N_{n\kappa}\,\frac{(2\lambda+1)!\,(n'-1)!}{(2\lambda+n')!}\,y^{\lambda}\exp(-y/2)$$
$$\times\left[-\alpha Z_\infty\,(2\lambda+n')\,n'\,L_{n'}^{2\lambda-1}(y)+(\kappa+\lambda)\,\frac{\kappa+\lambda\sqrt{1+\tau^2}}{\tau}\,y\,L_{n'-1}^{2\lambda+1}(y)\right],$$
$$Q_{n\kappa}(r) = N_{n\kappa}\,\frac{(2\lambda+1)!\,(n'-1)!}{(2\lambda+n')!}\,y^{\lambda}\exp(-y/2)$$
$$\times\left[(\kappa+\lambda)\,(2\lambda+n')\,n'\,L_{n'}^{2\lambda-1}(y)-\alpha Z_\infty\,\frac{\kappa+\lambda\sqrt{1+\tau^2}}{\tau}\,y\,L_{n'-1}^{2\lambda+1}(y)\right]. \quad (3.150)$$

Noting that, by virtue of Eqs. (3.137), (3.141) and (3.148),

$$(2\lambda+n')\,n' = \overline{\eta}^2-\lambda^2 = \frac{\kappa+\lambda\sqrt{1+\tau^2}}{\tau}\,\frac{\kappa-\lambda\sqrt{1+\tau^2}}{\tau}, \quad (3.151)$$

we can write

$$P_{n\kappa}(r) = \mathcal{A}\,y^{\lambda}\exp(-y/2)\left[-\alpha Z_\infty\,\frac{\kappa-\lambda\sqrt{1+\tau^2}}{\tau}\;L_{n'}^{2\lambda-1}(y)+(\kappa+\lambda)\,y\,L_{n'-1}^{2\lambda+1}(y)\right],$$
$$Q_{n\kappa}(r) = \mathcal{A}\,y^{\lambda}\exp(-y/2)\left[(\kappa+\lambda)\,\frac{\kappa-\lambda\sqrt{1+\tau^2}}{\tau}\,L_{n'}^{2\lambda-1}(y)-\alpha Z_\infty\,y\,L_{n'-1}^{2\lambda+1}(y)\right], \quad (3.152)$$

where

$$\mathcal{A} \equiv N_{n\kappa}\,\frac{\kappa+\lambda\sqrt{1+\tau^2}}{\tau}\,\frac{(2\lambda+1)!\,(n'-1)!}{(2\lambda+n')!}. \quad (3.153)$$

Then,

$$\mathcal{S} \equiv \int_0^\infty \left[P_{n\kappa}^2(r)+Q_{n\kappa}^2(r)\right]\mathrm{d}r = \frac{\mathcal{A}^2}{2a}\left\{\left[(\alpha Z_\infty)^2+(\kappa+\lambda)^2\right]\left(\frac{\kappa-\lambda\sqrt{1+\tau^2}}{\tau}\right)^2 I_1\right.$$
$$\left.-\,4\alpha Z_\infty\,(\kappa+\lambda)\,\frac{\kappa-\lambda\sqrt{1+\tau^2}}{\tau}\,I_2+\left[(\alpha Z_\infty)^2+(\kappa+\lambda)^2\right]I_3\right\} \quad (3.154)$$

with

$$I_1 \equiv \int_0^\infty \mathrm{e}^{-y}y^{2\lambda}\left[L_{n'}^{2\lambda-1}(y)\right]^2\,\mathrm{d}y = 2(\lambda+n')\,\frac{(2\lambda+n'-1)!}{n'!}, \quad (3.155a)$$

$$I_2 \equiv \int_0^\infty \mathrm{e}^{-y}y^{2\lambda+1}L_{n'}^{2\lambda-1}(y)\,L_{n'-1}^{2\lambda+1}(y)\,\mathrm{d}y = -2\frac{(2\lambda+n')!}{(n'-1)!}, \quad (3.155b)$$

$$I_3 \equiv \int_0^\infty \mathrm{e}^{-y}y^{2\lambda+2}\left[L_{n'-1}^{2\lambda+1}(y)\right]^2\,\mathrm{d}y = 2(\lambda+n')\,\frac{(2\lambda+n')!}{(n'-1)!}, \quad (3.155c)$$

where use has been made of the results (3.91) and (3.92). Inserting these expressions on the right-hand side of Eq. (3.154), we obtain

$$\begin{aligned}\mathcal{S} &= \frac{\mathcal{A}^2}{a}\frac{(2\lambda+n')!}{(n'-1)!}\left\{\left[(\alpha Z_\infty)^2+(\kappa+\lambda)^2\right]\left(\frac{\kappa-\lambda\sqrt{1+\tau^2}}{\tau}\right)^2\frac{\lambda+n'}{(2\lambda+n')n'}\right.\\ &\qquad\left.+4\alpha Z_\infty\,(\kappa+\lambda)\,\frac{\kappa-\lambda\sqrt{1+\tau^2}}{\tau}+\left[(\alpha Z_\infty)^2+(\kappa+\lambda)^2\right](\lambda+n')\right\}\\ &= \frac{N_{n\kappa}^2}{a}\,\frac{\kappa+\lambda\sqrt{1+\tau^2}}{\tau}\,[(2\lambda+1)!]^2\,\frac{(n'-1)!}{(2\lambda+n')!}\\ &\qquad\times\left\{\left[(\alpha Z_\infty)^2+(\kappa+\lambda)^2\right](\lambda+n')\,\frac{2\kappa}{\tau}+4\alpha Z_\infty\,(\kappa+\lambda)\,(2\lambda+n')\,n'\right\}. \quad (3.156)\end{aligned}$$

After simple manipulations, the quantity in braces can be expressed as

$$\{\cdots\}=\frac{4\lambda^2}{\tau}\,(\kappa+\lambda)(\lambda+n')(1+\tau^2).$$

From the normalisation condition, $\mathcal{S}=1$, we finally obtain the following expression for the normalisation constant,

$$\begin{aligned}N_{n\kappa} &= \frac{1}{2\lambda\,(2\lambda+1)!}\left[(\kappa+\lambda)(\lambda+n')\left(\kappa+\lambda\sqrt{1+\tau^2}\right)(1+\tau^{-2})\right]^{-1/2}\\ &\qquad\times\left[\frac{(2\lambda+n')!\,a}{(n'-1)!}\right]^{1/2}, \quad (3.157)\end{aligned}$$

which is valid for states with $n'>0$. Inserting this expression into Eqs. (3.149) we get final expressions for the normalised bound-state radial functions.

The case $n'=0$ ($n=|\kappa|$) requires a specific treatment. For states with $n'=0$, the second terms in expressions (3.140) vanish and the Kummer functions in the first terms reduce to unity [see Eq. (3.9)]. Therefore, the radial functions of these states have the form

$$\begin{aligned}P_{n\kappa}(r) &= N_{n\kappa}\,(2ar)^\lambda\,\exp(-ar)\,(-\alpha Z_\infty)\,2\lambda(2\lambda+1),\\ Q_{n\kappa}(r) &= N_{n\kappa}\,(2ar)^\lambda\,\exp(-ar)\,(\kappa+\lambda)\,2\lambda(2\lambda+1). \quad (3.158)\end{aligned}$$

The normalisation integral can then be evaluated easily with the aid of Eq. (3.89),

$$\begin{aligned}\mathcal{S} &\equiv \int_0^\infty \left[P_{n\kappa}^2(r)+Q_{n\kappa}^2(r)\right]\mathrm{d}r\\ &= \left[N_{n\kappa}\,2\lambda(2\lambda+1)\right]^2\left[(\alpha Z_\infty)^2+(\kappa+\lambda)^2\right]\int_0^\infty (2ar)^{2\lambda}\exp(-2ar)\,\mathrm{d}r\\ &= \left[N_{n\kappa}\,2\lambda(2\lambda+1)\right]^2\left[(\alpha Z_\infty)^2+(\kappa+\lambda)^2\right]\frac{(2\lambda)!}{2a}=1.\end{aligned}$$

We thus conclude that

$$N_{n\kappa} = \frac{1}{2\lambda(2\lambda+1)\sqrt{(\alpha Z_\infty)^2 + (\kappa+\lambda)^2}} \sqrt{\frac{2a}{(2\lambda)!}}. \tag{3.159}$$

Summarizing, the normalised radial functions for states with $n = |\kappa|$ are given by

$$\begin{aligned} P_{n\kappa}(r) &= \sqrt{\frac{2a}{(2\lambda)!\,[(\alpha Z_\infty)^2 + (\kappa+\lambda)^2]}}\ (2ar)^\lambda \exp(-ar), \\ Q_{n\kappa}(r) &= \sqrt{\frac{2a}{(2\lambda)!\,[(\alpha Z_\infty)^2 + (\kappa+\lambda)^2]}}\ (\kappa+\lambda)\,(2ar)^\lambda \exp(-ar). \end{aligned} \tag{3.160}$$

It is worth noting that the quantity $\lambda = \sqrt{\kappa^2 - (\alpha Z_\infty)^2}$, Eq. (3.103), is real (and positive) only if $|Z_\infty| < |\kappa|/\alpha$; otherwise, solutions that are regular at the origin do not exist. In particular, this implies that a point nucleus with (positive) charge Ze [$V(r) = -Ze^2/r$] is capable of binding an electron in a state of angular momentum $\kappa = \pm 1$ only if $Z < \alpha^{-1} \simeq 137$. In fact, for $\kappa = \pm 1$, λ is less than 1 (even for relatively small Z values) and the Dirac–Coulomb functions, Eq. (3.149), diverge slightly at the origin [$r^{-1}P(r) \simeq r^{\lambda-1}$], although they are square summable. This behaviour is in contrast with that of non-relativistic Coulomb functions, which are finite at $r = 0$.

In the non-relativistic limit ($c \to \infty$), the large radial function $P_{n\kappa}$, Eq. (3.149a), reduces to the non-relativistic radial function $P_{n\ell}$, Eq. (3.83), and the small radial function $Q_{n\kappa}$ vanishes. In this limit, the prefactor of either the first or the second of the Kummer functions in the expression (3.149a) vanishes, depending on the sign of κ. It is also worth noting that the number of zeros of the large radial function (excluding the one at $r = 0$) *is not* $n' = n - |\kappa|$, but

$$n_\mathrm{r} = n - (\ell + 1). \tag{3.161}$$

This becomes evident when considering the non-relativistic limit. Figure 4 displays the radial wave functions $P_{n\kappa}$ and $Q_{n\kappa}$ for bound states with $\kappa = -1$ and $+1$ of the Coulomb potential with $Z_\infty = -100$, and the corresponding non-relativistic radial function $P_{n\ell}^{(\mathrm{n.r.})}$, Eq. (3.83). For such a high value of $|Z_\infty|$, relativistic effects are important. The most visible consequence of these effects is that the small function $Q_{n\kappa}$ takes values that are comparable to those of $P_{n\kappa}$. The latter is similar in shape to the corresponding non-relativistic function, but somewhat contracted towards the centre of force.

Attractive Coulomb potentials hold an infinite number of bound states, whose energies have an accumulation point at $E = 0$. Since the radial functions $P_{n\kappa}$ and $Q_{n\kappa}$ of negative- and positive-energy states obey the same differential equations, these functions vary continuously with the energy E of the electron at $E = 0$. That is, the radial functions of a highly excited bound state, with $n \gg 1$, and of a "slow" free state, with a small positive energy E, have similar shapes near the origin, in the interval of radial distances where $|V(r)| \gg E$. To reveal the continuity of the radial functions at $E = 0$,

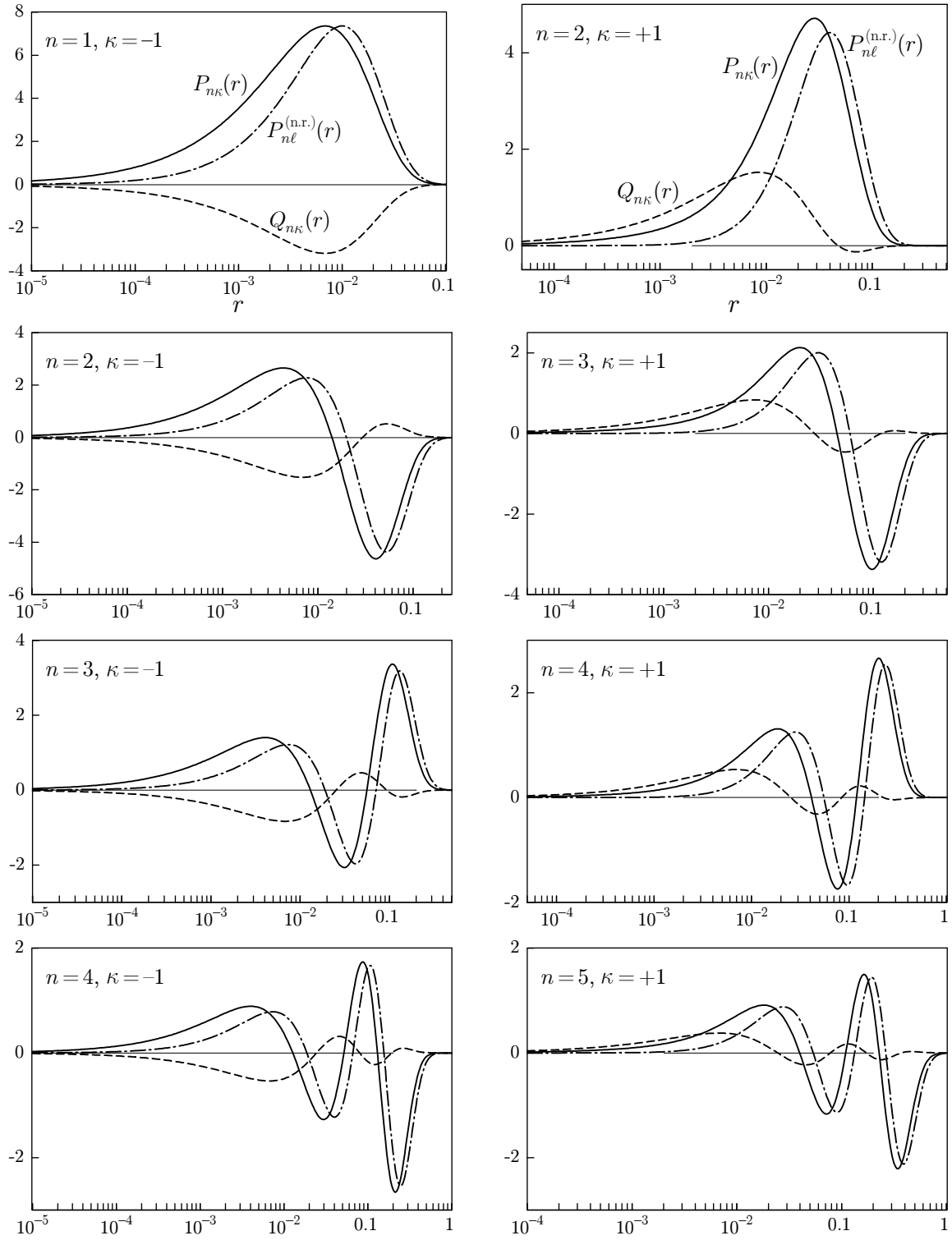

Figure 4: Dirac–Coulomb wave functions of bound states of the Coulomb potential with $Z_\infty = -100$. The continuous and dashed curves represent the large and small radial functions, $P_{n\kappa}(r)$ and $Q_{n\kappa}(r)$, respectively. The dot-dashed curves are the corresponding Schrödinger–Coulomb functions, $P^{(\mathrm{n.r.})}_{n\ell}(r)$ with $\ell = |\kappa| - [1 - \mathrm{sign}(\kappa)]/2$. All quantities are expressed in atomic units.

bound and free states should be normalised in an "analogous" way. Let us consider free states normalised on the energy scale [see Section 2.4, Eq. (2.49)],

$$P_{E\kappa}(r) = \sqrt{\frac{k}{\pi E}}\, f_\kappa^{(\mathrm{u})}(x) \underset{x\to\infty}{\sim} \sqrt{\frac{k}{\pi E}}\, \sin\left[x - \lambda\frac{\pi}{2} - \eta\ln(2x) + \Delta_\lambda\right]. \tag{3.162}$$

The analogous normalisation for bound states is obtained by observing that each energy level $W_{n\kappa}$ can be assigned the energy interval between the points

$$\frac{W_{n,\kappa} - W_{n-1,\kappa}}{2} \qquad \text{and} \qquad \frac{W_{n+1,\kappa} - W_{n,\kappa}}{2},$$

which are half way from the nearest levels, $W_{n-1,\kappa}$ and $W_{n+1,\kappa}$, respectively. The length of this interval is

$$\Delta E_{n\kappa} = \frac{W_{n+1,\kappa} - W_{n-1,\kappa}}{2}. \tag{3.163}$$

Bound states normalised "on the energy scale" satisfy the relation

$$\int_0^\infty \left[P_{n\kappa}^2(r) + Q_{n\kappa}^2(r)\right] \mathrm{d}r = \frac{1}{\Delta E_{n\kappa}}\,, \tag{3.164}$$

i.e., the radial functions of these states are $\sqrt{1/\Delta E_{n\kappa}}\, P_{n\kappa}(r)$ and $\sqrt{1/\Delta E_{n\kappa}}\, Q_{n\kappa}(r)$, where $P_{n\kappa}(r)$ and $Q_{n\kappa}(r)$ are the radial functions normalised to unity. Figure 5 compares the large components of Dirac–Coulomb functions of slow free states with $\kappa = 1$ for $Z_\infty = -1$ and $Z_\infty = -100$, with those of weakly bound states, all normalised on the energy scale. It is clear that, when $E \to 0$ and $n \to \infty$, the radial functions of free and bound states converge to a common limit. Of course, these functions differ at large radial distances, because the radial functions of free states oscillate with constant amplitude and very large wavelength, while those of the bound states vanish after $n - (\ell + 1)$ oscillations.

3.2.3 Regular Dirac–Coulomb functions

Dirac–Coulomb functions are utilised in quantum electrodynamics to account approximately for the effect of the Coulomb potential of the nucleus in the interactions of photons and charged particles with atomic electrons. In these calculations, it is customary to use the expressions of the regular Dirac–Coulomb functions derived by Rose (1961) (see also Greiner, 1990), which are slightly more compact than the ones obtained above. Rose's expressions for the free-state regular Dirac–Coulomb functions are as follows

$$f_\kappa^{(\mathrm{u})}(r) = A_\kappa\left[\mathcal{F}(r) + \mathcal{F}^*(r)\right], \qquad f_\kappa^{(\mathrm{l})}(r) = \frac{\mathrm{i}c\hbar k}{W + \mathrm{m_e}c^2}\, A_\kappa\left[\mathcal{F}(r) - \mathcal{F}^*(r)\right] \tag{3.165}$$

with

$$\mathcal{F}(r) = (\lambda - \mathrm{i}\eta)\, \exp(-\mathrm{i}kr + \mathrm{i}\nu)\, {}_1F_1(\lambda + 1 - \mathrm{i}\eta; 2\lambda + 1; 2\mathrm{i}kr) \tag{3.166}$$

and

$$A_\kappa = \pm\frac{\exp(-\pi\eta/2)|\Gamma(\lambda + \mathrm{i}\eta)|}{\Gamma(2\lambda + 1)}\, (2kr)^\lambda, \tag{3.167}$$

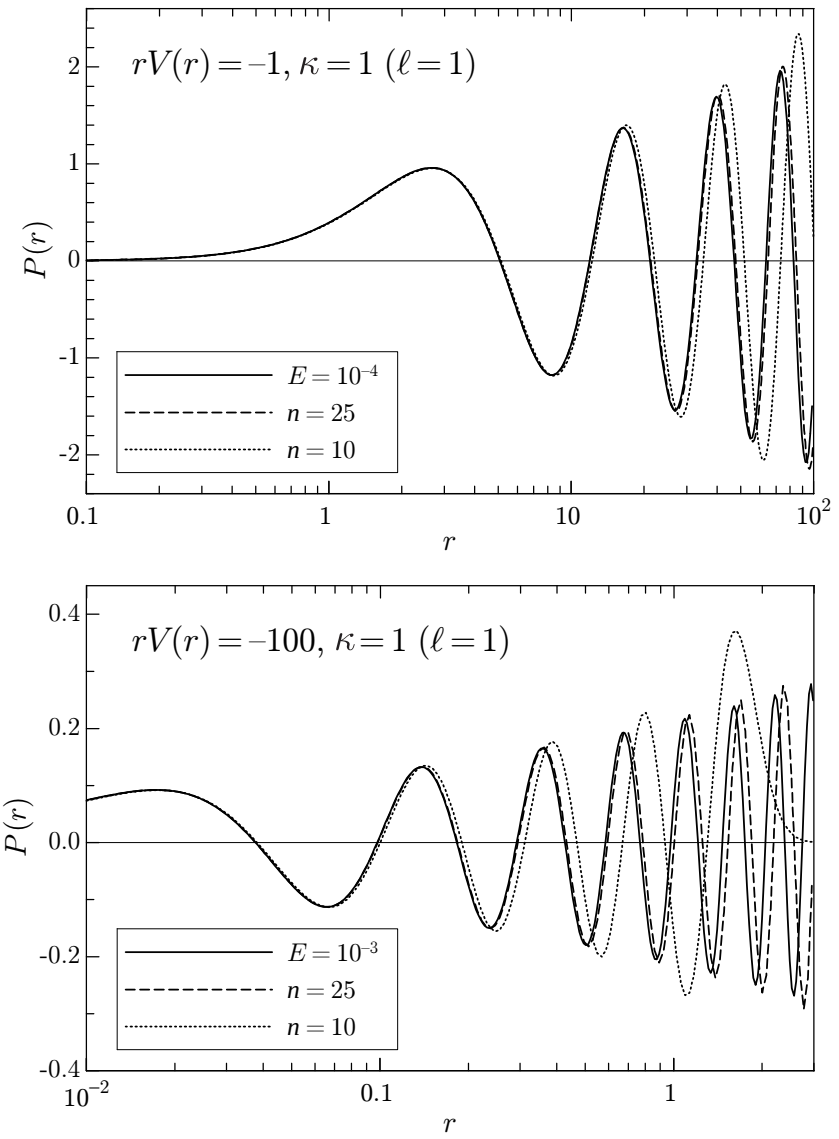

Figure 5: Dirac–Coulomb functions of bound states, $\sqrt{1/\Delta E_{n\kappa}}\, P_{n\kappa}(r)$ (normalised on the energy scale), and regular Dirac–Coulomb functions of free states, $\sqrt{k/\pi E}\, f_\kappa^{(\mathrm{u})}(kr)$ (also normalised in energy), for the indicated Coulomb potentials. All quantities are in atomic units.

where we have to take the minus sign when $Z_\infty < 0$ and $\kappa < 0$ and the plus sign otherwise. The constants in these expressions are defined by Eqs. (3.103), (3.107) and (3.124),

$$\lambda = \sqrt{\kappa^2 - (\alpha Z_\infty)^2}, \qquad \eta = \frac{\alpha Z_\infty W}{c\hbar k}, \qquad \nu = \arg\left[\alpha Z_\infty \left(W + \mathrm{m_e}c^2\right) - \mathrm{i}\,(\kappa + \lambda) c\hbar k\right].$$

The formulas (3.165) reproduce the regular Dirac–Coulomb functions derived in Section 3.2.1, including the normalisation and phase.

Rose also gave the following expressions for the radial functions of Dirac bound states for an attractive Coulomb potential, with $Z_\infty < 0$,

$$P_{n\kappa}(r) \;=\; B_{n\kappa} \sqrt{\frac{\mathrm{m_e}c^2 + W_{n\kappa}}{\mathrm{m_e}c^2}}\; (2ar)^\lambda \, \exp(-ar) \; J_+, \tag{3.168a}$$

$$Q_{n\kappa}(r) \;=\; B_{n\kappa} \sqrt{\frac{\mathrm{m_e}c^2 - W_{n\kappa}}{\mathrm{m_e}c^2}}\; (2ar)^\lambda \, \exp(-ar) \; J_-, \tag{3.168b}$$

where

$$J_\pm = n' \; {}_1F_1(-n'+1; 2\lambda+1; 2ar) \pm [\kappa - \alpha Z(\mathrm{m_e}c/\hbar a)] \; {}_1F_1(-n'; 2\lambda+1; 2ar), \tag{3.169}$$

$$B_{n\kappa} = \frac{\mathrm{sign}(\kappa)}{\Gamma(2\lambda+1)} \sqrt{\frac{a^3 \, \Gamma(2\lambda+n'+1)}{n'! \, 2 \, Z \, [Z - \kappa(\hbar a/\mathrm{m_e}c)]}}, \tag{3.170}$$

$$Z = -Z_\infty, \qquad n' = n - |\kappa|, \qquad a = \frac{\sqrt{\mathrm{m_e}^2c^4 - W_{n\kappa}^2}}{c\hbar}, \tag{3.171}$$

and $W_{n\kappa}$ is the energy of the bound state, given by Eq. (3.143). The radial functions of the ground state ($n = 1$, $\kappa = -1$) adopt the following simple expressions

$$P_{1,-1}(r) \;=\; \sqrt{\frac{1+\lambda}{2}} \sqrt{\frac{2Z/a_0}{\Gamma(2\lambda+1)}}\; (2Zr/a_0)^\lambda \, \exp\left(-Zr/a_0\right), \tag{3.172a}$$

$$Q_{1,-1}(r) \;=\; -\sqrt{\frac{1-\lambda}{2}} \sqrt{\frac{2Z/a_0}{\Gamma(2\lambda+1)}}\; (2Zr/a_0)^\lambda \, \exp\left(-Zr/a_0\right). \tag{3.172b}$$

Evidently, in the non-relativistic limit $P_{1,-1}(r)$ reduces to the Schrödinger radial function (3.95a) and $Q_{1,-1}(r)$ vanishes.

Expressions (3.165) and (3.168) are useful because they permit the exact analytical evaluation of certain integrals that occur in the theory of electromagnetic interactions with hydrogen atoms and one-electron ions (*e.g.*, photoelectric effect, internal conversion, pair production, ...). However, these expressions are of little use for computing the radial functions themselves because, when coded in a computer program, their numerical results may be affected by sizeable round-off errors. In the case of free states, at moderate and large radii, the radial functions (3.165) can be calculated with high accuracy by using the asymptotic expansion (3.11) of the Kummer functions. For bound states, the expressions (3.168) are strictly equivalent to the ones derived above [Eqs. (3.149) and (3.160)]. In the numerical calculation of the functions (3.168), round-off errors become manifest for states with principal quantum numbers larger than about 30 (*i.e.*, Rydberg states).

4 Power series solution of the radial equations

In the following Sections, and in the computer code, we use atomic units ($m_e = e = \hbar = 1$). In these units, the radial Schrödinger equation (2.6) takes the form

$$-\frac{1}{2}\frac{\mathrm{d}^2P}{\mathrm{d}r^2} + \left[V(r) + \frac{\ell(\ell+1)}{2r^2}\right]P = EP, \tag{4.1}$$

and the radial Dirac equations (2.21) read

$$\begin{aligned}\frac{\mathrm{d}P}{\mathrm{d}r} &= -\frac{\kappa}{r}P + \frac{E - V + 2c^2}{c}Q,\\ \frac{\mathrm{d}Q}{\mathrm{d}r} &= -\frac{E-V}{c}P + \frac{\kappa}{r}Q.\end{aligned} \tag{4.2}$$

Let us assume that the values $\mathcal{V}_i \equiv r_i V(r_i)$ have been given for a grid of points $r_1 = 0 < r_2 < \ldots < r_{\mathrm{NV}}$. In the calculations the function $\mathcal{V}(r)$ is approximated by the natural cubic spline (see Appendix A) which interpolates the input values, *i.e.*, by a piecewise cubic polynomial

$$\mathcal{V}(r) = v_0^{(i)} + v_1^{(i)} r + v_2^{(i)} r^2 + v_3^{(i)} r^3 \qquad \text{if } r_i \le r < r_{i+1} \tag{4.3}$$

with continuous first and second derivatives. Potentials having a finite number of discontinuities are dealt with by using different splines in each continuous region. In this case, the locations of the discontinuities are specified by simply introducing the two values of the potential for the *same* point; *i.e.*, when $r_i = r_{i+1}$ the adopted piecewise spline takes the values $\mathcal{V}_i$ and $\mathcal{V}_{i+1}$ to the left and right of r_i, respectively. The only requirements on the spacing of the grid points are: 1) the interpolation errors introduced by the spline approximation (4.3) have to be small and 2) the last grid point r_{NV} should be selected such that the potential function has reached its (constant) asymptotic value, *i.e.*, $\mathcal{V}(r) = \mathcal{V}(r_{\mathrm{NV}})$ for $r > r_{\mathrm{NV}}$. In fact, this last condition is implicitly assumed by RADIAL, which sets $\mathcal{V}(r) = \mathcal{V}(r_{\mathrm{NV}})$ for $r > r_{\mathrm{NV}}$. Notice that it is not necessary to use uniform grids.

4.1 Schrödinger equation

We consider that the values of the radial function and its first derivative at a given point r_a have already been computed. What we want to do is to evaluate the functions $P(r)$ and $P'(r) \equiv \mathrm{d}P/\mathrm{d}r$ in the interval between r_a and r_b, where the potential function $\mathcal{V}(r)$ is given by

$$\mathcal{V}(r) \equiv rV(r) = v_0 + v_1 r + v_2 r^2 + v_3 r^3. \tag{4.4}$$

Introducing the new variable

$$x \equiv (r - r_a)/h, \qquad h \equiv r_b - r_a, \tag{4.5}$$

the radial equation (4.1) transforms to

$$(r_{\rm a} + hx)^2 \, \frac{{\rm d}^2\mathcal{P}}{{\rm d}x^2} - h^2 \mathcal{U}(x)\, \mathcal{P} = 0, \tag{4.6}$$

with

$$\mathcal{P}(x) \equiv P(r) \tag{4.7}$$

and

$$\mathcal{U}(x) \equiv 2r^2[V(r) - E] + \ell(\ell+1) = u_0 + u_1 x + u_2 x^2 + u_3 x^3 + u_4 x^4, \tag{4.8}$$

where

$$\begin{aligned} u_0 &= \ell(\ell+1) + 2v_0 r_{\rm a} + 2(v_1 - E) r_{\rm a}^2 + 2v_2 r_{\rm a}^3 + 2v_3 r_{\rm a}^4, \\ u_1 &= 2\left[v_0 + 2(v_1 - E) r_{\rm a} + 3v_2 r_{\rm a}^2 + 4v_3 r_{\rm a}^3\right] h, \\ u_2 &= 2\left[(v_1 - E) + 3v_2 r_{\rm a} + 6v_3 r_{\rm a}^2\right] h^2, \\ u_3 &= 2\left(v_2 + 4v_3 r_{\rm a}\right) h^3, \\ u_4 &= 2v_3 h^4. \end{aligned} \tag{4.9}$$

The radial function $\mathcal{P}(x)$ is now expanded as a power series in x

$$\mathcal{P}(x) = \sum_{n=0}^{\infty} A_n x^n. \tag{4.10}$$

Introducing (4.10) in (4.6) we obtain the following recurrence relation for the coefficients in the series

$$\begin{aligned} A_n \;=\; & \frac{h}{n(n-1) r_{\rm a}} \left[-2(n-1)(n-2) A_{n-1} + \frac{h}{r_{\rm a}} \left\{ \Big(u_0 - (n-2)(n-3) \Big) A_{n-2} \right.\right. \\ & \left.\left. +\; u_1 A_{n-3} + u_2 A_{n-4} + u_3 A_{n-5} + u_4 A_{n-6} \right\} \right], \end{aligned} \tag{4.11}$$

which determines the values of all the A_n from the boundary conditions

$$A_0 = P(r_{\rm a}), \qquad A_1 = hP'(r_{\rm a}). \tag{4.12}$$

Generally we will only be interested in the values of $P(r)$ and $P'(r)$ at the end point $r_{\rm b}$ ($x = 1$):

$$P(r_{\rm b}) = \mathcal{P}(1) = \sum_{n=0}^{\infty} A_n, \qquad P'(r_{\rm b}) = h^{-1}\mathcal{P}'(1) = h^{-1} \sum_{n=0}^{\infty} n A_n. \tag{4.13}$$

In the numerical evaluation, the series $\mathcal{P}(1)$ and $\mathcal{P}'(1)$ may be summed *exactly*, *i.e.*, we can add enough terms to ensure that the relative error in the sum is smaller than a certain value ϵ ($\ll 1$), which should be of the order of 10^{-15} to get the optimum accuracy

attainable with double-precision arithmetic. We adopt the following convergence criteria: the summation of series (4.13) is stopped when the last added term, A_j, satisfies the two conditions

$$|A_j| < \epsilon \max\left\{\left|\sum_{n=0}^{j} A_n\right|, \frac{1}{j}\left|\sum_{n=0}^{j} nA_n\right|\right\} \tag{4.14a}$$

and

$$\left|r_{\rm b}^2\mathcal{P}''(1) - h^2\mathcal{U}(1)\mathcal{P}(1)\right| < \epsilon \max\left\{\left|\mathcal{P}(1)\right|, \left|\mathcal{P}'(1)\right|\right\}, \tag{4.14b}$$

so that the function $\mathcal{P}(x)$ fulfils differential equation (4.6) in the considered interval with the required accuracy. Notice that in order to check this last condition it is necessary to also sum the series for $\mathcal{P}''(1)$.

When $r_{\rm a} = r_1 = 0$, *i.e.*, to start the solution from the centre of force, we must proceed in a slightly different way. In this case we take

$$\mathcal{P}(x) = x^s \sum_{n=0}^{\infty} A_n x^n, \qquad x \equiv r/r_2, \tag{4.15}$$

with $A_0 = 1$. Introducing (4.15) in (4.6) we get the recurrence relation

$$A_n = \frac{u_1 A_{n-1} + u_2 A_{n-2} + u_3 A_{n-3} + u_4 A_{n-4}}{(s+n)(s+n-1) - u_0}, \tag{4.16}$$

where the coefficients u_i are given by Eqs. (4.9) with $h = r_2$. For $n = 0$, the denominator must vanish, and hence

$$s(s-1) = u_0 = \ell(\ell+1). \tag{4.17}$$

The regular solution is obtained for $s = \ell + 1$. The radial function at r_2 is evaluated by summing the series (4.15) and it is renormalised as follows

$$P(r_2) = \frac{\mathcal{P}(1)}{|\mathcal{P}(1)|}, \qquad P'(r_2) = \frac{\mathcal{P}'(1)}{r_2\,|\mathcal{P}(1)|}. \tag{4.18}$$

In the summation of the series we use the convergence criteria given by Eqs. (4.14).

4.2 Dirac equation

The Dirac equation (4.2) is solved in a similar way. We assume that the values of the radial functions P and Q at the point $r_{\rm a}$ are known. We wish to determine these functions in the interval between $r_{\rm a}$ and $r_{\rm b}$, where the potential function $\mathcal{V}(r)$ is again given by Eq. (4.4).

After changing to the new variable x, Eq. (4.5), the radial equations (4.2) are written in the form

$$\begin{aligned} &(r_{\rm a} + hx)\mathcal{P}' - \sigma|\kappa|h\mathcal{P} + \mathcal{U}h\mathcal{Q} - 2ch(r_{\rm a} + hx)\mathcal{Q} = 0, \\ &(r_{\rm a} + hx)\mathcal{Q}' + \sigma|\kappa|h\mathcal{Q} - \mathcal{U}h\mathcal{P} = 0, \end{aligned} \tag{4.19}$$

with

$$\mathcal{P}(x) \equiv P(r), \qquad \mathcal{Q}(x) \equiv Q(r), \tag{4.20}$$

$\sigma = -\text{sign}(\kappa)$, and

$$\mathcal{U}(x) \equiv \frac{r[V(r) - E]}{c} = u_0 + u_1 x + u_2 x^2 + u_3 x^3, \tag{4.21}$$

where

$$\begin{aligned} u_0 &= c^{-1}\left[v_0 + (v_1 - E)r_{\rm a} + v_2 r_{\rm a}^2 + v_3 r_{\rm a}^3\right], \\ u_1 &= c^{-1}\left[(v_1 - E) + 2v_2 r_{\rm a} + 3v_3 r_{\rm a}^2\right] h, \\ u_2 &= c^{-1}\left[v_2 + 3v_3 r_{\rm a}\right] h^2, \\ u_3 &= c^{-1} v_3 h^3. \end{aligned} \tag{4.22}$$

Introducing the series expansions

$$\mathcal{P}(x) = \sum_{n=0}^{\infty} A_n x^n, \qquad \mathcal{Q}(x) = \sum_{n=0}^{\infty} B_n x^n \tag{4.23}$$

in Eq. (4.19), we find the following recurrence relations for the coefficients

$$\begin{aligned} A_n &= -\frac{h}{n r_{\rm a}}\left[(\kappa + n - 1)A_{n-1}\right. \\ &\quad \left. + (u_0 - 2c r_{\rm a})B_{n-1} + (u_1 - 2ch)B_{n-2} + u_2 B_{n-3} + u_3 B_{n-4}\right], \\ B_n &= \frac{h}{n r_{\rm a}}\left[(\kappa - n + 1)B_{n-1} + u_0 A_{n-1} + u_1 A_{n-2} + u_2 A_{n-3} + u_3 A_{n-4}\right]. \end{aligned} \tag{4.24}$$

Using these relations and the boundary conditions

$$A_0 = P(r_{\rm a}), \qquad B_0 = Q(r_{\rm a}), \tag{4.25}$$

the coefficients A_n and B_n are completely determined. The values of $P(r)$ and $Q(r)$ at the end point $r_{\rm b}$ ($x = 1$) are given by

$$P(r_{\rm b}) = \mathcal{P}(1), \qquad Q(r_{\rm b}) = \mathcal{Q}(1). \tag{4.26}$$

In the numerical evaluation of the series $\mathcal{P}(1)$ and $\mathcal{Q}(1)$ we adopt a convergence criterion similar to (4.14). The summation is stopped when the last added terms, A_j and B_j, satisfy the two conditions

$$\max\left\{|A_j|, |B_j|\right\} < \epsilon \max\left\{\left|\sum_{n=0}^{j} A_n\right|, \left|\sum_{n=0}^{j} B_n\right|\right\} \tag{4.27a}$$

and

$$\max\left\{\left|r_{\rm b}\mathcal{P}'(1) - \sigma|\kappa| h\mathcal{P}(1) + (\mathcal{U}(1) - 2c r_{\rm b})\, h\mathcal{Q}(1)\right|,\right.$$

$$\left| r_{\rm b}\mathcal{Q}'(1) + \sigma|\kappa| h\mathcal{Q}(1) - \mathcal{U}(1)h\mathcal{P}(1) \right| \Big\} \; < \; \epsilon \max\left\{ |\mathcal{P}(1)|\,, |\mathcal{Q}(1)| \right\}. \quad (4.27b)$$

In order to check this last condition it is necessary to also sum the series for $\mathcal{P}'(1)$ and $\mathcal{Q}'(1)$.

As in the case of the Schrödinger equation, special series expansions must be used to start the solutions at $r_{\rm a} = r_1 = 0$. We take

$$\mathcal{P}(x) = x^s \sum_{n=0}^{\infty} A_n x^n, \qquad \mathcal{Q}(x) = x^{s+t} \sum_{n=0}^{\infty} B_n x^n \quad (4.28)$$

with $x \equiv r/r_2$. Introducing (4.28) in (4.19) we get

$$\begin{aligned} (s+n-\sigma|\kappa|)A_n + u_0 B_{n-t} + (u_1 - 2ch)B_{n-t-1} + u_2 B_{n-t-2} + u_3 B_{n-t-3} \; &= \; 0, \\ -(s+n+\sigma|\kappa|)B_{n-t} + u_0 A_n + u_1 A_{n-1} + u_2 A_{n-2} + u_3 A_{n-3} \; &= \; 0, \end{aligned} \quad (4.29)$$

where $h = r_2$.

The parameters s and t may be determined from the value of u_0 and the regularity condition at $r = 0$. The following different cases must be considered:

(i) $u_0 \neq 0$. We may take $t = 0$; Eqs. (4.29) for $n = 0$ simplify to

$$\begin{aligned} (s - \sigma|\kappa|)A_0 + u_0 B_0 &= 0, \\ u_0 A_0 - (s + \sigma|\kappa|)B_0 &= 0. \end{aligned} \quad (4.30)$$

Non-trivial solutions ($A_0 \neq 0$, $B_0 \neq 0$) exist only if the determinant vanishes, *i.e.*, $s^2 - \kappa^2 + u_0^2 = 0$. This yields

$$s = \left[\kappa^2 - u_0^2\right]^{1/2} \quad (4.31)$$

for the regular solutions. Equations (4.29) with $t = 0$ give the following recurrence relations

$$\begin{aligned} n(2s+n)A_n \; &= \; -u_0 A_n - (s+n+\sigma|\kappa|)B_n, \\ n(2s+n)B_n \; &= \; (s+n-\sigma|\kappa|)A_n - u_0 B_n, \end{aligned} \quad (4.32)$$

with

$$\begin{aligned} A_n \; &= \; u_1 A_{n-1} + u_2 A_{n-2} + u_3 A_{n-3}, \\ B_n \; &= \; (u_1 - 2ch)B_{n-1} + u_2 B_{n-2} + u_3 B_{n-3}. \end{aligned} \quad (4.33)$$

These relations, complemented with the values

$$A_0 = 1, \qquad B_0 = -(s - \sigma|\kappa|)/u_0, \quad (4.34)$$

suffice to determine the coefficients in series (4.28).

(ii) $u_0 = 0, \sigma = 1$. We take $s = |\kappa|$ and $t = 1$. With these values, Eqs. (4.29) yield

$$\begin{aligned} nA_n &= -(u_1 - 2ch)B_{n-2} - u_2 B_{n-3} - u_3 B_{n-4}, \\ (2|\kappa| + n + 1)\, B_n &= u_1 A_n + u_2 A_{n-1} + u_3 A_{n-2}. \end{aligned} \tag{4.35}$$

To start the series we set

$$A_0 = 1, \qquad B_0 = u_1/(2|\kappa| + 1). \tag{4.36}$$

(iii) $u_0 = 0, \sigma = -1$. We take $s = |\kappa| + 1$ and $t = -1$. From Eqs. (4.29) it follows that

$$\begin{aligned} (2|\kappa| + n + 1)\, A_n &= -(u_1 - 2ch)B_n - u_2 B_{n-1} - u_3 B_{n-2}, \\ nB_n &= u_1 A_{n-2} + u_2 A_{n-3} + u_3 A_{n-4}. \end{aligned} \tag{4.37}$$

The series are started with

$$B_0 = \pm 1, \qquad A_0 = -(u_1 - 2ch)B_0/(2|\kappa| + 1). \tag{4.38}$$

The sign of B_0 is selected so that A_0 is positive.

The series (4.28) are summed with convergence criteria given by Eqs. (4.27). The radial functions at r_2 are renormalised so that

$$P(r_2) = \frac{\mathcal{P}(1)}{|\mathcal{P}(1)|}, \qquad Q(r_2) = \frac{\mathcal{Q}(1)}{|\mathcal{P}(1)|}. \tag{4.39}$$

The subroutine package RADIAL uses the power-series method to solve the radial wave equations to a prescribed accuracy that is fixed by the input value of the parameter ϵ [see Eqs. (4.14) and (4.27)]. This parameter determines, to a large extent, the calculation time. A smaller value of ϵ yields more accurate solutions, but the calculation takes a longer computer time.

Values of the radial functions are delivered for the points of a grid specified by the user, which may be different from the grid where the potential function $\mathcal{V}(r)$ is tabulated. These two grids will be referred to as the "user" grid and the "potential" grid, respectively. In fact, RADIAL uses a combined grid, which is obtained by merging the user and potential grids. In what follows, the points of this combined grid are denoted as r_i (i =1, ..., NT). We consider that they are sorted in non-decreasing order (*i.e.*, $r_{i+1} - r_i \geq 0$) and that $r_1 = 0$. For bound states, the value of $r_{\rm NT}$ must be large enough to guarantee that the probability of finding the particle farther than $r_{\rm NT}$ is negligible (this is important for highly excited bound states). An interesting feature of the present solution method is that the accuracy of the computed wave functions is independent of the spacing of the user grid (except for bound states with many nodes, see below).

In principle, the wave function in each interval (r_i, r_{i+1}) is exactly given by the corresponding series expansion. In practice, however, it may be convenient to split this

interval into a number of shorter subintervals in order to speed up the convergence of the series. The RADIAL subroutines automatically select subinterval lengths such that convergence is achieved with less than 60 terms. However, only the values of the radial functions $P(r)$ and $Q(r)$ at the user grid points are transferred to the calling program. In the case of the Schrödinger equation, the output function $Q(r)$ is set equal to the derivative of $P(r)$, *i.e.*, $Q(r) \equiv P'(r)$.

Because of the renormalisation of the wave function at the second grid point r_2 [see Eqs. (4.18) and (4.39)], the computed radial wave functions may reach exceedingly large values (with the risk of leading to computer overflows). To prevent this undesirable effect during the calculation, each time the absolute value of $P(r_i)$ exceeds 100, the calculated radial functions are rescaled by dividing them by $|P(r_i)|$ (but the output radial functions are properly normalised).

5 Bound states. Eigenvalues

Let us now consider the problem of determining the energy ($E < 0$) and radial functions for bound states with specified quantum numbers. Discrete eigenvalues are located in the interval ($\sim E_{\rm inf}, E_{\rm sup}$) given by

$$E_{\rm inf} \simeq \min\left(V(r) + \frac{\ell(\ell+1)}{2r^2}\right), \qquad E_{\rm sup} \equiv \min\left\{V(r_{\rm NT}) + \frac{\ell(\ell+1)}{2r_{\rm NT}^2}, 0\right\}. \tag{5.1}$$

$E_{\rm inf}$, the minimum value of the effective radial potential, is a rigorous lower limit for the Schrödinger equation while it is only approximate in the case of the Dirac equation (small variations of this limit are allowed during the numerical calculations so that its exact value does not really matter). The upper limit is fixed by numerical requirements rather than by physical reasons.

The solution procedures for the radial Schrödinger and Dirac equations are similar. For a given energy E in the allowed interval (5.1), the numerical solution is started at $r = 0$ and extended outwards, by using the power-series method described in the previous Section 4, up to a certain grid point r_m farther than the outer node of the function $P(r)$ (see Appendix C). We determine r_m from the condition

$$V(r_i) > E - \frac{\ell(\ell+1)}{2r_i^2} \qquad \text{if } i \geq m, \tag{5.2}$$

which ensures that r_m is beyond the outer turning point of the non-relativistic radial motion.

The first step in the solution is to find a value of the energy E for which the outward solution (from 0 to r_m) has the correct number of zeros given by the radial quantum number $n_{\rm r} = n-(\ell+1)$, where n is the principal quantum number. This is accomplished by successive bisection of the energy interval (5.1). We start with the energy $E = (E_{\rm inf} + E_{\rm sup})/2$ and generate the outward solution up to r_m. If the number of zeros of $P(r)$ is too small (large), E replaces the lower (upper) end of the energy interval and the

process is repeated for the reduced interval. It is important to note that the number of zeros of $P(r)$ is determined from the function values *at the grid points*; as a consequence it is necessary to use dense enough grids to ensure that there is at most a single zero between consecutive grid points (otherwise, the program will probably ask for a denser user grid).

Once a value of the energy giving the correct number of zeros of the outward solution has been determined, we proceed to compute the solution starting from r_{NT} (or from a grid point far enough from the connection point r_m) and extending it inwards to r_m. The inward solution is then renormalised such that $P(r)$ is continuous at the matching point, *i.e.*, $P_{\mathrm{in}}(r_m) = P_{\mathrm{out}}(r_m)$. Successive corrections ΔE of the eigenvalue are determined from the discontinuity of $P'(r)$ or $Q(r)$ at r_m by using the method described by Mayers (1957). Potentials of finite range [*i.e.*, such that $\lim_{r\to\infty} rV(r) = 0$] hold a finite number of bound states; usually, the RADIAL subroutines are able to determine whether a certain bound state with given quantum numbers occurs, provided only that the radial grid is sufficiently dense. In the case of potentials with an attractive Coulomb tail [*i.e.*, such that $\lim_{r\to\infty} rV(r) < 0$], for each value of the relevant angular momentum quantum number (ℓ or κ) the number of bound states is infinite, and the set of bound energy levels has an accumulation point at $E = 0$. Of course, in this case the RADIAL subroutines are able to calculate only a finite number of bound states, and this number may vary with the extension and the spacing of the radial grid.

5.1 Schrödinger equation

The inward solution is started by means of the Wentzel–Kramers–Brillouin (WKB) approximation, which is expected to be fairly accurate for $r \to \infty$. The WKB solution of Eq. (4.1) in the region $r > r_m$ is given by (Schiff, 1968; Joachain, 1978)

$$P^{(\mathrm{WKB})}(r) = \mu^{-1/2} \exp\left\{ -\int_a^r \mu(r')\,\mathrm{d}r' \right\}, \tag{5.3}$$

where

$$\mu(r) \equiv \left\{ 2\,[V(r) - E] + \frac{\ell(\ell+1)}{r^2} \right\}^{1/2} \tag{5.4}$$

and a is an arbitrary point in the classically forbidden region ($a > r_m$). Approximation (5.3) implies that

$$\frac{P'(r)}{P(r)} = -\frac{1}{2}\mu'\mu^{-1} - \mu. \tag{5.5}$$

The inward solution is started at a point $r_\infty (\gg r_m)$, where we take $P(r_\infty) = 1$ and use (5.5) to approximate $P'(r_\infty)$, and extended inwards by using the power-series method. The point r_∞ is determined as the minimum grid point satisfying the condition

$$r_\infty\, \mu(r_\infty) > 150, \tag{5.6}$$

which ensures that $|P(r_\infty)| \ll |P(r_m)|$. If this last relation holds, the error introduced by the WKB approximation (5.5) does not propagate towards the connection point, *i.e.*,

the inward solution is stable. When $r_{\rm NT}\mu(r_{\rm NT}) < 150$ we take $r_\infty = r_{\rm NT}$. Further than r_∞ we set $P(r) = 0$. Notice that the last grid point $r_{\rm NT}$ should be larger than r_∞ or at least be far enough from r_m so that the error in the inward solution originating from the WKB formula (5.5) vanishes at the matching point.

For potentials such that $rV(r)$ is constant in the outer part of the integration interval, say, from $r_{\rm c}$ ($r_{\rm c} < r_\infty$) outwards, the inward integration could be started by using the asymptotic expansion (7.34) of the radial function (see Section 7.3). Although this procedure is more rigorous than the WKB approximation, usually it does not improve accuracy.

The formula for correcting the eigenvalue may be obtained as follows. Consider the radial Schrödinger equation (4.1) written in the form

$$P' = Q, \qquad Q' = 2\left[V(r) - E + \frac{\ell(\ell+1)}{2r^2}\right] P, \tag{5.7}$$

where P and Q are assumed to depend on r *and* E. From (5.7) it follows that

$$\frac{\mathrm{d}}{\mathrm{d}r}\left[P^2\,\frac{\mathrm{d}}{\mathrm{d}E}\left(\frac{Q}{P}\right)\right] = -2P^2, \tag{5.8}$$

and, integrating this equation over the arbitrary interval $(r_{\rm a}, r_{\rm b})$, we get

$$\left[P^2\,\frac{\mathrm{d}}{\mathrm{d}E}\left(\frac{Q}{P}\right)\right]_{r_{\rm a}}^{r_{\rm b}} = -2\int_{r_{\rm a}}^{r_{\rm b}} P^2(r)\,\mathrm{d}r. \tag{5.9}$$

Now we assume that the inward solution has been renormalised to match the outward one at the connection point, *i.e.*, $P_{\rm out}(r_m) = P_{\rm in}(r_m) \equiv P(r_m)$ and, moreover, that the entire function $P(r)$ has been normalised to unity. From Eq. (5.9) we have

$$\begin{aligned} 1 = \int_0^\infty P^2(r)\,\mathrm{d}r \;&=\; -\frac{1}{2}\left\{\left[P^2\,\frac{\mathrm{d}}{\mathrm{d}E}\left(\frac{Q}{P}\right)\right]_0^{r_m} + \left[P^2\,\frac{\mathrm{d}}{\mathrm{d}E}\left(\frac{Q}{P}\right)\right]_{r_m}^{\infty}\right\} \\ &=\; -\frac{1}{2}P^2(r_m)\,\frac{\mathrm{d}}{\mathrm{d}E}\left[\frac{Q_{\rm out}(r_m) - Q_{\rm in}(r_m)}{P(r_m)}\right], \end{aligned} \tag{5.10}$$

where the last quantity in the square brackets vanishes when E equals the eigenvalue $E_{n\ell}$. Finally, integrating (5.10) over E on the interval $(E, E_{n\ell} = E + \Delta E)$ we obtain the eigenvalue correction

$$\Delta E = P(r_m)\,[Q_{\rm out}(r_m) - Q_{\rm in}(r_m)]\left\{2\int_0^\infty P^2(r)\,\mathrm{d}r\right\}^{-1}. \tag{5.11}$$

5.2 Dirac equation

The methods used to start the inward solution and to correct the eigenvalue are analogous to those adopted for the Schrödinger equation. For large enough radii, the potential

energy $V(r)$ becomes negligibly small in comparison with $E + 2c^2$, and equations (4.2) may be combined to yield the following differential equation for the large component P

$$P''(r) - \mu(r)P(r) = 0, \tag{5.12}$$

where

$$\mu(r) \equiv \left[\frac{E + 2c^2}{c^2}\Big(V(r) - E\Big) + \frac{\ell(\ell+1)}{r^2}\right]^{1/2}. \tag{5.13}$$

The point r_∞ is determined as in the case of the Schrödinger equation [see Eq. (5.6)]. The inward solution is started there by using the first Dirac equation (4.2) and relation (5.5) which yield

$$\frac{Q(r)}{P(r)} \simeq \frac{c}{E + 2c^2}\left(\frac{\kappa}{r} + \frac{P'(r)}{P(r)}\right) = \frac{c}{E + 2c^2}\left(\frac{\kappa}{r} - \frac{1}{2}\mu'\mu^{-1} - \mu\right). \tag{5.14}$$

For potentials that are strictly Coulombian in the outer part of the integration interval (*i.e.*, such that $rV(r)$ is constant from some r_c out to r_∞) the inward integration can be started using the asymptotic formulas (7.43) (see Section 7.4). Normally this alternative method does not improve the accuracy of the results.

The formula for the eigenvalue correction reads (Mayers, 1957)

$$\Delta E = cP(r_m)\left[Q_\mathrm{out}(r_m) - Q_\mathrm{in}(r_m)\right]\left\{\int_0^\infty \Big[P^2(r) + Q^2(r)\Big]\,\mathrm{d}r\right\}^{-1}. \tag{5.15}$$

To derive this formula, we consider the quantity

$$\frac{\mathrm{d}}{\mathrm{d}r}\left[P^2\,\frac{\mathrm{d}}{\mathrm{d}E}\left(\frac{Q}{P}\right)\right] = P'\,\frac{\mathrm{d}Q}{\mathrm{d}E} + P\,\frac{\mathrm{d}Q'}{\mathrm{d}E} - Q'\,\frac{\mathrm{d}P}{\mathrm{d}E} - Q\,\frac{\mathrm{d}P'}{\mathrm{d}E}.$$

With the help of the radial equations (4.2) and the relations

$$\begin{aligned}
\frac{\mathrm{d}P'}{\mathrm{d}E} &= -\frac{\kappa}{r}\,\frac{\mathrm{d}P}{\mathrm{d}E} + \frac{1}{c}\,Q + \frac{E - V + 2c^2}{c}\,\frac{\mathrm{d}Q}{\mathrm{d}E},\\
\frac{\mathrm{d}Q'}{\mathrm{d}E} &= -\frac{1}{c}\,P - \frac{E - V}{c}\,\frac{\mathrm{d}P}{\mathrm{d}E} + \frac{\kappa}{r}\,\frac{\mathrm{d}Q}{\mathrm{d}E},
\end{aligned}$$

we can write

$$\frac{\mathrm{d}}{\mathrm{d}r}\left[P^2\,\frac{\mathrm{d}}{\mathrm{d}E}\left(\frac{Q}{P}\right)\right] = -\frac{1}{c}\left(P^2 + Q^2\right).$$

Hence,

$$\left[P^2\,\frac{\mathrm{d}}{\mathrm{d}E}\left(\frac{Q}{P}\right)\right]_{r_a}^{r_b} = -\frac{1}{c}\int_{r_a}^{r_b}\left[P^2(r) + Q^2(r)\right]\mathrm{d}r.$$

Taking $r_a = 0$ and $r_b = r_m$, we have

$$P_m^2\,\frac{\mathrm{d}}{\mathrm{d}E}\left(\frac{Q_m(\mathrm{out})}{P_m}\right) = -\frac{1}{c}\int_0^{r_m}\left[P^2(r) + Q^2(r)\right]\mathrm{d}r.$$

Similarly, with $r_a = r_m$ and $r_b = \infty$,

$$-P_m^2 \frac{\mathrm{d}}{\mathrm{d}E}\left(\frac{Q_m(\mathrm{in})}{P_m}\right) = -\frac{1}{c}\int_{r_m}^{\infty} \left[P^2(r) + Q^2(r)\right] \mathrm{d}r.$$

Adding the last two equations, we obtain

$$\frac{\mathrm{d}}{\mathrm{d}E}\left[\frac{Q_m(\mathrm{out}) - Q_m(\mathrm{in})}{P_m}\right] = -\frac{1}{c}\, P_m^{-2} \int_0^{\infty} \left[P^2(r) + Q^2(r)\right] \mathrm{d}r. \tag{5.16}$$

Notice that the difference $Q_m(\mathrm{out}) - Q_m(\mathrm{in})$ vanishes when E is the eigenvalue. On the other hand, the quantity on the right-hand side remains practically unaltered under small variations of E. Integration of Eq. (5.16) with respect to E over the interval $(E, E_{n\kappa} = E + \Delta E)$ leads to the Mayers formula (5.15).

5.3 Normalisation of bound states

In the first version of the RADIAL subroutines (Salvat *et al.*, 1995), the normalisation integrals in Eqs. (5.11) and (5.15) were evaluated by considering natural cubic splines that interpolated the calculated values of the radial functions $P(r)$ and $Q(r)$. Although the integrals of the squared splines were calculated analytically, this procedure introduced a slight relative error in the normalisation of bound-state wave functions (of the order of 10^{-6}). This source of error was revealed by a comparison of radial functions for Coulomb potentials, obtained through the numerical integration of the radial wave equations, with the Coulomb functions given by subroutines `SCOULB` and `DCOULB` (see Section 8.2), which employ the exact expressions described in Section 3.1.5.

To avoid this kind of systematic error, in the present version of RADIAL normalisation integrals are evaluated directly from the power-series expansions of the radial functions, Eqs. (4.10) or (4.23). That is, for Schrödinger bound states the contribution of each grid interval (r_i, r_{i+1}) $(i > 1)$ [or of each subinterval when the grid interval is split to improve the convergence of the series] to the normalisation integral is given by

$$\int_{r_i}^{r_{i+1}} P^2(r)\,\mathrm{d}r = h\int_0^1 \left(\sum_n A_n x^n\right)^2 \mathrm{d}x = h\sum_{n,m} \frac{A_n A_m}{n+m+1}\,, \tag{5.17}$$

where $h = r_{i+1} - r_i$. For Dirac bound states,

$$\begin{aligned}\int_{r_i}^{r_{i+1}} [P^2(r) + Q^2(r)]\,\mathrm{d}r \;&=\; h\int_0^1 \left[\left(\sum_n A_n x^n\right)^2 + \left(\sum_n B_n x^n\right)^2\right] \mathrm{d}x \\ &=\; h\sum_{n,m} \frac{A_n A_m + B_n B_m}{n+m+1}.\end{aligned} \tag{5.18}$$

The contribution of the first interval, from $r_1 = 0$ to r_2 (or to the endpoint of the first subinterval) is calculated by integrating the series (4.15) and (4.28). We thus obtain the normalisation integral with an accuracy similar to that of the radial functions.

6 Free states. Phase shifts

The series expansion method is also applied to compute radial wave functions for free states ($E > 0$). We recall that, for the considered class of potential functions, $\lim_{r\to\infty} \mathcal{V}(r) = Z_\infty$, where Z_∞ is a constant. Let r_c denote the grid point where the asymptotic value of $\mathcal{V}(r)$ is reached, *i.e.*, the smallest grid point such that $|\mathcal{V}(r)-Z_\infty| < \epsilon$ for $r > r_\mathrm{c}$, where ϵ is the accuracy parameter. Notice that the calculated radial functions have a relative uncertainty of the order of ϵ [see Eqs. (4.14) and (4.27)]. Accordingly, we consider that two quantities are numerically equal when their relative difference is less than ϵ.

In the region $r > r_\mathrm{c}$, the normalised solution of the Schrödinger equation can be expressed as (Schiff, 1968)

$$\begin{aligned} P(r) &= \cos\delta\ F_\ell(\eta, r) + \sin\delta\ G_\ell(\eta, r), \\ Q(r) &= \cos\delta\ F'_\ell(\eta, r) + \sin\delta\ G'_\ell(\eta, r), \end{aligned} \tag{6.1}$$

where $Q(r) = P'(r)$ and $F_\ell(\eta, r)$ and $G_\ell(\eta, r)$ are the regular and irregular Schrödinger–Coulomb functions with Z_∞=$\lim_{r\to\infty} \mathcal{V}(r)$ (Section 3.1.2). The normalised radial Dirac functions $P(r)$ and $Q(r)$ in the outer region ($r > r_\mathrm{c}$) satisfy

$$\begin{aligned} P(r) &= \cos\delta\ f_\kappa^{(\mathrm{u})}(r) + \sin\delta\ g_\kappa^{(\mathrm{u})}(r), \\ Q(r) &= \cos\delta\ f_\kappa^{(\mathrm{l})}(r) + \sin\delta\ g_\kappa^{(\mathrm{l})}(r), \end{aligned} \tag{6.2}$$

where $f_\kappa^{(\mathrm{u,l})}(r)$ and $g_\kappa^{(\mathrm{u,l})}(r)$ stand for the regular and irregular Dirac–Coulomb functions with Z_∞=$\lim_{r\to\infty} \mathcal{V}(r)$ (see Section 3.2.1).

The asymptotic behaviour of the Coulomb functions is (Section 3)

$$\begin{aligned} F(r), f^{(\mathrm{u})}(r) &\sim \sin\left(kr - \ell\frac{\pi}{2} - \eta\ln(2kr) + \Delta\right), \\ G(r), g^{(\mathrm{u})}(r) &\sim \cos\left(kr - \ell\frac{\pi}{2} - \eta\ln(2kr) + \Delta\right), \end{aligned} \tag{6.3}$$

where k is the particle wave number, η is Sommerfeld's parameter and Δ is the corresponding Coulomb phase shift. It then follows that, for large r,

$$P(r) \sim \sin\left(kr - \ell\frac{\pi}{2} - \eta\ln(2kr) + \Delta + \delta\right). \tag{6.4}$$

Schrödinger- and Dirac–Coulomb functions are calculated by subroutines `FCOUL` and `DCOULF` described above, which also give an estimate of the relative error of the delivered function values. The magnitude of this error is of the order of 10^{-15} for r larger than the Coulomb turning point, $r_\mathrm{TP}[0]$. For r less than this value, the accuracy of the calculated Coulomb functions worsens with decreasing r. When $|Z_\infty| > \epsilon$, we assume that for the outer grid points the errors in the calculated Coulomb functions are less than the tolerance ϵ (otherwise, the program asks for an extended grid). This implies that, for

r-values larger than a certain grid point r_m the radial functions $P(r)$ and $Q(r)$ can be calculated analytically from the expressions (6.1) and (6.2).

When $|Z_\infty| = 0$ (or, numerically, $< \epsilon$), the Schrödinger– and Dirac–Coulomb functions reduce to spherical Bessel and Neumann functions of integer order, which are accurately given by the function subprogram `SBESJN` for any value of r and E. In this case, we set $r_m = r_c$ and the radial functions for $r > r_c$ are evaluated by using Eqs. (6.1) and (6.2).

For both the Schrödinger and the Dirac equations, the numerical solution of the radial equation is started at $r = 0$ and extended outwards up to the matching point r_m by using the power-series method described in Section 4. Let $\overline{P}(r_i)$ and $\overline{Q}(r_i)$ (i=1,...,m) denote the resulting unnormalised radial functions. The normalised solution is obtained by matching the inner numerical function and the outer analytical function at r_m. Notice that, owing to difficulties in computing the Coulomb functions for distances r less than the turning point $r_{\rm TP}[0]$, it may be necessary to extend the inner numerical solution up to values of r that, in the case of low energies and repulsive potentials, may be quite large (and this can lengthen the calculation considerably). Of course, for completely screened Coulomb potentials ($Z_\infty = 0$), the inner solution can be stopped as soon as $|\mathcal{V}(r)| < \epsilon$. For a given radial grid, the RADIAL subroutines are able to calculate only free states with energy higher than a certain threshold value. The latter can be reduced by increasing the extension of the radial grid, that is, by integrating the radial equations up to larger radii. Needless to say, this will lengthen the calculation, which may become prohibitively slow when E is too small.

The inner and outer functions are matched by requiring continuity of the $P(r)$ function and its derivative,

$$\begin{aligned} A\,\overline{P}(r_m) &= \cos\delta\; F(r_m) + \sin\delta\; G(r_m), \\ A\,\overline{P}'(r_m) &= \cos\delta\; F'(r_m) + \sin\delta\; G'(r_m), \end{aligned} \tag{6.5}$$

where F and G stand for the corresponding regular and irregular Coulomb functions. Notice that

$$\begin{aligned} P'(r) &= Q(r) && \text{(Schrödinger)}, \\ P'(r) &= -\frac{\kappa}{r}\,P(r) + \frac{E - V + 2c^2}{c}\,Q(r) && \text{(Dirac)}. \end{aligned} \tag{6.6}$$

From Eqs. (6.5) the logarithmic derivatives of the inner and outer functions are (we suppress the argument r_m)

$$\frac{\overline{P}'}{\overline{P}} = \frac{F' + \tan\delta\; G'}{F + \tan\delta\; G} \tag{6.7}$$

and

$$\delta = \tan^{-1}\left(\frac{\overline{P}'\,F - \overline{P}\,F'}{\overline{P}\,G' - \overline{P}'\,G}\right), \qquad A = \frac{\cos\delta\; F + \sin\delta\; G}{\overline{P}}. \tag{6.8}$$

If $|\overline{P}| < \epsilon$, division by $\overline{P}$ is avoided by using the alternative formula

$$A = \frac{\cos\delta\; F' + \sin\delta\; G'}{\overline{P}'}. \tag{6.9}$$

The normalised inner function is

$$P(r_i) = A\,\overline{P}(r_i), \qquad Q(r_i) = A\,\overline{Q}(r_i) \qquad (i = 1, \ldots, m). \tag{6.10}$$

The "inner" phase shift δ is only due to the finite-range distortion of the asymptotic Coulomb potential, $\mathcal{V}_{\rm fr}(r) \equiv \mathcal{V}(r) - Z_\infty$; the effect of the Coulomb potential is accounted for by the logarithmic phase, $-\eta \ln(2kr)$, and the Coulomb phase shift Δ. For a pure Coulomb potential ($\mathcal{V}_{\rm fr} \equiv 0$), $\delta = 0$. Attractive (repulsive) finite-range potentials give positive (negative) inner phase shifts. These phase shifts are indeterminate in an integer multiple of π. Generally, we reduce the calculated values of δ to the interval $(-\pi/2,\pi/2)$ so as to get rid of this indeterminacy when $|\delta| < \pi/2$.

In the case of the Schrödinger equation, because the regular Schrödinger–Coulomb wave functions are positive near the origin, we can fix the global sign of the radial function by requiring $P(r)$ to be positive for small r. This is accomplished by taking the branch of the multivalued $\tan^{-1}$ function that makes the inner normalisation constant, A, positive. The calculated values of δ are then indeterminate in an integer multiple of 2π and can be reduced to the wider interval $(-\pi,\pi)$; thus, the reduced phase coincides with the absolute (or geometrical) phase shift $\delta_{\rm abs}$ (see below) when $|\delta_{\rm abs}| < \pi$. In addition, for a given energy, these reduced phase shifts tend to zero when ℓ increases and, hence, they vary "continuously" with ℓ for angular momenta larger than a certain cutoff value. This property is useful in calculations of scattering by a central potential (see, *e.g.*, Salvat *et al.*, 2005).

Unfortunately, the regular Dirac–Coulomb function $f_\kappa^{(\rm u)}(kr)$ for a repulsive potential ($Z_\infty > 0$) may be negative in a narrow interval between the origin and its first zero. If we require the large radial function to be positive near the origin, the resulting phase shifts may tend to $\pm\pi$ when κ tends to $-\infty$ or $+\infty$, while the geometrical phase shifts (see below) tend to zero. To avoid this inconsistency, Dirac phase shifts must be reduced to the interval $(-\pi/2, \pi/2)$

6.1 Absolute phase shifts

The absolute inner phase shift can be determined unambiguously by graphically comparing the radial wave function, $P_{E\ell}(r)$ or $P_{E\kappa}(r)$, calculated by RADIAL and the regular Coulomb function with the strength of the Coulomb tail, $Z_\infty = \lim_{r\to\infty} rV(r)$. The procedure is illustrated in Figs. 6 and 7 for the cases of Schrödinger and Dirac free states with $E = 0.5$ ($k \sim 1$) and angular momenta $\ell = 0, 1$ and $\kappa = \pm 1$ for finite-range potentials of the Yukawa type $V(r) = (Z/r)\exp(-r)$ with various values of Z. Note that in these examples $Z_\infty = 0$. Let r_n and $r_n^{(\rm C)}$ denote the n-th zeros of the calculated radial function, $P_{E\ell}(r)$ or $P_{E\kappa}(r)$, and of the large component of the regular Dirac–Coulomb function, $f_\kappa^{(\rm u)}(kr)$, respectively. Assuming that n is large enough for these zeros to be well beyond the onset $r_{\rm c}$ of the Coulomb tail, we can estimate the inner phase shift as $\delta \sim k(r_n^{(\rm C)} - r_n)$. That is, the integer multiple of π that has to be added or subtracted to the numerical phase shift to give the absolute phase shift is deduced from the number of oscillations of the calculated radial function between the points r_n and $r_n^{(\rm C)}$.

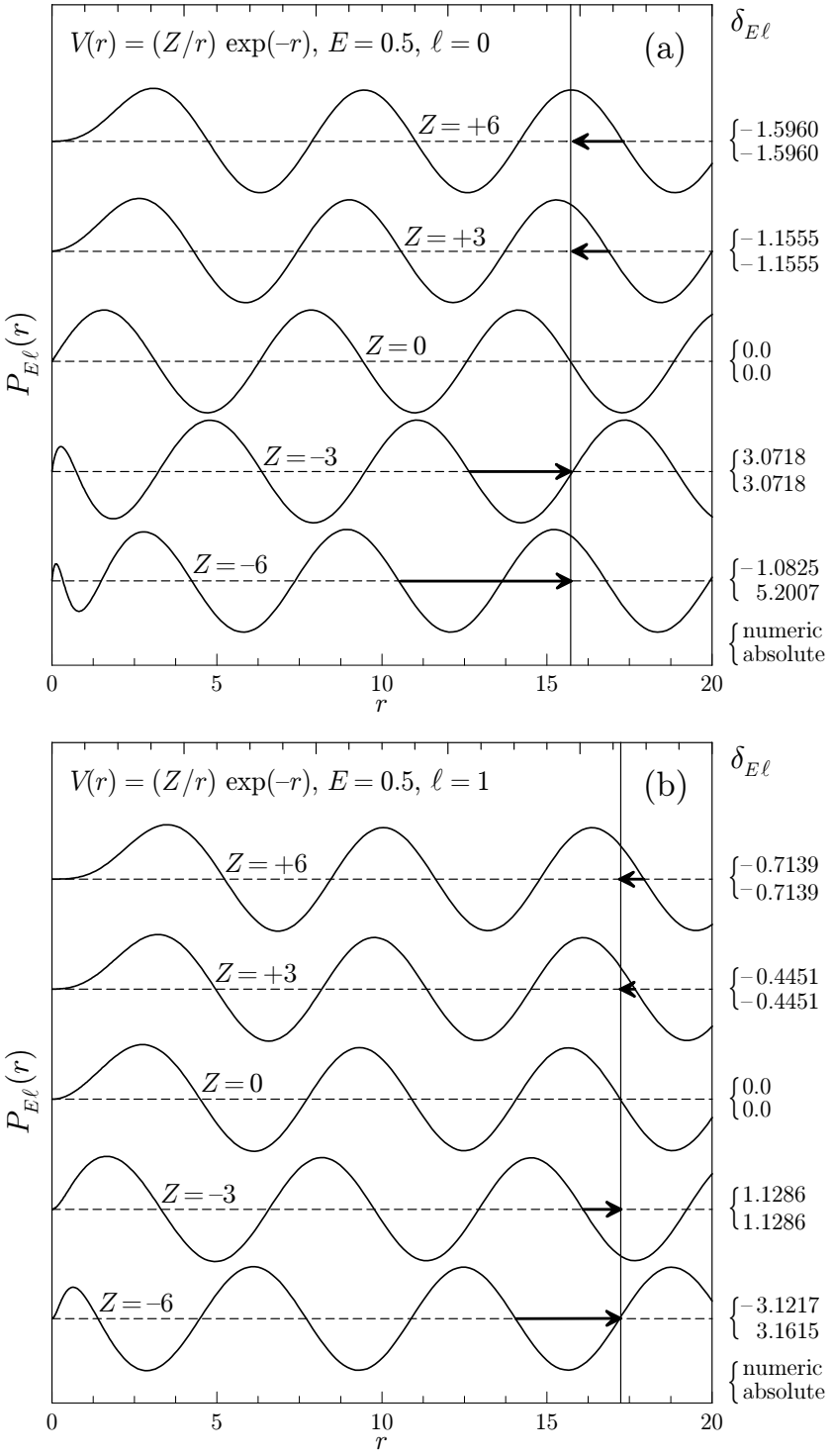

Figure 6: Radial Schrödinger wave functions of free states with energy $E = 0.5$ and angular momentum $\ell = 0$ (a) and $\ell = 1$ (b) for the finite-range potentials $V(r) = (Z/r)\exp(-r)$ with the indicated values of Z. The pair of values at the right of each plot are the numerical phase shift delivered by RADIAL (upper value) and the absolute phase shift (lover value) obtained from the numerical phase shift by adding the appropriate integer multiple of 2π. The length and direction of the arrows indicates the absolute phase shifts. All quantities in atomic units.

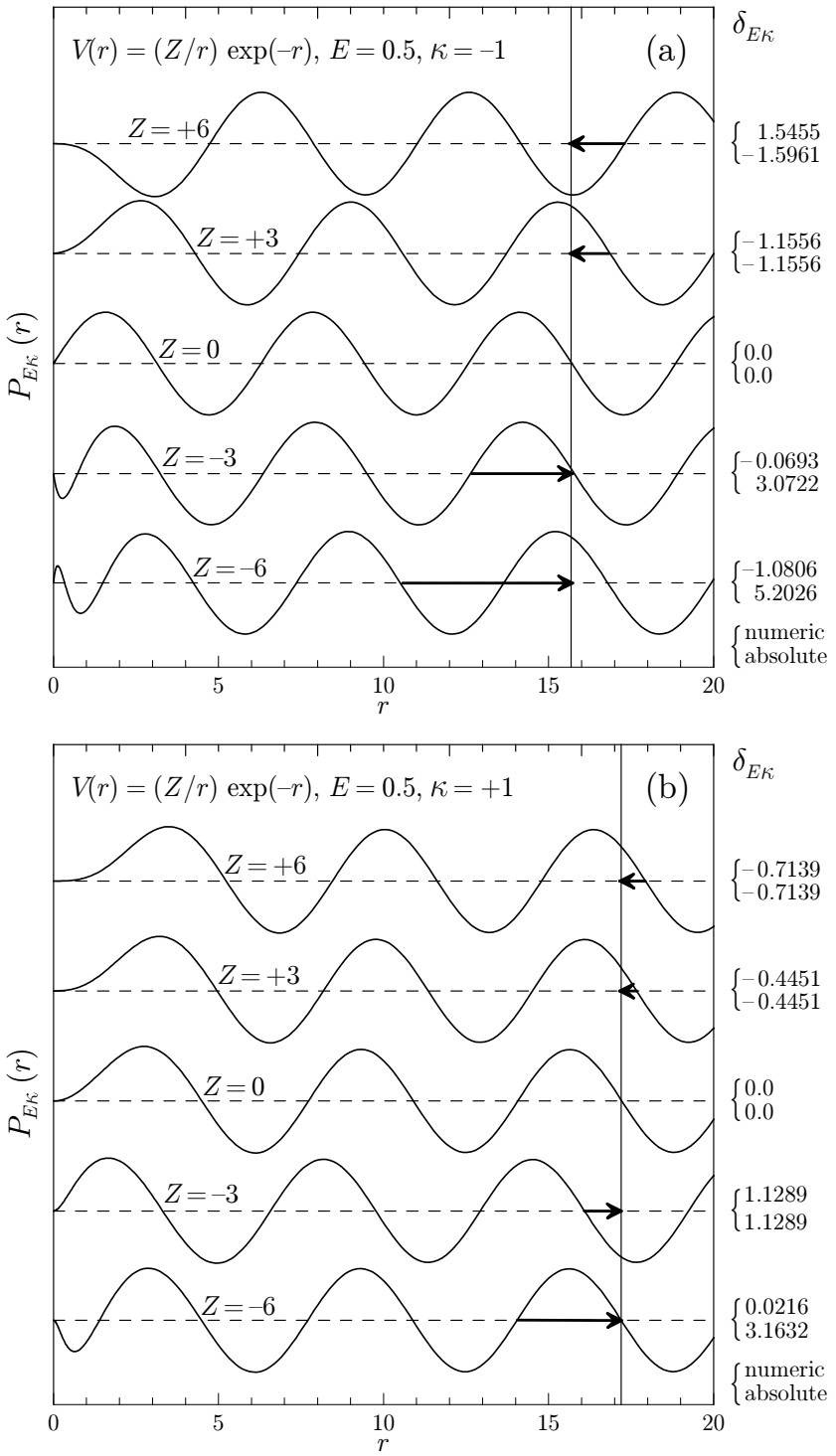

Figure 7: Radial Dirac wave functions of free states with energy $E = 0.5$ and $\kappa = -1$ (a) and $\kappa = +1$ (b) for the indicated potentials. The arrows show the inner absolute phase shifts obtained by adding the appropriate integer multiple of π to the numerical phase shift given by the RADIAL subroutines. Other details are the same as in Fig. 6.

It is worth observing that the calculated Schrödinger radial functions are positive near the origin (*i.e.*, their global sign is fixed) and, hence, the calculated phase shift, δ, coincides with the absolute phase when $|\delta| < \pi$. This is not the case for the Dirac functions, whose phase shifts are indeterminate in an integer multiple of π and, as a consequence, the global sign of the Dirac radial function remains indeterminate. In addition, the calculated Dirac phase shift equals the absolute phase only when $|\delta| < \pi/2$.

In the case of Schrödinger states, the absolute inner phase shifts tend to zero in the limit of high energies. Therefore, to determine the absolute phase shift $\delta_{E\ell}$, we can calculate this quantity using RADIAL for a grid of discrete energies, dense enough to reveal the 2π discontinuities of the numerical values, and then add the required integer multiples of 2π to obtain the absolute phase shift, which varies continuously with energy and vanishes for $E \to \infty$. Figure 8 shows the result from this procedure for the potential $V(r) = (-6/r)\exp(-r)$ and $\ell = 0$, which corresponds to the case in the lower plot in Fig. 6.

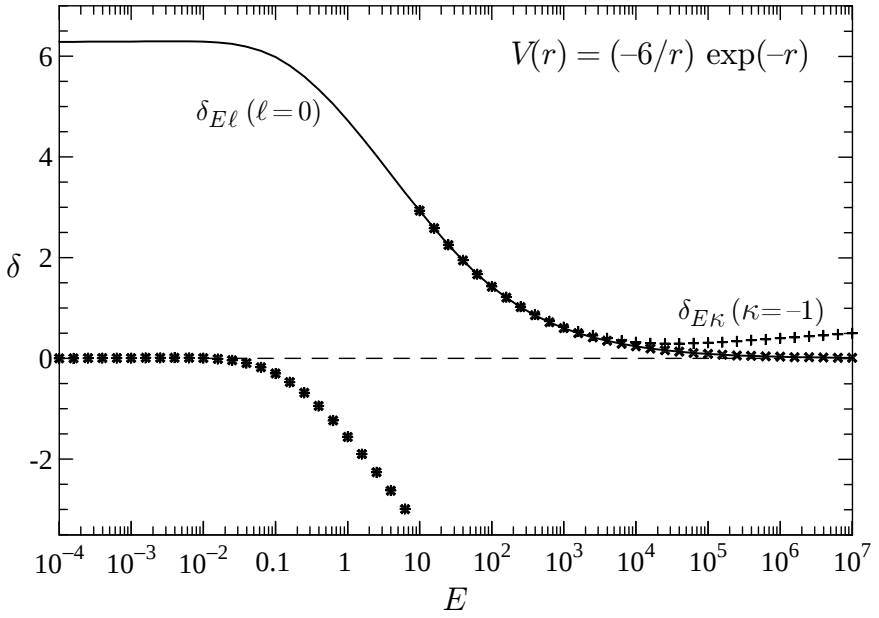

Figure 8: Schrödinger ($\times$) and Dirac ($+$) inner phase shifts for the potential $V(r) = (-6/r)\exp(-r)$ and free states with $\ell = 0$ and $\kappa = -1$, respectively. The continuous curve results from the numerical Schrödinger phase shifts by adding the appropriate integer multiples of 2π. All quantities are in atomic units.

The absolute inner phase shifts of Dirac free states do not vanish at high energies and, therefore, the method sketched here for determining absolute Schrödinger phase shifts from their high-energy limit may not work for Dirac phase shifts. However, Parzen (1950) showed that, if the finite-range component of the potential, $V_{\rm fr}(r) \equiv V(r) - Z_\infty/r$, has no pole at $r = 0$ [*i.e.*, if $\lim_{r\to 0} rV_{\rm fr}(r) = 0$], all the Dirac phase shifts $\delta_{E\kappa}$ tend to the same high-energy limit,

$$\lim_{E\to\infty} \delta_{E\kappa} = -\frac{1}{\hbar c}\int_0^\infty V_{\rm fr}(r)\,{\rm d}r \equiv \delta_\infty \qquad \forall\kappa. \tag{6.11}$$

This result provides a simple method for verifying the accuracy of the RADIAL subroutines for modified Coulomb potentials such that $V_{\rm fr}(r)$ is finite at $r = 0$. The subroutine `DELINF`, included in the `radial.f` source file, delivers the value of δ_∞ obtained by integrating the potential function $\mathcal{V}(r)$ described by the interpolating natural cubic spline. When the integral (6.11) is finite, calculated phase shifts for $E \gtrsim 10^7$ atomic units ($\gtrsim 3 \times 10^8$ eV) are found to agree with δ_∞ to 4 or more decimal digits, provided only that the tolerance ϵ is given a value of the order of 10^{-13} or smaller.

For potentials with an attractive Coulomb tail [*i.e.*, such that $Z_\infty = \lim_{r\to\infty} rV(r) < 0$], absolute inner phase shifts of free Dirac states with small energies can be determined from the theory of quantum defects (see, *e.g.*, Johnson and Cheng, 1979; Seaton, 1983, and references therein). This theory shows that the energies of bound levels can be parameterised in the form

$$E \equiv E_{n\kappa} = \mathrm{m_e}c^2 \left\{ \left[1 + \left(\frac{\alpha Z_\infty}{n^*} \right)^2 \right]^{-1/2} - 1 \right\}, \tag{6.12a}$$

where

$$n^* = n + \sqrt{\kappa^2 - \alpha^2} - |\kappa| - \mu_{n\kappa} \tag{6.12b}$$

is the effective principal quantum number. The quantity $\mu_{n\kappa}$ is the quantum defect, which depends strongly on the angular momentum quantum number κ but varies smoothly with n and approaches a finite value when n tends to infinity. The inner phase shift $\delta_{E\kappa}$ and the quantum defect are related by

$$\lim_{E\to 0^+} \delta_{E\kappa} = \pi \lim_{n\to\infty} \mu_{n\kappa}. \tag{6.13}$$

Hence, for states with a given value of κ, the quantum defect can be considered as a function of the energy E instead of n, and this function can be continued to positive energies by means of the relation (6.13), *i.e.*,

$$\mu_\kappa(E) = \frac{1}{\pi}\,\delta_{E\kappa} \qquad \text{for } E \geq 0. \tag{6.14}$$

Moreover, when the potential function $rV(r)$ is continuous, the function so defined varies smoothly near $E = 0$. In practice, $\mu_\kappa(E)$ can be evaluated numerically only for bound states with $n \lesssim 35$ [from the calculated eigenvalue $E_{n\kappa}$ through the relations (6.12)] and for free states with energy E higher than a certain threshold value, of the order of 10^{-4}. The integer multiple of π that has to be added to the numerical inner phase shift can be readily inferred from calculated quantum defects for bound levels with $n \sim 30$. Although the numerical solution of the radial Dirac equations is not possible for energies E closer to zero, the quantum defect function can be accurately represented as

$$\mu_\kappa(E) = \mu_\kappa(0) + a_\kappa E + b_\kappa E^2. \tag{6.15}$$

The subroutine `QNTDEF`, included in the `radial.f` source file, gives the parameters $\mu_\kappa(0)$, a_κ and b_κ obtained from a least-squares fit to calculated quantum defects of bound states with $n \geq 20$ and inner phase shifts of free states with energies E down to about 10^{-4}.

Figure 9 displays the fitted quantum-defect function (6.15) for the potential indicated in the legend, together with values of quantum defects and inner phase shifts computed by RADIAL with $\epsilon = 10^{-13}$. In this case, the relative error of the fit is less than 10^{-10}. When the tolerance ϵ is increased (*i.e.*, when accuracy is reduced), the quality of the fit deteriorates rapidly, and the associated relative error provides a direct measure of the accuracy of calculated radial functions.

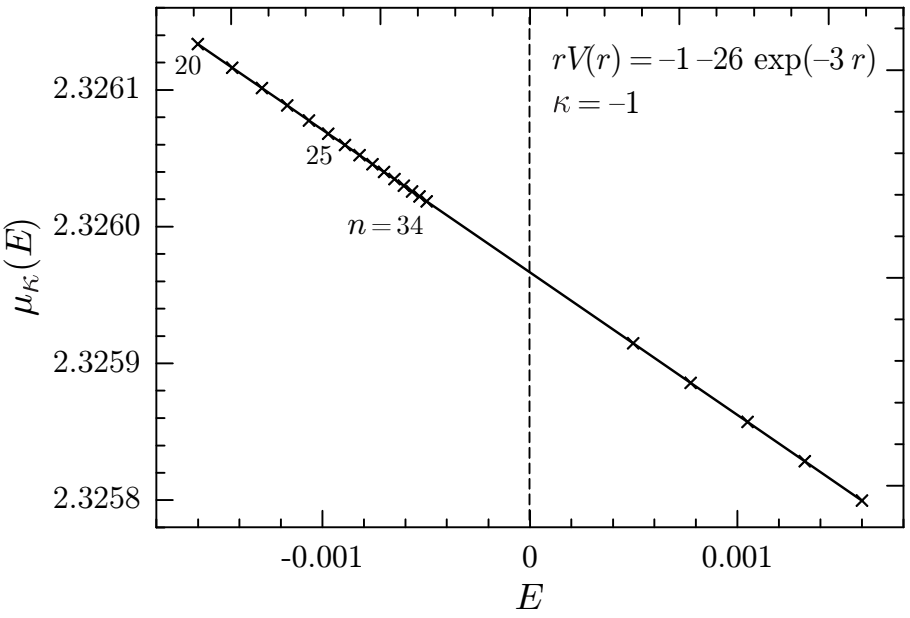

Figure 9: Quantum defect function for the indicated potential and $\kappa = -1$. Crosses are values obtained from the numerical solution of the radial Dirac equations, and the continuous curve represents the fitted quantum-defect function (6.15). The quantum defect at $E = 0$ is $\mu_\kappa(0) = 2.325\,967$. Note that the zero-energy inner phase shift is $\delta_{0\kappa} = \pi\mu_\kappa(0)$. Energies are in atomic units.

In the case of finite-range potentials, less singular than r^{-2} at the origin and vanishing faster than r^{-1} at $r = \infty$, the Levinson theorem (see, *e.g.*, Schiff, 1968; Ma, 1985) provides another interesting connection between the zero-energy limit of the absolute phase shift and the number of bound states. In its non-relativistic form (*i.e.*, for the Schrödinger equation), the theorem states that

$$\lim_{E\to 0^+} \delta_{E\ell} = \mathcal{N}_\ell\,\pi, \tag{6.16}$$

where $\delta_{E\ell}$ are the phase shifts and $\mathcal{N}_\ell$ is the number of Schrödinger bound states with orbital angular momentum ℓ. For $\ell = 0$ the Schrödinger equation may admit a zero-energy solution that vanishes at $r = 0$ and is finite at $r = \infty$, which is not normalisable. Such a solution is called a half-bound state or a zero-energy resonance and, when it exists, contributes as half a state to the right-hand side of the Levinson equality, Eq. (6.16), which becomes $(\mathcal{N}_0 + \frac{1}{2})\pi$. No zero-energy resonances are possible for $\ell > 0$. The theorem was generalised to the Dirac equation by Ma and Ni (1985), and re-considered by Poliatzky (1993) and Piekarewicz (1993). The relativistic version of the theorem

asserts that

$$\lim_{E\to 0^+} \left(\delta_{E\kappa} + \delta^-_{E,-\kappa}\right) = \left(\mathcal{N}_\kappa + \mathcal{N}^-_{-\kappa}\right)\pi, \tag{6.17}$$

where $\delta_{E\kappa}$ and $\mathcal{N}_\kappa$ are, respectively, the phase shifts and the number of positive-energy bound states for the potential $V(r)$ with angular momentum κ; $\delta^-_{E,-\kappa}$ and $\mathcal{N}^-_{-\kappa}$ are the corresponding quantities for the potential $-V(r)$ and the negative value of κ. Zero-energy resonances may exist, for either $V(r)$ or $-V(r)$, only when $\kappa = -1$ or $+1$. As in the non-relativistic case, a zero-energy resonance would contribute the amount $\frac{1}{2}\pi$ to the right-hand-side of Eq. (6.17).

The Levinson theorem can be used to check whether the RADIAL subroutines are able to calculate all bound states of a given finite-range potential. Figure 10 displays an illustration of the non-relativistic theorem for the potential $V(r) = -90\exp(-9r)/r$ and $\ell = 0$. As seen from the plot, the absolute phase shift of the free state with $E = 10^{-4}$ is $\sim 3\pi$ and, accordingly, the RADIAL subroutines calculate bound states with $n = 1$, 2 and 3, and they are unable to obtain bound states with $n > 3$. It is interesting to note that, in the case of screened attractive Coulomb potentials [such that $\lim_{r\to 0} rV(r)$ is negative], the bound states of zero angular momentum have their nodes at nearly the same positions. This is so because near the centre of force the negative potential outweighs the energy eigenvalue, *i.e.*, the radial functions of the various states satisfy nearly the same differential equations and, consequently, they have similar shapes. In the example of Fig. 10, the radial function of the bound state with higher energy has two nodes; free states with small E also present two nodes, at nearly the same positions as for the $n = 3$ bound state, before starting their "natural" oscillatory regime. At small radii, free states with small energies ($E \gtrsim 0$) inherit the shape and nodal structure of the highest bound state. At larger radii, the wave function of the free state runs parallel to that of the state of the same energy for the null potential, with a constant phase shift.

6.2 Partial-wave expansion of distorted plane waves

In collision theory, states of free particles ($E > 0$) in the initial and final channels are described as distorted plane waves (DPWs), which are solutions of the wave equation for the potential $V(r)$ that asymptotically behave as a plane wave plus an outgoing (+) or incoming (−) spherical wave (see, *e.g.*, Joachain, 1978).

6.2.1 Schrödinger DPWs

The Schrödinger DPWs of a spinless electron with momentum $\hbar\mathbf{k}$ in a potential $V(r)$ of finite range are solutions of the wave equation

$$\left[-\frac{\hbar^2}{2\mathrm{m_e}}\nabla^2 + V(r)\right]\psi^{(\pm)}_{\mathbf{k}}(\mathbf{r}) = E\,\psi^{(\pm)}_{\mathbf{k}}(\mathbf{r}), \qquad E = \frac{(\hbar k)^2}{2\mathrm{m_e}} \tag{6.18}$$

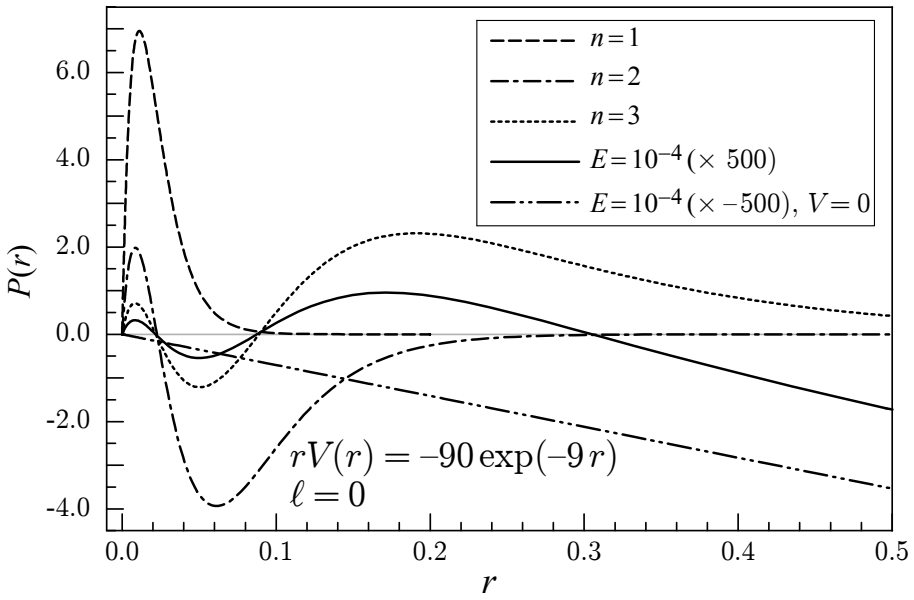

Figure 10: Calculated Schrödinger radial functions of bound states and of a free state with $E = 10^{-4}$ for the indicated potential and $\ell = 0$. The plot also shows the radial function of a free electron (*i.e.*, for $V = 0$) with the same energy. All quantities are in atomic units; the radial functions of the two free states have been multiplied by -500 for visual aid. For radii larger than about 1, the radial functions of these free states differ only by a small and constant shift. The absolute phase shift of the free state for the potential $V(r)$ is seen to be $\sim 3\pi$ (the numerical phase is $\delta_{E0} = -3.388\,277 \times 10^{-3}$) and, as predicted by the Levinson theorem, there are only 3 bound states.

with the asymptotic behaviour

$$\psi_{\mathbf{k}}^{(\pm)}(\mathbf{r}) \underset{r\to\infty}{\sim} \phi_{\mathbf{k}}(\mathbf{r}) + \psi_{\rm sc}^{(\pm)}(\mathbf{r}), \tag{6.19}$$

where

$$\phi_{\mathbf{k}}(\mathbf{r}) = \frac{1}{(2\pi)^{3/2}}\, \exp(\mathrm{i}\mathbf{k}\cdot\mathbf{r}) \tag{6.20}$$

is a plane wave, and

$$\psi_{\rm sc}^{(\pm)}(\mathbf{r}) = \frac{1}{(2\pi)^{3/2}}\, \frac{\exp(\pm \mathrm{i}kr)}{r}\, f^{(\pm)}(\hat{\mathbf{k}}\cdot\hat{\mathbf{r}}) \tag{6.21}$$

is an outgoing (+) or incoming (−) spherical wave. The function $f^{(\pm)}(\mathbf{k}\cdot\mathbf{r})$ is called the *scattering amplitude*. Physically, the DPW $\psi_{\mathbf{k}}^{(+)}(\mathbf{r})$ represents a stationary scattering state with a beam of electrons impinging in the direction $\hat{\mathbf{k}}$ and a spherical outgoing wave, modulated by the scattering amplitude $f^{(+)}(\hat{\mathbf{k}}\cdot\hat{\mathbf{r}})$, which describes electrons scattered in the direction $\hat{\mathbf{r}}$. The squared modulus of this scattering amplitude equals the scattering differential cross section (Schiff, 1968; see Section 11).

The DPWs can be expanded in the basis of spherical waves as

$$\psi_{\mathbf{k}}^{(\pm)}(\mathbf{r}) = \frac{1}{k}\sqrt{\frac{2}{\pi}}\sum_{\ell=0}^{\infty}\sum_{m=-\ell}^{\ell} \mathrm{i}^{\ell}\,\exp\left(\pm\mathrm{i}\delta_{E\ell}\right) Y_{\ell m}^{*}(\hat{\mathbf{k}})\,\psi_{E\ell m}(\mathbf{r}), \tag{6.22}$$

where $\delta_{E\ell}$ are the phase shifts. The expansion (6.22) is known as the *partial-wave series*. Inserting the expression (2.5) of the spherical waves, we have

$$\psi_{\mathbf{k}}^{(\pm)}(\mathbf{r}) = \frac{1}{kr}\sqrt{\frac{2}{\pi}}\sum_{\ell} \mathrm{i}^{\ell}\,\exp\left(\pm\mathrm{i}\delta_{E\ell}\right) P_{E\ell}(r)\sum_{m} Y_{\ell m}^{*}(\hat{\mathbf{k}})\,Y_{\ell m}(\hat{\mathbf{r}}). \tag{6.23}$$

The angular part can be simplified with the aid of the addition theorem of the spherical harmonics,

$$\sum_{m=-\ell}^{\ell} Y_{\ell m}^{*}(\hat{\mathbf{k}})\,Y_{\ell m}(\hat{\mathbf{r}}) = \frac{2\ell+1}{4\pi}\,P_{\ell}(\cos\theta), \qquad \cos\theta = \hat{\mathbf{k}}\cdot\hat{\mathbf{r}}, \tag{6.24}$$

where $P_{\ell}(\cos\theta)$ is the Legendre polynomial of degree ℓ, and θ is the angle between the vectors $\mathbf{k}$ and $\mathbf{r}$. Making use of the asymptotic form (2.8) of the radial functions, we can readily verify that the DPWs defined by the expansion (6.22) have the required asymptotic behaviour (6.19) with the scattering amplitudes given by the following partial-wave expansions

$$f^{(+)}(\hat{\mathbf{k}}\cdot\hat{\mathbf{r}}) = \frac{1}{2\mathrm{i}k}\sum_{\ell}(2\ell+1)\left[\exp(2\mathrm{i}\delta_{E\ell})-1\right]P_{\ell}(\cos\theta) \tag{6.25a}$$

and

$$f^{(-)}(\hat{\mathbf{k}}\cdot\hat{\mathbf{r}}) = \frac{1}{2\mathrm{i}k}\sum_{\ell}(-1)^{\ell}(2\ell+1)\left[1-\exp(-2\mathrm{i}\delta_{E\ell})\right]P_{\ell}(\cos\theta). \tag{6.25b}$$

The orthogonality of the radial functions (see Section 2.4) implies that the DPWs satisfy the orthogonality relation

$$\int\left[\psi_{\mathbf{k}'}^{(\pm)}(\mathbf{r})\right]^{*}\psi_{\mathbf{k}}^{(\pm)}(\mathbf{r})\,\mathrm{d}\mathbf{r} = \delta(\mathbf{k}'-\mathbf{k})\,. \tag{6.26}$$

From the partial-wave series (6.23) and (6.25), and the properties of the spherical harmonics, it follows that

$$\psi_{\mathbf{k}}^{(-)}(\mathbf{r}) = \left[\psi_{-\mathbf{k}}^{(+)}(\mathbf{r})\right]^{*} \qquad \text{and} \qquad f^{(-)}(\hat{\mathbf{k}}\cdot\hat{\mathbf{r}}) = \left[f^{(+)}(-\hat{\mathbf{k}}\cdot\hat{\mathbf{r}})\right]^{*}. \tag{6.27}$$

The first of these equalities indicates that the DPW $\psi_{\mathbf{k}}^{(-)}(\mathbf{r})$ describes the result of applying the time-reversal operator on the state corresponding to the DPW $\psi_{-\mathbf{k}}^{(+)}(\mathbf{r})$ (see, *e.g.*, Schiff, 1968).

Let us consider the continuous family of potentials $aV(r)$, with the strength parameter a taking values in the interval (0,1). Evidently, the DPWs for the potentials $aV(r)$ vary continuously with a. In the limit where a tends to zero, the phase shifts vanish,

the radial functions of free states ($E > 0$) are $P_{E\ell}(r) = kr\, j_\ell(kr)$, where $j_\ell(x)$ are the regular spherical Bessel functions [see Eq. (3.65a)], and the DPWs (6.23) become

$$\lim_{a\to 0} \psi_{\mathbf{k}}^{(\pm)}(\mathbf{r}) = \frac{1}{(2\pi)^{3/2}} \sum_\ell \mathrm{i}^\ell (2\ell+1)\, j_\ell(kr) \left[\frac{4\pi}{2\ell+1} \sum_m Y_{\ell m}^*(\hat{\mathbf{k}})\, Y_{\ell m}(\hat{\mathbf{r}}) \right], \tag{6.28}$$

which is the familiar Rayleigh expansion of the plane wave (6.20),

$$\phi_{\mathbf{k}}(\mathbf{r}) = \frac{1}{(2\pi)^{3/2}} \sum_\ell \mathrm{i}^\ell (2\ell+1)\, j_\ell(kr)\, P_\ell(\hat{\mathbf{k}}\cdot\hat{\mathbf{r}}). \tag{6.29}$$

In other words, the DPWs $\psi_{\mathbf{k}}^{(\pm)}(\mathbf{r})$ defined by Eq. (6.22) represent states that result from the continuous transformation of the normalised plane wave obtained by adiabatically rising the potential from 0 to $V(r)$, *i.e.*, varying the strength parameter a from 0 to 1.

In the case of the Coulomb potential, $V(r) = Z_\infty e^2/r$, the wave equation (6.18) for the DPW $\psi_{\mathbf{k}}^{(+)}(\mathbf{r})$ can be solved analytically by using parabolic coordinates (Joachain, 1978). The result is

$$\psi_{\mathbf{k}}^{(\mathrm{c},+)}(\mathbf{r}) = (2\pi)^{-3/2} \exp(-\pi\eta/2)\, \Gamma(1+\mathrm{i}\eta)\, \exp\left(\mathrm{i}\mathbf{k}\cdot\mathbf{r}\right)\, {}_1F_1(-\mathrm{i}\eta; 1; \mathrm{i}[kr - \mathbf{k}\cdot\mathbf{r}]), \tag{6.30}$$

where ${}_1F_1(a;b;z)$ is the Kummer function, Eq. (3.9), and η is the Sommerfeld parameter, Eq. (3.6). Far from the scattering centre, and for large "transverse distances", $d = r - \hat{\mathbf{k}}\cdot\mathbf{r}$, this DPW has the following asymptotic form,

$$\begin{aligned} \psi_{\mathbf{k}}^{(\mathrm{c},+)}(\mathbf{r}) \underset{d\to\infty}{\sim} & (2\pi)^{-3/2}\, \exp[\mathrm{i}\mathbf{k}\cdot\mathbf{r} + \mathrm{i}\eta \ln(kr - \mathbf{k}\cdot\mathbf{r})] \left[1 + \frac{\eta^2}{\mathrm{i}(kr - \mathbf{k}\cdot\mathbf{r})} + \ldots \right] \\ & + (2\pi)^{-3/2}\, \frac{\exp[\mathrm{i}kr - \mathrm{i}\eta \ln(2kr)]}{r} \left[1 + \frac{(1+\mathrm{i}\eta)^2}{\mathrm{i}(kr - \mathbf{k}\cdot\mathbf{r})} + \ldots \right] f^{(\mathrm{c},+)}(\hat{\mathbf{k}}\cdot\hat{\mathbf{r}}) \end{aligned} \tag{6.31}$$

with the scattering amplitude

$$f^{(\mathrm{c},+)}(\hat{\mathbf{k}}\cdot\hat{\mathbf{r}}) = -\eta\, \frac{\exp\{2\mathrm{i}\Delta_0 - \mathrm{i}\eta \ln[\sin^2(\theta/2)]\}}{2k \sin^2(\theta/2)}, \tag{6.32}$$

where $\theta = \arccos(\hat{\mathbf{k}}\cdot\hat{\mathbf{r}})$ is the angle between the vectors $\mathbf{k}$ and $\mathbf{r}$, and the quantity $\Delta_0 = \arg\Gamma(1+\mathrm{i}\eta)$ is the zeroth-order Coulomb phase shift, Eq. (3.21). The asymptotic form (6.31) does not reduce to the expression (6.19) characteristic of the DPWs for finite-range potentials. The long range of the Coulomb potential causes modifications that, when $d \to \infty$, affect only the phases of the two terms in the asymptotic form (6.31). Therefore, these two terms can still be interpreted as describing, respectively, an incident plane wave and an outgoing scattered wave.

The Coulomb DPW with incoming spherical component, $\psi_{\mathbf{k}}^{(\mathrm{c},-)}(\mathbf{r})$, and the corresponding scattering amplitude are determined by the formulas (6.27). That is,

$$\psi_{\mathbf{k}}^{(\mathrm{c},-)}(\mathbf{r}) \;=\; \left[\psi_{-\mathbf{k}}^{(\mathrm{c},+)}(\mathbf{r})\right]^*$$

$$= (2\pi)^{-3/2} \exp(-\pi\eta/2)\, \Gamma(1-\mathrm{i}\eta)\, \exp(\mathrm{i}\mathbf{k}\cdot\mathbf{r})\ {}_1F_1(\mathrm{i}\eta; 1; -\mathrm{i}[kr + \mathbf{k}\cdot\mathbf{r}]), \quad (6.33)$$

and

$$f^{(\mathrm{c},-)}(\hat{\mathbf{k}}\cdot\hat{\mathbf{r}}) = \left[f^{(\mathrm{c},+)}(-\hat{\mathbf{k}}\cdot\hat{\mathbf{r}})\right]^* = -\eta \exp(-2\mathrm{i}\Delta_0)\, \frac{\exp[\mathrm{i}\eta \ln(\sin^2(\theta/2))]}{2k\sin^2(\theta/2)}. \quad (6.34)$$

The Coulomb DPWs and the scattering amplitude can also be expressed in the form of partial-wave series,

$$\psi_{\mathbf{k}}^{(\pm)}(\mathbf{r}) = \frac{1}{kr}\sqrt{\frac{2}{\pi}} \sum_\ell \mathrm{i}^\ell\, \exp(\pm\mathrm{i}\Delta_\ell)\, F_\ell(\eta, kr) \sum_m Y^*_{\ell m}(\hat{\mathbf{k}})\, Y_{\ell m}(\hat{\mathbf{r}}). \quad (6.35)$$

and

$$f^{(\mathrm{c},+)}(\hat{\mathbf{k}}\cdot\hat{\mathbf{r}}) = \frac{1}{2\mathrm{i}k} \sum_\ell (2\ell+1) \left[\exp(2\mathrm{i}\Delta_\ell) - 1\right] P_\ell(\cos\theta), \quad (6.36)$$

where Δ_ℓ are the Coulomb phase shifts (3.21), and $F_\ell(\eta, kr)$ are the regular Coulomb functions (3.18).

In the general case of a modified Coulomb field, $V(r)$ such that $\lim_{r\to\infty} rV(r) = Z_\infty e^2$, the corresponding DPWs are given by the partial-wave series [cf. Eq. (6.23)]

$$\psi_{\mathbf{k}}^{(\pm)}(\mathbf{r}) = \frac{1}{kr}\sqrt{\frac{2}{\pi}} \sum_\ell \mathrm{i}^\ell\, \exp(\pm\mathrm{i}d_{E\ell})\, P_{E\ell}(r) \sum_m Y^*_{\ell m}(\hat{\mathbf{k}})\, Y_{\ell m}(\hat{\mathbf{r}}), \quad (6.37)$$

where $d_{E\ell} = \delta_{E\ell} + \Delta_\ell$ are the total phase shifts (*i.e.*, the sum of the inner and Coulomb phase shifts). Far from the scattering centre, the DPW $\psi_{\mathbf{k}}^{(+)}(\mathbf{r})$ has the asymptotic form,

$$\begin{aligned}\psi_{\mathbf{k}}^{(+)}(\mathbf{r}) \underset{d\to\infty}{\sim}\ & (2\pi)^{-3/2} \exp[\mathrm{i}\mathbf{k}\cdot\mathbf{r} + \mathrm{i}\eta\ln(kr - \mathbf{k}\cdot\mathbf{r})] \left[1 + \frac{\eta^2}{\mathrm{i}(kr - \mathbf{k}\cdot\mathbf{r})} + \ldots\right] \\ & + (2\pi)^{-3/2}\, \frac{\exp[\mathrm{i}kr - \mathrm{i}\eta\ln(2kr)]}{r} \left[1 + \frac{(1+\mathrm{i}\eta)^2}{\mathrm{i}(kr - \mathbf{k}\cdot\mathbf{r})} + \ldots\right] f^{(+)}(\hat{\mathbf{k}}\cdot\hat{\mathbf{r}}), \quad (6.38)\end{aligned}$$

with the scattering amplitude [see Eq. (6.25a)]

$$f^{(+)}(\hat{\mathbf{k}}\cdot\hat{\mathbf{r}}) = \frac{1}{2\mathrm{i}k} \sum_\ell (2\ell+1) \left[\exp(2\mathrm{i}d_{E\ell}) - 1\right] P_\ell(\cos\theta). \quad (6.39)$$

When the potential $V(r)$ has a Coulomb tail, the partial-wave series for the scattering amplitude may converge very slowly. The convergence of this series can be accelerated by adding the Coulomb scattering amplitude, Eq. (6.32), and subtracting the partial-wave series (6.36). This yields the modified series

$$f^{(+)}(\theta) = f^{(\mathrm{c},+)}(\theta) + \frac{1}{2\mathrm{i}k} \sum_\ell (2\ell+1) \exp(2\mathrm{i}\Delta_\ell) \left[\exp(2\mathrm{i}\delta_{E\ell}) - 1\right] P_\ell(\cos\theta), \quad (6.40)$$

where $\delta_{E\ell}$ are the inner phase shifts. This series converges as rapidly as the partial-wave series of the scattering amplitude for the finite-range component of the potential.

6.2.2 Dirac DPWs

We now consider the positive-energy Dirac DPWs for a central potential $V(r)$ of finite range[10]. The Dirac DPWs for an electron with momentum $\hbar\mathbf{k}$, and kinetic energy

$$E = \sqrt{(c\hbar k)^2 + (\mathrm{m_e}c^2)^2} - \mathrm{m_e}c^2, \tag{6.41}$$

in a pure spin state represented by the Pauli spinor χ_μ ($\mu = \pm 1/2$) are solutions of the wave equation

$$\left[-\mathrm{i}\, c\hbar\, \widetilde{\boldsymbol{\alpha}}\cdot\nabla + (\widetilde{\beta}-1)\mathrm{m_e}c^2 + V(r)\right] \psi^{(\pm)}_{\mathbf{k}\mu}(\mathbf{r}) = E\, \psi^{(\pm)}_{\mathbf{k}\mu}(\mathbf{r}) \tag{6.42}$$

with the asymptotic behaviour

$$\psi^{(\pm)}_{\mathbf{k}\mu}(\mathbf{r}) \underset{r\to\infty}{\sim} \phi_{\mathbf{k}\mu}(\mathbf{r}) + \psi^{(\pm)}_{\mathrm{sc}}(\mathbf{r}) \tag{6.43}$$

where

$$\phi_{\mathbf{k}\mu}(\mathbf{r}) = \frac{1}{(2\pi)^{3/2}}\, \exp(\mathrm{i}\mathbf{k}\cdot\mathbf{r}) \sqrt{\frac{E+2\mathrm{m_e}c^2}{2E+2\mathrm{m_e}c^2}} \begin{pmatrix} I_2 \\ \sqrt{\dfrac{E}{E+2\mathrm{m_e}c^2}}\, \boldsymbol{\sigma}\cdot\hat{\mathbf{k}} \end{pmatrix} \chi_\mu \tag{6.44}$$

is a positive-energy plane wave, and

$$\begin{aligned} \psi^{(\pm)}_{\mathrm{sc}}(\mathbf{r}) \;=\; & \frac{1}{(2\pi)^{3/2}}\, \frac{\exp(\pm\mathrm{i}kr)}{r} \sqrt{\frac{E+2\mathrm{m_e}c^2}{2E+2\mathrm{m_e}c^2}} \\ & \times \begin{pmatrix} I_2 \\ \pm\sqrt{\dfrac{E}{E+2\mathrm{m_e}c^2}}\, \boldsymbol{\sigma}\cdot\hat{\mathbf{r}} \end{pmatrix} \mathcal{F}(\pm\hat{\mathbf{k}},\hat{\mathbf{r}})\, \chi_\mu \end{aligned} \tag{6.45}$$

is an outgoing (+) or incoming (−) spherical wave. The factor $\mathcal{F}(\pm\hat{\mathbf{k}},\hat{\mathbf{r}})$, a 2×2 matrix independent of r, is the *scattering-amplitude matrix*.

The Dirac DPWs admit the following *partial-wave expansion* (see Rose, 1961, p. 207)

$$\psi^{(\pm)}_{\mathbf{k}\mu}(\mathbf{r}) = \frac{1}{k}\sqrt{\frac{E+2\mathrm{m_e}c^2}{\pi(E+\mathrm{m_e}c^2)}} \sum_{\kappa,m} \mathrm{i}^\ell\, \exp\left(\pm\mathrm{i}d_{E\kappa}\right) \left\{ \left[\Omega_{\kappa m}(\hat{\mathbf{k}})\right]^\dagger \chi_\mu \right\} \psi_{E\kappa m}(\mathbf{r})\,, \tag{6.46}$$

where $\psi_{E\kappa m}(\mathbf{r})$ are the spherical waves [see Eq. (2.16)]

$$\psi_{E\kappa m}(\mathbf{r}) = \frac{1}{r} \begin{pmatrix} P_{E\kappa}(r)\, \Omega_{\kappa,m}(\hat{\mathbf{r}}) \\ \mathrm{i}Q_{E\kappa}(r)\, \Omega_{-\kappa,m}(\hat{\mathbf{r}}) \end{pmatrix}. \tag{6.47}$$

[10]Modified Coulomb fields, such that $\lim_{r\to\infty} rV(r) \neq 0$, are not included in the present analysis. The case of pure Coulombian fields is studied, *e.g.*, in Rose's (1961) book.

The quantities $d_{E\kappa}$ are the total phase shifts,

$$d_{E\kappa} = \delta_{E\kappa} + \Delta_\kappa \tag{6.48}$$

where $\delta_{E\kappa}$ and Δ_κ are the inner phase shifts and the Dirac–Coulomb phase shifts [Eq. (3.129)], respectively. With the adopted normalisation for free spherical waves, Eq. (2.26), the DPWs satisfy the orthogonality relation

$$\int \left[\psi^{(\pm)}_{\mathbf{k}'\mu'}(\mathbf{r})\right]^\dagger \psi^{(\pm)}_{\mathbf{k}\mu}(\mathbf{r})\,\mathrm{d}\mathbf{r} = \delta(\mathbf{k}'-\mathbf{k})\,\delta_{\mu'\mu}\,. \tag{6.49}$$

In the case of the null potential ($V = 0$), the radial functions of free states reduce to regular spherical Bessel functions [see Eqs. (3.132)], and the DPW becomes the Dirac plane wave $\phi_{\mathbf{k}\mu}(\mathbf{r})$. The non-relativistic limit ($c \to \infty$) of the Dirac DPWs gives the Schrödinger–Pauli DPWs (see below).

The DPWs $\psi^{(+)}_{\mathbf{k}\mu}(\mathbf{r})$ represent stationary scattering states, and the scattering-amplitude matrix $\mathcal{F}(\hat{\mathbf{k}},\hat{\mathbf{r}})$ determines the scattering differential cross section. To simplify the formulas it is convenient to consider a reference frame with the z axis in the direction of the incident beam, so that $\mathbf{k} = k\hat{\mathbf{z}}$, and express the scattering-amplitude matrix as a function of the polar and azimuthal angles, θ and ϕ, of the direction $\hat{\mathbf{r}}$. We then have

$$\mathcal{F}(\hat{\mathbf{k}},\hat{\mathbf{r}}) \equiv \mathcal{F}(\theta,\phi) = \begin{pmatrix} f(\theta) & -\exp(-\mathrm{i}\phi)\,g(\theta) \\ \exp(\mathrm{i}\phi)\,g(\theta) & f(\theta) \end{pmatrix}. \tag{6.50}$$

The functions $f(\theta)$ and $g(\theta)$ are called the "direct" and "spin-flip" scattering amplitudes. They admit the following partial-wave expansions,

$$f(\theta) = \frac{1}{2\mathrm{i}k}\sum_\ell \Big\{(\ell+1)\left[\exp(2\mathrm{i}d_{E,\kappa=-\ell-1})-1\right] + \ell\left[\exp(2\mathrm{i}d_{E,\kappa=\ell})-1\right]\Big\} P_\ell(\cos\theta) \tag{6.51a}$$

and

$$g(\theta) = \frac{1}{2\mathrm{i}k}\sum_\ell \left[\exp(2\mathrm{i}d_{E,\kappa=\ell}) - \exp(2\mathrm{i}d_{E,\kappa=-\ell-1})\right] P^1_\ell(\cos\theta), \tag{6.51b}$$

where $P_\ell(\cos\theta)$ and $P^1_\ell(\cos\theta)$ are the Legendre polynomials and the associated Legendre functions, respectively. Note that the phase shifts $d_{E,\kappa=-\ell-1}$ and $d_{E,\kappa=\ell}$ correspond to $j-\ell = \frac{1}{2}$ (spin up) and $j-\ell = -\frac{1}{2}$ (spin down), respectively — see Table 1.

The partial-wave expansions (6.46) and (6.51) are also valid for the Coulomb potential (with $d_{E\kappa} = \Delta_\kappa$). Since the Coulomb phase shifts are given by analytical formulas, the calculation of the Coulomb scattering amplitudes $f^{(\mathrm{c})}(\theta)$ and $g^{(\mathrm{c})}(\theta)$ is relatively easy. Then, in the case of potentials $V(r)$ with a Coulomb tail, the number of inner phase shifts that need to be calculated to obtain the scattering amplitudes may be reduced by considering the series that result from adding and subtracting the Coulomb scattering amplitudes,

$$f(\theta) \;=\; f^{(\mathrm{c})}(\theta) + \frac{1}{2\mathrm{i}k}\sum_\ell \Big\{(\ell+1)\exp(2\mathrm{i}\Delta_{\kappa=-\ell-1})\left[\exp(2\mathrm{i}\delta_{E,\kappa=-\ell-1})-1\right]$$

$$+\,\ell\exp(2\mathrm{i}\Delta_{\kappa=\ell})\left[\exp(2\mathrm{i}\delta_{E,\kappa=\ell})-1\right]\Big\}\,P_\ell(\cos\theta) \tag{6.52a}$$

and

$$g(\theta) \;=\; g^{(\mathrm{c})}(\theta)+\frac{1}{2\mathrm{i}k}\sum_\ell\Big\{\exp(2\mathrm{i}\Delta_{\kappa=\ell})\left[\exp(2\mathrm{i}\delta_{E,\kappa=\ell})-1\right]$$

$$-\exp(2\mathrm{i}\Delta_{\kappa=-\ell-1})\left[\exp(2\mathrm{i}\delta_{E,\kappa=-\ell-1})-1\right]\Big\}\,P^1_\ell(\cos\theta). \tag{6.52b}$$

After computing the Coulomb scattering amplitudes, these series converge as rapidly as the partial-wave series for only the finite-range component of the potential.

6.2.3 Schrödinger–Pauli DPWs

The Schrödinger–Pauli DPWs for a modified Coulomb potential $V(r)$, with a finite-range component (which may include a spin orbit term) and a Coulomb tail such that $\lim_{r\to\infty} rV(r) = Z_\infty e^2$, are given by the partial-wave series [cf. Eq. (6.46)]

$$\psi^{(\pm)}_{\mathbf{k}\mu}(\mathbf{r}) = \frac{1}{k}\sqrt{\frac{2}{\pi}}\sum_{\kappa,m}\mathrm{i}^\ell\,\exp\left(\pm\mathrm{i}d_{E\kappa}\right)\left\{\left[\Omega_{\kappa m}(\hat{\mathbf{k}})\right]^\dagger\chi_\mu\right\}\,\psi_{E\kappa m}(\mathbf{r}), \tag{6.53}$$

where $\mathbf{k}$ is the wave vector, χ_μ is a Pauli spinor,

$$\psi_{E\kappa m}(\mathbf{r}) = \frac{1}{r}P_{E\kappa}(r)\,\Omega_{\kappa m}(\hat{\mathbf{r}}) \tag{6.54}$$

are spherical waves of energy $E = (\hbar k)^2/(2\mathrm{m_e})$, and $d_{E\kappa}$ are the total phase shifts. Considering the continuous family of potentials $aV(r)$, with $a\in(0,1)$, the DPW varies continuously with a. In the limit where the strength a of the potential tends to zero, the DPW reduces to the spinor plane wave

$$\phi_{\mathbf{k}\mu}(\mathbf{r}) = \frac{1}{(2\pi)^{3/2}}\,\exp(\mathrm{i}\mathbf{k}\cdot\mathbf{r})\,\chi_\mu. \tag{6.55}$$

To simplify the formulas, we consider a reference frame with the z axis in the direction of the incident beam, so that $\mathbf{k} = k\hat{\mathbf{z}}$. Then, far from the scattering centre, the DPW has the asymptotic form,

$$\psi^{(+)}_{k\hat{\mathbf{z}},\mu}(\mathbf{r}) \underset{|r-z|\to\infty}{\sim} (2\pi)^{-3/2}\,\exp[\mathrm{i}kz+\mathrm{i}\eta\ln(kr(1-\cos\theta))]\left[1+\frac{\eta^2}{\mathrm{i}kr(1-\cos\theta)}+\ldots\right]\chi_\mu$$

$$+\,(2\pi)^{-3/2}\,\frac{\exp[\mathrm{i}kr-\mathrm{i}\eta\ln(2kr)]}{r}\left[1+\frac{(1+\mathrm{i}\eta)^2}{\mathrm{i}kr(1-\cos\theta)}+\ldots\right]\mathcal{F}(\theta,\phi)\,\chi_\mu\,, \tag{6.56}$$

where θ and ϕ are the polar and azimuthal angles of the direction $\hat{\mathbf{r}}$, and $\mathcal{F}(\theta,\phi)$ is a scattering-matrix amplitude of the form (6.50). The direct and spin-flip scattering amplitudes are given by the partial-wave expansions (6.51).

It is worth noticing that for a pure Coulomb potential, $\delta_{E\kappa} = 0$, and $\Delta_{\kappa=-\ell-1} = \Delta_{\kappa=\ell} = \Delta_\ell$, the Schrödinger–Coulomb phase shift. From Eqs. (6.51)we have

$$f^{(\mathrm{c})}(\theta) = \frac{1}{2\mathrm{i}k}\sum_\ell (2\ell+1)\left[\exp(2\mathrm{i}\Delta_\ell) - 1\right] P_\ell(\cos\theta), \qquad g^{(\mathrm{c})}(\theta) = 0. \tag{6.57}$$

Because the Coulomb potential is independent of the spin, the interaction does not alter the spin state and, hence, the spin-flip scattering amplitude vanishes.

When the potential $V(r)$ has a Coulomb tail, the partial-wave series for the scattering amplitudes [Eqs. (6.51)] may converge very slowly. The convergence of these series can be accelerated by adding the Coulomb scattering amplitude, Eq. (6.32), and subtracting the partial-wave series (6.36). This yields the modified series

$$\begin{aligned} f(\theta) \;=\; & f^{(\mathrm{c})}(\theta) + \frac{1}{2\mathrm{i}k}\sum_\ell \exp(2\mathrm{i}\Delta_\ell)\left\{(\ell+1)\left[\exp(2\mathrm{i}\delta_{E,\kappa=-\ell-1}) - 1\right]\right. \\ & \left. + \ell\left[\exp(2\mathrm{i}\delta_{E,\kappa=\ell}) - 1\right]\right\} P_\ell(\cos\theta) \end{aligned} \tag{6.58a}$$

and, recalling that $g^{(\mathrm{c})} = 0$,

$$g(\theta) = \frac{1}{2\mathrm{i}k}\sum_\ell \exp(2\mathrm{i}\Delta_\ell)\left[\exp(2\mathrm{i}\delta_{E,\kappa=\ell}) - \exp(2\mathrm{i}\delta_{E,\kappa=-\ell-1})\right] P_\ell^1(\cos\theta), \tag{6.58b}$$

where $\delta_{E\kappa}$ are the inner phase shifts. These series converge as rapidly as the partial-wave series of the scattering amplitudes for the finite-range component of the potential.

6.3 Free states and complex optical potentials

Elastic collisions of fast particles with atoms and nuclei are frequently described by using the static-field approximation, in which the target is regarded as a frozen distribution of bound particles and the interaction with the projectile is represented as a time-independent, spherically symmetrical potential $V_{\mathrm{st}}(r)$. This approximation amounts to neglecting the fact that the interaction with the projectile can alter the structure of the target. In particular, elastic scattering usually coexists with inelastic collisions which cause the excitation of the target. As these collisions involve the transfer of a certain amount of energy from the projectile to the target, they effectively remove projectile particles from the elastic channel. In the so-called *optical-model potential* calculations (see, *e.g.*, Fröbrich and Lipperheide, 1996; Salvat, 2003, and references therein) this "inelastic absorption" effect is modelled by adding a negative imaginary part, $\mathrm{i}W_{\mathrm{abs}}(r)$, to the static potential. That is, the optical-model potential is expressed as

$$V(r) = V_{\mathrm{st}}(r) + \mathrm{i}W_{\mathrm{abs}}(r) \tag{6.59}$$

with $W_{\mathrm{abs}} \leq 0$. It can be easily shown that the quantity $(2/\hbar)|W_{\mathrm{abs}}(r)|$ represents the absorption probability per unit time of the projectile at r (see, *e.g.*, Section 20 of Schiff, 1968). The function $W_{\mathrm{abs}}(r)$ will be referred to as the *absorption potential*.

The theory of scattering by central potentials can be formally generalised to the case of complex potentials. In particular, one can build exact solutions of the wave equation with the form of distorted plane waves (DPWs), which admit the usual partial-wave expansion in terms of spherical waves (see Section 6.2). The only modification introduced by the imaginary potential is that the reduced radial functions and the phase shifts are now complex.

The radial Schrödinger and Dirac equations for spherical waves of a particle in the optical potential (6.59) can be solved by using essentially the same numerical algorithm as for real potentials, extended to allow complex potentials and radial functions. We limit our considerations to the case where the absorption potential has a finite range, $r_{\rm ca}$; the static potential is assumed to have the properties of the real potentials considered in previous Sections, that is, the function $rV_{\rm st}(r)$ is finite everywhere and reduces to a real constant at radii larger than $r_{\rm cs}$. That is

$$rV(r) = Z_\infty \qquad \text{for } r > r_{\rm c} = \max\{r_{\rm cs}, r_{\rm ca}\}. \tag{6.60}$$

The outward integration, from the origin up to $r_{\rm c}$, can be performed by using the power-series method with complex coefficients; the integration algorithms described in Section 4 are also valid for complex potentials.

The radial functions are calculated using the same scheme as for real potentials. The radial equations are integrated from $r = 0$ up to a certain grid point r_m beyond the range $r_{\rm c}$ of the inner component of the potential. The resulting unnormalised radial function is denoted by $\overline{P}(r_i)$. The normalised radial function for $r < r_m$ is $P(r) = A\overline{P}(r)$. Because the potential is Coulombian (or zero) for $r > r_m$, the radial function in the outer region can be expressed as a linear combination of the regular and irregular Coulomb functions [see Eq. (6.5)], with due regard to the fact that the phase shift is generally complex. That is, for $r \geq r_m$, we can write

$$P(r) = \cos\delta\; F(r) + \sin\delta\; G(r), \tag{6.61}$$

where F and G stand for the corresponding (Schrödinger or Dirac) regular and irregular Coulomb functions. The inner phase shift δ and the normalisation constant A of the inner solution are determined by matching this outer analytical form to the inner numerical solution at r_m, by requiring continuity of the radial function $P(r)$ and its derivative;

$$A\overline{P}(r_m) \;=\; \frac{\exp(\mathrm{i}\delta) + \exp(-\mathrm{i}\delta)}{2}\, F(r_m) + \frac{\exp(\mathrm{i}\delta) - \exp(-\mathrm{i}\delta)}{2\mathrm{i}}\, G(r_m), \tag{6.62a}$$

$$A\overline{P}'(r_m) \;=\; \frac{\exp(\mathrm{i}\delta) + \exp(-\mathrm{i}\delta)}{2}\, F'(r_m) + \frac{\exp(\mathrm{i}\delta) - \exp(-\mathrm{i}\delta)}{2\mathrm{i}}\, G'(r_m). \tag{6.62b}$$

Taking the ratio of these equations, we obtain the equality

$$\exp(2\mathrm{i}\delta) = \frac{\overline{P}(r_m)\,[F'(r_m) + \mathrm{i}G'(r_m)] - \overline{P}'(r_m)\,[F(r_m) + \mathrm{i}G(r_m)]}{\overline{P}'(r_m)\,[F(r_m) - \mathrm{i}G(r_m)] - \overline{P}(r_m)\,[F'(r_m) - \mathrm{i}G'(r_m)]}\,, \tag{6.63}$$

which determines the phase shift $\delta = \delta_1 + \mathrm{i}\delta_2$. To reduce the indeterminacy of the phase shifts, we proceed as in the case of real potentials, *i.e.*, we add or subtract an integer multiple of π so that the real part δ_1 of the phase lies in the interval $(-\pi/2, \pi/2)$.

If $\overline{P}(r_m)$ is not null, the normalisation of the inner solution is determined by Eq. (6.62a)

$$A = \frac{1}{\overline{P}(r_m)} \left[\frac{\exp(\mathrm{i}\delta) + \exp(-\mathrm{i}\delta)}{2} F(r_m) + \frac{\exp(\mathrm{i}\delta) - \exp(-\mathrm{i}\delta)}{2\mathrm{i}} G(r_m) \right]. \tag{6.64}$$

When $|\overline{P}(r_m)| < \epsilon$, we protect the program against computer overflows by using the alternative formula that results from (6.62b),

$$A = \frac{1}{\overline{P}'(r_m)} \left[\frac{\exp(\mathrm{i}\delta) + \exp(-\mathrm{i}\delta)}{2} F'(r_m) + \frac{\exp(\mathrm{i}\delta) - \exp(-\mathrm{i}\delta)}{2\mathrm{i}} G'(r_m) \right]. \tag{6.65}$$

6.3.1 Normalisation

For a complex optical potential, radial functions having the form (6.61) beyond the matching radius r_m are not normalised in the same form as for real potentials, that is, with $P(r)$ oscillating asymptotically with unit amplitude [see Eqs. (2.8) and (2.26)]. To obtain the normalisation condition obeyed by free states of electrons in a complex potential we can proceed as in Section 2.4.

Again we consider the case of the Dirac equation, because in the non-relativistic limit it yields the results for the Schrödinger and Schrödinger–Pauli equations. The upper-component radial function has the asymptotic behaviour

$$P_{E\kappa}(r) \underset{r\to\infty}{\sim} \sin\phi_E, \tag{6.66}$$

with

$$\phi_E = k_E r - \ell\frac{\pi}{2} - \eta_E \ln(2k_E r) + \Delta_\kappa + \delta_{E\kappa}, \tag{6.67}$$

where k_E, η_E, Δ_κ, and $\delta_{E\kappa} = \delta_1 + \mathrm{i}\delta_2$ are, respectively, the wave number, the Sommerfeld parameter, the Coulomb phase shift, and the complex inner phase shift. The squared modulus of $P_{E\kappa}(r)$ in the asymptotic region is

$$|P_{E\kappa}(r)|^2 \underset{r\to\infty}{\sim} |\sin\phi_E|^2 = \frac{1}{2}\left[1 - \exp(-2\delta_2)\,\cos(2\phi_1)\right] \tag{6.68a}$$

where

$$\phi_1 = k_E r - \ell\frac{\pi}{2} - \eta_E \ln(2k_E r) + \Delta_\kappa + \delta_1. \tag{6.68b}$$

The asymptotic form of the lower-component Dirac function is determined by the first of Eqs. (2.21). Neglecting terms of order $(1/r)$, we have

$$Q_{E\kappa}(r) \underset{r\to\infty}{\sim} \sqrt{\frac{E}{E + 2\mathrm{m_e}c^2}}\,\cos\phi_E. \tag{6.69}$$

We wish to evaluate the orthogonality integral,

$$\int_0^\infty (P^*_{E\kappa}P_{E'\kappa} + Q^*_{E\kappa}Q_{E'\kappa})\,\mathrm{d}r,$$

which defines a distribution and in actual calculations occurs only as a factor in the integrand of integrals over the energy E of the particle. We consider the radial Eqs. (2.21),

$$P'_{E\kappa} + \frac{\kappa}{r}\, P_{E\kappa} \;=\; \frac{E - V + 2\mathrm{m_e}c^2}{c\hbar}\, Q_{E\kappa}, \tag{6.70a}$$

$$Q'_{E\kappa} - \frac{\kappa}{r}\, Q_{E\kappa} \;=\; -\,\frac{E - V}{c\hbar}\, P_{E\kappa}. \tag{6.70b}$$

Multiplying Eqs. (6.70a) and (6.70b) from the left by $Q^*_{E'\kappa}$ and $P^*_{E'\kappa}$, respectively,

$$Q^*_{E'\kappa}P'_{E\kappa} + \frac{\kappa}{r}\, Q^*_{E'\kappa}P_{E\kappa} \;=\; \frac{E - V + 2\mathrm{m_e}c^2}{c\hbar}\, Q^*_{E'\kappa}Q_{E\kappa},$$

$$P^*_{E'\kappa}Q'_{E\kappa} - \frac{\kappa}{r}\, P^*_{E'\kappa}Q_{E\kappa} \;=\; -\,\frac{E - V}{c\hbar}\, P^*_{E'\kappa}P_{E\kappa}.$$

We can write a pair of analogous equations by interchanging E and E' and taking the complex conjugate,

$$Q_{E\kappa}P'^*_{E'\kappa} + \frac{\kappa}{r}\, Q_{E\kappa}P^*_{E'\kappa} \;=\; \frac{E' - V^* + 2\mathrm{m_e}c^2}{c\hbar}\, Q_{E\kappa}Q^*_{E'\kappa},$$

$$P_{E\kappa}Q'^*_{E'\kappa} - \frac{\kappa}{r}\, P_{E\kappa}Q^*_{E'\kappa} \;=\; -\,\frac{E' - V^*}{c\hbar}\, P_{E\kappa}P^*_{E'\kappa}.$$

Subtracting from the equations in the first pair those in the second pair, we get

$$Q^*_{E'\kappa}P'_{E\kappa} - Q_{E\kappa}P'^*_{E'\kappa} + \frac{\kappa}{r}\,(Q^*_{E'\kappa}P_{E\kappa} - Q_{E\kappa}P^*_{E'\kappa}) \;=\; \frac{E - E' - V + V^*}{c\hbar}\, Q^*_{E'\kappa}Q_{E\kappa},$$

$$P^*_{E'\kappa}Q'_{E\kappa} - P_{E\kappa}Q'^*_{E'\kappa} - \frac{\kappa}{r}\,(P^*_{E'\kappa}Q_{E\kappa} - P_{E\kappa}Q^*_{E'\kappa}) \;=\; -\,\frac{E - E' - V + V^*}{c\hbar}\, P^*_{E'\kappa}P_{E\kappa},$$

and, finally, subtracting the second from the first of these equations we have

$$\begin{aligned}\frac{E - E' + 2\mathrm{i}W_{\mathrm{abs}}}{c\hbar}\,[P^*_{E'\kappa}P_{E\kappa} + Q^*_{E'\kappa}Q_{E\kappa}] \;&=\; P_{E\kappa}Q'^*_{E'\kappa} + P'_{E\kappa}Q^*_{E'\kappa} - P^*_{E'\kappa}Q'_{E\kappa} - P'^*_{E'\kappa}Q_{E\kappa} \\ &=\; \frac{\mathrm{d}}{\mathrm{d}r}\left(Q^*_{E'\kappa}P_{E\kappa} - P^*_{E'\kappa}Q_{E\kappa}\right). \end{aligned} \tag{6.71}$$

Then, for any value of R,

$$\int_0^R \frac{E - E' + 2\mathrm{i}W_{\mathrm{abs}}}{c\hbar}\,(P^*_{E'\kappa}P_{E\kappa} + Q^*_{E'\kappa}Q_{E\kappa})\,\mathrm{d}r = Q^*_{E'\kappa}(R)P_{E\kappa}(R) - P^*_{E'\kappa}(R)Q_{E\kappa}(R) \tag{6.72}$$

because $P_{E\kappa}(0) = Q_{E\kappa}(0) = 0$. The main contribution to the integral comes from large radial distances, where the asymptotic forms (6.66) and (6.69) are valid. Introducing these expressions into Eq. (6.72) we obtain

$$\int_0^R \left(1 + 2\mathrm{i}\,\frac{W_{\mathrm{abs}}}{E - E'}\right)(P^*_{E'\kappa}P_{E\kappa} + Q^*_{E'\kappa}Q_{E\kappa})\,\mathrm{d}r$$

$$= \frac{c\hbar}{E-E'}\left\{\sqrt{\frac{E'}{E'+2\mathrm{m_e}c^2}}\cos\phi^*_{E'}\sin\phi_E - \sqrt{\frac{E}{E+2\mathrm{m_e}c^2}}\sin\phi^*_{E'}\cos\phi_E\right\}$$

$$= \frac{c\hbar}{E-E'}\left\{\sqrt{\frac{E'}{E'+2\mathrm{m_e}c^2}}\sin\Big[\,(k_E-k_{E'})\,R\Big] + X_{E',E}(R)\right\}, \tag{6.73}$$

where

$$X_{E',E}(R) \equiv \sqrt{\frac{E'}{E'+2\mathrm{m_e}c^2}}\left(\cos\phi^*_{E'}\,\sin\phi_E - \sin\Big[\,(k_E-k_{E'})\,R\Big]\right)$$

$$- \sqrt{\frac{E}{E+2\mathrm{m_e}c^2}}\,\sin\phi^*_{E'}\cos\phi_E. \tag{6.74}$$

If $E \neq E'$, $X_{E',E}(R)$ oscillates infinitely rapidly as $R \to \infty$ and contributes nothing. When $E = E'$, the familiar equality

$$\sin\phi_E\,\cos\phi^*_E - \sin\phi^*_E\,\cos\phi_E = \sin(\phi_E - \phi^*_E)$$

implies that

$$\begin{aligned}\sin\phi^*_E\,\cos\phi_E &= \cos\phi^*_E\sin\phi_E - \sin(\phi_E-\phi^*_E)\\ &= \cos\phi^*_E\sin\phi_E - \mathrm{i}\sinh(2\delta_2),\end{aligned} \tag{6.75}$$

where δ_2 is the imaginary part of $\delta_{E\kappa}$. Evidently, the real part of $X_{E,E}(R)$ vanishes and, taking the real parts of Eq. (6.73), we can write

$$\begin{aligned}&\int_0^\infty (P^*_{E'\kappa}P_{E\kappa} + Q^*_{E'\kappa}Q_{E\kappa})\,\mathrm{d}r\\ &= c\hbar\sqrt{\frac{E'}{E'+2\mathrm{m_e}c^2}}\,\frac{k_E-k_{E'}}{E-E'}\,\lim_{R\to\infty}\left\{\frac{1}{k_E-k_{E'}}\sin\Big[\,(k_E-k_{E'})\,R\Big]\right\}\\ &= \frac{E'}{k_{E'}}\,\frac{k_E-k_{E'}}{E-E'}\,\pi\,\delta(k_E-k_{E'}) = \frac{\pi E'}{k_{E'}}\,\frac{k_E-k_{E'}}{E-E'}\,\frac{\mathrm{d}E}{\mathrm{d}k_E}\,\delta(E-E')\\ &= \frac{\pi E}{k_E}\,\delta(E-E').\end{aligned}$$

Consequently, the calculated radial functions (6.61) for the complex optical potential (6.59) satisfy the same orthogonality relation

$$\int_0^\infty (P^*_{E'\kappa}P_{E\kappa} + Q^*_{E'\kappa}Q_{E\kappa})\,\mathrm{d}r = \frac{\pi E}{k_E}\,\delta(E-E') \tag{6.76}$$

as the radial functions for real potentials [cf. Eq. (2.48)]. This property implies that the DPWs for the complex optical potential are still given by Eq. (6.46), and they satisfy the orthogonality relation (6.49). Evidently, an analogous conclusion holds for the Schrödinger and the Schrödinger–Pauli equations.

7 Asymptotic expansions

Practical calculations in collision theory and quantum electrodynamics involve matrix elements of operators with bound and free states, that is, integrals of radial functions that extend from 0 to ∞. In some cases (*e.g.*, in studies of bremsstrahlung emission by charged particles) the integrals contain only free states and are difficult to compute, because of the fast oscillations of the radial functions. The calculation can be eased by using asymptotic expansions of the radial functions, which allow the analytical evaluation of the integrals from a certain finite radius, $r_{\rm a}$, to ∞. In this Section we present asymptotic expansions for the radial functions of states with arbitrary energies in a Coulomb potential, $rV(r) = Z_\infty$. These expansions are valid for modified Coulomb potentials, although their validity is limited to the Coulomb tail, *i.e.*, to radii beyond the range $r_{\rm c}$ of the finite-range component of the potential. They can also be used for complex optical potentials with a finite-range imaginary part, in which case the phase-dependent coefficients are complex.

7.1 Schrödinger free states

The radial function of a non-relativistic electron in the outer region, $r > r_{\rm c}$, is given by [see Eq. (6.1)],

$$P(r) = \cos\delta\; F_\ell(\eta, x) + \sin\delta\; G_\ell(\eta, x), \tag{7.1}$$

where $F_\lambda(\eta, x)$ and $G_\lambda(\eta, x)$ are the Schrödinger–Coulomb functions (see Section 3.1.2), which we consider as functions of the dimensionless variable $x = kr$. Asymptotic expansions of these functions can be obtained directly from the relation [see Eqs. (3.50) and (3.54)]

$$G_\lambda(\eta, x) + {\rm i}F_\lambda(\eta, x) = {}_2F_0\left({\rm i}\eta - \lambda, {\rm i}\eta + \lambda + 1; (2{\rm i}x)^{-1}\right)\, \exp({\rm i}\theta_\lambda), \tag{7.2}$$

where ${}_2F_0$ is the hypergeometric function given by Eq. (3.53) and [see Eqs. (3.29) and (3.21)]

$$\theta_\lambda = x - \lambda\frac{\pi}{2} - \eta\ln(2x) + {\rm arg}\Gamma(\lambda + 1 + {\rm i}\eta). \tag{7.3}$$

We have,

$$\begin{aligned} F_\lambda(\eta, x) &= \mathcal{G}_\lambda(x)\cos\theta_\lambda + \mathcal{F}_\lambda(x)\sin\theta_\lambda, \\ G_\lambda(\eta, x) &= \mathcal{F}_\lambda(x)\cos\theta_\lambda - \mathcal{G}_\lambda(x)\sin\theta_\lambda, \end{aligned} \tag{7.4}$$

with

$$\begin{aligned} \mathcal{F}_\lambda(x) &= {\rm Re}\;{}_2F_0\left({\rm i}\eta - \lambda, {\rm i}\eta + \lambda + 1; (2{\rm i}x)^{-1}\right), \\ \mathcal{G}_\lambda(x) &= {\rm Im}\;{}_2F_0\left({\rm i}\eta - \lambda, {\rm i}\eta + \lambda + 1; (2{\rm i}x)^{-1}\right). \end{aligned} \tag{7.5}$$

Inserting the expansions (7.4) into Eq. (7.1), we obtain

$$P(r) = \cos(\delta + \theta_\ell)\,\mathcal{G}_\ell(x) + \sin(\delta + \theta_\ell)\,\mathcal{F}_\ell(x). \tag{7.6}$$

It is now convenient to introduce the quantity

$$\phi_\ell \equiv \delta + \theta_\ell = kr - \eta \ln r + d_\ell^{(0)}, \tag{7.7}$$

where

$$d_\ell^{(0)} \equiv \delta - \ell\frac{\pi}{2} - \eta \ln(2k) + \mathrm{arg}\Gamma(\ell + 1 + \mathrm{i}\eta) \tag{7.8}$$

is an r-independent phase. We can thus write

$$P(r) = \mathcal{A}_1(r)\, \cos\phi_\ell + \mathcal{A}_2(r)\, \sin\phi_\ell \tag{7.9}$$

with the functions $\mathcal{A}_1(r) = \mathcal{G}_\ell(x)$ and $\mathcal{A}_2(r) = \mathcal{F}_\ell(x)$ defined in Eq. (7.5) as power series in r^{-1}. This is the sought asymptotic expansion for $P(r)$. The corresponding expansion for $Q(r) = P'(r)$,

$$Q(r) = \mathcal{A}_3(r)\, \cos\phi_\ell + \mathcal{A}_4(r)\, \sin\phi_\ell, \tag{7.10}$$

can be obtained by straight differentiation.

7.2 Dirac free states

The Dirac radial functions of the electron in the outer region of the potential, $r > r_\mathrm{c}$, can be expressed as [see Eq. (6.2)]

$$\begin{aligned} P(r) &= \cos\delta\, f_\kappa^{(\mathrm{u})}(r) + \sin\delta\, g_\kappa^{(\mathrm{u})}(r), \\ Q(r) &= \cos\delta\, f_\kappa^{(\mathrm{l})}(r) + \sin\delta\, g_\kappa^{(\mathrm{l})}(r), \end{aligned} \tag{7.11}$$

where $f_\kappa^{(\mathrm{u,l})}$ and $g_\kappa^{(\mathrm{u,l})}$ are, respectively, the regular and irregular Dirac–Coulomb functions (see Section 3.2.1). It is convenient to use the relations (3.118) and express these functions in terms of the non-relativistic Coulomb functions $F_\lambda(\eta, x)$ and $G_\lambda(\eta, x)$ (see Section 3.1.2), which again we consider as functions of the dimensionless variable $x = kr$. We have

$$\begin{aligned} u_\kappa^{(\mathrm{u})}(r) &= N\left[(\kappa+\lambda)\sqrt{\lambda^2+\eta^2}\; c\hbar k\; U_\lambda(\eta,x) + \alpha Z_\infty\left(\lambda\, \mathrm{m_e}c^2 - \kappa\, W\right)\; U_{\lambda-1}(\eta,x)\right], \\ u_\kappa^{(\mathrm{l})}(r) &= -N\left[\alpha Z_\infty\sqrt{\lambda^2+\eta^2}\; c\hbar k\; U_\lambda(\eta,x)\right. \\ &\qquad \left. + (\kappa+\lambda)\left(\lambda\, \mathrm{m_e}c^2 - \kappa\, W\right)\; U_{\lambda-1}(\eta,x)\right], \end{aligned} \tag{7.12}$$

where $u_\kappa^{(\mathrm{u,l})} = f_\kappa^{(\mathrm{u,l})}$ or $g_\kappa^{(\mathrm{u,l})}$, $U_\lambda = F_\lambda$ or G_λ, and [see Eq. (3.126)]

$$N = (1 - 2\mathcal{S}_{Z_\infty,\kappa})\,\frac{1}{\lambda}\left[(\alpha Z_\infty)^2\left(W + \mathrm{m_e}c^2\right)^2 + (\kappa+\lambda)^2(c\hbar k)^2\right]^{-1/2} \tag{7.13}$$

with $\mathcal{S}_{Z_\infty,\kappa} = 1$ if $Z_\infty < 0$ and $\kappa < 0$, and $= 0$ otherwise.

Inserting the expressions (7.12) into the right-hand side of Eq. (7.11), and using the expansions (7.4), the large radial function in the outer region, $r > r_\mathrm{c}$, is expressed as

$$P(r) = N\left\{(\kappa+\lambda)\sqrt{\lambda^2+\eta^2}\; c\hbar k\; \left[\mathcal{G}_\lambda(x)\cos(\phi_\kappa + \Delta\theta) + \mathcal{F}_\lambda(x)\sin(\phi_\kappa + \Delta\theta)\right]\right.$$

$$+ \alpha Z_\infty \left(\lambda\, \mathrm{m_e}c^2 - \kappa\, W\right)\, \left[\mathcal{G}_{\lambda-1}(x)\, \cos\phi_\kappa + \mathcal{F}_{\lambda-1}(x)\, \sin\phi_\kappa\right] \Big\}\,, \tag{7.14}$$

where

$$\phi_\kappa \equiv \delta + \theta_{\lambda-1} \qquad \text{and} \qquad \Delta\theta \equiv \theta_\lambda - \theta_{\lambda-1}. \tag{7.15}$$

From the definition (7.3) and the properties of the Γ function, we have

$$\Delta\theta = -\frac{\pi}{2} + \arg\frac{\Gamma(\lambda+1+\mathrm{i}\eta)}{\Gamma(\lambda+\mathrm{i}\eta)} = -\frac{\pi}{2} + \arg(\lambda+\mathrm{i}\eta). \tag{7.16}$$

Expanding the trigonometric functions in (7.14) and rearranging terms, we arrive at the desired asymptotic expansion,

$$P(r) = \mathcal{A}_1(r)\cos\phi_\kappa + \mathcal{A}_2(r)\sin\phi_\kappa, \tag{7.17}$$

where

$$\begin{aligned}\mathcal{A}_1(r) \;=\; & N(\kappa+\lambda)\sqrt{\lambda^2+\eta^2}\; c\hbar k\; \left[\mathcal{F}_\lambda(x)\sin\Delta\theta + \mathcal{G}_\lambda(x)\cos\Delta\theta\right] \\ & + N\alpha Z_\infty \left(\lambda\, \mathrm{m_e}c^2 - \kappa\, W\right) \mathcal{G}_{\lambda-1}(x)\end{aligned} \tag{7.18}$$

and

$$\begin{aligned}\mathcal{A}_2(r) \;=\; & N(\kappa+\lambda)\sqrt{\lambda^2+\eta^2}\; c\hbar k\; \left[\mathcal{F}_\lambda(x)\cos\Delta\theta - \mathcal{G}_\lambda(x)\sin\Delta\theta\right] \\ & + N\alpha Z_\infty \left(\lambda\, \mathrm{m_e}c^2 - \kappa\, W\right) \mathcal{F}_{\lambda-1}(x).\end{aligned} \tag{7.19}$$

Notice that

$$\phi_\kappa = kr - \eta\ln r + d_\kappa^{(0)} \tag{7.20}$$

with

$$d_\kappa^{(0)} = \delta + \arg\Gamma(\lambda+\mathrm{i}\eta) - \eta\ln(2k) - (\lambda-1)\frac{\pi}{2}. \tag{7.21}$$

Similarly, for the small radial function we obtain

$$Q(r) = \mathcal{A}_3(r)\cos\phi_\kappa + \mathcal{A}_4(r)\sin\phi_\kappa, \tag{7.22}$$

where

$$\begin{aligned}\mathcal{A}_3(r) \;=\; & -N\,\alpha Z_\infty\sqrt{\lambda^2+\eta^2}\; c\hbar k\; \left[\mathcal{F}_\lambda(x)\sin\Delta\theta + \mathcal{G}_\lambda(x)\cos\Delta\theta\right] \\ & - N(\kappa+\lambda)\left(\lambda\, \mathrm{m_e}c^2 - \kappa\, W\right) \mathcal{G}_{\lambda-1}(x)\end{aligned} \tag{7.23}$$

and

$$\begin{aligned}\mathcal{A}_4(r) \;=\; & -N\,\alpha Z_\infty\sqrt{\lambda^2+\eta^2}\; c\hbar k\; \left[\mathcal{F}_\lambda(x)\cos\Delta\theta - \mathcal{G}_\lambda(x)\sin\Delta\theta\right] \\ & - N(\kappa+\lambda)\left(\lambda\, \mathrm{m_e}c^2 - \kappa\, W\right) \mathcal{F}_{\lambda-1}(x).\end{aligned} \tag{7.24}$$

When $Z_\infty = 0$ and $\kappa < 0$, the above expressions are indeterminate and have to be replaced with

$$\mathcal{A}_1 = \mathcal{G}_{\lambda-1}, \quad \mathcal{A}_2 = \mathcal{F}_{\lambda-1}, \quad \mathcal{A}_3 = \sqrt{\frac{\epsilon}{W+\mathrm{m_e}c^2}}\,\mathcal{F}_\lambda, \quad \mathcal{A}_4 = -\sqrt{\frac{\epsilon}{W+\mathrm{m_e}c^2}}\,\mathcal{G}_\lambda. \tag{7.25}$$

For both Schrödinger and Dirac free states, the functions $\mathcal{A}_i(r)$ are defined as series in powers of r^{-1}. It is convenient to express them in the form

$$\mathcal{A}_i(r) = \sum_{\nu=0}^{\nu_\mathrm{a}} A_{i\nu} \left(\frac{r_\mathrm{a}}{r}\right)^\nu , \tag{7.26}$$

where we have introduced the radius of convergence r_a. Although the (real-valued) coefficients $A_{i\nu}$ have complicated expressions, it is easy to obtain their values numerically. In the RADIAL code, the series are truncated at $\nu_\mathrm{a} = 49$ (50 terms). The subroutines `SFAS0` (Schrödinger) and `DFAS0` (Dirac) generate the coefficients $A_{i\nu}$ ($i = 1$ to 4, $\nu = 0$ to 49) and store them in the common blocks `CSFAS` and `CDFAS`. These subroutines also determine the convergence radius of the truncated series, *i.e.*, a radius r_a such that for $r > r_\mathrm{a}$ the series converge within the required accuracy (specified by the parameter ϵ). Once the coefficients A_{in} have been evaluated, the subroutine `SFAS` (Schrödinger) or `DFAS` (Dirac) can be called to calculate the radial functions at $r > r_\mathrm{a}$ from their asymptotic expansions (7.9), (7.17) and (7.22). With the considered 50 terms, the convergence radius r_a is of the order of the classical turning point,

$$r_\mathrm{TP}[\lambda] = k^{-1} x_\mathrm{TP}[\lambda] = k^{-1}\left[\eta + \sqrt{\eta^2 + \lambda(\lambda+1)}\right]. \tag{7.27}$$

In the interval from r_a to infinity, the truncated asymptotic series approximate the radial functions P and Q with relative accuracy better than ϵ.

For $Z_\infty = 0$, the Coulomb functions reduce to spherical Bessel and Neumann functions; in this case, the present formulas are equivalent to the well-known asymptotic expansions of the spherical functions.

7.3 Schrödinger bound states

In the Coulomb tail (*i.e.*, for $r > r_\mathrm{c}$) of potentials with $Z_\infty < 0$, the Schrödinger equation for bound states ($E < 0$),

$$-\frac{\hbar^2}{2\mathrm{m_e}}\frac{\mathrm{d}^2}{\mathrm{d}r^2}P_{E\ell}(r) + \left[\frac{\hbar^2}{2\mathrm{m_e}}\frac{\ell(\ell+1)}{r^2} + \frac{Z_\infty e^2}{r}\right] P_{E\ell}(r) = E\, P_{E\ell}(r), \tag{7.28}$$

can be recast in dimensionless form by introducing the familiar change of variable $z = 2ar$, with

$$a = \sqrt{\frac{2\mathrm{m_e}}{\hbar^2}(-E)}. \tag{7.29}$$

We have

$$\frac{\mathrm{d}^2}{\mathrm{d}z^2}P_{E\ell}(z) + \left[-\frac{1}{4} + \frac{\overline{\eta}}{z} + \frac{\frac{1}{4} - (\ell+\frac{1}{2})^2}{z^2}\right] P_{E\ell}(z) = 0\,, \tag{7.30}$$

which is the Whittaker standard form of the confluent hypergeometric equation with

$$\overline{\eta} = \sqrt{\frac{Z_\infty^2}{2(-E)}\,E_\mathrm{h}}\,. \tag{7.31}$$

Hence, for any negative energy E, and at radii beyond the start of the Coulomb tail, the radial function of bound states is proportional to the Whittaker function regular at $r = \infty$,

$$P_{E\ell}(r) = N\mathcal{W}_{\overline{\eta},\ell+1/2}(2ar)\,, \tag{7.32}$$

where N is a normalisation constant.

The asymptotic expansion of the Whittaker function, Eq. (3.16),

$$\mathcal{W}_{\overline{\eta},\ell+1/2}(2ar) = (2ar)^{\overline{\eta}}\,\mathrm{e}^{-ar}\left[\sum_{\nu=0}^{R-1}\frac{(\ell+1-\overline{\eta})_\nu\;(-\ell-\overline{\eta})_\nu}{\nu!\;(-2ar)^\nu} + O(|2ar|^{-R})\right], \tag{7.33}$$

gives the sought expansion of the radial function,

$$P_{E\ell}(r) \;=\; N(2ar)^{\overline{\eta}}\,\mathrm{e}^{-ar}\sum_\nu \mathcal{A}_\nu^{(\ell)}\,\left(\frac{r_\mathrm{a}}{r}\right)^\nu, \tag{7.34}$$

with

$$\mathcal{A}_\nu^{(\ell)} = \frac{(\ell+1-\overline{\eta})_\nu\;(-\ell-\overline{\eta})_\nu}{\nu!\;(-2ar_\mathrm{a})^\nu}\,. \tag{7.35}$$

Here we have introduced a "convergence radius", r_a, so that convergence at $r = r_\mathrm{a}$ ensures convergence at any larger r. The derivative of the radial function is given by

$$Q_{E\ell}(r) \equiv \frac{\mathrm{d}}{\mathrm{d}r}P_{E\ell}(r) = N(2ar)^{\overline{\eta}}\,\mathrm{e}^{-ar}\sum_\nu\left(\frac{\overline{\eta}-\nu+1}{r_\mathrm{a}}\,\mathcal{A}_{\nu-1}^{(\ell)} - a\,\mathcal{A}_\nu^{(\ell)}\right)\left(\frac{r_\mathrm{a}}{r}\right)^\nu. \tag{7.36}$$

It is interesting to observe that when E is an exact eigenvalue of the Coulomb potential, $E_n = -(Z_\infty^2/2n^2)\,E_\mathrm{h}$ and $\overline{\eta} = n$ [see Section 3.1.5], the solution (7.32) regular at $r = \infty$ coincides with the solution of the pure Coulomb potential that is regular at $r = 0$. In this case, the asymptotic series (7.33) terminates after $n_\mathrm{r} + 1 = n - \ell$ terms, being identical to the familiar polynomial form (3.83) of the regular Schrödinger–Coulomb function. That is, the asymptotic series for bound eigenstates of a Coulomb potential converge for all r!

7.4 Dirac bound states

Asymptotic expansions of the Dirac radial functions for bound states can be obtained easily by using the relation (3.112) between Dirac– and Schrödinger–Coulomb radial functions, and the result (7.32),

$$\begin{pmatrix} P_{E\kappa}(r) \\ Q_{E\kappa}(r) \end{pmatrix} = D^{-1}\begin{pmatrix} P_{E,\lambda}(r) \\ q\;P_{E,\lambda-1}(r) \end{pmatrix} = N\begin{pmatrix} \kappa+\lambda & \alpha Z_\infty \\ -\alpha Z_\infty & -\kappa-\lambda \end{pmatrix}\begin{pmatrix} \mathcal{W}_{\overline{\eta},\lambda+1/2}(2ar) \\ q\,\mathcal{W}_{\overline{\eta},\lambda-1/2}(2ar) \end{pmatrix}, \tag{7.37}$$

where

$$\lambda = \sqrt{\kappa^2 - (\alpha Z_\infty)^2}, \qquad a = \frac{\sqrt{-E(E+2\mathrm{m_e}c^2)}}{\hbar c} \qquad \text{and} \qquad \overline{\eta} \equiv -\,\frac{\alpha Z_\infty\,(E+\mathrm{m_e}c^2)}{c\hbar a}\,, \tag{7.38}$$

and the normalisation constant N absorbs all the common factors. That is,

$$\begin{aligned} P_{E\kappa}(r) &= N\left[(\kappa+\lambda)\mathcal{W}_{\overline{\eta},\lambda+1/2}(2ar) + \alpha Z_\infty\, q\, \mathcal{W}_{\overline{\eta},\lambda-1/2}(2ar)\right] \\ Q_{E\kappa}(r) &= N\left[-\alpha Z_\infty\, \mathcal{W}_{\overline{\eta},\lambda+1/2}(2ar) - (\kappa+\lambda)\, q\, \mathcal{W}_{\overline{\eta},\lambda-1/2}(2ar)\right] \end{aligned} \tag{7.39}$$

Then, from Eq. (7.33), we obtain the following asymptotic expansions,

$$\begin{aligned} P_{E\kappa}(r) &= N(2ar)^{\overline{\eta}}\, \mathrm{e}^{-ar} \sum_\nu \left[(\kappa+\lambda)\mathcal{A}_\nu^{(\lambda)} + \alpha Z_\infty\, q\, \mathcal{A}_\nu^{(\lambda-1)}\right] \left(\frac{r_\mathrm{a}}{r}\right)^\nu \\ Q_{E\kappa}(r) &= N(2ar)^{\overline{\eta}}\, \mathrm{e}^{-ar} \sum_\nu \left[-\alpha Z_\infty\, \mathcal{A}_\nu^{(\lambda)} - (\kappa+\lambda)\, q\, \mathcal{A}_\nu^{(\lambda-1)}\right] \left(\frac{r_\mathrm{a}}{r}\right)^\nu , \end{aligned} \tag{7.40}$$

with $\mathcal{A}_\nu^{(\lambda)}$ given by Eq. (7.35). Inserting these expansions into the Dirac radial equations for the Coulomb tail,

$$\begin{aligned} \frac{\mathrm{d}P}{\mathrm{d}r} &= -\frac{\kappa}{r}\, P + \frac{E+2\mathrm{m_e}c^2}{\hbar c}\, Q - \frac{Z_\infty \alpha}{r}\, Q\,, \\ \frac{\mathrm{d}Q}{\mathrm{d}r} &= -\frac{E}{\hbar c}\, P + \frac{Z_\infty \alpha}{r}\, P + \frac{\kappa}{r}\, Q\,, \end{aligned} \tag{7.41}$$

and equating the coefficients of terms with $\nu = 0$ on both sides of the equalities we obtain the following equivalent expressions for the parameter q in Eq. (7.37),

$$q = \frac{-a(\kappa+\lambda) + \dfrac{E+2\mathrm{m_e}c^2}{\hbar c}\alpha Z_\infty}{a\alpha Z_\infty - \dfrac{E+2\mathrm{m_e}c^2}{\hbar c}(\kappa+\lambda)} = \frac{-a\alpha Z_\infty - \dfrac{E}{\hbar c}(\kappa+\lambda)}{a(\kappa+\lambda) + \dfrac{E}{\hbar c}\alpha Z_\infty}\,. \tag{7.42}$$

We thus arrive at the desired asymptotic expansions of the radial functions,

$$P_{E\kappa}(r) = N(2ar)^{\overline{\eta}}\, \mathrm{e}^{-ar} \sum_\nu \mathcal{B}_\nu \left(\frac{r_\mathrm{a}}{r}\right)^\nu , \tag{7.43a}$$

$$Q_{E\kappa}(r) = N(2ar)^{\overline{\eta}}\, \mathrm{e}^{-ar} \sum_\nu \mathcal{C}_\nu \left(\frac{r_\mathrm{a}}{r}\right)^\nu , \tag{7.43b}$$

with

$$\mathcal{B}_\nu = (\kappa+\lambda)\left[a(\kappa+\lambda) + \frac{E}{\hbar c}\alpha Z_\infty\right]\mathcal{A}_\nu^{(\lambda)} - \alpha Z_\infty \left[a\alpha Z_\infty + \frac{E}{\hbar c}(\kappa+\lambda)\right]\mathcal{A}_\nu^{(\lambda-1)}\,, \tag{7.44a}$$

$$\mathcal{C}_\nu = -\alpha Z_\infty \left[a(\kappa+\lambda) + \frac{E}{\hbar c}\alpha Z_\infty\right]\mathcal{A}_\nu^{(\lambda)} + (\kappa+\lambda)\left[a\alpha Z_\infty + \frac{E}{\hbar c}(\kappa+\lambda)\right]\mathcal{A}_\nu^{(\lambda-1)}\,. \tag{7.44b}$$

The expansions (7.34) and (7.43) represent exact solutions of the corresponding wave equation in the Coulomb tail (*i.e.*, for $r > r_\mathrm{c}$), and can be used as analytical expressions of the radial functions for radii larger than a certain r_a, at which the expansions converge within the required accuracy (defined by the parameter ϵ). As in the case of free states,

the series are truncated at $\nu_{\rm a} = 49$ (50 terms). The package RADIAL contains subroutines `SBAS0` (Schrödinger) and `DBAS0` (Dirac) that generate the coefficients $\mathcal{A}_\nu^{(\lambda)}$, $\mathcal{B}_\nu$ and $\mathcal{C}_\nu$ ($\nu = 0$ to 49), store them in the common blocks `CSBAS` and `CDBAS`, and determine $r_{\rm a}$. Once these quantities have been set, the subroutine `SBAS` (Schrödinger) or `DBAS` (Dirac) can be called to calculate the radial functions at any $r \geq r_{\rm a}$ from the corresponding asymptotic expansions. The normalisation constant N can be determined by matching the radial functions calculated numerically at some radius r beyond $r_{\rm a}$.

• Integrals of asymptotic expansions

As indicated above, in calculations of collision theory we may find integrals involving products of free states, bound states, and powers of r. For radii beyond the onset $r_{\rm c}$ of the Coulomb tail, we can introduce the asymptotic expansions and reduce the radial integral from r_0 to infinity to a finite sum of integrals that are the real or the imaginary parts of the following

$$\int_{r_0}^{\infty} \exp\left[\mathrm{i}(ar - b\ln r)\right] \frac{1}{r^{n+1}}\,\mathrm{d}r = (-\mathrm{i}a)^{n+\mathrm{i}b}\,\Gamma(-n-\mathrm{i}b, -\mathrm{i}ar_0), \tag{7.45}$$

where $\Gamma(\alpha, z)$ is the incomplete gamma function with complex arguments (Abramowitz and Stegun, 1974),

$$\Gamma(\alpha, z) \equiv \int_z^{\infty} \mathrm{e}^{-t}\, t^{\alpha-1}\,\mathrm{d}t = z^\alpha \int_1^{\infty} \mathrm{e}^{-zu}\, u^{\alpha-1}\,\mathrm{d}u. \tag{7.46}$$

Introducing the continued fraction representation (Abramowitz and Stegun, 1974),

$$\Gamma(\alpha, z) = \mathrm{e}^{-z} z^\alpha \left(\frac{1}{z+} \frac{1-\alpha}{1+} \frac{1}{z+} \frac{2-\alpha}{1+} \frac{2}{z+} \frac{3-\alpha}{1+} \cdots \right), \tag{7.47}$$

the integral (7.45) can be expressed as

$$\int_{r_0}^{\infty} \exp\left[\mathrm{i}(ar - b\ln r)\right] \frac{1}{r^{n+1}}\,\mathrm{d}r = \mathrm{e}^{\mathrm{i}ar_0}\, r_0^{-n-\mathrm{i}b}\, \mathcal{G}(\alpha, z) \tag{7.48}$$

with the continued fraction

$$\mathcal{G}(\alpha, z) = \frac{1}{z+} \frac{1-\alpha}{1+} \frac{1}{z+} \frac{2-\alpha}{1+} \frac{2}{z+} \frac{3-\alpha}{1+} \cdots, \tag{7.49}$$

which can be calculated to high accuracy by using the Wallis algorithm (see Appendix B).

---

8 Structure and operation of the RADIAL subroutines

In the Fortran programs all the real variables are handled in double precision (`REAL*8`), all the integers are of `INTEGER*4` type. The input of the solution subroutines contains the parameter `EPS` [$= \epsilon$, cf. Eqs. (4.14) and (4.27)] which controls the global accuracy of

the numerical procedure; the relative numerical uncertainty in the results is of the order of 100×EPS. Calculation time increases when EPS is reduced. With double-precision arithmetic, optimum accuracy is obtained with EPS$\simeq 10^{-15}$. We recall that all quantities are in atomic units ($m_e = e = \hbar = 1$); the units of length and energy are, respectively, the Bohr radius a_0 and the Hartree energy E_h —Eqs. (2.1) and (2.2). The code can also be used to solve the radial equations for particles other than electrons and positrons, in which case all quantities will be expressed in generalised atomic units, $M = e = \hbar = 1$, where M is the mass of the particle. The generalised atomic units of length and energy are $a_M = (m_e/M)a_0$ and $E_M = (M/m_e)E_h$, respectively.

RADIAL is structured as a stand-alone package. To solve a radial equation the user must enter a table of the potential function, suitably spaced to ensure that natural cubic spline interpolation is sufficiently accurate, define the grid of radii where the radial functions are to be tabulated, and call the appropriate solution routine. The lists of input-output arguments of the solution subroutines are minimal; the radial grid and the table of function values are transferred through a single common block. The package contains subroutines for computing Schrödinger– and Dirac–Coulomb wave functions and phase shifts. Numerical tools (cubic spline interpolation, integration) and a subroutine that builds radial grids with flexible spacing are also included.

8.1 Solution routines

The subroutines to be called from the main program are the following:

1) `SUBROUTINE VINT(R,RV,NV)`.

This is an initialisation subroutine which determines the natural cubic spline that interpolates the table of potential values provided by the user. The values of the potential function $\mathcal{V}(r_i) = r_i V(r_i)$ and the grid points r_i ($i = 1, \ldots,$ NV) are entered as the first NV components of the arrays RV and R respectively, which are kept unaltered. The dimension of these arrays must be less than, or equal to NDIM (see below). The r values must be given in non-decreasing order with R(1)=0.0D0. A pair of repeated r values is interpreted as a discontinuity of the potential (or its derivatives); we use a separate interpolating spline in each continuous region of the potential.

The function RVSPL(R) returns the value of $\mathcal{V}(r)$ at the point $r = R$ calculated from the interpolating cubic spline, that is, the value of the potential function actually used by the solution subroutines. This function can be used for verifying the correctness of the spline interpolation (see Section 4 and Appendix A). The function VRANGE() gives the range of the "inner component" of the potential, *i.e.*, the radius where the Coulomb tail starts.

When the potential function $\mathcal{V}(r)$ is given in numerical form, the error introduced by the interpolating spline may be difficult to estimate. As indicated above, one must at least make sure that the spline does not wiggle between the tabulated data; this may happen when the potential grid points are spaced too far apart. To get an idea of the magnitude of the interpolation error in the vicinity of the grid point r_k, we can consider the natural cubic spline that interpolates the potential table with the k-th

point removed. The difference between the value of this spline at r_k and the datum $\mathcal{V}(r_k)$ then gives the sought error estimate. The subroutine `SPLERR`, which is included in the `radial.f` source file, uses this method to estimate the maximum relative error introduced by natural cubic spline interpolation in a given table. This subroutine may be helpful to check whether a given radial grid is adequately spaced to permit spline interpolation of $\mathcal{V}(r)$ to the required accuracy.

When the potential is given by an analytical expression, the subroutine `SPLSET` (Appendix A) can be used to define an optimal radial grid. This subroutine not only generates a table suited for spline interpolation of the potential but also provides a realistic estimate of the interpolation error, which can always be reduced by simply increasing the number of grid points.

2) `SUBROUTINE SBOUND(E,EPS,N,L)`.

Calculation of Schrödinger bound-state radial functions and eigenvalues.

INPUT: `E` = estimated eigenvalue (a good estimate speeds up the calculation but it is not essential).
`N` = principal quantum number n. `L` = ℓ.

OUTPUT: `E` = eigenvalue.
Radial functions $P(r)$ and $Q(r) \equiv P'(r)$ (see below).

3) `SUBROUTINE SFREE(E,EPS,PHASE,L,IRWF)`.

Calculation of Schrödinger free-state radial functions and phase shifts.

INPUT: `E` = kinetic energy. `L` = ℓ.
`IRWF`: when = 0 the radial functions are not returned. This serves to avoid unnecessary calculations when only the phase shift is required.

OUTPUT: `PHASE` = inner phase shift δ (in radians).
Radial functions $P(r)$ and $Q(r) \equiv P'(r)$ (see below), only if `IRWF`$\neq 0$.

4) `SUBROUTINE DBOUND(E,EPS,N,K)`.

Calculation of Dirac bound-state radial functions and eigenvalues.

INPUT: `E` = estimated eigenvalue.
`N` = principal quantum number n. `K` = κ.

OUTPUT: `E` = eigenvalue.
Radial functions $P(r)$ and $Q(r)$ (see below).

5) `SUBROUTINE DFREE(E,EPS,PHASE,K,IRWF)`.

Calculation of Dirac free-state radial functions and phase shifts.

INPUT: `E` = kinetic energy. `K` = κ.
`IRWF`: when = 0 the radial functions are not returned. This serves to avoid unnecessary calculations when only the phase shift is required.

OUTPUT: PHASE = inner phase shift δ (in radians).
Radial functions $P(r)$ and $Q(r)$ (see below), only if IRWF$\neq 0$.

The values of the radial functions at the points r_i ($i = 1, \ldots,$ NGP) of a grid arbitrarily selected by the user (which may be different from the grid where the potential function is tabulated) are delivered through the named common block

```
COMMON/RADWF/RAD(NDIM),P(NDIM),Q(NDIM),NGP,ILAST,IER
```

The input array RAD contains the grid points r_i ($i = 1, \ldots,$ NGP) in the first NGP positions. Although it is advisable to have the radial grid points sorted in non-decreasing order, this is not strictly necessary; the solution subroutines do not alter the ordering of the input radii. At the output, the arrays P and Q contain the values of P(RAD(I)) and Q(RAD(I)) stored in their I-th positions ($Q \equiv P'$ for the Schrödinger equation). The physical dimension of the arrays is defined by the parameter NDIM in the Fortran module CONSTANTS, which is set to 25,000. This value must be changed by the user, by editing the radial.f source file, if a larger number of grid points is required.

The variable IER in the common block RADWF is an error flag: its output value is zero when the calculation has been successfully ended, and a positive value is returned when some fatal error is found during the calculation (in this case an error message is also written in the output file). The output value of IER indicates the type of detected error. A list of error codes and tentative solutions can be found in the heading comments of the radial.f source file. The program stops when an obvious inconsistency in the input data is detected.

For bound states, ILAST is the index corresponding to the practical infinity, *i.e.*, RAD(ILAST)$= r_\infty$; for $r >$ RAD(ILAST), $P(r)$ and $Q(r)$ are set equal to zero. In the case of free states, ILAST is the index of the matching point, RAD(ILAST)$= r_m$; the free-state radial functions for $r >$RAD(NGP) can be obtained analytically from Eqs. (6.1) and (6.2), with the help of subroutines SCOULF and DCOULF (see Section 8.2), which compute Schrödinger– and Dirac–Coulomb free functions, respectively. For potentials such that $\lim_{r\to\infty} \mathcal{V}(r) = 0$, the radial functions for $r >$RAD(NGP) should be calculated in terms of the spherical Bessel functions of integer order (which are computed by function SBESJN). At output from SFREE and DFREE, the common block

```
COMMON/OCOUL/RK,ETA,DELTA
```

contains the values of the wave number, k (=RK), the Sommerfeld parameter, η (=ETA), and the Coulomb phase shift, Δ (=DELTA) in radians.

Although values of the radial functions are delivered only at the points of the user grid r_i, the subroutines calculate the solution in a denser grid, which is obtained by merging the user grid and the potential grid. Bound-state radial functions are normalised to unity; the normalisation integral is evaluated using the power-series expansions of the radial functions, Eqs. (4.10) or (4.23) (see Section 5.3). Evidently, to ensure proper normalisation of the calculated functions, the outer point of the merged grid must be beyond the practical infinity. Free-state radial functions are normalised to asymptotic unit amplitude by matching the inner solution with the asymptotic solution, Eqs. (6.5), at a grid point larger than a radius r_m in the Coulomb tail of the potential where

the asymptotic solution can be calculated with the required accuracy. Notice that normalisation of free states is possible only if the outer radius of the merged grid is larger than r_m. Otherwise, subroutines SFREE and DFREE seek a convenient matching radius by progressively increasing the value of the outer point of the merged grid. The program stops when the matching radius is found to be larger than 10^4, which normally occurs when the energy is too small. Free-state radial functions are not delivered when IRWF = 0; in this case the subroutines SFREE and DFREE keep the contents of arrays P and Q unaltered.

For large enough values of r, the radial functions of Schrödinger and Dirac states can be calculated from their asymptotic expansions (see Section 7), which are applicable for radii larger than the range r_c of the finite-range component of the potential, which is given by the function VRANGE(). The maximum number of terms in the asymptotic expansions, which is defined by the parameter MNT in the Fortran module CONSTANTS, is set equal to 50. For free states, these expansions usually converge for radii larger than about the classical turning point $r_{TP}[\lambda]$, that is, for $r > \max(r_{TP}[\lambda], r_c)$. The subroutines

```
SUBROUTINE SFAS0(Z,E,L,PHASE,RCI,RACONV,EPS)    (Schrödinger)
SUBROUTINE DFAS0(Z,E,K,PHASE,RCI,RACONV,EPS)    (Dirac)
```

calculate the coefficients $A_{i,n}$ of the asymptotic series for free states in a Coulomb potential with Z_∞ = Z and load them in the common blocks CSFAS and CDFAS. The argument RCI is the user cutoff radius, *i.e.*, the smaller radius for which we need to use the asymptotic expansions (usually equal to RAD(ILAST)). The output value RACONV is the effective convergence radius r_a of the truncated asymptotic expansions (7.26); these expansions converge (to within the required relative uncertainty, EPS) only for $r >$ RACONV. When the user cutoff radius is large enough, RACONV is set equal to RCI so as to minimize the number of terms needed to ensure convergence. The user should be aware of the fact that the expansion coefficients may take quite large values when the radius r_a is not far enough from the turning point. After invoking SFAS0 [DFAS0], subroutine SFAS(R,P,Q,IER) [DFAS(R,P,Q,IER)] calculates the radial wave functions at r = R from their asymptotic expansions. The output argument IER is an error flag. When the radius R is larger than RACONV, IER is set to zero and the radial functions are calculated. When R < RACONV, the truncated expansions do not converge (the radial functions are set to zero) and IER is set to 1.

Similarly, the subroutines

```
SUBROUTINE SBAS0(Z,E,L,RCI,RACONV,EPS)    (Schrödinger)
SUBROUTINE DBAS0(Z,E,K,RCI,RACONV,EPS)    (Dirac)
```

calculate the coefficients of the asymptotic series for bound states [Eqs. (7.34) and (7.43)] and load them in the common blocks CSBAS and CDBAS. As for free states, the argument RCI is the user cutoff radius, and the output value RACONV is the effective convergence radius r_a of the truncated asymptotic expansions, which converge (to within the relative uncertainty EPS) for $r >$ RACONV. After calling SBAS0 [DBAS0], subroutine SFAS(R,P,Q,IER) [DFAS(R,P,Q,IER)] calculates the radial wave functions at r = R from their asymptotic expansions. When the radius R is larger than RACONV, the asymptotic

series converge, `IER` is set to zero, and the calculated radial functions are delivered. When `R` $<$ `RACONV`, the truncated expansions do not converge necessarily, the output value of `IER` is 1, and both `P` and `Q` are set to zero.

Although RADIAL has been devised to handle potentials such that $V(r)$ goes to zero at large distances, it can also be used to compute bound states for potentials that diverge at $r = \infty$ (*e.g.*, the isotropic harmonic oscillator potential, $V(r) \propto r^2$). For these potentials, we can start from a table of values of $V(r)$ for a certain grid r_i ($i = 1, \ldots, \mathrm{NT}$), suitably spaced to minimize spline interpolation errors, and define the shifted potential function $\mathcal{V}(r) \equiv r[V(r) - V(r_{\mathrm{NT}})]$, which vanishes at the outer grid point. This point must be selected such that, for the considered bound state, the probability of having the particle farther than r_{NT} is negligible. It is important to meet this condition, since RADIAL sets $\mathcal{V}(r) = \mathcal{V}(r_{\mathrm{NT}})$ for $r > R_{\mathrm{NT}}$. With the shifted potential, RADIAL then gives the desired bound-state radial functions; the output value of the energy is $E' = E - V(r_{\mathrm{NT}})$, where E is the eigenenergy for the actual potential $V(r)$. It is advisable to check whether the computed value of $E = E' + V(r_{\mathrm{NT}})$ is altered by round-off errors. This occurs, for instance, when both $-E'$ and $V(r_{\mathrm{NT}})$ have large positive values and E is small. In such a case, the energy E should be obtained as the expectation value of the Hamiltonian;

$$E = \int \psi^\dagger(\mathbf{r})\, \mathcal{H}_{\mathrm{S\,or\,D}}\, \psi(\mathbf{r})\, \mathrm{d}\mathbf{r}. \tag{8.1}$$

Thus, the Schrödinger energy eigenvalue is given by

$$E_{n\ell} = \int_0^\infty \left\{ \frac{\hbar^2}{2\mathrm{m_e}} \left[P'_{n\ell}(r)\right]^2 + P_{n\ell}(r) \left[V(r) + \frac{\ell(\ell+1)\hbar^2}{2\mathrm{m_e} r^2} \right] P_{n\ell}(r) \right\} \mathrm{d}r, \tag{8.2}$$

the energy eigenvalue of the Dirac equation is

$$\begin{aligned} E_{n\kappa} \;=\; & \int_0^\infty \Big\{ P_{n\kappa}(r) \left[V(r)\, P_{n\kappa}(r) + c\hbar \left(\frac{\kappa}{r}\, Q_{n\kappa}(r) - Q'_{n\kappa}(r) \right) \right] \\ & + Q_{n\kappa}(r) \left[c\hbar \left(\frac{\kappa}{r}\, P_{n\kappa}(r) + P'_{n\kappa}(r) \right) + \left(V(r) - 2\mathrm{m_e}c^2 \right)\, Q_{n\kappa}(r) \right] \Big\}\, \mathrm{d}r, \end{aligned} \tag{8.3}$$

and the eigenvalue of the Schrödinger–Pauli equation is obtained as [see Eq. (2.34)]

$$E_{n\kappa} = \int_0^\infty \left\{ \frac{\hbar^2}{2\mathrm{m_e}} \left[P'_{n\kappa}(r)\right]^2 + P_{n\kappa}(r) \left[V_\kappa(r) + \frac{\ell(\ell+1)\hbar^2}{2\mathrm{m_e} r^2} \right] P_{n\kappa}(r) \right\} \mathrm{d}r. \tag{8.4}$$

8.2 Coulomb wave functions

Coulomb wave functions of free states are required to extend the calculated radial functions to radii beyond `RAD(NGP)`. On the other hand, the Coulomb functions of bound states can be used for verifying the accuracy of calculated radial functions for attractive Coulomb potentials. The following subroutines deliver accurate values of Schrödinger– and Dirac–Coulomb wave functions, which are calculated from the analytical expressions

and the continued fraction method derived above (see Section 3). Notice that free-state irregular Coulomb functions diverge at $r = 0$ and cannot be calculated for very small radii.

6) `SUBROUTINE SCOULB(Z,N,L,E,R,P)`.

Calculation of Schrödinger–Coulomb radial functions for bound states.

INPUT: `Z` = potential strength, Z_∞ (must be negative for bound states).
`N` = n, `L` = ℓ, `R` = r (> 0).

OUTPUT: `E` = binding energy, $E_{n\ell}$. `P` = $P_{n\ell}(r)$.

7) `SUBROUTINE DCOULB(Z,N,K,E,R,P,Q)`.

Calculation of Dirac–Coulomb radial functions for bound states.

INPUT: `Z` = potential strength, Z_∞ (must be negative for bound states).
`N` = n, `K` = κ, `R` = r (> 0).

OUTPUT: `E` = binding energy, $E_{n\kappa}$. `P` = $P_{n\kappa}(r)$, `Q` = $Q_{n\kappa}(r)$.

8) `SUBROUTINE SCOULF(Z,E,L,R,F,FP,G,GP,ERRF,ERRG)`.

Calculation of Schrödinger–Coulomb radial functions for free states.

INPUT: `Z` = potential strength, Z_∞.
`E` = kinetic energy, E (> 0).
`L` = ℓ, `R` = r (> 0).

OUTPUT: `F`, `FP` = regular Coulomb function and its derivative with respect to r, $F_\ell(\eta, kr)$ and $\mathrm{d}F_\ell(\eta, kr)/\mathrm{d}r$.
`G`, `GP` = irregular Coulomb function and its derivative with respect to r, $G_\ell(\eta, kr)$ and $\mathrm{d}G_\ell(\eta, kr)/\mathrm{d}r$.
`ERRF`, `ERRG` = accuracy (relative uncertainty) of the calculated functions.

9) `SUBROUTINE DCOULF(Z,E,K,R,FU,FL,GU,GL,ERRF,ERRG)`.

Calculation of Dirac–Coulomb radial functions for free states.

INPUT: `Z` = potential strength, Z_∞.
`E` = kinetic energy, E (> 0).
`K` = κ, `R` = r (> 0).

OUTPUT: `FU`, `FL` = upper and lower components of the regular Dirac–Coulomb function, $f_\kappa^{(\mathrm{u})}(kr)$ and $f_\kappa^{(\mathrm{l})}(kr)$.
`GU`, `GL` = upper and lower components of the irregular Dirac–Coulomb function, $g_\kappa^{(\mathrm{u})}(kr)$ and $g_\kappa^{(\mathrm{l})}(kr)$.
`ERRF`, `ERRG` = accuracy (relative uncertainty) of the calculated functions.

At the output of `SCOULF` and `DCOULF`, the wave number, k, the Sommerfeld parameter, η, and the Coulomb phase shift, Δ, are delivered through the common block `OCOUL`.

In the case of attractive Coulomb potentials, subroutines `SCOULB` and `DCOULB` deliver nominally exact radial functions for bound states with small and moderate values of the principal quantum number; for states with n larger than about 20, the sum of the hypergeometric series may be affected by considerable round-off errors. For the hydrogen atom ($Z_\infty = -1$) and states with $n \leq 20$, it is found that the ratio of the radial functions calculated by subroutines `SBOUND` and `DBOUND` to these exact values differs from unity in less than 10^{-11} when $\epsilon = 10^{-15}$. We thus confirm that the numerical integration algorithm (Section 4) meets the accuracy level prescribed by the tolerance parameter ϵ. For free states of Coulomb potentials, such a direct verification of accuracy is not possible, because the outward numerical integration is discontinued at a very small radius, r_m (see Section 6). For larger radii, the delivered wave function is simply the regular Coulomb function, because the inner phase shift vanishes.

8.3 Complex optical potentials

The RADIAL package includes subroutines for computing Schrödinger and Dirac radial wave functions of free states for complex optical potentials (see Section 6.3) of the type

$$V_{op}(r) = V(r) + \mathrm{i}W(r) \tag{8.5}$$

where $V(r)$ is a modified Coulomb potential [*i.e.*, such that the function $\mathcal{V}(r) = rV(r)$ is finite for all r and tends to a constant value when $r \to \infty$] and $W(r)$ is a finite-range negative (*i.e.*, absorptive) potential such that $rW(r)$ is finite everywhere.

The radial wave functions of the free states of optical potentials are calculated by the subroutines `ZVINT` and `ZSFREE` or `ZDFREE`. These subroutines use complex double precision arithmetic and operate similarly to their analogues for real potentials (`VINT`, `SFREE`, `DFREE`).

1c) `SUBROUTINE ZVINT(R,RV,RW,NV)`.

This initialisation subroutine determines two natural cubic splines that interpolate the potential functions $\mathcal{V}(r) = rV(r)$ and $\mathcal{W}(r) = rW(r)$. The array `R` contains the potential grid poins r_i ($i = 1, \ldots,$ `NV`), the values $\mathcal{V}(r_i)$ and $\mathcal{W}(r_i)$ are entered as the first `NV` components of the arrays `RV` and `RW`, respectively, which are kept unaltered. The dimension of these arrays must be less than, or equal to `NDIM` (see above). The r values must be given in non-decreasing order with `R(1)=0.0D0`. A pair of repeated r values is interpreted as a discontinuity of the potential functions (or their derivatives); we use separate interpolating splines in each continuous region of the potential.

The subroutine `ZRVSPL(R,RVS,RWS)` returns the interpolated values `RVS` and `RWS` of the respective functions $\mathcal{V}(r)$ and $\mathcal{W}(r)$ at $r =$ `R`, *i.e.*, the potential functions effectively used in the numerical solution. The function `VRANGE()` gives the range r_c of the "inner potentials", Eq. (6.60), which is the radius where the Coulomb tail starts.

2c) `SUBROUTINE ZSFREE(E,EPS,PHASER,PHASEI,L,IRWF)`.

Calculation of Schrödinger free-state radial functions and phase shifts.

INPUT: `E` = kinetic energy. `L` = ℓ.
`IRWF`: when = 0 the radial functions are not returned. This serves to avoid unnecessary calculations when only the phase shift is required.

OUTPUT: `PHASER`, `PHASEI` = real and imaginary parts of the inner phase shift δ (in radians).
Radial functions $P(r)$ and $Q(r) \equiv P'(r)$ (see below), only if `IRWF`$\neq 0$.

3c) `SUBROUTINE ZDFREE(E,EPS,PHASER,PHASEI,K,IRWF)`.

Calculation of Dirac free-state radial functions and phase shifts.

INPUT: `E` = kinetic energy. `K` = κ.
`IRWF`: when = 0 the radial functions are not returned. This serves to avoid unnecessary calculations when only the phase shift is required.

OUTPUT: `PHASER`, `PHASEI` = real and imaginary parts of the inner phase shift δ (in radians).
Radial functions $P(r)$ and $Q(r)$ (see below), only if `IRWF`$\neq 0$.

The values of the calculated radial functions at the points r_i ($i = 1, \ldots,$ `NGP`) of the user grid are delivered through the named common blocks

```
COMMON/RADWF/RAD(NDIM),P(NDIM),Q(NDIM),NGP,ILAST,IER
```

and

```
COMMON/RADWFI/PIM(NDIM),QIM(NDIM)
```

The input array `RAD` contains the user grid points r_i ($i = 1, \ldots,$ `NGP`) in the first `NGP` positions. At the output, when `IRWF` $\neq 0$, the real and imaginary parts of the calculated radial wave functions are given in the pairs of arrays `P`, `Q` and `PIM`, `QIM`, respectively. Specifically the radial functions at the i-th grid point, `RAD(I)` $= r_i$, are

$$P(r_i) = \texttt{P(I)} + \mathrm{i}\,\texttt{PIM(I)},$$
$$Q(r_i) = \texttt{Q(I)} + \mathrm{i}\,\texttt{QIM(I)}.$$

In contrast to the case of real potentials, free-state radial functions are not normalised to asymptotic unit amplitude.

8.4 Defining the radial grids

As mentioned above, the accuracy of the calculated radial functions is practically independent of the user grid spacing, provided only that in the case of bound states there are no multiple zeros between consecutive grid points. However, for practical calculations (of, *e.g.*, transition matrix elements), the user grid `RAD(I)` (`I` $= 1, \ldots,$ `NGP`) should be dense enough to ensure that radial functions can be accurately calculated by interpolation of their values at the grid points. Thus, the accuracy of calculation results depends critically on the spacing of the user grid. To facilitate the definition of radial grids that

are suitably spaced to allow accurate interpolations, RADIAL includes the subroutine `SGRID`, which generates non-uniform grids with prescribed spacing.

10) `SUBROUTINE SGRID(R,DR,RN,R2,DRN,N,NMAX,IER)`.

INPUT: `NMAX` = physical dimensions of the arrays `R` and `DR` (`NMAX` $\leq$ `NDIM`)
`N` = number of grid points (`N` $\leq$ `NMAX`).
`RN` = outer radius r_N (must be greater than 10^{-5}).
The grid extends from $r_1 = 0$ up to r_N.
`R2` = approximate position of the second grid point r_2 (must be less than 10^{-2} and less than r_N).
This value controls the grid spacing at small radii.
`DRN` = an upper bound for the distance between the last grid points, $r_N - r_{N-1}$, which controls the grid spacing at large radii.

OUTPUT: `N` = number of grid points (it may be greater than the input value).
`R(I)` = r_i, radial grid points.
`DR(I)` = values of $1/\mathcal{G}'(r_i)$ (see below), which are required, *e.g.*, for evaluating integrals using Simpson's rule.
`IER` = error flag:
= 0, the grid has been successfully defined.
> 0, the grid could not be defined.

The grid is set by means of the continuous transformation

$$\mathcal{G}(r_i) \equiv a\, r_i + b\, \ln(c + r_i) + d = i \quad (i = 1, 2, \ldots, N), \tag{8.6}$$

where the parameters a, b, c and d are determined by solving the system of equations

$$\mathcal{G}(0) = b\, \ln c + d = 1, \qquad [r_1 = 0], \tag{8.7a}$$

$$\mathcal{G}'(0) = a + \frac{b}{c} = \frac{1}{r_2}, \qquad \left[\mathcal{G}'(0) \simeq \frac{1}{r_2 - r_1} = \frac{1}{r_2}\right], \tag{8.7b}$$

$$\mathcal{G}(r_N) = a\, r_N + b\, \ln(c + r_N) + d = N, \tag{8.7c}$$

$$\mathcal{G}'(r_N) = a + \frac{b}{c + r_N} = \frac{1}{\texttt{DRN}}. \tag{8.7d}$$

When the quantity

$$A_{\rm grid} \equiv \frac{r_N - (N-1)r_2}{r_N}\, \frac{\texttt{DRN}}{\texttt{DRN} - r_2} \tag{8.8}$$

lies in the interval (0.5,1), Eqs. (8.7) have a unique solution given by

$$c = x r_N\,, \quad b = \frac{x(c + r_N)(\texttt{DRN} - r_2)}{\texttt{DRN}\, r_2}\,, \quad a = \frac{c - b r_2}{c r_2}\,, \quad \text{and} \quad d = 1 - b \ln c\,, \tag{8.9}$$

where x is the positive root of the equation

$$(x+1)\left[1 - x \ln\left(\frac{x+1}{x}\right)\right] = A_{\rm grid}\,. \tag{8.10}$$

In subroutine SGRID Eqs. (8.6) and (8.10) are solved by the bisection method.

When r_N is large (say, larger than $\sim$10) and r_2 is small (of the order of 10^{-5} or less), the grid is nearly logarithmic in the vicinity of $r = 0$ and nearly uniform at large r. In this case we get a high density of points near the origin (which is convenient in order to have a good representation of bound states) and a nearly uniform grid at large distances from the origin (as required to follow the regular oscillations of free-state wave functions in the asymptotic region). For instance, for bound states of screened Coulomb potentials the following values are normally adequate: r_N of the order of 50, r_2 about 10^{-5} or smaller, DRN about 0.5 and $N = 750$ or larger. For free states, we can set DRN equal to 0.05 times the wavelength λ ($= 2\pi/k$). We thus get about 20 grid points within a wavelength. As a rule of thumb, the grid is properly set if the output radial functions look smooth when plotted using straight segments to join the data points.

It is worth noting that the grids defined by Eq. (8.6) are convenient for further numerical calculations. Thus, interpolation from the uniform i-grid is easier than from the r-grid. Also, to evaluate integrals of functions $f(r)$ of the radial variable, we simply change to the new variable $x = \mathcal{G}(r)$ to get the integrand tabulated in a uniform grid, with unit spacing,

$$\int_0^{r_N} f(r)\,\mathrm{d}r \;=\; \int_1^{N} f(r_i)\,\frac{1}{\mathcal{G}'(r_i)}\,\mathrm{d}i. \tag{8.11}$$

The integral on the right-hand side can be routinely calculated by using, *e.g.*, the extended Simpson rule or Lagrange quadrature formulas (Abramowitz and Stegun, 1974). Simpson's rule can be applied when the number N of grid points is odd, and gives

$$\int_0^{r_N} f(r)\,\mathrm{d}r \simeq \frac{1}{3}\left[F_1 + 4F_2 + 2F_3 + 4F_4 + \cdots + 2F_{N-2} + 4F_{N-1} + F_N\right], \tag{8.12}$$

with $F_i = f(r_i)/\mathcal{G}'(r_i) = f(r_i)\,\mathtt{DR}(i)$.

In our calculations we prefer to use the 6-point Lagrange quadrature formulas, which are more general and slightly more accurate than Simpson's rule (see, *e.g.* Abramowitz and Stegun, 1974). If r_1, r_2, ..., r_6 are six successive grid points, the 6-point Lagrange formulas read

$$\begin{aligned}
\int_{r_1}^{r_2} f(r)\,\mathrm{d}r &\simeq \frac{1}{1440}\left(475F_1 + 1427F_2 - 798F_3 + 482F_4 - 173F_5 + 27F_6\right),\\
\int_{r_2}^{r_3} f(r)\,\mathrm{d}r &\simeq \frac{1}{1440}\left(-27F_1 + 637F_2 + 1022F_3 - 258F_4 + 77F_5 - 11F_6\right),\\
\int_{r_3}^{r_4} f(x)\,\mathrm{d}r &\simeq \frac{1}{1440}\left(11F_1 - 93F_2 + 802F_3 + 802F_4 - 93F_5 + 11F_6\right),\\
\int_{r_4}^{r_5} f(r)\,\mathrm{d}r &\simeq \frac{1}{1440}\left(-11F_1 + 77F_2 - 258F_3 + 1022F_4 + 637F_5 - 27F_6\right),\\
\int_{r_5}^{r_6} f(r)\,\mathrm{d}r &\simeq \frac{1}{1440}\left(27F_1 - 173F_2 + 482F_3 - 798F_4 + 1427F_5 + 475F_6\right),
\end{aligned} \tag{8.13}$$

where $F_i = f(r_i)\,\mathtt{DR}(i)$. The source file `radial.f` contains a subroutine named `SLAG6` which implements these formulas to calculate the integrals of $f(r)$ over the intervals $(0, r_i)$ between the first and the i-th grid points.

9 Test programs

The RADIAL package is accompanied with a main program called `demorad` that calculates bound- and free-state radial functions for modified Coulomb potentials of the following types:

$$\text{Coulomb + spherical step:} \qquad V(r) = \frac{Z}{r} + V_0\,\Theta(A - r), \tag{9.1a}$$

$$\text{Coulomb + exponential:} \qquad V(r) = \frac{Z}{r} + V_0\exp(-Ar), \tag{9.1b}$$

$$\text{Coulomb + Gaussian:} \qquad V(r) = \frac{Z}{r} + V_0\exp(-Ar^2), \tag{9.1c}$$

and

$$\text{Partially-screened Coulomb:} \qquad V(r) = \frac{Z}{r} + \frac{V_0}{r}\exp(-Ar), \tag{9.1d}$$

where $\Theta(x)$ is the unit step function (= 1 if $x > 0$ and = 0 otherwise). The parameters Z, V_0 and A define, respectively, the Coulomb tail, and the strength and range of the finite-range component of the potential. With $Z = 0$, the potentials have finite ranges, and their shapes are varied enough to allow numerical verification of many theoretical analyses. With properly selected parameters, the partially-screened Coulomb potential may be used to approximate the interactions that occur in atomic physics (atomic structure, photoionisation, collisions of charged particles with atoms and ions, ...).

The accuracy of the solution is mostly determined by the grid of radii where the potential function $\mathcal{V}(r)$ is tabulated, which will be referred as the potential grid. In `demorad.f` the potential grid is determined automatically by subroutine `SPLSET` (see Appendix A) which uses an adaptive strategy to reduce interpolation errors. The user grid is generated by subroutine `SGRID`, with parameters selected to describe properly the oscillations of the radial functions. The program `demorad` can be run interactively and the input/output is self-explanatory. Radial functions are written in an output file, named `schrodinger.dat` or `dirac.dat`, in a format ready to be imported by a plotting program for visualisation. Optionally, for potentials with an attractive Coulomb tail [$\lim_{r\to\infty} rV(r) < -0.5$], the program can also determine the quantum-defect function (6.15); the consistency of the results of this delicate calculation provides direct evidence of the accuracy of the RADIAL routines.

Examples of results produced by `demorad` are given in Table 2, which shows the contents of the output file `res.dat` generated by running the program in batch mode with the input file `demorad.in`. These data were obtained on a personal computer with

Windows 7 operating system by using the executable binaries produced by the Fortran compiler gfortran from the GNU Compiler Collection (`https://gcc.gnu.org/`). Notice that results obtained in different platforms or with different compilers may differ slightly due to accumulated round-off errors.

The distribution package also includes the main program `numpoten`, which solves the radial equations for numerical potentials. This program reads the potential function $\mathcal{V}(r)$ from an input file. The example provided in the distribution package, file `dhfs079.tab`, is the Dirac–Hartree–Fock–Slater potential of the gold atom (see Section 10). `numpoten` operates in the same way as `demorad`; it calculates radial functions for bound and free states and, in the case of attractive partially-screened Coulomb potentials, it can also determine the quantum-defect function.

The calculation of radial functions of free states for complex optical potentials (see Section 6.2) is illustrated in the main program `zdemorad.f`, which operates similarly to `demorad.f`. The real and imaginary parts of the potential are defined by the functions `VPOTR(R)` and `VPOTI(R)` respectively; the example in the program imitates the potentials used for describing the scattering of nucleons by nuclei. The potential grid used in `zdemorad.f` is generated automatically by subroutine `SPLSET`, which optimizes only the interpolation of the real part of the potential (see Appendix A); the imaginary part of the potential is tabulated on the same grid. The program outputs the calculated radial functions in a formatted file named `zschrodinger.dat` or `zdirac.dat`.

To visualise the contents of output files, we use the plotting program gnuplot, which is small in size, available for various platforms (including Windows and Linux) and free (distribution sites are listed at the Gnuplot Central site, `http://www.gnuplot.info`). The distribution package of RADIAL contains gnuplot scripts that display the various output files. Each script has the filename of the output file that is plotted and the extension `.gnu` (*i.e.*, the script `filename.gnu` displays the tables in the output file `filename.ext`).

RADIAL provides radial functions, eigenvalues and phase shifts *for the potential function given by the cubic spline* (4.3). Calculation results are affected by numerical uncertainties that arise not only from round-off errors (which can be reduced by using a smaller accuracy parameter ϵ) but also from differences between the spline approximation and the actual potential function $\mathcal{V}(r)$. In general, we shall deal with potentials that are either given in analytical form or defined numerically by means of a table $\mathcal{V}(r_i)$ $(i = 1, \ldots, N)$. For analytical potentials, we can always determine a radial grid r_i that is dense enough to make sure that the corresponding natural cubic spline differs from the actual potential function by less than a selected tolerance. For the analytical potentials (9.1) and the radial grids used in `demorad`, the relative error introduced by the spline interpolation is usually less than 10^{-8}. In a few particular cases (namely, piecewise Coulomb, constant, linear or quadratic potentials) the spline interpolation is exact, irrespective of the number of grid points, and the calculated results are only affected by round-off errors.

The programs `demorad`, `zdemorad`, and `numpoten` generate files with tables of the original and the interpolated potential functions. The input table of $\mathcal{V}(r)$ at the points

Table 2: Test run output generated by running `demorad.f` in batch mode with the input file `demorad.in`.

```
# **** Schrodinger Eq. Potential: V(R)=Z/R+V0*EXP(-A*R)/R
#      Z=-1.000000E+00, V0=-5.000000E+01, A= 5.000000E+00
#      Bound state: N=   1, L=   0  (EPS= 1.0E-15)
#      Binding energy=-1.067816660452936E+03

# **** Dirac equation. Potential: V(R)=Z/R+V0*EXP(-A*R)/R
#      Z=-1.000000E+00, V0=-5.000000E+01, A= 5.000000E+00
#      Bound state: N=   1, K=  -1  (EPS= 1.0E-15)
#      Binding energy=-1.115472538970607E+03

# **** Schrodinger Eq. Potential: V(R)=Z/R+V0*EXP(-A*R)/R
#      Z=-1.000000E+00, V0=-5.000000E+01, A= 5.000000E+00
#      Bound state: N=  10, L=   5  (EPS= 1.0E-15)
#      Binding energy=-5.000000000004944E-03

# **** Dirac equation. Potential: V(R)=Z/R+V0*EXP(-A*R)/R
#      Z=-1.000000E+00, V0=-5.000000E+01, A= 5.000000E+00
#      Bound state: N=  10, K=   5  (EPS= 1.0E-15)
#      Binding energy=-5.000003328218323E-03

# **** Schrodinger Eq. Potential: V(R)=Z/R+V0*EXP(-A*R)/R
#      Z=-1.000000E+00, V0=-5.000000E+01, A= 5.000000E+00
#      Free state: E= 1.000000E+02, L=   0  (EPS= 1.0E-15)
#        Inner phase shift=-8.870875020160565E-01
#      Coulomb phase shift= 4.067401266228893E-02  (ETA=-7.071068E-02)

# **** Dirac equation. Potential: V(R)=Z/R+V0*EXP(-A*R)/R
#      Z=-1.000000E+00, V0=-5.000000E+01, A= 5.000000E+00
#      Free state: E= 1.000000E+02, K=  -1  (EPS= 1.0E-15)
#        Inner phase shift=-7.124212601851576E-01
#      Coulomb phase shift= 4.069204642967206E-02  (ETA=-7.099277E-02)

# **** Schrodinger Eq. Potential: V(R)=Z/R+V0*EXP(-A*R)/R
#      Z=-1.000000E+00, V0=-5.000000E+01, A= 5.000000E+00
#      Free state: E= 1.000000E+02, L=   5  (EPS= 1.0E-15)
#        Inner phase shift= 5.109874526307268E-01
#      Coulomb phase shift=-1.206426693445067E-01  (ETA=-7.071068E-02)

# **** Dirac equation. Potential: V(R)=Z/R+V0*EXP(-A*R)/R
#      Z=-1.000000E+00, V0=-5.000000E+01, A= 5.000000E+00
#      Free state: E= 1.000000E+02, K=   5  (EPS= 1.0E-15)
#        Inner phase shift= 5.165576031574922E-01
#      Coulomb phase shift=-1.210779425821564E-01  (ETA=-7.099277E-02)

# **** Dirac equation. Potential: V(R)=Z/R+V0*EXP(-A*R)/R
#      Z=-1.000000E+00, V0=-5.000000E+01, A= 5.000000E+00
#      Free state: E= 1.000000E+02, K=  10  (EPS= 1.0E-15)
#        Inner phase shift= 5.837929361036831E-02
#      Coulomb phase shift=-1.669349756747289E-01  (ETA=-7.099277E-02)
```

of the potential grid is written in file `potential.dat`. The file `pot-spline.dat` contains a table of the potential function effectively used by the solution subroutines (*i.e.*, calculated from the interpolating cubic spline) at a denser grid, which has five uniformly spaced radii in each subinterval of the potential grid. The gnuplot script `potential.gnu` displays the contents of these two files in a single plot, allowing the user to verify that the spline does not wiggle artificially in regions where $\mathcal{V}(r)$ is either constant or changes abruptly, such a wiggling would spoil the accuracy of the calculated radial functions.

10 DHFS self-consistent method for atoms

As a practical application of the RADIAL subroutines, we consider the self-consistent solution of the Dirac–Hartree–Fock–Slater (DHFS) equations for the ground-state configuration of neutral atoms and positive ions of atomic number Z with N bound electrons (Liberman *et al.*, 1965, 1971).

The DHFS method is based on the central-field independent-electron approximation. The states of the atom are represented by single Slater determinants built with central-field orbitals of the form (2.16),

$$\psi_{n\kappa m}(\mathbf{r}) = \frac{1}{r}\begin{pmatrix} P_{n\kappa}(r)\,\Omega_{\kappa,m}(\hat{\mathbf{r}}) \\ \mathrm{i}Q_{n\kappa}(r)\,\Omega_{-\kappa,m}(\hat{\mathbf{r}}) \end{pmatrix} . \tag{10.1}$$

We consider the ground-state configuration of the atom or ion, which is specified by giving the occupied (sub)shells $(n_a\kappa_a)$ and the corresponding occupation numbers q_a $(\leq 2j_a+1 = 2|\kappa_a|)$;

$$(n_1\kappa_1)^{q_1}\,,\ (n_2\kappa_2)^{q_2}\,\ldots\,. \tag{10.2}$$

The electronic configurations of ground states of neutral atoms are provided by subroutine `ELEMNT` (source file `elemnt.f`).

The orbitals $\psi_{n\kappa m}(\mathbf{r})$ are solutions of the DHFS equations,

$$\left[c\,\widetilde{\boldsymbol{\alpha}}\cdot\mathbf{p} + (\widetilde{\beta}-1)\mathrm{m_e}c^2 + V_{\mathrm{DHFS}}(r)\right]\psi_{n\kappa m}(\mathbf{r}) = E_{n\kappa}\,\psi_{n\kappa m}(\mathbf{r})\,, \tag{10.3}$$

for a common central potential $V_{\mathrm{DHFS}}(r)$. These equations are obtained from the single-configuration Dirac–Fock equations (see, *e.g.* Grant, 1970) by replacing the non-local exchange potential with the local average approximation due to Slater (1951), which is derived from non-relativistic free-electron gas theory. Since Eqs. (10.3) have the form of the Dirac equation for an electron in a central potential, the radial functions $P_{n\kappa}(r)$ and $Q_{n\kappa}(r)$ of the DHFS orbitals satisfy the radial equations (2.21),

$$\begin{aligned} \frac{\mathrm{d}P_{n\kappa}}{\mathrm{d}r} &= -\frac{\kappa}{r}\,P_{n\kappa} + \frac{E_{n\kappa} - V_{\mathrm{DHFS}} + 2\mathrm{m_e}c^2}{c\hbar}\,Q_{n\kappa}, \\ \frac{\mathrm{d}Q_{n\kappa}}{\mathrm{d}r} &= -\frac{E_{n\kappa} - V_{\mathrm{DHFS}}}{c\hbar}\,P_{n\kappa} + \frac{\kappa}{r}\,Q_{n\kappa}. \end{aligned} \tag{10.4}$$

The electron density is given by

$$\rho(\mathbf{r}) = \sum \psi^{\dagger}_{n\kappa m}(\mathbf{r})\, \psi_{n\kappa m}(\mathbf{r})\,, \tag{10.5}$$

where the summation runs over the N orbitals that are occupied. We recall that, by virtue of Unsöld's theorem (see,*e.g.*, Condon and Odabaşi, 1980), the electron density of a closed shell (with $q_a = 2j_a + 1$ electrons) is spherically symmetric. Consequently, for closed-shell configurations we have

$$\rho(r) = \frac{1}{4\pi r^2} \sum_a q_a \left[P^2_{n_a\kappa_a}(r) + Q^2_{n_a\kappa_a}(r)\right]\,, \tag{10.6}$$

where the summation is over occupied subhells. In calculations with arbitrary configurations, expression (10.6) is adopted as the definition of the local electron density. Thus, for configurations with open shells, spherical symmetry of the density (and the potential) is enforced by considering that the orbitals of an open shell $(n_a\kappa_a)$ with q_a electrons have a fractional occupancy equal to $q_a/(2j_a + 1)$.

The DHFS potential is given by

$$V_{\rm DHFS}(r) = V_{\rm nuc}(r) + V_{\rm el}(r) + V_{\rm ex}(r)\,. \tag{10.7}$$

The term $V_{\rm nuc}(r)$ is the nuclear potential (*i.e.*, the electrostatic interaction energy of an electron at r with the nucleus, which is assumed to be spherical). For a point nucleus,

$$V_{\rm nuc}(r) = -Ze^2/r. \tag{10.8}$$

The finite size of the nucleus has a small effect on the atomic structure, which can be approximately accounted for by using simple models for the nuclear charge distribution. A convenient parameterisation of the proton density is provided by the Fermi distribution (Hahn *et al.*, 1956),

$$\rho_{\rm p}(r) = \frac{\rho_0}{\exp\left[(r - R_{\rm n})/z\right] + 1}\,, \tag{10.9}$$

with

$$R_{\rm n} = 1.07\, A^{1/3}\,{\rm fm}, \qquad \text{and} \qquad z = 0.546\,{\rm fm}\,, \tag{10.10}$$

where A is the mass number, which is usually replaced by the atomic weight (mean relative atomic mass) of the element. The constant ρ_0, which equals twice the proton density at $r = R_{\rm n}$, is to be determined by normalisation. The nuclear potential for the Fermi distribution has to be calculated numerically,

$$\begin{aligned} V_{\rm nuc}(r) &= -e^2 \int \frac{\rho_{\rm p}(r')}{|\mathbf{r} - \mathbf{r}'|}\, {\rm d}\mathbf{r}' \\ &= -\frac{e^2}{r} \int_0^r \rho_{\rm p}(r')\, 4\pi r'^2\, {\rm d}r' - e^2 \int_r^{\infty} \rho_{\rm p}(r')\, 4\pi r'\, {\rm d}r'\,. \end{aligned} \tag{10.11}$$

The second term in expression (10.7) is the electronic potential (*i.e.*, the interaction energy of an electron at r with the whole atomic electron cloud),

$$V_{\rm el}(r) = e^2 \int \frac{\rho(r')}{|\mathbf{r} - \mathbf{r}'|}\, {\rm d}\mathbf{r}'$$

$$= \frac{e^2}{r}\int_0^r \rho(r')\,4\pi r'^2\,\mathrm{d}r' + e^2\int_r^\infty \rho(r')\,4\pi r'\,\mathrm{d}r'\,. \tag{10.12}$$

The last term on the right-hand side of Eq. (10.7) is the exchange potential, which can be expressed as

$$V_{\rm ex}(r) = C_{\rm ex}\,V_{\rm ex}^{\rm (TF)}(r)\,, \tag{10.13}$$

where $C_{\rm ex}$ is a constant and

$$V_{\rm ex}^{\rm (TF)}(\mathbf{r}) = -e^2(3/\pi)^{1/3}\,[\rho(\mathbf{r})]^{1/3} \tag{10.14}$$

is the exchange potential of a free-electron gas of density $\rho(\mathbf{r})$. Slater (1951), applied the Thomas–Fermi approximation to the non-relativistic Hartree–Fock exchange potential (after variation) and obtained $C_{\rm ex} = 3/2$. Later, Kohn and Sham (1965) using arguments that are equivalent to a variational formulation in which the non-relativistic Hartree–Fock exchange energy (before variation) is estimated by means of the Thomas–Fermi approximation, obtained an exchange potential of the same form but with $C_{\rm ex} = 1$. This indicates that there is a certain arbitrariness in the value of this parameter, which has been exploited to seek improved approximations (see, *e.g.*, Condon and Odabaşi, 1980, and references therein). Since the value $C_{\rm ex} = 3/2$ results from applying the Thomas–Fermi approximation to the exchange potential, the corresponding energy eigenvalues $E_{n\kappa}$ keep the physical significance of one-electron binding energies, as in the Dirac–Fock method (Koopmans' theorem).

Near the nucleus, the electron density is relatively large and the Thomas–Fermi (statistical) approximation to the exchange potential is nearly correct. However, for large r, the electron density is very small and the statistical approximation is not accurate; the resulting local exchange potential is so weak there that it cannot cancel the self-interaction term in the electronic potential. We have,

$$\lim_{r\to\infty} rV_{\rm DHFS}(r) = -(Z-N)e^2, \tag{10.15}$$

which is incorrect. To obtain the correct asymptotic behaviour [$= -(Z-N+1)e^2$] it is customary to introduce an *ad hoc* correction, known as the Latter tail (Latter, 1955), which consists of replacing $rV_{\rm DHFS}(r)$ by $-(Z-N+1)e^2$ at large distances where the original DHFS potential becomes higher than this value. The corrected exchange potential is

$$V_{\rm ex}(r) = \begin{cases} C_{\rm ex}V_{\rm ex}^{\rm (TF)}(r) & \text{if } r < r_{\rm Latter}, \\ -(Z-N-1)\dfrac{e^2}{r} - V_{\rm nuc}(r) - V_{\rm el}(r) & \text{if } r \geq r_{\rm Latter}, \end{cases} \tag{10.16}$$

where the cutoff radius $r_{\rm Latter}$ is the outer root of the equation

$$r\left[V_{\rm nuc}(r) + V_{\rm el}(r) + C_{\rm ex}V_{\rm ex}^{\rm (TF)}(r)\right] = -(Z-N+1)e^2. \tag{10.17}$$

Evidently, this correction yields a continuous exchange potential with the correct large-r behaviour, although the derivative of $V_{\rm ex}(r)$ has a discontinuity at $r_{\rm Latter}$.

10.1 Free-atom and Wigner–Seitz boundary conditions

The RADIAL subroutines compute one-electron eigenvalues $E_{n\kappa}$ and radial functions by solving the Dirac equations (10.4) with the usual free-atom boundary conditions. That is, by requiring that $P_{n\kappa}(r)$ and $Q_{n\kappa}(r)$ go to zero when r tends to infinity (see Section 5.2).

In many practical cases, atoms are bound in solids and it is of interest to study what is the effect of aggregation on the atomic orbitals and ionisation energies, at least in an approximate manner. To simplify arguments, we consider a single-element solid of mass density ρ (g/cm^3). A simple and convenient approach is provided by the Wigner–Seitz model (see, *e.g.*, Tucker *et al.*, 1969), which assumes that the atomic charge is fully contained within a sphere of radius $r_{\rm WS}$ and volume equal to the average atomic volume, *i.e.*,

$$\frac{4\pi}{3}\, r_{\rm WS}^3 = A_{\rm w}/(N_{\rm A}\rho), \tag{10.18}$$

where $A_{\rm w}$ is the atomic weight (g/mol) and $N_{\rm A}$ is Avogadro's constant. Inserting the numerical values of the constants,

$$r_{\rm WS} = 1.3882\,(A_{\rm w}/\rho)^{1/3}\, a_0. \tag{10.19}$$

Alternatively, for elementary solids one can set $r_{\rm WS}$ equal to half the nearest neighbour distance (see, *e.g.*, Kittel, 1976); this corresponds to the so-called muffin-tin model. The potential is spherically symmetric inside the sphere and constant outside it. To account for the periodicity of the solid lattice, we would like equivalent orbitals in neighbouring spheres to join smoothly at their surfaces. In a non-relativistic formulation, this is accomplished (again, approximately) by requiring that the radial functions $r^{-1}P(r)$ of odd (even) orbitals vanish (have null derivative) at the surface of the Wigner–Seitz sphere. In a relativistic calculation with Dirac wave functions, it is not possible to match simultaneously the large and small radial functions of corresponding orbitals of neighbouring atoms, because they have opposite parities. Nonetheless, the only orbitals that extend to distances of the order of $r_{\rm WS}$ are those of outer shells; these are weakly relativistic and, therefore, the small components of their wave functions at $r_{\rm WS}$ are negligible [$|Q(r_{\rm WS})| \ll |P(r_{\rm WS})|$]. We can, therefore, get quite a smooth joining of orbitals of neighbouring atoms by simply matching the large radial functions. The practical recipe is to require

$$\begin{aligned} &P(r_{\rm WS}) = 0 && \text{if } \ell \text{ is odd,} \\ &\frac{\rm d}{{\rm d}r}\left[r^{-1}P(r_{\rm WS})\right] = 0 && \text{if } \ell \text{ is even.} \end{aligned} \tag{10.20}$$

Combining these conditions with the radial equations (10.4) we obtain the following boundary values at $r_{\rm WS}$ (apart from a normalisation constant)

$$\begin{aligned} &P(r_{\rm WS}) = 0, \quad Q(r_{\rm WS}) = 1 && \text{if } \ell \text{ is odd,} \\ &P(r_{\rm WS}) = 1, \quad Q(r_{\rm WS}) = \frac{c\hbar}{E - V(r_{\rm WS}) + 2{\rm m_e}c^2}\,\frac{1+\kappa}{r_{\rm WS}} && \text{if } \ell \text{ is even.} \end{aligned} \tag{10.21}$$

These values determine the start of the inward power-series solution of the radial equations unambiguously. Notice that inner-shell orbitals which do not extend appreciably beyond $r_{\rm WS}$ are not affected by these boundary conditions. The program `DHFS` contains the subroutine `DBNDWS`, which calculates Dirac bound orbitals with Wigner–Seitz boundary conditions by using the same numerical strategy as in subroutine `DBOUND`; inner-shell orbitals that effectively vanish at $r = r_{\rm WS}$ are calculated with the usual free-atom boundary conditions. In subroutine `DBNDWS` both the potential and the radial functions are defined only for radii less than $r_{\rm WS}$.

10.2 Self-consistent solution method

The program `DHFS` uses the RADIAL subroutines to calculate one-electron energy eigenvalues, $E_{n\kappa}$, radial functions and DHFS potentials for neutral atoms and positive ions with either free-atom or Wigner-Seitz boundary conditions. The results for free atoms are equivalent to those from the similar code developed by Liberman *et al.* (1965), which is available from the Computer Physics Communications Program Library (Liberman *et al.*, 1971). In our program, all calculations are performed using Hartree atomic units. Radial functions are tabulated on a grid of up to 1,500 radii, extending from $r = 0$ up to an outer radius `RN` of the order of 75 a_0, which is generated by subroutine `SGRID` (see Section 8.4). The integrals (10.11) and (10.12) are evaluated using 6-point Lagrange quadrature formulas, Eq. (8.13), after introducing the change of variable (8.6).

The self-consistent solution of the DHFS equations (10.4) is started by considering an approximate electron density $\rho_0(r)$, which is obtained from the Molière (1947) parameterisation of the Thomas–Fermi potential of neutral atoms,

$$\rho_0(r) = \frac{N}{4\pi r b^2}\left[3.60\,\mathrm{e}^{-6r/b} + 0.792\,\mathrm{e}^{-1.2r/b} + 0.0315\,\mathrm{e}^{-0.3r/b}\right], \tag{10.22}$$

where $b = 0.885\,34\,Z^{-1/3}\,a_0$ is the Thomas–Fermi radius. The self-consistent solution then proceeds as follows. From the initial density ρ_0 we compute a first approximation to the DHFS potential, Eq. (10.7), which we call V_1. With this potential, a set of radial functions and energy eigenvalues is obtained by solving the radial Dirac equations (10.4) for the various shells. This yields a new electronic density ρ_1 from which we obtain a new approximation to the DHFS potential, which we indicate as $V_{2\rm n}$. The potential for the next iteration is the weighted average

$$V_2 = (1 - w)V_1 + wV_{2\rm n}. \tag{10.23}$$

Inserting this potential into the radial equations, we compute a new set of radial functions and energy eigenvalues, from which we calculate a new electron density ρ_2, etc. The calculation continues by repeating these steps and ends when the maximum relative difference between the potentials in successive iterations is less than the specified tolerance, 10^{-9}, in the `DHFS` program. At the beginning, the weight w is set equal to 0.05 and its value is gradually increased as the calculation progresses, to reach a maximum value of 0.5. This kind of mixture of the "new" and "old" potentials is necessary to ensure convergence for all atoms and positive ions.

Ground-state configurations of atoms with one or two electrons ($N = 1, 2$) in a single shell are handled separately. In these cases we take $C_{\rm ex} = 0$ and set the exchange potential equal to the self interaction energy, *i.e.*, N^{-1} times the electronic potential. This gives exact results for the hydrogen atom and one-electron ions in any state. The method is also exact for helium and two-electron ions in their ground configuration and doubly excited symmetric configurations of the type $(n\kappa)^2$ with $\kappa = -1$.

The program `DHFS` reads input data from a formatted file with the structure shown in Table 3 (see the heading comments of the source file `DHFS.f`). Data are read from the fields in parentheses; information outside these fields is just a reminder to the user. If the number of shells is set equal to zero or negative (and lines `C3` are removed from the input file), the program performs the self-consistent calculation for a neutral atom in its ground-state configuration (which is defined internally by subroutine `ELEMNT`). The atomic weight (in g/mol) in line `C4` is used to determine the nuclear radius, Eq. (10.10) [a point nucleus is assumed when $-0.5 < A_{\rm w} < 0.5$]. If the input value of the atomic weight is less than -0.5, the programs replaces it by the average atomic weight of the element for natural isotopic abundances. The exchange parameter $C_{\rm ex}$ in line `C5` should be set equal to 1.5 to perform a true DHFS calculation (*i.e.*, with Slater's exchange potential); with $C_{\rm ex} = 1$, the program uses the potential of Kohn and Sham (1965). The outer radius `RN` is read from line `C6`. In the case of free atoms this parameter should be larger than about $= 75a_0$; when the input value is smaller, and positive, it is replaced by `RN` $= 75a_0$. A negative input value of `RN` instructs the program to use Wigner-Seitz boundary conditions with $r_{\rm WS} = -$`RN`. The line `C8`, with the keyword `Compton` in columns 4–10, is optional; it activates the calculation of momentum wave functions and Compton profiles (see Section 10.4).

Table 3: Example of input data file of the `DHFS` program. The scale lines are not part of the input file. A line `C3` is expected for each shell $(n\ell_j)^q$.

```
C...+....1....+....2....+....3....+....4....+....5....+....6....+....7..
C1 (Neon, Z= 10. Neutral atom                                      )  Title
C2 (Ne, 10,  4)       Chemical symbol, atomic number Z, number of shells
C3 ( 1, 0, 1, 2.000)   2  He                n, l, 2j, occupation number
C3 ( 2, 0, 1, 2.000)   4                    n, l, 2j, occupation number
C3 ( 2, 1, 1, 2.000)   6                    n, l, 2j, occupation number
C3 ( 2, 1, 3, 4.000)  10  Ne                n, l, 2j, occupation number
C4 (  20.1797)                                Aw (atomic weight, g/mol)
C5 (   1.5000)          Exchange parameter (1.5, Slater; 1.0, Kohn-Sham)
C6 (  75.0000)             RN, outer radius; -Rws for Wigner-Seitz atoms
C7 (1000,Eh)        Number of radial grid points, energy unit (Eh or Ry)
C8 Compton                     Compute shell Compton profiles (optional)
C...+....1....+....2....+....3....+....4....+....5....+....6....+....7..
```

The program stops when an incorrect or inconsistent input datum is found; normally, the wrong quantity is printed in the last line of the standard output unit (`UNIT=6`). At the end of the calculation, when the self-consistent procedure has converged, results are

delivered through several output files with the extension ".dat". In the output files, energy eigenvalues are given in either Hartrees or Rydbergs (1 Ry = $\frac{1}{2}E_{\rm h}$) (as selected in line C7 of the input file) and in eV, all lengths are in Bohr radii. The file dhfs.dat contains a detailed report of the calculation, including energy eigenvalues, expectation values of various powers of the radial distance,

$$\langle r^n \rangle \equiv \frac{1}{N} \int_0^\infty r^n \, \rho(r) \, 4\pi r^2 \, {\rm d}r, \tag{10.24}$$

as well as a table with the electron density and the potential. The file rwavefcts.dat contains the radial wave functions for the various shells in a format appropriate for visualisation with a plotting program, such as gnuplot (http://www.gnuplot.info). All output files have heading comments describing the file contents and format. DHFS also generates a gnuplot script named dhfsplot.gnu, which can be used for displaying the results on the computer screen.

Figure 11 displays the various components of the self-consistent DHFS potential of copper ($Z = 29$) with a finite nucleus; the corresponding electron density is shown in Fig. 12. For radii smaller than $r_{\rm Latter}$, the exchange potential varies smoothly with r; at $r_{\rm Latter}$ the exchange potential changes form (it is forced to cancel the electron self-interaction) and there is a discontinuity in the first derivative of $rV_{\rm ex}(r)$. We recall that the electrostatic interaction energy of the atom and an external particle with electric charge $Z_0 e$ is $-Z_0[V_{\rm nuc}(r) + V_{\rm el}(r)]$ where r is the distance of the particle to the centre of the nucleus. The electronic potential $V_{\rm el}(r)$ accounts for the screening of the nuclear charge by the atomic electrons. The function $rV_{\rm el}$ practically vanishes for radii less than about 10^{-3}, showing that electronic screening is negligible at small r.

The self-consistent radial electron density of copper calculated by the program DHFS is shown in Fig. 12a. Electron densities for free atoms and Wigner-Seitz copper atoms calculated with the DHFS method, are displayed in Fig. 12b. Differences between the electron densities of free and bound atoms are appreciable only for relatively large radii. Notice that, as a result of the boundary conditions (10.21), the electron density at $r = r_{\rm WS}$ ($= 2.42 a_0$) is "flat".

The DHFS energy eigenvalues, $-E_{n\kappa}$, of neutral atoms are compared to the experimental shell ionisation energies (Carlson, 1975) in Fig. 13. As mentioned above, DHFS eigenvalues keep the significance of one-electron binding energies and, indeed, they are close to the actual ionisation energies for shells with $-E_{n\kappa}$ larger than about 200 eV. Because of this peculiarity, the self-consistent DHFS potential is employed in many calculations of interactions of high-energy radiations with inner-shell electrons (see, *e.g.*, Pratt *et al.*, 1973; Bote and Salvat, 2008).

Slater (1951) proposed his approximation to the exchange potential, Eq. (10.13) with $C_{\rm ex} = 3/2$, as a simplification of the non-relativistic Hartree–Fock method which leads to the so-called Hartree–Fock–Slater (HFS) equations. The book of Condon and Odabaşi (1980) contains a historical review of HFS calculations and some sample results. The HFS equations can be regarded as the non-relativistic limit of the DHFS equations, because they are obtained from the latter by replacing the one-electron kinetic energy operator, $c\,\widetilde{\boldsymbol{\alpha}}\cdot\mathbf{p} + (\widetilde{\beta} - 1){\rm m_e}c^2$, by its non-relativistic form, $\mathbf{p}^2/(2{\rm m_e})$.

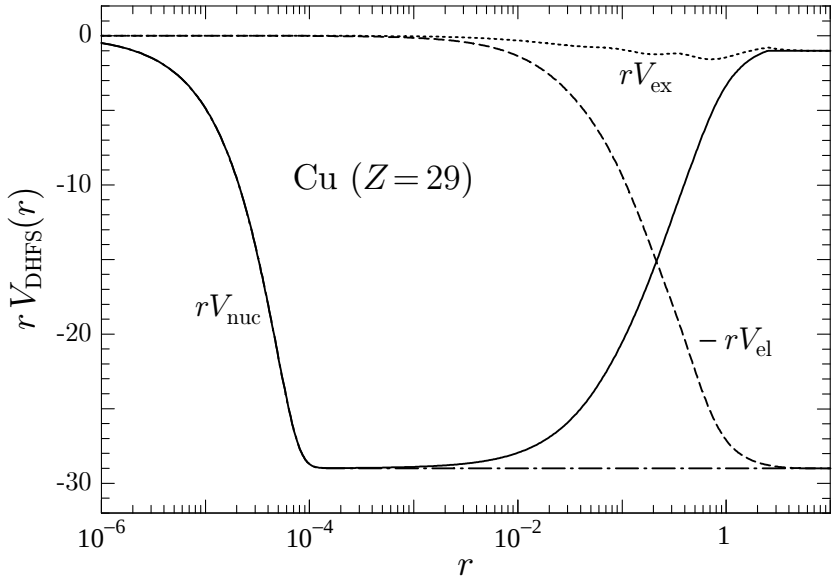

Figure 11: DHFS self-consistent potential $rV_{\rm DHFS}(r)$ of the copper atom (solid curve). The nuclear potential (dot-dashed curve) corresponds to a finite nucleus, represented by the Fermi distribution, Eq. (10.9). The exchange potential includes the Latter tail correction, Eq. (10.16). All quantities are in atomic units.

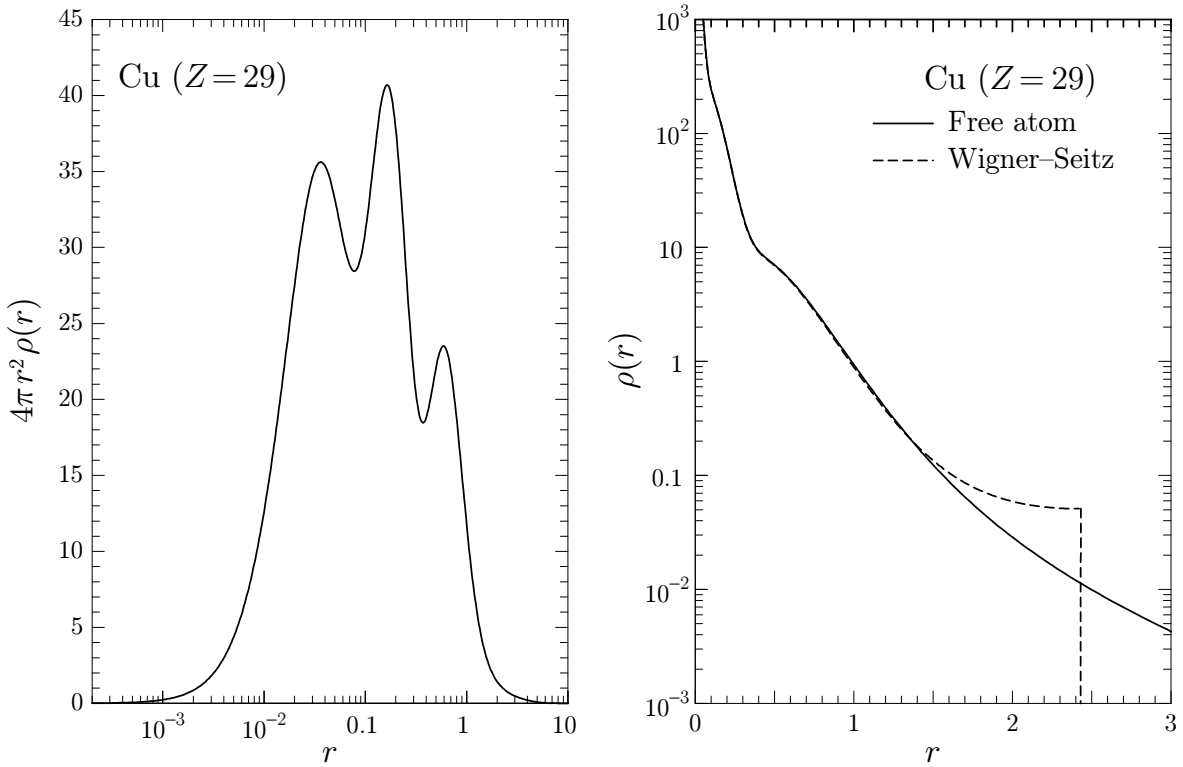

Figure 12: a) DHFS radial electron density, $4\pi r^2\rho(r)$, of the copper atom ($Z = 29$). b) Electron densities of copper atoms calculated with free-atom and Wigner–Seitz boundary conditions. Lengths in atomic units.

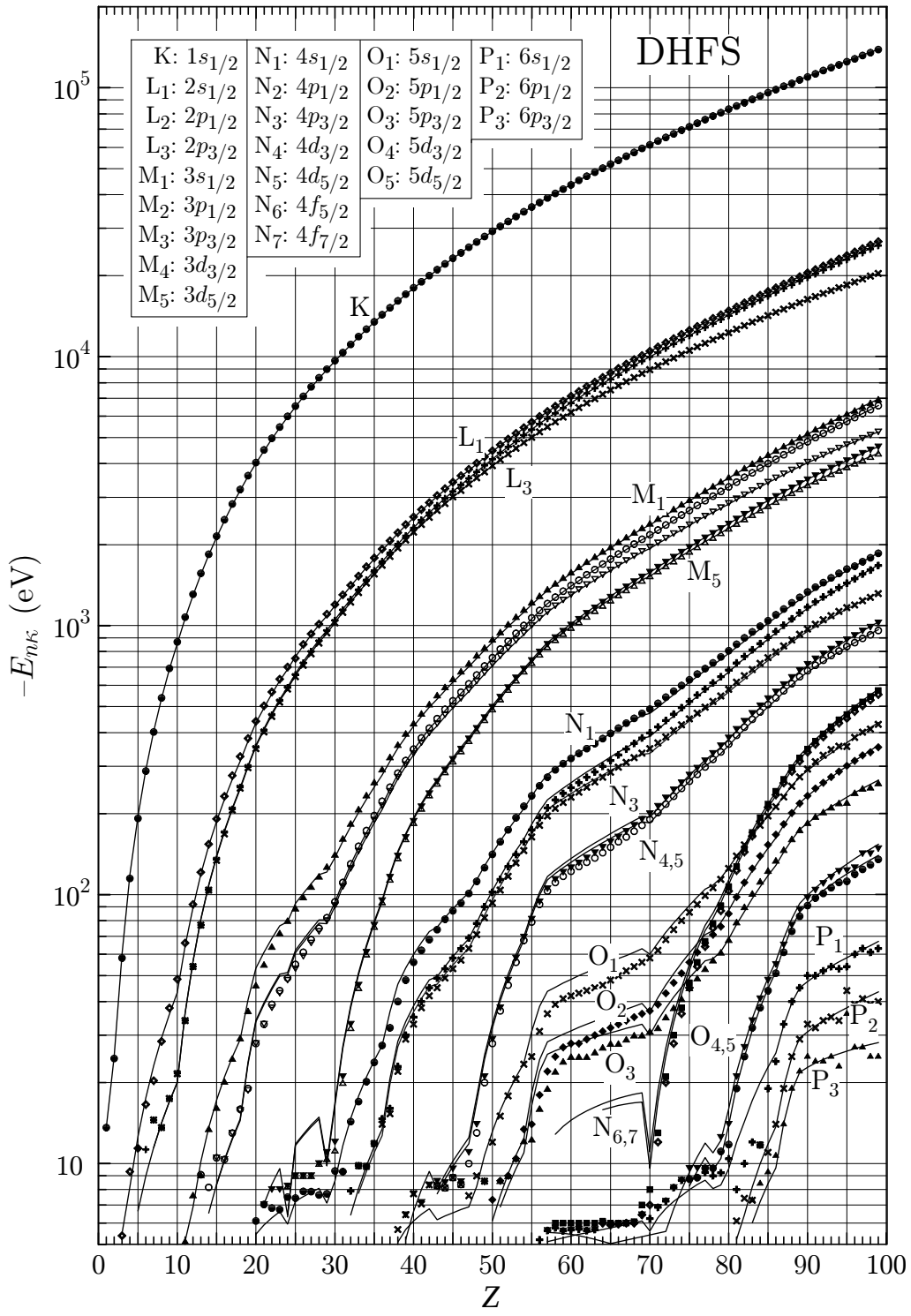

Figure 13: Ionisation energies of neutral atoms, in eV. Symbols are experimental values taken from Carlson (1975). Lines represent the absolute values of the one-electron energy levels, $-E_{n\kappa}$, for the DHFS potential (with $C_{\rm ex} = 3/2$). Electron shells are indicated by using the x-ray notation, in which the value of the principal quantum number $n = 1, 2, 3, 4, \ldots$ is represented by the respective capital letters K, L, M, N, ..., and angular momenta are indicated by the numeral i (see Table 1).

10.3 Evaluation of the total binding energy

The Fortran source files of the RADIAL package contain the main tools needed to evaluate matrix elements of the atomic Hamiltonian,

$$\mathcal{H} = \sum_{i=1}^{N} \Big[c\widetilde{\boldsymbol{\alpha}}_i \cdot \mathbf{p}_i + (\widetilde{\beta}_i - 1)\mathrm{m_e}c^2 \Big] + \sum_{i=1}^{N} V_{\mathrm{nuc}}(\mathbf{r}_i) + \sum_{i<j=1}^{N} \frac{e^2}{|\mathbf{r}_i - \mathbf{r}_j|}, \tag{10.25}$$

where $\mathbf{p}_i$, $\mathbf{r}_i$ are the momentum and position operators of the i-th electron and $\widetilde{\boldsymbol{\alpha}}_i$, $\widetilde{\beta}_i$ are the Dirac matrices, (2.12). The expression in square brackets in Eq. (10.25) is the Dirac "kinetic energy" operator of the i-th electron, which results from subtracting the rest energy $\mathrm{m_e}c^2$ from the Dirac Hamiltonian of a free electron.

As mentioned above, the DHFS model assumes that atomic wave functions Ψ are represented as Slater determinants formed with N Dirac spin orbitals, $\psi_1(\mathbf{r}), \ldots, \psi_N(\mathbf{r})$, normalised and mutually orthogonal,

$$\Psi = \frac{1}{\sqrt{N!}} \begin{vmatrix} \psi_1(\mathbf{r}_1) & \ldots & \psi_1(\mathbf{r}_N) \\ \vdots & \ddots & \vdots \\ \psi_N(\mathbf{r}_1) & \ldots & \psi_N(\mathbf{r}_N) \end{vmatrix}, \qquad \langle \psi_i | \psi_j \rangle \equiv \int \psi_i^\dagger(\mathbf{r})\, \psi_j(\mathbf{r})\, \mathrm{d}\mathbf{r} = \delta_{ij}. \tag{10.26}$$

To illustrate the calculation of matrix elements of $\mathcal{H}$ with Slater determinants, we consider the total (electronic) binding energy, $E[\Psi] \equiv \langle \Psi | \mathcal{H} | \Psi \rangle$, which using the Slater–Condon rules (Slater, 1929; Condon, 1930) can be expressed as

$$E[\Psi] = E_{\mathrm{kin}} + E_{\mathrm{nuc}} + E_{\mathrm{el}} + E_{\mathrm{ex}}, \tag{10.27}$$

where the terms

$$E_{\mathrm{kin}} = \sum_i \int \psi_i^\dagger(\mathbf{r}) \Big\{ c\, \widetilde{\boldsymbol{\alpha}} \cdot \mathbf{p} + (\widetilde{\beta} - 1)\mathrm{m_e}c^2 \Big\} \psi_i(\mathbf{r})\, \mathrm{d}\mathbf{r}, \tag{10.28a}$$

$$E_{\mathrm{nuc}} = \sum_i \int \psi_i^\dagger(\mathbf{r})\, V_{\mathrm{nuc}}(r)\, \psi_i(\mathbf{r})\, \mathrm{d}\mathbf{r}, \tag{10.28b}$$

$$E_{\mathrm{el}} = \frac{1}{2}\, e^2 \sum_{i,j} \iint \Big\{ \psi_i^\dagger(\mathbf{r}) \psi_i(\mathbf{r}) \Big\} \Big\{ \psi_j^\dagger(\mathbf{r}') \psi_j(\mathbf{r}') \Big\} \frac{1}{|\mathbf{r} - \mathbf{r}'|}\, \mathrm{d}\mathbf{r}\, \mathrm{d}\mathbf{r}' \tag{10.28c}$$

and

$$E_{\mathrm{ex}} = -\frac{1}{2}\, e^2 \sum_{i,j} \iint \Big\{ \psi_i^\dagger(\mathbf{r}) \psi_j(\mathbf{r}) \Big\} \Big\{ \psi_j^\dagger(\mathbf{r}') \psi_i(\mathbf{r}') \Big\} \frac{1}{|\mathbf{r} - \mathbf{r}'|}\, \mathrm{d}\mathbf{r}\, \mathrm{d}\mathbf{r}' \tag{10.28d}$$

are, respectively, the kinetic energy, the interaction energy with the nucleus, the total electron-electron interaction energy and the exchange energy. The last two quantities include self-interaction terms with $i = j$, which cancel by pairs in the sum (10.27). The

actual electron-electron interaction energy and the exchange energy are given, respectively, by the sums in expressions (10.28c) and (10.28d) *excluding* the self-interaction terms.

To be consistent with the spherical average implicit in the DHFS central-field equations, we shall limit ourselves to considering the average energy of the ground-state configuration, which is defined as

$$E_{\rm av} \equiv \frac{1}{\mathcal{D}} \sum_{\Psi} \langle \Psi | \mathcal{H} | \Psi \rangle \,, \tag{10.29}$$

where the summation extends over the $\mathcal{D}$ equivalent states in the configuration (corresponding to various combinations of occupied orbitals in the open shells). For a closed-shell configuration, $\mathcal{D} = 1$ and the average energy coincides with the energy of the state. The average energy of the configuration can be split into its kinetic and potential parts,

$$E_{\rm av} = E_{\rm av,kin} + E_{\rm av,pot} \,, \tag{10.30}$$

which are given by (see, *e.g.*, Grant, 1970),

$$\begin{aligned} E_{\rm av,kin} \,=\, & \sum_a q_a \int \left\{ P_{n_a\kappa_a}\, c\hbar \left(\frac{\kappa_a}{r}\, Q_{n_a\kappa_a} - Q'_{n_a\kappa_a} \right) \right. \\ & \left. + Q_{n_a\kappa_a} \left[c\hbar \left(\frac{\kappa_a}{r}\, P_{n_a\kappa_a} + P'_{n_a\kappa_a} \right) - 2{\rm m_e}c^2\, Q_{n_a\kappa_a} \right] \right\} {\rm d}r, \end{aligned} \tag{10.31}$$

$$\begin{aligned} E_{\rm av,pot} \,=\, & \sum_a q_a \left\{ \int \left(P^2_{n_a\kappa_a} + Q^2_{n_a\kappa_a} \right) V_{\rm nuc}\, {\rm d}r \right. \\ & + \frac{e^2}{2}\, (q_a - 1) \left(F^0(a,a) - \sum_{L=1}^{\infty} \frac{d^L(\kappa_a,\kappa_a)}{2j_a}\, F^L(a,a) \right) \\ & \left. + \frac{e^2}{2} \sum_{b\neq a} q_b \left(F^0(a,b) - \sum_{L=0}^{\infty} \frac{d^L(\kappa_a,\kappa_b)}{2j_b+1}\, G^L(a,b) \right) \right\}, \end{aligned} \tag{10.32}$$

where the summations run over the occupied shells a. The quantities

$$F^L(a,b) \equiv R^L(a\,b, a\,b) \qquad \text{and} \qquad G^L(a,b) \equiv R^L(a\,b, b\,a) \tag{10.33}$$

are radial integrals of the form (Slater integrals),

$$\begin{aligned} R^L(a\,b, c\,d) \,\equiv\, & \int_0^\infty \int_0^\infty \left[P_{n_a\kappa_a}(r_1)\, P_{n_c\kappa_c}(r_1) \,+ Q_{n_a\kappa_a}(r_1)\, Q_{n_c\kappa_c}(r_1) \right] \frac{r_<^L}{r_>^{L+1}} \\ & \times \left[P_{n_b\kappa_b}(r_2)\, P_{n_d\kappa_d}(r_2) \,+ Q_{n_b\kappa_b}(r_2)\, Q_{n_d\kappa_d}(r_2) \right] {\rm d}r_1\, {\rm d}r_2, \end{aligned} \tag{10.34}$$

with $r_> \equiv \max(r, r')$ and $r_< \equiv \min(r, r')$. The coefficients $d^L(\kappa_a, \kappa_b)$ are given by

$$d^L(\kappa_a,\kappa_b) \equiv v(L,\ell_a,\ell_b)\, \frac{2j_b+1}{2j_a+1}\, \left\langle L j_b 0 \tfrac{1}{2} \middle| j_a \tfrac{1}{2} \right\rangle^2 \tag{10.35}$$

with the parity factor

$$\upsilon(L,\ell_a,\ell_b) \equiv \begin{cases} 1 \text{ if } L+\ell_a+\ell_b \text{ is even,} \\ 0 \text{ otherwise.} \end{cases} \tag{10.36}$$

The Clebsch–Gordan coefficient $\left\langle Lj_b0\frac{1}{2}\middle|\, j_a\frac{1}{2}\right\rangle$ can be evaluated using the relation (see Edmonds, 1960, Eq. 3.7.12)

$$\begin{aligned}\sqrt{2j'(2j+1)}\,\left\langle L,j,0,\tfrac{1}{2}\middle|\, j',\tfrac{1}{2}\right\rangle &= \sqrt{(K-2L)(K+1)}\,\left\langle L,j-\tfrac{1}{2},0,0\middle|\, j'-\tfrac{1}{2},0\right\rangle \\ &+ \sqrt{(K-2j)(K-2j'+1)}\,\left\langle L,j+\tfrac{1}{2},0,0\middle|\, j'-\tfrac{1}{2},0\right\rangle, \end{aligned} \tag{10.37}$$

where $K \equiv L+j+j'$. The coupling coefficients on the right-hand side are of the form $\langle j_1 j_2 00|j_3 0\rangle$ and vanish if $j_1+j_2+j_3$ is odd. When $j_1+j_2+j_3 \equiv 2J$ is even,

$$\langle j_1 j_2 00|j_3 0\rangle = (-1)^{J-j_3}\sqrt{\frac{2j_3+1}{2J+1}}\left[\frac{\tau(J)}{\tau(J-j_1)\tau(J-j_2)\tau(J-j_3)}\right]^{1/2} \tag{10.38a}$$

with

$$\tau(n) \equiv \frac{2^n(n!)^2}{(2n)!} = \frac{n!}{1\cdot 3\cdot 5\cdots(2n-1)}. \tag{10.38b}$$

It is worth mentioning that the DHFS solution does not satisfy Koopmans' theorem (Condon and Odabaşi, 1980), *i.e.*, the absolute value of the one-electron eigenvalue, $|E_{n_a\kappa_a}| = -E_{n_a\kappa_a}$, is not equal to the shell ionisation energy, $I_{n_a\kappa_a}$, which is defined as the energy required to extract an electron from this shell leaving the other occupied orbitals frozen. $I_{n_a\kappa_a}$ can be estimated as the difference between the average energy $E_{\rm av}(N)$ of the initial configuration and the average energy $E_{\rm av}(N-1)$ of the configuration that results from emptying an orbital $(n_a\kappa_a)$,

$$I_{n_a\kappa_a} = E_{\rm av}(N) - E_{\rm av}(N-1). \tag{10.39}$$

The program `DHFS` calculates the ionisation energies $I_{n_a\kappa_a}$, as well as the one-electron kinetic and potential energies, of the occupied shells. Interestingly, at least for inner shells with binding energies larger than about 200 eV, the DHFS eigenvalues $-E_{n\kappa}$ are much closer to the experimental ionisation energies than the values obtained from Eq. (10.39).

It should be noted that the concept of ionisation energy is somewhat ambiguous. In a real ionisation process, *e.g.*, in the photoabsorption of photons with energy $E_{\rm ph}$, the ejected electron leaves the atom with a finite speed. If this speed is high, the ionisation is "sudden" and the inactive orbitals remain frozen during the process; the electron would then be ejected with energy $\simeq E_{\rm ph} - I_{n\kappa}$. On the other hand, for photons with energies slightly above the ionisation edge, the photoelectron leaves the parent atom very slowly and the orbitals that remain occupied have time to relax in the course of the process. This implies that the amount of energy needed to extract the electron is smaller than for sudden ionisation and, in particular, that photon absorption edges occur at energies which are smaller than $I_{n\kappa}$. In the so-called "adiabatic approximation", the ionisation energy is calculated as the difference between the total energies (or average configuration energies) of the initial and final configurations, *i.e.*, allowing *complete* relaxation of the inactive electron orbitals (see Grant, 1970).

10.3.1 Calculation of Slater integrals

The calculation of matrix elements of the Coulomb interaction, $e^2/|\mathbf{r}-\mathbf{r}'|$, involves double radial integrals of Slater's type,

$$I_L \equiv \int_0^\infty \mathrm{d}r\, g(r) \int_0^\infty \mathrm{d}s\, \frac{r_<^L}{r_>^{L+1}}\, f(s), \tag{10.40}$$

where $r_< \equiv \min(r,s)$ and $r_> \equiv \max(r,s)$, *i.e.*,

$$I_L = \int_0^\infty \mathrm{d}r\, g(r) \left\{ \frac{1}{r^{L+1}} \int_0^r s^L\, f(s)\, \mathrm{d}s + r^L \int_r^\infty \frac{1}{s^{L+1}}\, f(s)\, \mathrm{d}s \right\}. \tag{10.41}$$

The straightforward evaluation of I_L (*e.g.*, using Lagrange quadrature formulas) is very time consuming and not particularly accurate. It is much more efficient to use the following method, which was described by Hartree in his book "The Calculation of Atomic Structures" 1957. We define the function

$$\begin{aligned} Y(r) &\equiv r \int_0^\infty \frac{r_<^L}{r_>^{L+1}}\, f(s)\, \mathrm{d}s \\ &= \int_0^r \left(\frac{s}{r}\right)^L f(s)\, \mathrm{d}s + \int_r^\infty \left(\frac{r}{s}\right)^{L+1} f(s)\, \mathrm{d}s, \end{aligned} \tag{10.42}$$

so that

$$I_L = \int_0^\infty g(r)\, \frac{1}{r}\, Y(r)\, \mathrm{d}r. \tag{10.43}$$

The function

$$Z(r) \equiv \int_0^r \left(\frac{s}{r}\right)^L f(s)\, \mathrm{d}s \tag{10.44}$$

vanishes at $r = 0$ and satisfies the differential equation

$$\frac{\mathrm{d}Z(r)}{\mathrm{d}r} = f(r) - \frac{L}{r} Z(r). \tag{10.45}$$

Multiplying the relation

$$Y(r) = Z(r) + \int_r^\infty \left(\frac{r}{s}\right)^{L+1} f(s)\, \mathrm{d}s \tag{10.46}$$

by $r^{-(L+1)}$, differentiating both sides, and using Eq. (10.45), we find that $Y(r)$ satisfies the following equation

$$\frac{\mathrm{d}Y(r)}{\mathrm{d}r} = \frac{1}{r}\Big[(L+1)Y(r) - (2L+1)Z(r)\Big]. \tag{10.47}$$

Hartree's method consists of first determining $Z(r)$ by solving the differential equation (10.45), starting from the origin with the initial value $Z(0) = 0$ and integrating outwards up to a distance r_a for which $Z(r)$ attains its asymptotic value $Z(\infty)$. Then, $Y(r)$ is obtained from Eq. (10.47), which is integrated inwards, starting from r_a with the initial

value $Y(r_\mathrm{a}) = Z(r_\infty)$. In the interval (r_a, ∞), $f(s) = 0$, $Y(r) = Z(r)$ and Eq. (10.47) reduces to

$$\frac{\mathrm{d}Y(r)}{\mathrm{d}r} = -\frac{L}{r}Y(r). \tag{10.48}$$

Hence,

$$Y(r) = \frac{Z(\infty)\, r_\mathrm{a}^L}{r^L} \qquad \text{for } r > r_\mathrm{a}. \tag{10.49}$$

The function `SLATER` in the source file `DHFS.f` computes the Slater integrals (10.40) by using Hartree's method. To solve the differential equation (10.45), the function $f(r)$ is replaced by the interpolating natural cubic spline and $Z(r)$ is determined by using a power-series method similar to the one employed in Section 4. After solving Eq. (10.45), the function $Z(r)$ is also replaced by a natural cubic spline and Eq. (10.47) is integrated inwards by again using the power-series method. The convergence of the power series is accelerated, when needed, by halving the interval between successive points of the grid. Errors in the resulting $Y(r)$ values arise only from possible inaccuracies of the spline interpolations, since the power-series method effectively eliminates truncation errors. The only practical difficulty is found in the last stages of the integration of Eq. (10.47) for large L's; when we approach the origin the magnitude of $Z(r)$ is exceedingly small and $Y(r)$ also tends to zero, which makes the numerical solution unstable. The problem is avoided by simply discontinuing the integration when $Y(r)$ is less than 10^{-14} or when it shows any tendency to increase in magnitude for decreasing r. Finally, the integral (10.43) is evaluated using the 6-point Lagrange quadrature formulas (8.13).

10.4 Momentum distributions and Compton profiles

With the radial wave functions obtained from the self-consistent calculation, we can calculate momentum distributions and Compton profiles for the various shells. These quantities are useful, *e.g.*, to derive cross sections for incoherent (Compton) scattering of x-rays within the impulse approximation (see, *e.g.*, Ribberfors, 1975, and references therein).

The Dirac Hamiltonian of a free electron $\mathcal{H}_0 = c\widetilde{\boldsymbol{\alpha}}\cdot\mathbf{p} + (\widetilde{\beta}-1)\mathrm{m_e}c^2$ ($V \equiv 0$) commutes with the linear momentum operator $\mathbf{p}$. A complete set of common eigenfunctions of these two operators are the plane waves

$$\phi_{\mathbf{p}\mu\tau}(\mathbf{r}) = \frac{\exp(\mathrm{i}\mathbf{p}\cdot\mathbf{r}/\hbar)}{(2\pi\hbar)^{3/2}}\, u_{\mathbf{p}\mu\tau}, \tag{10.50}$$

where the index τ ($= \pm 1$) denotes the sign of the energy, $\mu = \pm 1/2$ and $u_{\mathbf{p}\mu\tau}$ are the double spinors

$$u_{\mathbf{p},\mu,+1} = \left[1 + \frac{(cp)^2}{(|\mathcal{W}| + \mathrm{m_e}c^2)^2}\right]^{-1/2} \begin{pmatrix} I_2 \\ +\dfrac{c\,\boldsymbol{\sigma}\cdot\mathbf{p}}{|\mathcal{W}| + \mathrm{m_e}c^2} \end{pmatrix} \chi_\mu, \tag{10.51a}$$

$$u_{\mathbf{p},\mu,-1} \;=\; \left[1+\frac{(cp)^2}{(|\mathcal{W}|+\mathrm{m_e}c^2)^2}\right]^{-1/2} \begin{pmatrix} -\dfrac{c\,\boldsymbol{\sigma}\cdot\mathbf{p}}{|\mathcal{W}|+\mathrm{m_e}c^2} \\ I_2 \end{pmatrix} \chi_\mu, \qquad (10.51b)$$

with the Pauli spinors χ_μ defined by (2.18). The plane wave $\phi_{\mathbf{p}\mu\tau}(\mathbf{r})$ describes a free electron with momentum $\mathbf{p}$, total energy $\mathcal{W}=\tau[(cp)^2+\mathrm{m_e}^2c^4]^{1/2}$ and spin projection μ, in the coordinate representation. It can be easily verified that, for a given $\mathbf{p}$,

$$u^\dagger_{\mathbf{p}\mu'\tau'}\,u_{\mathbf{p}\mu\tau}=\delta_{\mu',\mu}\,\delta_{\tau',\tau} \qquad \text{and} \qquad \sum_{\mu\tau} u_{\mathbf{p}\mu\tau}\,u^\dagger_{\mathbf{p}\mu\tau}=I_4, \qquad (10.52)$$

where I_4 is the 4×4 unit matrix. From the properties of the three-dimensional Fourier transform, it follows that the plane waves (10.50) constitute a complete basis for the states of free Dirac particles. They satisfy the orthonormality relation

$$\langle\,\phi_{\mathbf{p}'\mu'\tau'}|\,\phi_{\mathbf{p}\mu\tau}\,\rangle=\int \phi^\dagger_{\mathbf{p}'\mu'\tau'}(\mathbf{r})\,\phi_{\mathbf{p}\mu\tau}(\mathbf{r})\,\mathrm{d}\mathbf{r}=\delta(\mathbf{p}'-\mathbf{p})\,\delta_{\mu',\mu}\,\delta_{\tau',\tau}. \qquad (10.53)$$

The momentum distribution of an electron in the bound orbital $\psi_{n\kappa m}$ is given by

$$\begin{aligned}\rho_{n\kappa m}(\mathbf{p}) \;&=\; \sum_{\mu,\tau}|\langle\phi_{\mathbf{p}\mu\tau}|\,\psi_{n\kappa m}\rangle|^2=\sum_{\mu,\tau}\langle\psi_{n\kappa m}|\,\phi_{\mathbf{p}\mu\tau}\rangle\,\langle\phi_{\mathbf{p}\mu\tau}|\,\psi_{n\kappa m}\rangle \\ &=\left[\int\psi^\dagger_{n\kappa m}(\mathbf{r})\,\frac{\exp(\mathrm{i}\mathbf{p}\cdot\mathbf{r}/\hbar)}{(2\pi\hbar)^{3/2}}\,\mathrm{d}\mathbf{r}\right] \\ &\quad\times\left(\sum_{\mu,\tau}u_{\mathbf{p}\mu\tau}u^\dagger_{\mathbf{p}\mu\tau}\right)\left[\int\frac{\exp(-\mathrm{i}\mathbf{p}\cdot\mathbf{r}/\hbar)}{(2\pi\hbar)^{3/2}}\,\psi_{n\kappa m}(\mathbf{r})\,\mathrm{d}\mathbf{r}\right]. \qquad (10.54)\end{aligned}$$

Using the closure relation (10.52) of the 4-spinors $u_{\mathbf{p}\mu\tau}$, we can write

$$\rho_{n\kappa m}(\mathbf{p})=\widetilde{\psi}^\dagger_{n\kappa m}(\mathbf{p})\,\widetilde{\psi}_{n\kappa m}(\mathbf{p}), \qquad (10.55)$$

where

$$\widetilde{\psi}_{n\kappa m}(\mathbf{p})\equiv\frac{1}{(2\pi\hbar)^{3/2}}\int\exp(-\mathrm{i}\mathbf{p}\cdot\mathbf{r}/\hbar)\,\psi_{n\kappa m}(\mathbf{r})\,\mathrm{d}\mathbf{r}. \qquad (10.56)$$

is the Fourier transform of the bound orbital $\psi_{n\kappa m}(\mathbf{r})$. Inserting the Rayleigh expansion of the Schrödinger plane waves [see Eq. (6.29)],

$$\exp(\mathrm{i}\mathbf{p}\cdot\mathbf{r}/\hbar)=4\pi\sum_{\lambda=0}^{\infty}\sum_{\nu=-\lambda}^{\lambda}\mathrm{i}^\lambda\,j_\lambda(pr/\hbar)\,Y^*_{\lambda,\nu}(\hat{\mathbf{p}})\,Y_{\lambda,\nu}(\hat{\mathbf{r}}), \qquad (10.57)$$

where $j_\lambda(x)$ are the spherical Bessel functions, Eqs. (3.65a) and (3.68), we have

$$\begin{aligned}\widetilde{\psi}_{n\kappa m}(\mathbf{p}) &= \sqrt{\frac{2}{\pi\hbar^3}}\sum_{\lambda,\nu}\mathrm{i}^{-\lambda}\,Y_{\lambda,\nu}(\hat{\mathbf{p}})\int j_\lambda(pr/\hbar)\,Y^*_{\lambda,\nu}(\hat{\mathbf{r}})\begin{pmatrix}P_{n\kappa}(r)\,\Omega_{\kappa,m}(\hat{\mathbf{r}})\\ \mathrm{i}Q_{n\kappa}(r)\,\Omega_{-\kappa,m}(\hat{\mathbf{r}})\end{pmatrix} r\,\mathrm{d}r\,\mathrm{d}\hat{\mathbf{r}} \\ &= \begin{pmatrix}\mathrm{i}^{-\ell}\,\widetilde{P}_{n\kappa}(p)\,\Omega_{\kappa,m}(\hat{\mathbf{p}})\\ \mathrm{i}^{1-\bar{\ell}}\,\widetilde{Q}_{n\kappa}(p)\,\Omega_{-\kappa,m}(\hat{\mathbf{p}})\end{pmatrix}=\mathrm{i}^{-\ell}\begin{pmatrix}\widetilde{P}_{n\kappa}(p)\,\Omega_{\kappa,m}(\hat{\mathbf{p}})\\ \dfrac{-\kappa}{|\kappa|}\,\widetilde{Q}_{n\kappa}(p)\,\Omega_{-\kappa,m}(\hat{\mathbf{p}})\end{pmatrix} \qquad (10.58)\end{aligned}$$

with

$$\widetilde{P}_{n\kappa}(p) \;=\; \sqrt{\frac{2}{\pi\hbar^3}} \int_0^\infty j_\ell(pr/\hbar)\, P_{n\kappa}(r)\; r\,\mathrm{d}r,$$

$$\widetilde{Q}_{n\kappa}(p) \;=\; \sqrt{\frac{2}{\pi\hbar^3}} \int_0^\infty j_{\bar{\ell}}(pr/\hbar)\, Q_{n\kappa}(r)\; r\,\mathrm{d}r. \tag{10.59}$$

Here ℓ and $\bar{\ell} = \ell - \kappa/|\kappa|$ are the orbital angular momenta corresponding to κ and $-\kappa$, respectively. Notice that

$$\int \widetilde{\psi}^\dagger_{n'\kappa'm'}(\mathbf{p})\, \widetilde{\psi}_{n\kappa m}(\mathbf{p})\, \mathrm{d}\mathbf{p} = \delta_{n',n}\, \delta_{\kappa',\kappa}\, \delta_{m',m}, \tag{10.60}$$

which follows directly from the definition (10.56). The average over degenerate magnetic states

$$\rho_{n\kappa}(\mathbf{p}) = \frac{1}{2j+1} \sum_m \rho_{n\kappa m}(\mathbf{p}) = \frac{1}{4\pi} \left[\widetilde{P}^2_{n\kappa}(p) + \widetilde{Q}^2_{n\kappa}(p) \right] \tag{10.61}$$

is the probability density of the momentum of an electron in the $(n\kappa)$ shell, which is spherically symmetric.

The Compton profile of the $(n\kappa)$ shell is defined by

$$J_{n\kappa}(p_z) \equiv \int \rho_{n\kappa}(\mathbf{p})\, \mathrm{d}p_x\, \mathrm{d}p_y\,. \tag{10.62}$$

That is, $J(p_z)\,\mathrm{d}p_z$ represents the probability that the z-component of the electron's linear momentum $\mathbf{p}$ has a value between p_z and $p_z + \mathrm{d}p_z$. Since the averaged momentum distribution (10.61) is isotropic, we have

$$\begin{aligned} J_{n\kappa}(p_z) \;&\equiv\; \frac{1}{4\pi} \int \left[\widetilde{P}^2_{n\kappa}(p) + \widetilde{Q}^2_{n\kappa}(p) \right] \mathrm{d}p_x\, \mathrm{d}p_y \\ &=\; \frac{1}{2} \int_{|p_z|}^\infty \left[\widetilde{P}^2_{n\kappa}(p) + \widetilde{Q}^2_{n\kappa}(p) \right] p\,\mathrm{d}p, \qquad p \equiv \sqrt{p_x^2 + p_y^2 + p_z^2}. \end{aligned} \tag{10.63}$$

From its definition, it follows that the shell Compton profile is symmetric and normalised to unity,

$$J_{n\kappa}(p_z) = J_{n\kappa}(-p_z), \qquad \int_{-\infty}^\infty J_{n\kappa}(p_z)\, \mathrm{d}p_z = 1. \tag{10.64}$$

The total Compton profile $J(p_z)$ of the atom or ion is

$$J(p_z) \equiv \int \rho(\mathbf{p})\, \mathrm{d}p_x\, \mathrm{d}p_y = \sum_a q_a\, J_{n_a\kappa_a}(p_z), \tag{10.65}$$

i.e., $N^{-1}J(p_z)\,\mathrm{d}p_z$ is the average probability that the z-component of the linear momentum $\mathbf{p}$ of an orbiting electron has a value between p_z and $p_z + \mathrm{d}p_z$. Evidently,

$$\int_{-\infty}^\infty J(p_z)\, \mathrm{d}p_z = N. \tag{10.66}$$

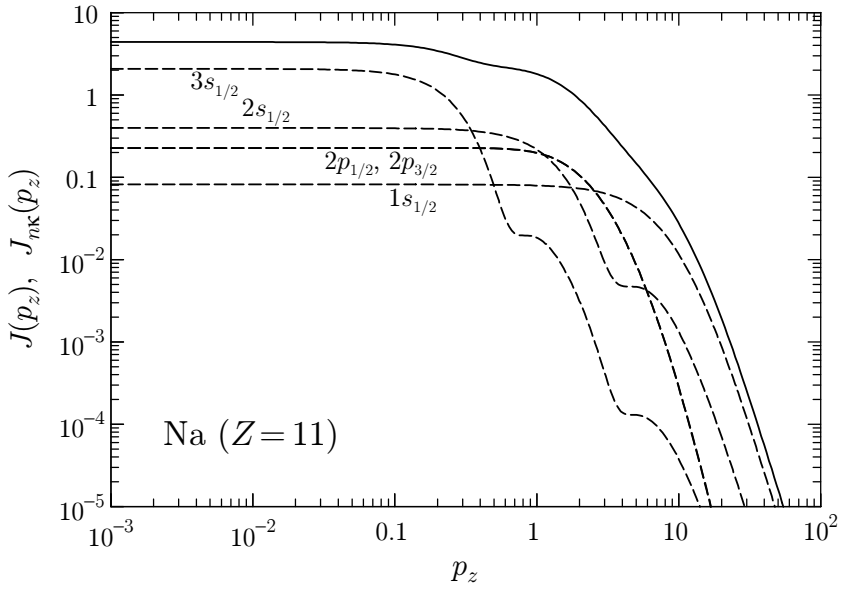

Figure 14: Total Compton profile $J(p_z)$ (solid curve) and shell profiles $J_{n\kappa}(p_z)$ (dashed curves) of the sodium atom, in atomic units, calculated by the `DHFS` code.

The program `DHFS` offers the option of evaluating the radial functions (10.59) and the Compton profiles for all the occupied shells. The calculation of Compton profiles is activated by the line `C8` of the input data file (see Table 3). The "radial" functions $\widetilde{P}_{n\kappa}(p)$ and $\widetilde{Q}_{n\kappa}(p)$ are computed from the definitions (10.59) by using cubic spline interpolation of the radial functions $P_{n\kappa}(r)$ and $Q_{n\kappa}(r)$ and the adaptive 20-point Gauss–Legendre quadrature function `SUMGA` (see the source file `DHFS.f`). Results from this calculation are printed in a file named `compton.dat`; the program also generates a gnuplot script named `Cprofiles.gnu` that plots the "radial" momentum wave functions and Compton profiles. Figure 14 displays the calculated total Compton profile $J(p_z)$ of Na ($Z = 11$) together with the various shell contributions $J_{n\kappa}(p_z)$.

11 Elastic scattering of electrons and positrons by atoms

The RADIAL subroutines allow the easy calculation of the differential cross section (DCS) for elastic collisions of electrons and positrons by atoms. By definition, elastic collisions are interactions that do not cause excitation of the target atom, which is assumed to be in its ground state. These collisions are usually described by means of the static-field approximation, *i.e.*, as scattering of the projectile by the electrostatic field of the target atom, suitably averaged over directions. The interaction is represented by a potential energy function $V(r)$ depending only on the distance r of the projectile to the atomic nucleus. The scattering DCS can then be calculated by the partial-wave expansion method, that is, from the asymptotic behaviour of the distorted plane waves (see Section 6.2) of the potential $V(r)$.

In this Section we consider the calculation of DCSs for scattering of high-energy electrons and positrons by neutral atoms of the element of atomic number Z using the non-relativistic (Schrödinger) and the relativistic (Dirac) partial-wave methods. For simplicity, the target atom is assumed to be fixed at the origin of coordinates. We also disregard the effects of electron exchange and of the dipole polarizability of the atom; these effects may be accounted for by introducing additional terms in the interaction potential (see, *e.g.*, Salvat, 2003) without altering the structure of the calculations.

11.1 Scattering potential

Within the static-field approximation, the interaction energy of a projectile electron or positron at $\mathbf{r}$ with the target atom is

$$V(r) = Z_1 e\, \varphi_{\rm es}(r)\,, \tag{11.1}$$

where $Z_1 e$ is the projectile charge, and $\varphi_{\rm es}(r)$ is the electrostatic potential of the atomic charge distribution,

$$\varphi_{\rm es}(r) = \varphi_{\rm nuc}(r) + \varphi_{\rm el}(r), \tag{11.2}$$

where

$$\varphi_{\rm nuc}(r) = e\left[\frac{1}{r}\int_0^r \rho_{\rm p}(r')\,4\pi r'^2\,{\rm d}r' + \int_r^\infty \rho_{\rm p}(r')\,4\pi r'\,{\rm d}r'\right] \tag{11.3}$$

and

$$\varphi_{\rm el}(r) = -e\left[\frac{1}{r}\int_0^r \rho(r')\,4\pi r'^2\,{\rm d}r' + \int_r^\infty \rho(r')\,4\pi r'\,{\rm d}r'\right] \tag{11.4}$$

are the contributions from the nucleus and of the atomic electron cloud. The quantities $\rho_{\rm p}(r)$ and $\rho(r)$ are the particle densities of protons in the nucleus and of atomic electrons, respectively.

If the nucleus is represented as a point charge, the electrostatic potential of the atom can be written as

$$\varphi_{\rm es}(r) = \frac{Ze}{r}\,\Phi(r), \tag{11.5}$$

where $\Phi(r)$ is the screening function, which describes the electrostatic shielding of the nuclear charge by the atomic electrons. This function equals unity at $r = 0$, where the projectile "sees" the full charge of the nucleus, and decreases monotonously with r, tending to zero at large radii, because the Z atomic electrons completely screen the nuclear charge.

In the program `electronscat` described below we can use the numerical potentials generated by the program `DHFS` (see Section 10), which correspond to the self-consistent DHFS atomic electron density for a point or finite nucleus. Alternatively, to allow rapid calculations for different atoms, we can also use approximate potentials expressed in the form (11.5) with screening functions of the type

$$\Phi(r) = \sum_{i=1}^{3} A_i \exp(-a_i r), \tag{11.6}$$

where A_i and a_i are parameters determined by fitting the numerical potentials obtained from various atomic models. In the calculations we consider the following sets of parameters:

• **Thomas–Fermi–Molière (TFM) screening function**
The Thomas–Fermi model yields a "universal" screening function for neutral atoms. Molière (1947) approximated the numerical Thomas–Fermi screening function by the expression (11.6) with the parameters

$$\begin{aligned} &A_1 = 0.10, \quad A_2 = 0.55, \quad A_3 = 0.35, \\ &a_1 = 6.0/b, \quad a_2 = 1.2/b, \quad a_3 = 0.3/b, \end{aligned} \tag{11.7}$$

where

$$b = 0.885\,34\, Z^{-1/3}\, a_0 \tag{11.8}$$

is a radial scale parameter known as the Thomas–Fermi radius. The values given by formula (11.6) with these parameters differ from the numerical Thomas–Fermi screening function in less than 0.002 in the region where the latter takes appreciable values ($r \lesssim 6b$).

• **Analytical Dirac–Hartree–Fock–Slater (DHFS) screening function**
The program `electronscat` implements the screening function (11.6) with the parameters given by Salvat *et al.* (1987) for the elements with $Z = 1$ to 99 (hydrogen to einsteinium), which were obtained by fitting the screening function of neutral atoms calculated from the DHFS self-consistent atomic electron densities (see Section 10).

11.2 Scattering amplitudes and cross sections

Let us consider the scattering of projectile electrons or positrons with kinetic energy E in the potential $V(r)$ of atoms of atomic number Z. Notice that the potential of neutral atoms is of finite range, *i.e.*, $\lim_{r\to\infty} rV(r) = 0$. The derivations that follow are valid only for potentials with finite ranges. The formulas can be extended to the case of potentials with a Coulomb tail by simply adding to the phase shifts $\delta_{E,\ell}$ or $\delta_{E,\kappa}$ the corresponding Coulomb phase shifts of the potential tail.

We assume that before the interaction the projectiles move in the direction of the z axis; after the interaction they emerge in directions defined by the polar and azimuthal angles, θ and ϕ, respectively. Because of the spherical symmetry of the potential, the scattering DCS per unit solid angle, $\mathrm{d}\sigma/\mathrm{d}\Omega$, is independent of the azimuthal angle ϕ.

11.2.1 Schrödinger theory

The DCS obtained from the non-relativistic Schrödinger theory is (Mott and Massey, 1965)

$$\frac{\mathrm{d}\sigma^{(\mathrm{S})}}{\mathrm{d}\Omega} = \left|f^{(\mathrm{S})}(\theta)\right|^2, \tag{11.9}$$

with the scattering amplitude $f^{(\mathrm{S})}(\theta)$ given by Eq. (6.25a). It is customary to introduce the scattering matrix elements

$$S_{E,\ell} \equiv \exp(2\mathrm{i}\delta_{E,\ell}) \tag{11.10}$$

and express the scattering amplitude as

$$f^{(\mathrm{S})}(\theta) = \frac{1}{2\mathrm{i}k} \sum_{\ell} (2\ell+1) \left[S_{E,\ell} - 1 \right] P_\ell(\cos\theta), \tag{11.11}$$

where $P_\ell(\cos\theta)$ are the Legendre polynomials. The total scattering cross section is

$$\sigma^{(\mathrm{S})} = \int \frac{\mathrm{d}\sigma^{(\mathrm{S})}}{\mathrm{d}\Omega}\, \mathrm{d}\Omega = 2\pi \int_{-1}^{1} \frac{\mathrm{d}\sigma^{(\mathrm{S})}}{\mathrm{d}\Omega}\, \mathrm{d}(\cos\theta) \tag{11.12}$$

and the transport cross section is

$$\sigma_{\mathrm{tr}}^{(\mathrm{S})} = \int (1-\cos\theta) \frac{\mathrm{d}\sigma^{(\mathrm{S})}}{\mathrm{d}\Omega}\, \mathrm{d}\Omega = 2\pi \int_{-1}^{1} (1-\cos\theta) \frac{\mathrm{d}\sigma^{(\mathrm{S})}}{\mathrm{d}\Omega}\, \mathrm{d}(\cos\theta). \tag{11.13}$$

• Integrals of three Legendre functions

The total cross section and the transport cross section can be expressed in the form of partial-wave series by using the integral properties of the associated Legendre functions. The integrals occurring in the calculations are given by the following general formula

$$\begin{aligned} \int_{-1}^{1} P_{\ell_2}^{m_2}(x)\, P_\ell^m(x)\, P_{\ell_1}^{m_1}(x)\, \mathrm{d}x = \\ = \frac{2}{2\ell_2+1} \sqrt{\frac{(\ell_2+m_2)!\,(\ell+m)!\,(\ell_1+m_1)!}{(\ell_2-m_2)!\,(\ell-m)!\,(\ell_1-m_1)!}} \\ \times \langle \ell\ell_1 00|\ell_2 0\rangle\, \langle \ell\ell_1 m m_1|\ell_2 m_2\rangle, \end{aligned} \tag{11.14}$$

which follows from the formula for the integral of three spherical harmonics (see, *e.g.*, Edmonds, 1960; Varshalovich *et al.*, 1988) and the relation between the associated Legendre functions $P_\ell^m(\cos\theta)$ and the spherical harmonics $Y_{\ell m}(\theta,\phi)$,

$$P_\ell^m(\cos\theta) = \sqrt{\frac{4\pi}{2\ell+1} \frac{(\ell+m)!}{(\ell-m)!}}\, \exp(-\mathrm{i}m\phi)\, Y_{\ell m}(\theta,\phi). \tag{11.15}$$

The present calculations involve integrals of the type (11.14) with $\ell = 0, 1$ and $m = 0$. Notice that $P_0^0(\cos\theta) = 1$ and $P_1^0(\cos\theta) = \cos\theta$. Introducing the analytical expressions of the Clebsch–Gordan coefficients (see, *e.g.*, Rose, 1995), we obtain

$$\int_{-1}^{1} P_\ell^m(x)\, P_{\ell'}^{m'}(x)\, \mathrm{d}x = \frac{2}{2\ell+1} \frac{(\ell+m)!}{(\ell-m)!}\, \delta_{\ell,\ell'}\, \delta_{m,m'}, \tag{11.16a}$$

$$\int_{-1}^{1} x\, P_\ell(x)\, P_{\ell'}(x)\, \mathrm{d}x = \begin{cases} \dfrac{2(\ell+1)}{(2\ell+1)(2\ell+3)} & \text{if } \ell' = \ell+1, \\ \dfrac{2\ell}{(2\ell-1)(2\ell+1)} & \text{if } \ell' = \ell-1, \end{cases} \tag{11.16b}$$

and

$$\int_{-1}^{1} x\, P^1_\ell(x)\, P^1_{\ell'}(x)\, \mathrm{d}x = \begin{cases} \dfrac{2\ell(\ell+1)(\ell+2)}{(2\ell+1)(2\ell+3)} & \text{if } \ell' = \ell+1, \\ \dfrac{2(\ell-1)\ell(\ell+1)}{(2\ell-1)(2\ell+1)} & \text{if } \ell' = \ell-1. \end{cases} \tag{11.16c}$$

Inserting the partial-wave expansion of the scattering amplitude, Eq. (11.11), performing the integrals over $\cos\theta$ by using the formulas (11.16), and after some algebra, we obtain the expansions,

$$\sigma^{(\mathrm{S})} = \frac{\pi}{k^2} \sum_\ell (2\ell+1) \left| 1 - S_{E,\ell} \right|^2 \tag{11.17}$$

and

$$\sigma^{(\mathrm{S})}_{\mathrm{tr}} = \frac{4\pi}{k^2} \sum_\ell (\ell+1)\, \sin^2(\delta_{E,\ell} - \delta_{E,\ell+1}). \tag{11.18}$$

The total cross section can also be obtained from the optical theorem, which expresses the conservation of the number of projectile particles (see, *e.g.*, Merzbacher, 1970). That is,

$$\sigma^{(\mathrm{S})} = \frac{4\pi}{k} \,\mathrm{Im}\left[f^{(\mathrm{S})}(\theta = 0) \right]. \tag{11.19}$$

11.2.2 Dirac theory

In the relativistic Dirac theory, the DCS for scattering of spin-unpolarised electrons or positrons is (Walker, 1971; Salvat *et al.*, 2005)

$$\frac{\mathrm{d}\sigma^{(\mathrm{D})}}{\mathrm{d}\Omega} = |f^{(\mathrm{D})}(\theta)|^2 + |g^{(\mathrm{D})}(\theta)|^2 \tag{11.20}$$

with the direct and spin-flip scattering amplitudes given by the partial-wave expansions (6.51). Introducing the scattering matrix elements

$$S_{E,\kappa} = \exp\left(2\mathrm{i}\delta_{E,\kappa}\right) \tag{11.21}$$

we express the scattering amplitudes as

$$f^{(\mathrm{D})}(\theta) \;=\; \frac{1}{2\mathrm{i}k} \sum_\ell \Big\{ (\ell+1) \Big[S_{E,-\ell-1} - 1 \Big] + \ell \Big[S_{E,\ell} - 1 \Big] \Big\}\, P_\ell(\cos\theta) \tag{11.22a}$$

and

$$g^{(\mathrm{D})}(\theta) \;=\; \frac{1}{2\mathrm{i}k}\sum_{\ell}\Big[S_{E,\ell}-S_{E,-\ell-1}\Big]\,P^{1}_{\ell}(\cos\theta), \tag{11.22b}$$

where $P_\ell(\cos\theta)$ and $P^1_\ell(\cos\theta)$ are the Legendre polynomials and the associated Legendre functions, respectively.

Particles scattered in directions with polar angle θ have their spin partially polarised. The degree of polarisation is given by the spin-polarisation function, also known as the Sherman function,

$$P(\theta) = \mathrm{i}\,\frac{f^{(\mathrm{D})}(\theta)\left[g^{(\mathrm{D})}(\theta)\right]^{*} - \left[f^{(\mathrm{D})}(\theta)\right]^{*} g^{(\mathrm{D})}(\theta)}{|f^{(\mathrm{D})}(\theta)|^2 + |g^{(\mathrm{D})}(\theta)|^2}\,. \tag{11.23}$$

The total scattering cross section is

$$\sigma^{(\mathrm{D})} = 2\pi\int_{-1}^{1}\frac{\mathrm{d}\sigma^{(\mathrm{D})}}{\mathrm{d}\Omega}\,\mathrm{d}(\cos\theta), \tag{11.24}$$

and the transport cross section is

$$\sigma^{(\mathrm{D})}_{\mathrm{tr}} = 2\pi\int_{-1}^{1}(1-\cos\theta)\,\frac{\mathrm{d}\sigma^{(\mathrm{D})}}{\mathrm{d}\Omega}\,\mathrm{d}(\cos\theta). \tag{11.25}$$

Inserting the partial-wave expansions of the scattering amplitudes, Eqs. (11.22), performing the integrals over $\cos\theta$ using the formulas (11.16), and after a good deal of algebra, we obtain the following partial-wave expansions,

$$\sigma^{(\mathrm{D})} \;=\; \frac{\pi}{k^2}\sum_{\ell}\left\{(\ell+1)\left|1-S_{E,-\ell-1}\right|^2 + \ell\left|1-S_{E,\ell}\right|^2\right\}, \tag{11.26}$$

and

$$\sigma^{(\mathrm{D})}_{\mathrm{tr}} = \frac{4\pi}{k^2}\sum_{\kappa}|\kappa|\left\{\frac{\kappa-1}{2\kappa-1}\,\sin^2(\delta_{E,\kappa}-\delta_{E,\kappa-1}) + \frac{1}{2(4\kappa^2-1)}\,\sin^2(\delta_{E,\kappa}-\delta_{E,-\kappa})\right\}. \tag{11.27}$$

Notice that the summation in the last expression runs over positive and negative values of κ. It is readily verified that the total cross section can also be obtained from the optical theorem, that is,

$$\sigma^{(\mathrm{D})} = \frac{4\pi}{k}\,\mathrm{Im}\left[f^{(\mathrm{D})}(\theta=0)\right]. \tag{11.28}$$

It is worth mentioning that the expansions derived from the Dirac theory are also valid for the scattering of non-relativistic electrons described by the Schrödinger–Pauli wave equation. The scattering amplitude and cross sections for a spinless particle are obtained from the above expansions by putting $\delta_{E,\kappa=-\ell-1} = \delta_{E,\kappa=\ell}$. Evidently, by the same substitution we obtain the familiar non-relativistic formulas (see the last Section).

11.3 The program `electronscat`

The phase shifts $\delta_{E,\ell}$ and $\delta_{E,\kappa}$ are determined by the asymptotic behaviour of the radial functions with the corresponding angular momenta, and they can be calculated by using the subroutines `SFREE` and `DFREE` of the RADIAL package. With these numerical phase shifts, the scattering amplitudes can be evaluated very accurately, provided only their partial-wave series converge sufficiently fast.

The program `electronscat` calculates scattering amplitudes and DCSs for elastic collisions of electrons and positrons by atoms, using either the TFM or DHFS analytical potentials or the numerical DHFS potential (which may be generated by running the program `DHFS`). The program computes the phase shifts numerically from the solution of the corresponding radial wave equation, up to an angular momentum such that phase shifts with higher ℓ or $|\kappa|$ are less than 10^{-9} in magnitude. To reduce the calculation time, phase shifts of waves with ℓ or $|\kappa|$ higher than about 100 are computed from the solution of the radial equation only for a sparse grid of angular momenta; the phase shifts with angular momenta not included in this grid are obtained by lin-log cubic spline interpolation. With this simplification, `electronscat` allows considering phase shifts of partial waves with angular momentum ℓ or $|\kappa|$ up to 25,000, and it can effectively compute collisions of projectiles with energies up to about 5 MeV. For higher energies, depending on the atomic number of the target atom, the RADIAL subroutines are not able to calculate phase shifts with very large angular momenta because of accumulated round-off errors.

At least for scattering angles that are not too small, the convergence of the partial-wave series can be accelerated by applying the "reduced series" method described by Yennie *et al.* (1954), which is based on the fact that, if a function $f(\theta)$ is strongly peaked at $\theta = 0$, the function $(1 - \cos\theta) f(\theta)$ is smoother than $f(\theta)$, and hence its Legendre expansion may be more rapidly convergent. Explicitly, to sum up a series of the form

$$f(\theta) = \sum_{\ell=0}^{\infty} \mathcal{F}_\ell^0 \, P_\ell(\cos\theta) \tag{11.29}$$

that is weakly convergent (*i.e.*, $\mathcal{F}_\ell^0$ decreases slowly with ℓ for large ℓ), we consider the transformed series

$$\hat{f}(\theta) = (1 - \cos\theta)^n \, f(\theta) = \sum_{\ell=0}^{\infty} \mathcal{F}_\ell^n \, P_\ell(\cos\theta) \tag{11.30}$$

and compute $f(\theta)$ as $(1 - \cos\theta)^{-n} \hat{f}(\theta)$. The coefficients $\mathcal{F}_\ell^n$ are given by

$$\mathcal{F}_\ell^n = \mathcal{F}_\ell^{n-1} - \frac{\ell + 1}{2\ell + 3} \mathcal{F}_{\ell+1}^{n-1} - \frac{\ell}{2\ell - 1} \mathcal{F}_{\ell-1}^{n-1} \tag{11.31}$$

and, for large ℓ, they decrease more rapidly with ℓ than the coefficients $\mathcal{F}_\ell^0$ of the original series. It can be shown that if $\mathcal{F}_\ell^n \approx \mathcal{O}(\ell^b)$, then $\mathcal{F}_\ell^{n+1} \approx \mathcal{O}(\ell^{b-2})$. In the case of a series in associated Legendre functions such as $g^{(\mathrm{D})}(\theta)$,

$$g(\theta) = \sum_{\ell=0}^{\infty} \mathcal{G}_\ell^0 \, P_\ell^1(\cos\theta), \tag{11.32}$$

the transformed series is

$$\hat{g}(\theta) = (1 - \cos\theta)^n \, g(\theta) = \sum_{\ell=0}^{\infty} \mathcal{G}_\ell^n \, P_\ell^1(\cos\theta) \tag{11.33}$$

with

$$\mathcal{G}_\ell^n = \mathcal{G}_\ell^{n-1} - \frac{\ell+2}{2\ell+3}\,\mathcal{G}_{\ell+1}^{n-1} - \frac{\ell-1}{2\ell-1}\,\mathcal{G}_{\ell-1}^{n-1}. \tag{11.34}$$

For large ℓ, $\mathcal{G}_\ell^n$ decreases more rapidly with ℓ than the coefficients $\mathcal{G}_\ell^0$. Again, if $\mathcal{G}_\ell^n \approx \mathcal{O}(\ell^b)$, then $\mathcal{G}_\ell^{n+1} \approx \mathcal{O}(\ell^{b-2})$. Of course, the reduced-series method cannot be used when $\theta \approx 0$. In the program `electronscat` the reduced series method is applied with $n = 2$ for angles θ larger than 1 degree, whenever the number of calculated phase shifts is larger than 200.

The program `electronscat` does the calculation for both the Schrödinger and Dirac equations, and it generates respective output files, named `sdcs.dat` and `ddcs.dat`, that contain tables of DCSs from the two calculations for a predefined grid of ~ 600 scattering angles, which is densely spaced to allow accurate spline interpolation of the DCS. The output files also include the corresponding values of the total cross section,

$$\sigma = 2\pi \int_{-1}^{1} \frac{\mathrm{d}\sigma}{\mathrm{d}\Omega}\,\mathrm{d}(\cos\theta) \tag{11.35}$$

and the transport cross section,

$$\sigma_{\mathrm{tr}} = 2\pi \int_{-1}^{1} (1 - \cos\theta)\,\frac{\mathrm{d}\sigma}{\mathrm{d}\Omega}\,\mathrm{d}(\cos\theta). \tag{11.36}$$

These integrals are computed from the natural cubic splines that interpolate the DCSs. The quantities σ and σ_{tr} are also evaluated by summing the partial-wave series derived above; comparison of the values obtained in this way with the results of integrating the splines serves to assess the accuracy of the spline interpolations. `electronscat` also produces the output files `spwa.dat` and `dpwa.dat` which contain the lists of calculated Schrödinger and Dirac phase shifts, and tables of the scattering amplitudes for the same scattering angles where the DCSs are tabulated. The program also produces a file named `potential.dat` which contains the table of the potential function $rV(r)$ that is effectively passed to the RADIAL subroutines. Notice that the output files are overwritten at each run of the program.

The distribution package contains the gnuplot scripts `potential.gnu` and `dcs.gnu`. The former displays the scattering potential used by `electronscat`, while the latter shows the DCSs obtained from the Schrödinger and Dirac equations *for the same potential*. Comparison of these two DCSs reveals the net effect of relativity and spin on the DCS. Example results, for scattering of 500 eV electrons and positrons by the analytical DHFS potential of gold atoms ($Z = 79$), are displayed in Fig. 15. Notice that the potentials for electrons and positrons have equal magnitudes and opposite signs; electrons (positrons) are attracted towards (repelled from) the nucleus. Differences between the Schrödinger and Dirac DCSs for positrons are seen to be much less than for electrons.

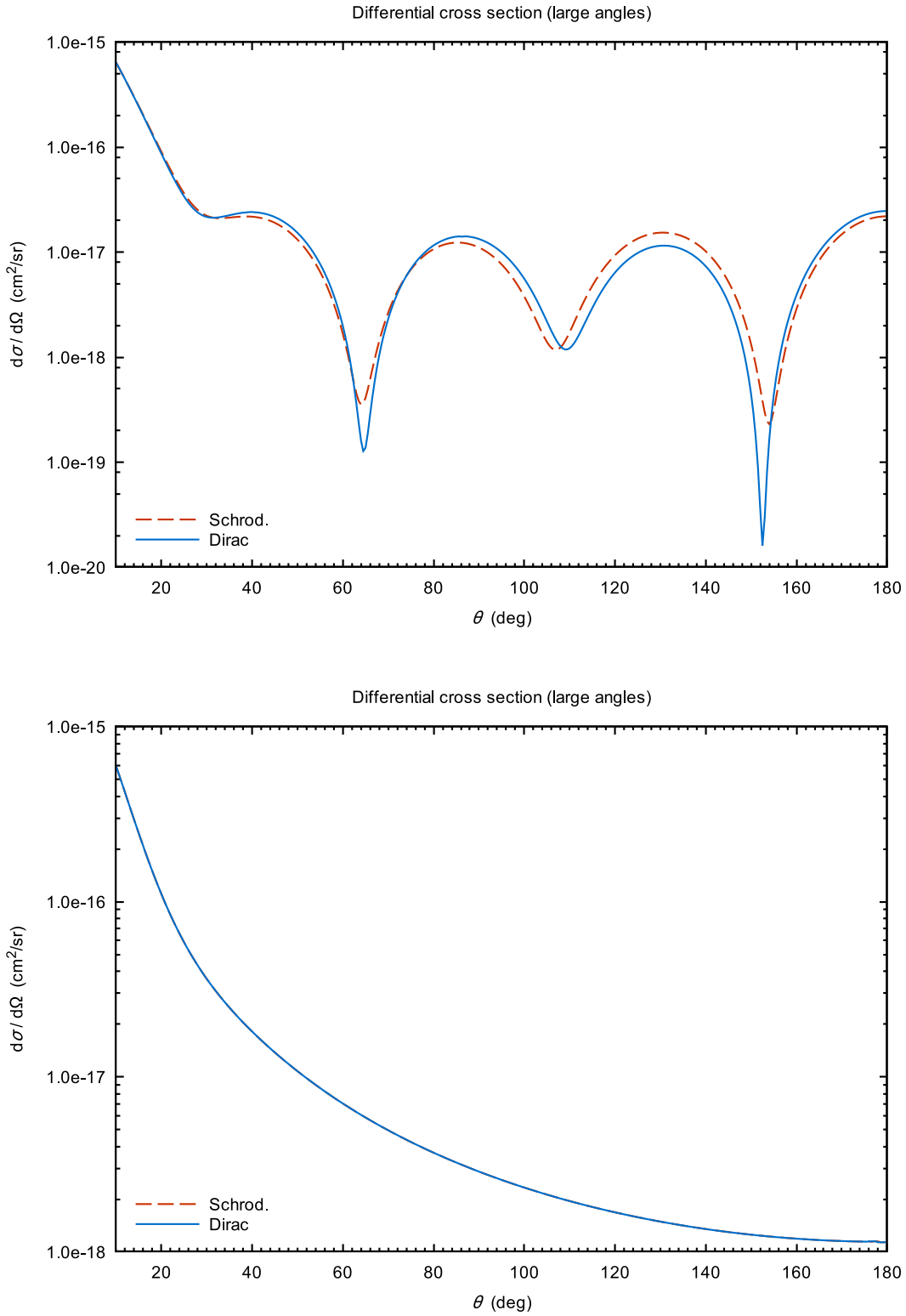

Figure 15: Examples of results from the program `electronscat`. DCSs for scattering of 500 eV electrons (top) and positrons (bottom) in the analytical DHFS potential of gold atoms ($Z = 79$). The plots were generated with the gnuplot script `dcs.gnu`.

12 Elastic collisions of nucleons with nuclei

In this Section we consider the calculation of elastic collisions of neutrons and protons with nuclei of atomic number Z and mass number A. A fairly realistic description of these collisions is obtained by using the partial-wave expansion method (see Section 6.2) with a phenomenological complex optical-model potential (op),

$$V_{\rm op}(r) = V(r) + {\rm i}W(r), \tag{12.1}$$

where $V(r)$ is a real potential and ${\rm i}W(r)$ is an absorptive (negative) imaginary potential, that accounts for the loss of projectile particles from the elastic channel caused by inelastic processes. The imaginary part of the potential has a finite range, and at large radii $V_{\rm op}(r)$ reduces to the Coulomb tail,

$$\lim_{r\to\infty} rV_{\rm op}(r) = Z_0 Z e^2, \tag{12.2}$$

where $Z_0 e$ is the charge of the projectile.

Parameterisations of optical-model potentials have been proposed by various authors (*e.g.*, Becchetti and Greenlees, 1969; Hodgson, 1971). They are generally written as a combination of Woods–Saxon volume terms,

$$f(R,a;r) = \frac{1}{1+\exp[(r-R)/a]}\,, \tag{12.3}$$

and surface derivative (d) terms,

$$\begin{aligned} g(R,a;r) \;&=\; \frac{\rm d}{{\rm d}r}\, f(R,a;r) = -\frac{1}{a}\,\frac{\exp[(r-R)/a]}{\{1+\exp[(r-R)/a]\}^2} \\ &=\; \frac{1}{a}\, f(R,a;r)\,[f(R,a;r)-1]\,. \end{aligned} \tag{12.4}$$

The parameters in these functions are the radius R and the diffuseness a; typically, the radius is expressed as $R = r_0 A^{1/3}$. We consider a generic potential having the form

$$\begin{aligned} V_{\rm op}(E;r) \;=\; & V_{\rm v}(E;r) + V_{\rm d}(E;r) + V_{\rm c}(r) + V_{\rm so}(E;r)\,2\,\mathbf{L}\cdot\mathbf{S}_{\rm P} \\ & + {\rm i}\left[W_{\rm v}(E;r) + W_{\rm d}(E;r) + W_{\rm so}(E;r)\,2\,\mathbf{L}\cdot\mathbf{S}_{\rm P}\right] \end{aligned} \tag{12.5}$$

with the following terms:

1) Real volume (v) potential:

$$V_{\rm v}(E;r) = V_{\rm v}(E)\, f(R_{\rm v}, a_{\rm v}; r). \tag{12.6a}$$

2) Real surface (d) potential:

$$V_{\rm d}(E;r) = V_{\rm d}(E)\, 4a_{\rm d}\, g(R_{\rm d}, a_{\rm d}; r). \tag{12.6b}$$

3) Coulomb (c) potential:

$$V_{\rm c}(r) = Z_0 Z e^2 \begin{cases} \dfrac{1}{2R_{\rm c}}\left(3 - \dfrac{r^2}{R_{\rm c}^2}\right) & \text{if } r < R_{\rm c}, \\ \dfrac{1}{r} & \text{if } r \geq R_{\rm c}. \end{cases} \tag{12.6c}$$

4) Real spin-orbit (so) potential:

$$V_{\rm so}(E;r) = V_{\rm so}(E)\,\frac{1}{r}\,g(R_{\rm so}, a_{\rm so}; r). \tag{12.6d}$$

5) Imaginary volume (w) potential:

$$W_{\rm v}(E;r) = W_{\rm v}(E)\,f(R_{\rm w}, a_{\rm w}; r). \tag{12.6e}$$

6) Imaginary surface (wd) potential:

$$W_{\rm d}(E;r) = W_{\rm d}(E)\,4a_{\rm wd}\,g(R_{\rm wd}, a_{\rm wd}; r). \tag{12.6f}$$

7) Imaginary spin-orbit (wso) potential:

$$W_{\rm so}(E;r) = W_{\rm so}(E)\,\frac{1}{r}\,g(R_{\rm wso}, a_{\rm wso}; r). \tag{12.6g}$$

The operators $\mathbf{L}$ and $\mathbf{S}_{\rm P}$ are the orbital and spin angular momenta (both in units of $\hbar$), respectively. We have indicated explicitly that the strengths of the potential terms are generally functions of the kinetic energy E of the projectile in the reference frame of the laboratory, where the target nucleus is at rest.

It should be noted that, since the mass of the projectile may be appreciable in comparison with that of the target, the collision has to be described as a two-body process. The scattering observables are then determined by the asymptotic behaviour of the distorted plane wave (DPW) that represents the relative motion of the projectile and the target nucleus *in the centre-of-mass* (CM) *frame*. Due to the spin-orbit term in the optical-model potential, that DPW satisfies a wave equation having the form of the Schrödinger–Pauli equation (see Section 2.3),

$$\left[-\frac{\hbar^2}{2\mu}\,\nabla^2 + V_{\rm op}(E;r)\right]\psi^{(+)}_{\mathbf{k},i}(\mathbf{r}) = \frac{p^2}{2\mu}\,\psi^{(+)}_{\mathbf{k},i}(\mathbf{r}), \tag{12.7}$$

where μ is the reduced mass and p is the linear momentum in the CM frame. Since we may consider projectiles with kinetic energies that are not negligible in front of their rest energies, we use the relativistic expressions of these quantities. That is, the linear momentum in CM is given by

$$p = M(Z,A)c\,\sqrt{\frac{E(E+2mc^2)}{\left[mc^2 + M(Z,A)c^2\right]^2 + 2M(Z,A)c^2\,E}}, \tag{12.8}$$

where m and $M(Z,A)$ are the rest masses of the projectile and the target atom, respectively. The relativistic reduced mass is

$$\mu = c^{-1}\,\frac{\sqrt{m^2c^2+p^2}\,\sqrt{M^2(Z,A)c^2+p^2}}{\sqrt{m^2c^2+p^2}+\sqrt{M^2(Z,A)c^2+p^2}}. \tag{12.9}$$

In spite of the non-relativistic appearance of Eq. (12.7), when p and μ are replaced with the relativistic forms of the linear momentum and the reduced mass the resulting equation incorporates the main relativistic kinematical effects. It can be shown that Eq. (12.7) describes the relative motion of the colliding particles under the assumptions that 1) the potential $V_{\rm op}(E;r)$ represents their interaction in the CM frame and 2) $|V_{\rm op}(E;r)| \ll 2\mu c^2$. Because of the Lorentz–FitzGerald contraction, assumption 1) holds only when the speed of the projectile in the laboratory frame is much less than c.

In most practical circumstances the target nucleus is in a neutral atom, that is, dressed with the atomic electron cloud, although electronic screening is neglected in the present calculations of proton collisions (see below). Hence, $M(Z,A)$ represents the atomic mass, which we estimate by means of the mass formula (Royer and Gautier, 2006)

$$M(Z,A)c^2 = Zm_{\rm p}c^2 + Nm_{\rm n}c^2 - B_{\rm nuc} + Z{\rm m}_{\rm e}c^2 - B_{\rm e}, \tag{12.10}$$

where $m_{\rm n}$ and $m_{\rm p}$ are the masses of the neutron and the proton, respectively, $N = A-Z$ is the number of neutrons in the nucleus, $B_{\rm nuc}$ is the nuclear binding energy and $B_{\rm e}$ is the total binding energy of the Z atomic electrons. These binding energies are approximated by the following empirical expressions, which were determined from fits to available calculated or measured data,

$$B_{\rm e} = (14.4381\ {\rm eV})\,Z^{2.39} + (1.55468\times10^{-6}\ {\rm eV})\,Z^{5.35}, \tag{12.11}$$

and

$$\begin{aligned} B_{\rm nuc} = {} & (15.7335\times10^{6}\ {\rm eV})\left(1-1.6949\,I^2\right)A - (17.8048\times10^{6}\ {\rm eV})\left(1-1.0884\,I^2\right)A^{2/3} \\ & - \frac{3}{5}\,\frac{Z^2e^2}{R_0} + E_{\rm pair}, \end{aligned} \tag{12.12}$$

where $I = (N-Z)/A$ is the charge asymmetry parameter, $R_0 = 1.2181\,A^{1/3}$ fm, and

$$E_{\rm pair} = \begin{cases} -(11\times10^{6}\ {\rm eV})\,A^{-1/2} & \text{for nuclei with odd } Z \text{ and odd } N, \\ 0 & \text{for nuclei with odd } A, \\ (11\times10^{6}\ {\rm eV})\,A^{-1/2} & \text{for nuclei with even } Z \text{ and even } N. \end{cases} \tag{12.13}$$

The formula (12.10) approximates the experimental atomic masses of naturally occurring isotopes (Coursey *et al.*, 2015) with a relative accuracy better than about 10^{-4}, which is sufficient for the present purposes.

The potentials and kinematical parameters passed to the RADIAL subroutines must be given in generalised atomic units (defined by setting $\hbar = e = \mu = 1$); the units of

length and energy are $a_\mu = (\mathrm{m_e}/\mu)a_0$ and $E_\mu = (\mu/\mathrm{m_e})E_\mathrm{h}$, respectively [cf. Eqs. (2.1) and (2.2)]. The calculated wave functions are also expressed in these units.

Scattering observables are obtained from the asymptotic form of the DPW [cf. Eq. (6.53)]

$$\psi^{(+)}_{\mathbf{k},i}(\mathbf{r}) = \frac{1}{kr}\sqrt{\frac{2}{\pi}}\sum_{\ell=0}^{\infty}\sum_{j=\ell\pm1/2}\sum_{m=-j}^{j}\mathrm{i}^\ell\,\exp\left(\mathrm{i}d_{\ell j}\right)\,P_{\ell j}(r)\,\left\{\left[\Omega^\ell_{jm}(\hat{\mathbf{k}})\right]^\dagger\chi_i\right\}\Omega^\ell_{jm}(\hat{\mathbf{r}}), \tag{12.14}$$

where $\mathbf{k} = p/\hbar$ is the CM wave vector before the interaction, $\Omega^\ell_{jm}(\hat{\mathbf{r}})$ are the spherical spinors, and the radial functions $P_{E\ell j}(r)$ satisfy the radial wave equation

$$-\frac{\hbar^2}{2\mu}\frac{\mathrm{d}^2}{\mathrm{d}r^2}P_{\ell j}(r) + \left[V_{\ell j}(r) + \frac{\hbar^2}{2\mu}\frac{\ell(\ell+1)}{r^2}\right]P_{\ell j}(r) = \frac{p^2}{2\mu}P_{\ell j}(r) \tag{12.15}$$

with

$$\begin{aligned} V_{\ell j}(r) \;=\; & V_\mathrm{v}(E;r) + V_\mathrm{d}(E;r) + V_\mathrm{c}(r) + \mathrm{i}\,[W_\mathrm{v}(E;r) + W_\mathrm{d}(E;r)] \\ & + [V_\mathrm{so}(E;r) + \mathrm{i}\;W_\mathrm{so}(E;r)]\,\frac{1}{2}\left[j(j+1) - \ell(\ell+1) - \tfrac{1}{2}\left(\tfrac{1}{2}+1\right)\right]. \end{aligned} \tag{12.16}$$

The radial functions are normalised so that

$$P_{\ell j}(r) \underset{r\to\infty}{\sim} \sin\left(kr - \ell\frac{\pi}{2} - \eta\ln(2kr) + d_{\ell j}\right), \tag{12.17}$$

where

$$\eta = \frac{Z_0 Z e^2 \mu}{\hbar^2 k} \tag{12.18}$$

is the Sommerfeld parameter, and $d_{\ell j} = \Delta_\ell + \delta_{E,\ell,j}$ is the total phase shift, *i.e.*, the sum of the Schrödinger–Coulomb phase shift Δ_ℓ [Eq. (3.21)] and the complex "inner" phase shift $\delta_{E,\ell,j}$ caused by the finite-range component of the potential. Hereafter, the inner phase shifts are denoted by the abridged notation $\delta_{E\ell a}$ with $a = 2(j-\ell)$, *i.e.*, $\delta_{E,\ell,+} \equiv \delta_{E,\ell,j=\ell+1/2}$ and $\delta_{E,\ell,-} \equiv \delta_{E,\ell,j=\ell-1/2}$.

Assuming that the projectile moves in the direction of the positive z axis before the collision, the DPW has the familiar asymptotic form [see Eq. (6.56)]. The direct and spin-flip scattering amplitudes are given by the partial-wave expansions (6.58). It is customary to introduce the quantities

$$S_{E,\ell,a} = \exp(2\mathrm{i}\delta_{E,\ell,a}), \tag{12.19}$$

which are the nuclear parts of the S-matrix elements, and write the expansions (6.58) in the form

$$\begin{aligned} f(\theta) \;=\; & f^{(\mathrm{c})}(\theta) + \frac{1}{2\mathrm{i}k}\sum_\ell \exp(2\mathrm{i}\Delta_\ell)\left\{(\ell+1)\left[S_{E,\ell,+}-1\right]\right. \\ & \left. + \ell\left[S_{E,\ell,-}-1\right]\right\}\,P_\ell(\cos\theta) \end{aligned} \tag{12.20a}$$

and

$$g(\theta) = \frac{1}{2\mathrm{i}k} \sum_{\ell} \exp(2\mathrm{i}\Delta_\ell) \left[S_{E,\ell,-} - S_{E,\ell,+} \right] \, P_\ell^1(\cos\theta), \tag{12.20b}$$

where

$$f^{(\mathrm{c})}(\theta) = -\eta \, \frac{\exp\{2\mathrm{i}\Delta_0 - \mathrm{i}\eta \ln[\sin^2(\theta/2)]\}}{2k \sin^2(\theta/2)} \tag{12.21}$$

is the Coulomb scattering amplitude, Eq. (6.32).

For spin-unpolarised projectiles, the elastic DCS per unit solid angle in the CM frame is given by

$$\frac{\mathrm{d}\sigma_{\mathrm{CM}}}{\mathrm{d}\Omega} = |f(\theta)|^2 + |g(\theta)|^2 \, . \tag{12.22}$$

The total elastic cross section is

$$\sigma_{\mathrm{CM}} = \int \frac{\mathrm{d}\sigma_{\mathrm{CM}}}{\mathrm{d}\Omega} \, \mathrm{d}\Omega = 2\pi \int_{-1}^{1} \frac{\mathrm{d}\sigma_{\mathrm{CM}}}{\mathrm{d}\Omega} \, \mathrm{d}(\cos\theta). \tag{12.23}$$

In the case of proton collisions, the DCS diverges at $\theta = 0$ and the total elastic cross section is infinite because of the infinite range of the Coulomb interaction. The origin of this spurious divergence is the neglect of the screening of the nuclear charge by the atomic electrons, which reduces the range of the electrostatic interaction to a finite value. For projectile neutrons, the Coulomb interaction vanishes, so that $f^{(\mathrm{c})}(\theta) = 0$ and $\Delta_\ell = 0$, and the total elastic cross section is finite. It is then reasonable to consider the "nuclear" elastic DCS, defined by subtracting the Coulomb scattering amplitude from the direct amplitude, that is,

$$\frac{\mathrm{d}\sigma_{\mathrm{CM}}^{\mathrm{nucl}}}{\mathrm{d}\Omega} = \left| f(\theta) - f^{(\mathrm{c})}(\theta) \right|^2 + |g(\theta)|^2 \, . \tag{12.24}$$

Evidently, for neutrons this is the usual (shape) elastic DCS. In the case of protons, the nuclear elastic DCS is finite for all angles. Using the properties of the Legendre functions we obtain the following partial-wave expansion of the integrated nuclear DCS,

$$\begin{aligned} \sigma_{\mathrm{CM}}^{\mathrm{nucl}} &= 2\pi \int_{-1}^{1} \frac{\mathrm{d}\sigma_{\mathrm{CM}}^{\mathrm{nucl}}}{\mathrm{d}\Omega} \, \mathrm{d}(\cos\theta) \\ &= \frac{\pi}{k^2} \sum_{\ell} \left\{ (\ell+1) \left| 1 - S_{E,\ell,+} \right|^2 + \ell \left| 1 - S_{E,\ell,-} \right|^2 \right\} . \end{aligned} \tag{12.25}$$

Because in proton collisions the effect of nuclear interactions is limited to relatively large scattering angles, it is customary to display the measured and calculated proton data as the ratio of the DCS to the Rutherford DCS,

$$\frac{\mathrm{d}\sigma_{\mathrm{R}}}{\mathrm{d}\Omega} = \left| f^{(\mathrm{c})}(\theta) \right|^2 = \frac{\eta^2}{4k^2 \sin^4(\theta/2)}. \tag{12.26}$$

As expected, the ratio $\mathrm{d}\sigma_{\mathrm{CM}}/\mathrm{d}\sigma_{\mathrm{R}}$ equals unity at $\theta = 0$.

The loss of projectile particles from the elastic channel is related to the reaction cross section, *i.e.*, the total cross section for inelastic interactions, given by

$$\sigma_{\rm react} = \frac{\pi}{k^2}\sum_{\ell}\Big\{(\ell+1)\left[1-|S_{E,\ell,+}|^2\right]+\ell\left[1-|S_{E,\ell,-}|^2\right]\Big\}\,. \tag{12.27}$$

The quantities $T_{E,\ell a}=1-|S_{E,\ell a}|^2$, the so-called transmission coefficients, measure the fraction of flux lost from each partial wave. In the case of neutrons, the total cross section

$$\sigma_{\rm T} = \sigma_{\rm CM} + \sigma_{\rm react} \tag{12.28}$$

can be obtained from the optical theorem (see, *e.g.*, Schiff, 1968) as

$$\sigma_{\rm T} = \frac{4\pi}{k}\,{\rm Im}\,f(0). \tag{12.29}$$

Elastic collisions cause the spin polarisation of initially unpolarised particles. The degree of polarisation of projectiles scattered in the direction θ is given by the spin polarisation function

$$P(\theta) = {\rm i}\,\frac{f(\theta)g^*(\theta)-f^*(\theta)g(\theta)}{|f(\theta)|^2+|g(\theta)|^2}\,. \tag{12.30}$$

It is worth noticing that the optical-model potential (12.5) represents the interaction of the projectile with the bare target nucleus. The results from the present partial-wave calculations provide a realistic description of collisions of neutrons with atoms. In the case of proton collisions, however, it is very difficult to account for the screening of the nuclear charge by the atomic electrons within a partial-wave calculation. The practical difficulty of including screening effects arises from the fact that the proton wavelength,

$$\lambda_{\rm dB} = \frac{2\pi}{k} = \frac{2\pi c\hbar}{\sqrt{E(E+2mc^2)}}, \tag{12.31}$$

is much smaller than the range of the screened atomic potential. For example, in collisions of 10 MeV protons with Au atoms $\lambda_{\rm dB} = 1.7\times10^{-4}\,a_0$ and to determine each phase shift we would have to extend the outward solution of the radial equation up to a matching radius of the order of $4a_0$; along this distance the radial function has about 23,500 oscillations! Electronic screening has an effect only for relatively small angles and can be introduced as a correction [based, *e.g.*, on the eikonal approximation Salvat (2013)] to the DCS calculated for the bare nucleus.

12.1 The program `nucleonscat`

The program `nucleonscat` computes scattering amplitudes and DCSs for elastic collisions of neutrons and protons with nuclei. The source file contains subroutines that provide the parameters of the global optical-model potential of Koning and Delaroche (2003), and the atomic masses $M(A,Z)$ obtained from the empirical mass formula (12.10). The adopted potential is adequate for neutrons and protons with kinetic energies from 1 keV to 200 MeV. For projectiles with higher energies, the potential is

assumed to be independent of energy (*i.e.*, it is calculated for $E = 200$ MeV). The program computes all the phase shifts numerically from the solution of the corresponding radial wave equation, up to an angular momentum such that phase shifts with higher ℓ are less than 10^{-9} in magnitude. In the summation of the partial-wave series, the reduced-series method (see Section 11.3) is applied with $n = 2$ for angles θ larger than 1 degree, whenever the number of calculated phase shifts is larger than 200. `nucleonscat` can effectively compute collisions of projectiles with energies up to about 1 GeV, well beyond the range of validity of the potential. Notice that results at these high energies are not expected to be realistic owing to the lack of spherical symmetry of the interaction in the CM frame. At higher energies, the RADIAL subroutines have difficulties to calculate phase shifts with very large angular momenta because of accumulated round-off errors.

`nucleonscat` calculates the phase shifts $\delta_{E,\ell,a}$ and the scattering amplitudes and the DCS for a predefined grid of ~ 1200 scattering angles, which is densely spaced to allow accurate spline interpolation of the DCS. The table of the potential function $rV_{\rm op}(r)$ that is effectively passed to the RADIAL subroutines is written in an output file named `voptical.dat`. The program generates an output file named `ndcs.dat` that contains the DCS table, the total nuclear cross section and the reaction cross section, Eqs. (12.25) and (12.27). The total nuclear cross section $\sigma_{\rm CM}^{\rm nucl}$ is calculated by summing up its partial-wave series (12.25) and also by integrating the spline that interpolates the DCS table. The agreement between the values calculated with these two methods serves to verify the adequacy of the adopted angular grid and the accuracy of the spline interpolation. In addition, `nucleonscat` produces an output file named `npwa.dat` that contains the list of calculated phase shifts, and a table of the scattering amplitudes for the same scattering angles where the DCSs is tabulated. Notice that the output files are overwritten at each new run of the program.

The distribution package contains the gnuplot scripts `voptical.gnu` and `ndcs.gnu`. The former displays the complex optical-model potential used by `nucleonscat`, while the latter shows the calculated DCS. Example results for scattering of 40 MeV protons by ^{90}Zr ($Z = 40$, $A = 90$) nuclei are shown in Fig. 16.

Acknowledgements

We are thankful to Dr D. Bote for helping to improve the RADIAL subroutines to meet the needs of calculations of inelastic electron-atom collisions. We are also indebted to Prof. A. Stauffer for identifying and correcting a bug in the subroutine `FCOUL`, and to Prof. J. Piekarewicz for his advice on the Levinson theorem for the Dirac equation. Dr F. Salvat-Pujol kindly provided useful comments, found a bug in the subroutine `SBESJN`, and helped to improve the robustness of the program. Financial support from the Spanish Ministerio de Economía y Competitividad and ERDF (projects nos. FPA2013-44549-P and FPA2016-77689-C2-2-R) and from the Generalitat de Catalunya (grant 2014 SGR 846) is gratefully acknowledged.

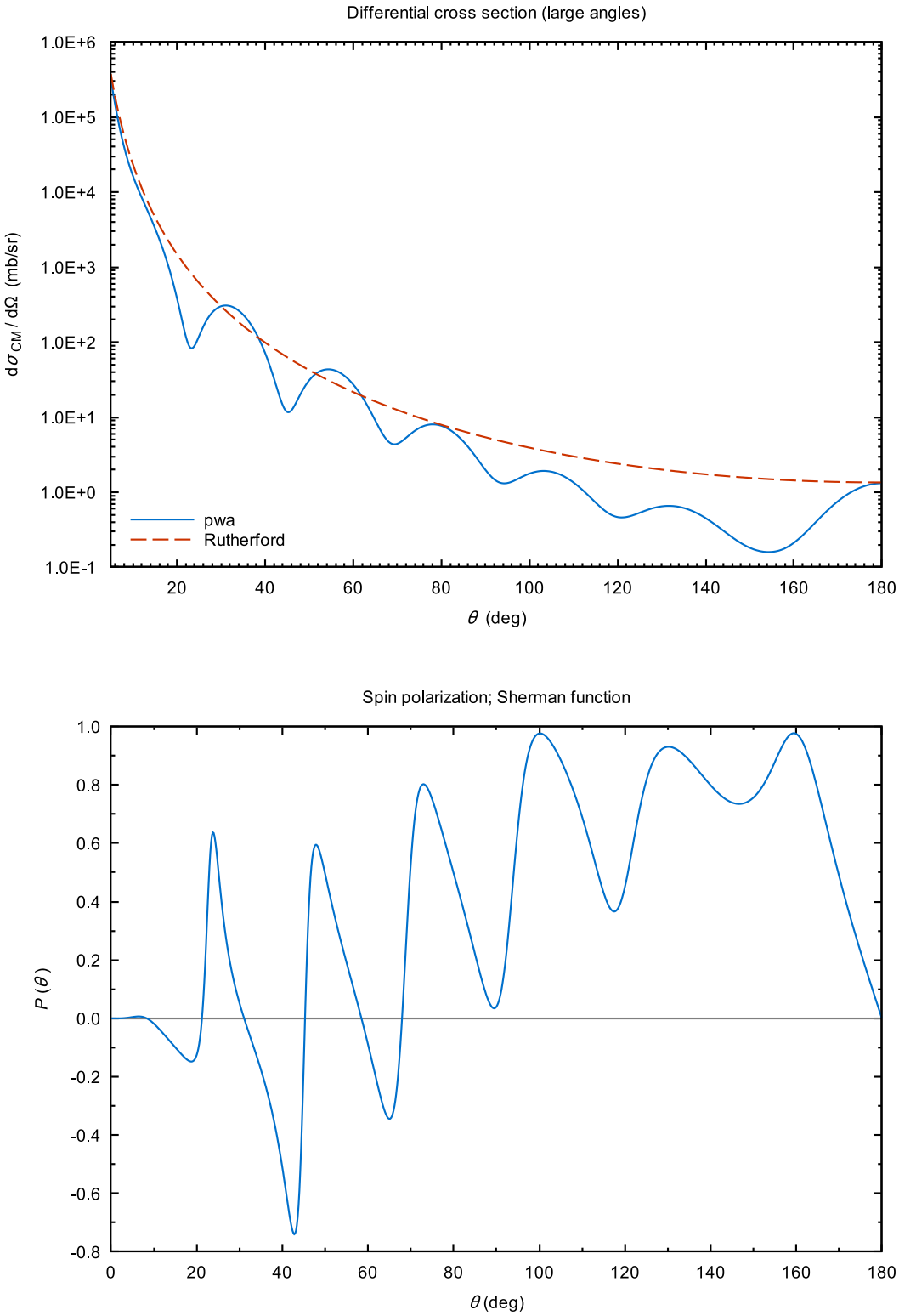

Figure 16: Examples of results from the program `nucleonscat` for elastic collisions of 40 MeV protons with ^{90}Zr ($Z = 40$, $A = 90$) nuclei. In the upper plot, the solid and dashed curves represent, respectively, the partial-wave (pwa) and Rutherford DCSs. The lower plot displays the spin polarisation function. These plots were generated with the gnuplot script `ndcs.gnu`.

A Cubic spline interpolation

In this Appendix we follow the presentation of Maron (1982). Suppose that a function $f(x)$ is given in numerical form, *i.e.*, as a table of values

$$f_i = f(x_i) \qquad (i = 1, \ldots, N). \tag{A.1}$$

The points (knots) x_i do not need to be equispaced, but we assume that they are in (strictly) increasing order

$$x_1 < x_2 < \cdots < x_N. \tag{A.2}$$

A function $\varphi(x)$ is said to be an interpolating cubic spline if
1) It reduces to a cubic polynomial within each interval $[x_i,x_{i+1}]$, *i.e.*, if $x_i \le x \le x_{i+1}$

$$\varphi(x) = a_i + b_i x + c_i x^2 + d_i x^3 \equiv p_i(x) \qquad (i = 1, \ldots, N-1). \tag{A.3}$$

2) The polynomial $p_i(x)$ matches the values of $f(x)$ at the end-points of the i-th interval,

$$p_i(x_i) = f_i, \quad p_i(x_{i+1}) = f_{i+1} \qquad (i = 1, \ldots, N-1), \tag{A.4}$$

so that $\varphi(x)$ is continuous in $[x_1,x_N]$.
3) The first and second derivatives of $\varphi(x)$ are continuous in $[x_1,x_N]$

$$p_i'(x_{i+1}) = p_{i+1}'(x_{i+1}) \qquad (i = 1, \ldots, N-2), \tag{A.5a}$$

$$p_i''(x_{i+1}) = p_{i+1}''(x_{i+1}) \qquad (i = 1, \ldots, N-2). \tag{A.5b}$$

Consequently, the curve $y = \varphi(x)$ interpolates the tabulated values (A.1) and has a continuously turning tangent.

To obtain the spline coefficients a_i, b_i, c_i, d_i $(i = 1, \ldots, N-1)$ we start from the fact that $\varphi''(x)$ is linear in $[x_i,x_{i+1}]$. Introducing the quantities

$$h_i \equiv x_{i+1} - x_i \qquad (i = 1, \ldots, N-1) \tag{A.6}$$

and

$$\sigma_i = \varphi''(x_i) \qquad (i = 1, \ldots, N), \tag{A.7}$$

we can write the obvious identity

$$p_i''(x) = \sigma_i \frac{x_{i+1} - x}{h_i} + \sigma_{i+1} \frac{x - x_i}{h_i} \qquad (i = 1, \ldots, N-1). \tag{A.8}$$

Notice that x_{i+1} must be larger than x_i in order to have $h_i > 0$. Integrating Eq. (A.8) twice with respect to x gives for $i = 1, \ldots, N-1$

$$p_i(x) = \sigma_i \frac{(x_{i+1} - x)^3}{6h_i} + \sigma_{i+1} \frac{(x - x_i)^3}{6h_i} + A_i(x - x_i) + B_i(x_{i+1} - x), \tag{A.9}$$

where A_i and B_i are constants. These can be determined by introducing the expression (A.9) into Eqs. (A.4); this gives the pair of Eqs.

$$\sigma_i \frac{h_i^2}{6} + B_i h_i = f_i \qquad \text{and} \qquad \sigma_{i+1} \frac{h_i^2}{6} + A_i h_i = f_{i+1}. \tag{A.10}$$

Finally, solving for A_i and B_i and substituting the result in (A.9), we obtain

$$\begin{aligned} p_i(x) \;=\; & \frac{\sigma_i}{6}\left[\frac{(x_{i+1}-x)^3}{h_i} - h_i(x_{i+1}-x)\right] + f_i\frac{x_{i+1}-x}{h_i} \\ & + \frac{\sigma_{i+1}}{6}\left[\frac{(x-x_i)^3}{h_i} - h_i(x-x_i)\right] + f_{i+1}\frac{x-x_i}{h_i}. \end{aligned} \tag{A.11}$$

To be able to use $\varphi(x)$ to approximate $f(x)$, we must find the second derivatives σ_i $(i = 1, \ldots, N)$. To this end, we impose the conditions (A.5). Differentiating (A.11) gives

$$p_i'(x) = \frac{\sigma_i}{6}\left[-\frac{3(x_{i+1}-x)^2}{h_i} + h_i\right] + \frac{\sigma_{i+1}}{6}\left[\frac{3(x-x_i)^2}{h_i} - h_i\right] + \delta_i, \tag{A.12}$$

where

$$\delta_i = \frac{y_{i+1}-y_i}{h_i}. \tag{A.13}$$

Hence,

$$p_i'(x_{i+1}) = \sigma_i\frac{h_i}{6} + \sigma_{i+1}\frac{h_i}{3} + \delta_i, \tag{A.14a}$$

$$p_i'(x_i) = -\sigma_i\frac{h_i}{3} - \sigma_{i+1}\frac{h_i}{6} + \delta_i, \tag{A.14b}$$

and, similarly,

$$p_{i+1}'(x_{i+1}) = -\sigma_{i+1}\frac{h_{i+1}}{3} - \sigma_{i+2}\frac{h_{i+1}}{6} + \delta_{i+1}. \tag{A.14c}$$

Replacing (A.14a) and (A.14c) in (A.5a), we find

$$h_i\sigma_i + 2(h_i + h_{i+1})\sigma_{i+1} + h_{i+1}\sigma_{i+2} = 6\,(\delta_{i+1} - \delta_i) \qquad (i = 1, \ldots, N-2). \tag{A.15}$$

The system (A.15) is linear in the N unknowns σ_i $(i = 1, \ldots, N)$. However, since it contains only $N-2$ equations, it is underdetermined. This means that we need either to add two additional (independent) equations or to fix arbitrarily two of the N unknowns. The usual practice is to adopt *end-point strategies* that introduce constraints on the behaviour of $\varphi(x)$ near x_1 and x_N. An end-point strategy fixes the values of σ_1 and σ_N, yielding an $(N-2)\times(N-2)$ system in the variables σ_i $(i = 2, \ldots, N-1)$. The resulting system is, in matrix form,

$$\begin{pmatrix} H_2 & h_2 & 0 & \cdots & 0 & 0 & 0 \\ h_2 & H_3 & h_3 & \cdots & 0 & 0 & 0 \\ 0 & h_3 & H_4 & \cdots & 0 & 0 & 0 \\ \vdots & \vdots & \vdots & \ddots & \vdots & \vdots & \vdots \\ 0 & 0 & 0 & \cdots & H_{N-3} & h_{N-3} & 0 \\ 0 & 0 & 0 & \cdots & h_{N-3} & H_{N-2} & h_{N-2} \\ 0 & 0 & 0 & \cdots & 0 & h_{N-2} & H_{N-1} \end{pmatrix} \begin{pmatrix} \sigma_2 \\ \sigma_3 \\ \sigma_4 \\ \vdots \\ \sigma_{N-3} \\ \sigma_{N-2} \\ \sigma_{N-1} \end{pmatrix} = \begin{pmatrix} D_2 \\ D_3 \\ D_4 \\ \vdots \\ D_{N-3} \\ D_{N-2} \\ D_{N-1} \end{pmatrix}, \tag{A.16}$$

where

$$H_i = 2(h_{i-1} + h_i) \qquad (i = 2, \ldots, N-1) \tag{A.17}$$

and

$$\begin{aligned} D_2 &= 6(\delta_2 - \delta_1) - h_1\sigma_1, \\ D_i &= 6(\delta_i - \delta_{i-1}) \qquad\qquad (i = 3, \ldots, N-2), \\ D_{N-1} &= 6(\delta_{N-1} - \delta_{N-2}) - h_{N-1}\sigma_N. \end{aligned} \tag{A.18}$$

(σ_1 and σ_N are removed from the first and last equations, respectively). The matrix of coefficients is symmetric, tridiagonal and diagonally dominant (the larger coefficients are in the diagonal), so that the system (A.16) can be easily (and accurately) solved by Gauss elimination. The spline coefficients a_i, b_i, c_i, d_i ($i = 1, \ldots, N-1$) —see Eq. (A.3)— can then be obtained by expanding the expressions (A.11):

$$\begin{aligned} a_i &= \frac{1}{6h_i}\left[\sigma_i x_{i+1}^3 - \sigma_{i+1}x_i^3 + 6\left(f_i x_{i+1} - f_{i+1}x_i\right)\right] + \frac{h_i}{6}\left(\sigma_{i+1}x_i - \sigma_i x_{i+1}\right), \\ b_i &= \frac{1}{2h_i}\left[\sigma_{i+1}x_i^2 - \sigma_i x_{i+1}^2 + 2\left(f_{i+1} - f_i\right)\right] + \frac{h_i}{6}\left(\sigma_i - \sigma_{i+1}\right), \\ c_i &= \frac{1}{2h_i}\left(\sigma_i x_{i+1} - \sigma_{i+1}x_i\right), \\ d_i &= \frac{1}{6h_i}\left(\sigma_{i+1} - \sigma_i\right). \end{aligned} \tag{A.19}$$

In order to allow moderate extrapolation we extend the spline to the intervals $(-\infty, x_1)$ and (x_N, ∞) by means of quadratic polynomials that match the values of the spline and its first and second derivatives at the end-points. That is, we set

$$\varphi(x) = (a_1 + d_1 x_1^3) + (b_1 - 3d_1 x_1^2)x + (c_1 + 3d_1 x_1)x^2 \qquad \text{if } x \le x_1, \tag{A.20a}$$

and

$$\begin{aligned} \varphi(x) &= (a_{N-1} + d_{N-1}x_N^3) + (b_{N-1} - 3d_{N-1}x_N^2)x \\ &\quad + (c_{N-1} + 3d_{N-1}x_N)x^2 \qquad \text{if } x \ge x_N, \end{aligned} \tag{A.20b}$$

We thus obtain a continuous function with continuous first and second derivatives, *i.e.*, a cubic spline in $(-\infty,\infty)$.

When accurate values of $f''(x)$ are known, the best strategy is to set $\sigma_1 = f''(x_1)$ and $\sigma_N = f''(x_N)$, since this will minimize the spline interpolation errors near the end-points. Unfortunately, the exact values $f''(x_1)$ and $f''(x_N)$ are not always available. The so-called *natural spline* corresponds to taking $\sigma_1 = \sigma_N = 0$. It results in a $y = \varphi(x)$ curve with the shape that would be taken by a flexible rod (such as a draughtsman's spline) if it were bent around pegs at the knots but allowed to maintain its natural (straight) shape outside the interval $[x_1,x_N]$.

The accuracy of the spline interpolation is mainly determined by the density of knots in the regions where $f(x)$ has strong variations. For constant, linear, quadratic and cubic functions the interpolation errors can be reduced to zero by using the exact values of σ_1 and σ_N. Evidently, in the case of quadratic or cubic polynomials the natural spline may introduce considerable errors near the end-points. It is also important to keep in mind that a cubic polynomial has, at most, one inflexion point. As a consequence,

we should have at least a knot between each pair of inflexion points of $f(x)$ to ensure proper interpolation. Special care must be taken when interpolating functions that have a practically constant value in a partial interval, since the spline tends to wiggle instead of staying constant. In this particular case, it may be more convenient to use linear interpolation in the interval where the function is constant.

Obviously, the interpolating cubic spline $\varphi(x)$ can be used not only to obtain interpolated values of $f(x)$ between the knots, but also to calculate integrals such as

$$\int_a^b f(x)\, x^k \,\mathrm{d}x \simeq \int_a^b \varphi(x)\, x^k \,\mathrm{d}x \tag{A.21}$$

analytically. In addition, it is worth recalling that derivatives of $\varphi(x)$ other than the first one may differ significantly from those of $f(x)$.

To obtain the interpolated value $\varphi(x_\mathrm{c})$ —see Eq. (A.3)— of $f(x)$ at the point x_c, we must first determine the interval $[x_i,x_{i+1}]$ that contains the point x_c. To reduce the effort to locate the point, we use the following binary search algorithm

1. Set i =1 and $j = N$.
2. Set $k = [(i + j)/2]$, where $[x]$ indicates the integer part of x.
3. If $x_k < x_\mathrm{c}$ set $i = k$, otherwise set $j = k$.
4. If $j - i > 1$ go to step 2.
5. Deliver i.

Notice that the maximum delivered value of i is $N - 1$. Hence, the cases $x < x_1$ and $x > x_N$ (where the quadratic extrapolation applies) should be considered separately.

A.1 The spline toolkit

Because the power-series solution algorithm implemented in RADIAL rests heavily on cubic spline interpolation, the distribution package includes a set of tools that facilitate the definition and the use of interpolating cubic splines. Although some of these subprograms are interconnected, the set is standalone and can be used independently. Notice that the physical dimensions of all input-output arrays must be defined in the calling program.

The spline toolkit consists of the following seven subprograms:

1) `SUBROUTINE SPLINE(X,Y,A,B,C,D,S1,SN,N)`

This subroutine determines the coefficients of a piecewise cubic spline that interpolates the input table of variable and function values defined as a double array `(X,Y)` of dimension `N`. Duplicated abscissas are considered as discontinuities; a separate spline is used for each interval between consecutive discontinuities, with "natural" end-point shape (null second derivative) at the discontinuities.

INPUT: `X(1:N)` = grid points x_i, must be in non decreasing order.
`Y(1:N)` = corresponding function values, $y_i = f(x_i)$.
`S1`, `SN` = σ_1 and σ_N, second derivatives at x_1 and x_N, respectively.
The natural cubic spline is considered when `S1` = 0 and `SN=0`.
`N` = N, number of grid points.

OUTPUT: `A`(1:N), `B(1:N)`, `C(1:N)`, `D(1:N)` = arrays of spline coefficients.

OTHER SUBPROGRAMS USED: subroutine `SPLIN0`.

The interpolating cubic polynomial in the `I`-th interval, from `X(I)` to `X(I+1)`, is

$$\varphi(x) = \mathtt{A(I)} + x(\mathtt{B(I)} + x(\mathtt{C(I)} + x\mathtt{D(I)}))). \tag{A.22}$$

2) `SUBROUTINE SPLIN0(X,Y,A,B,C,D,S1,SN,N)`

Initialisation of cubic spline interpolation of tabulated data. It is assumed that the function and its first two derivatives are continuous; duplicate abscissas are not allowed.

INPUT: `X(1:N)` = grid points x_i, must be in strictly increasing order.
`Y(1:N)` = corresponding function values, $y_i = f(x_i)$.
`S1`, `SN` = σ_1 and σ_N, second derivatives at x_1 and x_N, respectively.
The natural cubic spline is considered when `S1` = 0 and `SN=0`.
`N` = N, number of grid points.

OUTPUT: `A(1:N)`, `B(1:N)`, `C(1:N)`, `D(1:N)` = arrays of spline coefficients.

This subroutine is standalone.

3) `SUBROUTINE FINDI(XC,X,N,I)`

This subroutine finds the interval (`X(I)`,`X(I+1)`) that contains the value `XC` by using the binary search algorithm.

INPUT: `XC` = point to be located.
`X(1:N)` = grid points x_i.
`N` = N, number of grid points.

OUTPUT: `I` = interval index.

4) `FUNCTION SPLVAL(XC,X,A,B,C,D,N)`

This function evaluates a cubic spline at the point `XC`; quadratic extrapolation is used for points outside the interval (x_1, x_N).

INPUT: `XC` = spline argument.
`X(1:N)` = grid points x_i, must be in non decreasing order.
`A(1:N)`, `B(1:N)`, `C(1:N)`, `D(1:N)` = arrays of spline coefficients.
`N` = N, number of grid points.

OUTPUT: `SPLVAL` = value of the spline function at `XC`.

5) `SUBROUTINE SPLERR(X,Y,S1,SN,ERR,N,IWR)`

This subroutine estimates the error introduced by the cubic spline interpolation of a table (`X`,`Y`). The interpolation error in the neighbourhood of `X(K)` is estimated from the relative difference between `Y(K)` and the value obtained from the spline that interpolates the table with the `K`-th point removed. Generally, the error of the spline is slightly overestimated.

INPUT: `X(1:N)` = grid points x_i, must be in non decreasing order.
`Y(1:N)` = corresponding function values, $y_i = f(x_i)$.
`S1`, `SN` = σ_1 and σ_N, second derivatives at x_1 and x_N, respectively. The natural cubic spline is considered when `S1` = 0 and `SN=0`.
`N` = N, number of grid points.
`IWR` = printing flag. When `IWR` is greater than zero, a table of input function values, spline values, and the relative differences is written in a file named `SPLERR.dat`, which is open as unit `IWR`.

OUTPUT: `ERR` = estimated largest relative error of the interpolating spline.

OTHER SUBPROGRAMS USED: subroutines `SPLINE` and `SPLIN0`.

6) `SUBROUTINE SPLSET(FUNC,XL,XU,X,Y,TOL,ERR,NPM,NFIX,NU,N)`

This subroutine determines a table `(X,Y)` of the external function `FUNC(X)` suited for natural cubic spline interpolation in the interval (`XL`,`XU`).

The `X` grid is built by starting from an initial subgrid consisting of `NU` uniformly spaced points in (`XL`,`XU`). If `NU` is negative, the initial grid points are logarithmically spaced within that interval. The grid is refined by adding new points in regions where the interpolation seems to have the larger errors. Optionally a number `NFIX` of `X`-values can be fixed by the user; they are to be entered in the first `NFIX` positions of the input array `X`. `TOL` is the tolerance; the subroutine ends when the largest relative error is estimated to be less than `TOL`.

INPUT: `FUNC`: name of the external function.
`XL`, `XU` = endpoints of the considered interval.
`TOL` = tolerance, desired relative error of the interpolation.
`NPM` = physical dimension of arrays `X` and `Y`.
`NFIX` = number of fixed points. Their abscissas must be entered as the first `NFIX` elements of the array `X`. A doubled value is considered as a discontinuity.
`NU` = number of points in the initial "uniform" subgrid.
`N` = desired number of points in the table. Must be larger than `NFIX+ABS(NU)` and less than `NPM`.

OUTPUT: `X(1:N)` = generated array of grid points x_i, in non-decreasing order.
`Y(1:N)` = corresponding function values, $y_i = f(x_i)$.
`ERR` = estimated largest relative error of the interpolating spline.
`N` = number of points in the generated grid.

OTHER SUBPROGRAMS USED: subroutines `SPLINE` and `SPLERR`.

The number of grid points in the grid may differ from the input value `N`, either because the subroutine stopped adding grid points as soon as the required tolerance was attained or because `N` was too small to initiate the process. Notice that subroutine `SPLSET` does not give the spline coefficients, which have to be generated by calling subroutine `SPLINE` after the call to `SPLSET`.

7) `FUNCTION SPLINT(X,A,B,C,D,XL,XU,N,NPOW)`

This function calculates the integral of a cubic spline function $\varphi(x)$ multiplied by a power of x, *i.e.*,

$$\int_{\mathtt{XL}}^{\mathtt{XU}} \varphi(x)\, x^{\mathtt{NPOW}}\, \mathrm{d}x. \tag{A.23}$$

INPUT: `X(1:N)` = spline grid points x_i.
`A(1:N)`, `B(1:N)`, `C(1:N)`, `D(1:N)` = arrays of spline coefficients.
`XL` and `XU`= lower and upper limits of the integral.
`N` = N, number of spline grid points.
`NPOW` = power of x in the integrand.

OUTPUT: `SPLINT` = value of the integral.

OTHER SUBPROGRAMS USED: subroutines `FINDI` and `SPLIN1`.

B Continued fractions

Continued fractions are often useful to evaluate special functions (see Press *et al.*, 1992). A continued fraction is defined as

$$f(x) = b_0 + \cfrac{a_1}{b_1 + \cfrac{a_2}{b_2 + \cfrac{a_3}{b_3 + \cdots}}}, \tag{B.1}$$

where the a's and b's can themselves be simple functions of x. The continued fraction (B.1) is frequently written in the typographically simpler form

$$f(x) = b_0 + \frac{a_1}{b_1+}\,\frac{a_2}{b_2+}\,\frac{a_3}{b_3+\cdots}. \tag{B.2}$$

If the number of terms is finite, f is called a terminating continued fraction. If the number of terms is infinite, f is called an infinite continued fraction and the terminating fraction

$$f_n(x) = b_0 + \frac{a_1}{b_1+}\,\frac{a_2}{b_2+}\cdots\frac{a_n}{b_n} \tag{B.3}$$

is called the n-th convergent of f. If $\lim_{n\to\infty} f_n(x)$ exists, the infinite continued fraction $f(x)$ is said to be convergent, and the limit is then the value of the continued fraction. Continued fractions frequently converge much more rapidly than power series expansions and in a wider domain of the complex plane.

In the calculation of terminating continued fractions, is seems natural to proceed from right to left, but this is not possible for infinite continued fractions. A practical solution is to proceed from left to right by using the following recursion method, which was invented by Wallis a long while ago (in 1655!). Let us define two sequences, A_n and B_n, by the initial values

$$A_{-1} = 1, \quad A_0 = b_0, \quad B_{-1} = 0, \quad B_0 = 1 \tag{B.4}$$

and the recurrence relations

$$A_n = A_{n-1}\, b_n + A_{n-2}\, a_n, \qquad B_n = B_{n-1}\, b_n + B_{n-2}\, a_n; \tag{B.5}$$

then, the n-th convergent of f is

$$f_n(x) = \frac{A_n}{B_n}. \tag{B.6}$$

This result can be easily proved by induction. The recurrence relations (B.5) frequently generate very large or very small values of the partial numerators and denominators A_n and B_n, with the risk of overflow or underflow of the floating-point representation. However, as the recurrences (B.5) are linear, this can be fixed by simply rescaling the values A_n, A_{n-1}, B_n, and B_{n-1}, for instance dividing all them by $|B_n|$, when an overflow is imminent[11]. A brute-force solution, easier to program, is to rescale after each iteration. If one of the denominators B_n equals 0 (as it may happen in the case of Coulomb functions), we must skip the rescaling and evaluation of the ratio (B.6) and continue with the next iteration of (B.5); a second zero could indicate that the continued fraction is not convergent. We assume that the numerical evaluation of the continued fraction can be terminated when the values $f_n(x)$ and $f_{n-1}(x)$ of the last iterations differ in less than the selected tolerance. This is normally a good termination method (it certainly works for Coulomb functions), although it may yield wrong results with peculiar fractions (such that $f_{n-1} = f_n$ but $f_{n+1} \neq f_n$). More sophisticated algorithms for evaluating continued fractions, which avoid the need for rescaling intermediate results, have been proposed by Steed (Barnett *et al.*, 1974) and by Lentz (see Press *et al.*, 1992).

The equivalence transformation

$$a_k \to c a_k, \quad b_k \to c b_k, \quad a_{k+1} \to c a_{k+1}, \tag{B.7}$$

with $c \neq 0$, keeps the value of the continued fraction unchanged. Successive equivalence transformations with different c's can be applied to successive terms to simplify the form of the a and b coefficients:

$$f(x) = b_0 + \frac{c_1 a_1}{c_1 b_1 +}\, \frac{c_1 c_2 a_2}{c_2 b_2 +} \cdots \frac{c_{n-1} c_n a_n}{c_n b_n + \cdots}. \tag{B.8}$$

[11] The use of a positive scaling factor is important so as to keep track of the true sign of the partial denominator, which is required to determine the sign of the Coulomb functions computed by Steed's continued fraction method (see Section 3.1.3).

C Nodes of the radial functions

In the calculation of bound-state wave functions, the outward and inward solutions are matched at a point r_m such that the interval $(0, r_m)$ contains all nodes of the radial functions (see Section 5). This makes sure that the inward solution has no nodes and, therefore, trial energies that are too far from the eigenvalue can be discarded by computing only the outward solution. Obviously, the adopted value of the matching radius r_m is quite arbitrary, any value larger than the outer node of the $P(r)$ function is acceptable (but the calculation time increases with r_m). In this Appendix we discuss the strategies used to determine r_m for the Schrödinger and Dirac equations.

The radial Schrödinger equation (2.6) can be written in the form[12]

$$P''(r) = -\frac{2\mathrm{m_e}}{\hbar^2}\left[E - V(r) - \frac{\hbar^2}{2\mathrm{m_e}}\,\frac{\ell(\ell+1)}{r^2}\right] P(r). \tag{C.1}$$

It is instructive to consider the radial motion under the effective potential (see Fig. 17)

$$V_{\mathrm{eff}}(r) = V(r) + \frac{\hbar^2}{2\mathrm{m_e}}\,\frac{\ell(\ell+1)}{r^2}. \tag{C.2}$$

Evidently, the set of inflexion points ($P'' = 0$) of the radial function consists of the nodes of $P(r)$ and the turning points of the radial motion ($V_{\mathrm{eff}} = E$). In the classically allowed regions of motion ($E > V_{\mathrm{eff}}$), the radial function is convex toward the axis ($P''/P < 0$). Within a forbidden region ($E < V_{\mathrm{eff}}$), $P(r)$ is concave toward the axis ($P''/P > 0$) and, therefore, it has at most a single node. As long as $P(r)$ does not vanish at the turning points, there is a finite distance from a turning point to the nearest node.

For Schrödinger bound states, the matching radius r_m may be taken equal to the outmost turning point, *i.e.*, the largest root of the equation

$$V(r_m) + \frac{\hbar^2}{2\mathrm{m_e}}\,\frac{\ell(\ell+1)}{r_m^2} - E = 0. \tag{C.3}$$

This is the outer inflexion point of the radial function. In the forbidden region $r > r_m$, $P(r)$ is convex towards the axis, *i.e.*, $|P(r)|$ decreases monotonously when r increases and tends to zero when $r \to \infty$. Obviously, all the nodes of the radial function of a bound state are within the interval $(0,r_m)$.

Let us now consider the radial Dirac equations (2.21). It is interesting to transform these equations into a single equation of the Schrödinger form. By elimination of the function $Q(r)$ we have

$$P''(r) = \frac{\kappa(\kappa+1)}{r^2}\,P(r) + \frac{\kappa}{r}\,\frac{A'}{A}\,P(r) - \left(\frac{2\mathrm{m_e}c^2}{c\hbar}\right)^2 A(A-1)\,P(r) + \frac{A'}{A}\,P'(r)\,, \tag{C.4}$$

where

$$A(r) \equiv \frac{E - V(r) + 2\mathrm{m_e}c^2}{2\mathrm{m_e}c^2}. \tag{C.5}$$

[12]Here primes indicate differentiation with respect to r.

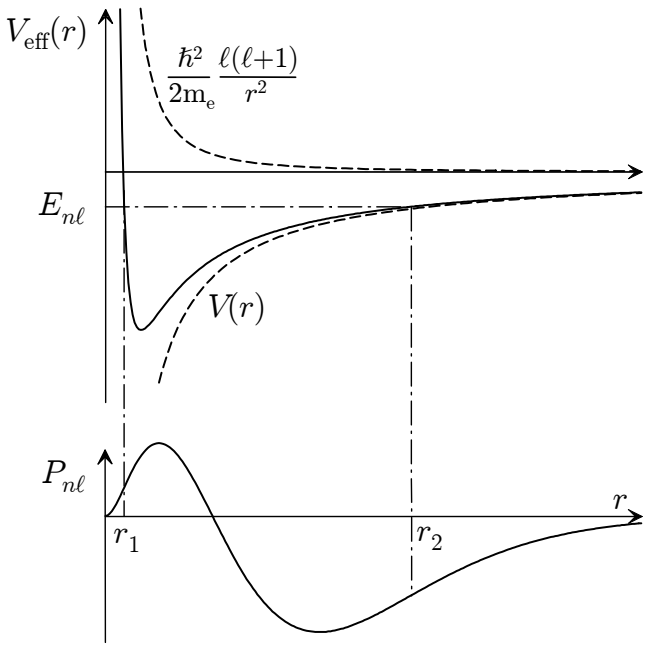

Figure 17: Effective potential $V_{\rm eff}(r)$, for a purely attractive potential $V(r)$, and reduced radial function $P_{n\ell}(r)$ of a bound state. Within the classically allowed interval (r_1, r_2), the radial function is convex toward the axis. Outside this interval $P_{n\ell}(r)$ is concave toward the axis, *i.e.*, it increases or decreases monotonically. All zeros of $P_{n\ell}(r)$ are inside the interval $(r_1,\, r_2)$ except, evidently, those at $r = 0$ and $r = \infty$.

With the substitution

$$P(r) = \sqrt{A(r)}\, F(r), \tag{C.6}$$

and recalling that $\kappa(\kappa+1) = \ell(\ell+1)$, Eq. (C.4) transforms into

$$F''(r) = -\left[\frac{E(E+2m_e c^2)}{c^2\hbar^2} - \frac{2m_e}{\hbar^2}\, V_{\rm rel}(r) - \frac{\ell(\ell+1)}{r^2}\right] F(r) \tag{C.7}$$

with

$$V_{\rm rel}(r) \equiv V + \left\{ V\, \frac{2E-V}{2m_e c^2} + \frac{\hbar^2}{2m_e}\left[\frac{\kappa}{r}\,\frac{A'}{A} + \frac{3}{4}\left(\frac{A'}{A}\right)^2 - \frac{1}{2}\,\frac{A''}{A}\right]\right\}. \tag{C.8}$$

Equation (C.7), which is strictly equivalent to the Dirac equations (2.21), has the form of the Schrödinger equation (C.1) with the relativistic potential $V_{\rm rel}(r)$ given by Eq. (C.8). The terms in curly braces (which depend on the potential and its derivatives, as well as on E and κ) account for the relativistic corrections. We see again that, in the non-relativistic limit, $A(r) = 1$ and the function $F(r) = P(r)$ reduces to the Schrödinger radial function.

In the region where $V(r)$ is less than $E + 2m_e c^2$, the zeros of the Dirac function $P(r)$ coincide with those of $F(r)$, see Eq. (C.6). As before, the inflexion points of the function $F(r)$ are the nodes ($F = 0$) and the points for which

$$\frac{E(E+2m_e c^2)}{c^2\hbar^2} - \frac{2m_e}{\hbar^2}\, V_{\rm rel}(r) - \frac{\ell(\ell+1)}{r^2} = 0. \tag{C.9}$$

All the nodes of $P(r)$ are within the interval $(0, r_m)$, where r_m is the largest root of Eq. (C.9). For most bound states, $E - V(r_m)$ is much less than $2\mathrm{m_e}c^2$ and the derivatives of the function $A(r)$ are negligible for $r > r_m$. Under these circumstances, Eq. (C.9) reduces to Eq. (C.3), *i.e.*, the matching radius r_m is approximately equal to the outermost turning point of the classical non-relativistic motion. In the RADIAL subroutines, r_m is always evaluated in this approximate way but, if the outward function $P(r)$ is not concave towards the axis at r_m, the outward solution is continued up to the first grid point where $P(r)$ and $P''(r)$ have the same sign. This point is beyond the last zero of $P(r)$, as required.

Within each allowed region of motion ($E > V$), the nodes of the small radial function $Q(r)$ alternate with those of $P(r)$. To prove this assertion, let us assume that r_a and r_b ($> r_a$) are two consecutive nodes of P and consider that $P'(r_a) > 0$ and $P'(r_b) < 0$, *i.e.*, $P(r)$ is positive between r_a and r_b. From the first of Eqs. (2.21),

$$Q(r) = \frac{c\hbar}{E - V + 2\mathrm{m_e}c^2} \left(P' + \frac{\kappa}{r} P \right), \tag{C.10}$$

it then follows that $Q(r_a)$ is positive and $Q(r_b)$ is negative. Therefore, $Q(r)$ has (at least) one node in the interval (r_a, r_b). Exchanging the roles of P and Q and considering the second of Eqs. (2.21), we conclude that P has a node between each pair of consecutive nodes of Q. This implies that between each pair of nodes of P there is a single node of Q.

References

Abramowitz, M., and I.A. Stegun (1974), *Handbook of Mathematical Functions* (Dover, New York).

Auvil, P.R., and L.M. Brown (1978), "The relativistic hydrogen atom: a simple solution." *Am. J. Phys.* **46**, 679–681.

Bardin, C., Y. Dandeu, L. Gauthier, J. Guillermin, T. Lena, J.-M. Pernet, H.H. Wolter, and T. Tamura (1972), "Coulomb functions in entire (θ,ρ)-plane." *Comput. Phys. Commun.* **3**, 73–87.

Barnett, A.R., D.H. Feng, J.W. Steed, and L.J.B. Goldfarb (1974), "Coulomb wave functions for all real η and ρ." *Comput. Phys. Commun.* **8**, 377–395.

Barnett, A.R. (1981), "An algorithm for regular and irregular Coulomb and Bessel functions of real order to machine accuracy." *Comput. Phys. Commun.* **21**, 297–314.

Becchetti, F.D., and G.W. Greenlees (1969), "Nucleon-nucleus optical-model parameters, $A > 40$, $E < 50$ MeV." *Phys. Rev.* **182**, 1190–1209.

Bethe, H.A., and E.E. Salpeter (1957) *Quantum Mechanics of One- and Two-electron Atoms* (Springer-Verlag OHG, Berlin).

Bote, D., and F. Salvat (2008) "Calculations of inner-shell ionization by electron impact with the distorted-wave and plane-wave Born approximations." *Phys. Rev. A* **77**, 042701 (24 pp).

Bransden, B.H., and C.J. Joachain (1983) *Physics of Atoms and Molecules* (Addison Wesley Longman Ltd., Essex).

Bühring, W. (1965), "Computational improvements in phase shift calculations of elastic electron scattering." *Z. Phys.* **187**, 180–196.

Carlson, T.A. (1975) *Photoelectron and Auger Spectroscopy* (Plenum Press, New York and London).

Condon, E.U. (1930) "The theory of complex spectra." *Phys. Rev.* **36**, 1121–1133.

Condon, E.U., and H. Odabaşi (1980) *Atomic Structure* (Cambridge Univ. Press, New York).

Coursey, J.S., D.J. Schwab, J.J. Tsai, and R.A. Dra (2015) "Atomic and isotopic compositions for all elements," NIST Standard Reference Database 144.
`https://www.nist.gov/srd/nist-standard-reference-databases-chemistry`

Dennery, P., and A. Krzywicki (1995), *Mathematics for Physicists* (Dover, New York).

Edmonds, A.R. (1960) *Angular Momentum in Quantum Mechanics* (Princeton Univ. Press, Princeton NJ).

Erdélyi, A., Ed. (1953) *Higher Transcendental Functions*, Vol. I (McGraw-Hill Book Company, New York).

Fröberg, C.-E. (1955) "Numerical treatment of Coulomb wave functions." *Rev. Mod. Phys.* **27**, 399–411.

Fröbrich, P., and R. Lipperheide (1996) *Theory of Nuclear Reactions. Oxford Studies in Nuclear Physics*, Vol. 18 (Oxford University Press, Oxford).

Gradshteyn, I.S., and I.M. Ryzhik (1980), *Table of Integrals, Series and Products* (Academic Press, New York).

Grant, I.P. (1970) "Relativistic calculation of atomic structures." *Advances in Physics* **19**, 747–811.

Greiner, W. (1990), *Relativistic Quantum Mechanics – Wave Equations* (Springer, Berlin).

Hahn, B., D.G. Ravenhall, and R. Hofstadter (1956). "High-energy electron scattering." *Phys. Rev.* **101**, 1131–1142.

Hartree, D.R. (1957) *The Calculation of Atomic Structures* (John Wiley and Sons, New York).

Hodgson, P.E. (1971) "The nuclear optical model." *Rep. Prog. Phys.* **34**, 765–819.

Joachain, C.J. (1978), *Quantum Collision Theory* (North Holland, Amsterdam).

Johnson, W.R., and K.T. Cheng (1979), "Quantum defects for highly stripped ions." *J. Phys. B: At. Mol. Phys.* **12**, 863–879.

Kittel, C. (1976), *Introduction to Solid State Physics* (John Wiley and Sons, New York).

Kohn, W., and L.J. Sham (1965) "Self-consistent equations including exchange and correlation effects." *Phys. Rev.* **140 A**, 1133–1138.

Kolsrud, M. (1966), "On the solution of Dirac's equation with Coulomb potential." *Physica Norvegica* **2**, 43–50.

Koning, A.J., and J.P. Delaroche (2003) "Local and global nucleon optical models from 1 keV to 200 MeV." *Nucl. Phys.* **A 713**, 231–310.

Latter, R. (1955) "Atomic energy levels for the Thomas-Fermi and Thomas-Fermi-Dirac potential." *Phys. Rev.* **99**, 510–519.

Liberman, D., J.T. Waber, and D.T. Cromer (1965) "Self-consistent-field Dirac-Slater wave functions for atoms and ions I. Comparison with previous calculations." *Phys. Rev.* **1A**, 27–34.

Liberman, D., D.T. Cromer, and J.T. Waber (1971) "Relativistic self-consitent field program for atoms and ions." *Comput. Phys. Commun.* **2**, 107–113.

Ma, Z.-Q. (1985), "Proof of the Levinson theorem by the Sturm-Liouville theory." *J. Mat. Phys.* **26**, 1995–1999.

Ma, Z.-Q., and G.-J. Ni (1985), "Levinson theorem for Dirac particles." *Phys. Rev. D* **31**, 1482–1488.

Maron, M.J. (1982), *Numerical Analysis: A Practical Approach* (Macmillan, New York).

Mayers, D.F. (1957), "Relativistic self-consistent field calculations for mercury." *Proc. Roy. Soc.* (London) **A241**, 93–98.

Merzbacher, E. (1970), *Quantum Mechanics*, 2nd edition (John Wiley and Sons, New York).

Mohr, P.J., D.B. Newell, and B.N. Taylor (2016), "CODATA recommended values of the fundamental physical constants: 2014." *Rev. Mod. Phys.* **88**, 035009 (73 pp).

Molière, G. (1947) " Theorie der Streuung schneller geladener Teilchen I. Einzelstreuung am abgeschirmten Coulomb-Feld." *Z. Naturforsch.* **2a**, 133–145.

Mott, N.F., and H.S.W. Massey (1965), *The Theory of Atomic Collisions*, 3rd edition (Oxford Univ. Press, London).

Olver, F.W.J., D.W. Lozier, R.F. Boisvert, and C.W. Clark, Eds. (2010) *NIST Handbook of Mathematical Functions*, (Cambridge University Press, New York). Print companion to the NIST Digital Library of Mathematical Functions (DLMF), `http://dlmf.nist.gov/`

Parzen, G. (1950), "On the scattering theory of the Dirac equation." *Phys. Rev.* **80**, 261–268.

Piekarewicz, J. (1993), "Levinson's theorem for Dirac particles." *Phys. Rev. C* **48**, 2174–2181.

Poliatzky, N. (1993), "Levinson's theorem for the Dirac equation." *Phys. Rev. Lett.* **70**, 2507–2510.

Pratt, R.H., A. Ron, and H.K. Tseng (1973), "Atomic photoelectric effect above 10 keV." *Rev. Mod. Phys.* **45**, 273–325. Erratum (1973) *ibid.* **45**, 663–664.

Press, W.H., S.A. Teukolsky, W.T. Vetterling, and B.P. Flannery (1992), *Numerical Recipes*, 2nd. ed. (Cambridge Univ. Press, New York).

Ribberfors, R. (1975) "Relationship of the relativistic Compton cross section to the momentum distribution of bound electron states." *Phys. Rev. B* **12**, 2067–2074.

Rose, M.E. (1961), *Relativistic Electron Theory* (John Wiley and Sons, New York).

Rose, M.E. (1995), *Elementary Theory of Angular Momentum* (Dover Publications, Inc., New York).

Royer, G., and C. Gautier (2006) "Coefficients and terms of the liquid drop model and mass formula." *Phys. Rev. C* **73**, 067302 (4 pp).

Sabbatucci, L., and F. Salvat (2016), "Theory and calculation of the atomic photoeffect." *Radiat. Phys. Chem.* **121**, 122–140.

Sakurai, J.J. (1967), *Advanced Quantum Mechanics* (Addison-Wesley Publ. Co., Reading, Massachusetts).

Salvat, F. (2003), "Optical-model potential for electron and positron elastic scattering by atoms." *Phys. Rev. A* **68**, 012708 (17 pp).

Salvat, F., and R. Mayol (1991), "Accurate numerical solution of Schrödinger and Dirac wave equations for central fields." *Comput. Phys. Commun.* **62**, 65–79.

Salvat, F., J.M. Fernández-Varea, and W. Williamson, Jr. (1995), "Accurate numerical solution of the radial Schrödinger and Dirac wave equations." *Comput. Phys. Commun.* **90**, 151–168.

Salvat, F., A. Jablonski, and C.J. Powell (2005), "ELSEPA–Dirac partial-wave calculation of elastic scattering of electrons and positrons by atoms, positive ions and molecules." *Comput. Phys. Commun.* **165**, 157–190.

Salvat, F., J.D. Martínez, R. Mayol, and J. Parellada (1987), "Analytical Dirac–Hartree–Fock–Slater screening function for atoms (Z = 1–92)." *Phys. Rev. A* **36**, 467–474.

Salvat, F. (2013), "A generic algorithm for Monte Carlo simulation of proton transport." *Nucl. Instrum. Meth. B* **316**, 144–159.

Schiff, L.I. (1968), *Quantum Mechanics* (McGraw-Hill Kogakusha, Tokyo).

Seaton, M.J. (1983), "Quantum defect theory." *Rep. Prog. Phys.* **46**, 167–257.

Segui, S., M. Dingfelder, J.M. Fernández-Varea, and F. Salvat (2003), "The structure of the Bethe ridge. Relativistic Born and impulse approximations." *J. Phys. B: At. Mol. Opt. Phys.* **35**, 33–53.

Segui, S., M. Dingfelder, and F. Salvat (2003), "Distorted-wave calculation of cross sections for inner-shell ionization by electron and positron impact." *Phys. Rev. A* **67**, 062710 (12 pp).

Slater, J.C. (1929) "The theory of complex spectra." *Phys. Rev.* **34**, 1293–1322.

Slater, J.C. (1951) "A simplification of the Hartree-Fock method." *Phys. Rev.* **81**, 385–390.

Tucker, T.C., L.D. Roberts, C.W. Nestor, T.A. Carlson and F.B. Malik (1969), "Relativistic self-consistent-field calculation of the wave functions, eigenvalues, isotope shifts, and the 6s hyperfine-structure coupling constant as a function of pressure for metallic gold in the Wigner-Seitz model." *Phys. Rev.* **178**, 998–1008.

Varshalovich, D.A., A.N. Moskalev, and V.K. Khersonskii (1988), *Quantum Theory of Angular Momentum* (World Scientific, Singapore).

Walker, D.W. (1971), "Relativistic effects in low energy electron scattering from atoms." *Adv. Phys.* **20**, 257–323.

Yennie, D.R., D.G. Ravenhall and R.N. Wilson (1954), "Phase-shift calculation of high-energy electron scattering." *Phys. Rev.* **95**, 500–512.